

RADIONUCLIDE AND RARE EARTH ELEMENT GEOCHEMISTRY
OF THE CRIFFEL PLUTON, SOUTHWEST SCOTLAND:
AN ANALOGUE STUDY FOR NUCLEAR WASTE DISPOSAL

by

Daud Bin Mohamad, BSc. (Hons.), M.Sc.

A thesis submitted for the degree of Doctor of Philosophy at
the University of Glasgow

Department of Geology and Applied Geology
University of Glasgow
Scotland

October, 1993

ProQuest Number: 13834126

All rights reserved

INFORMATION TO ALL USERS

The quality of this reproduction is dependent upon the quality of the copy submitted.

In the unlikely event that the author did not send a complete manuscript and there are missing pages, these will be noted. Also, if material had to be removed, a note will indicate the deletion.



ProQuest 13834126

Published by ProQuest LLC (2019). Copyright of the Dissertation is held by the Author.

All rights reserved.

This work is protected against unauthorized copying under Title 17, United States Code
Microform Edition © ProQuest LLC.

ProQuest LLC.
789 East Eisenhower Parkway
P.O. Box 1346
Ann Arbor, MI 48106 – 1346

CONTENTS

	Page	
Contents	i	
List of tables	iv	
List of figures	vii	
List of plates	xv	
Acknowledgements	xvii	
Summary	xix	
Declaration	xxiii	
CHAPTER 1	INTRODUCTION	
1.1	Overview	1
1.2	The geochemistry of uranium and thorium	7
1.3	The natural radioactive decay series	15
1.4	Geochemistry of the rare earth elements	25
1.5	Radioactive waste disposal	30
1.5.1	Origin and types of radioactive wastes	30
1.5.2	Methods of disposal	35
1.6	Natural analogues	46
1.6.1	Analogue studies for the waste form	46
1.6.2	Analogue studies for canister materials	50
1.6.3	Analogue studies for bentonite backfill	52
1.6.4	Analogue studies for far-field radionuclide movement	54
1.7	The study area	59
1.8	Objectives of the study	67
CHAPTER 2	SAMPLING AND ANALYTICAL METHODS	
2.1	Summary of samples analysed	69
2.1.1	Granite and granodiorite samples from different zones of the Criffel pluton	69
2.1.2	Fracture and redox front samples from Craignair quarry, Dalbeattie	72
2.1.3	Weathering profile samples of granite and granodiorite	78
2.1.4	Soil samples and radioactivity survey at Beeswing	81
2.1.5	Stream water samples	85
2.2	Analytical methods	87
2.2.1	Instrumental neutron activation analysis	87
2.2.2	Direct gamma spectroscopy analysis	92
2.2.3	Radiochemical analysis of uranium and thorium	96

2.2.3.1	Whole rock analysis	96
2.2.3.2	Soil leaching	102
2.2.3.3	Water analysis	105
2.2.4	Fission track analysis	105
2.2.5	Inductively coupled plasma-mass spectrometry (ICP-MS)	107
CHAPTER 3	RESULTS	112
CHAPTER 4	DISCUSSION AND CONCLUSION	
4.1	Uranium and thorium concentrations and distributions and decay series disequilibrium in the different zones of the Criffel pluton	135
4.2	Natural decay series radionuclide and REE behaviour in fissures and at redox fronts in rock sections from Craignair quarry, Dalbeattie	156
4.2.1	CQ1 rock section studies	156
4.2.1.1	Natural decay series studies	156
4.2.1.2	Rare earth element studies of rock section CQ1	169
4.2.2	CQ2 rock section studies	178
4.2.2.1	Natural decay series studies	178
4.2.2.2	Rare earth element studies of rock section CQ2	196
4.3	Natural decay series radionuclide and REE distributions in granite and granodiorite cores from outcrops subject to post-glacial weathering	202
4.3.1	Weathering profile study of a granite core (GR) sample from Kinharvie	202
4.3.1.1	Natural decay series radionuclide distributions	202
4.3.1.2	Rare earth element studies of granite core GR	214
4.3.2	Weathering profile study of a granodiorite core (GD) sample from Clifton	223
4.3.2.1	Natural decay series radionuclide distributions	223
4.3.2.2	Rare earth element studies of granite core GD	234

4.4	Uranium transport and distribution of ^{210}Pb , ^{226}Ra , ^{134}Cs and ^{137}Cs radionuclides in soil in the vicinity of uranium mineralised veins at Beeswing	239
4.5	Uranium and thorium studies in stream water around the Criffel pluton	256
4.6	Conclusions.	261
References		267

List of Tables	page
Table 1.1: Ionic potentials, radii and general solubility characteristics of some selected elements (Henderson, 1982; Mason and Moore, 1982; Greenword and Earnshaw, 1984).	10
Table 1.2: Some important radionuclides of high-level waste (Chapman et al., 1984; Chapman and Smellie, 1986).	33
Table 1.3: Modes of typical granite and granodiorite of the Criffel pluton, southwest Scotland (Stephens and Halliday, 1980).	63
Table 1.4: Petrologic range for typical BM-, MB- and B-granite and HB- and CHB-granodiorite of the Criffel pluton, southwest Scotland (Stephens and Halliday, 1980).	64
Table 2.1: Results of alpha spectroscopic analyses of uranyl nitrate and thorium nitrate for preparation of uranium and thorium standards for instrumental neutron activation analysis.	89
Table 2.2: Results of neutron activation analysis of IAEA standard reference material Soil-7 along with certified values (IAEA, 1984).	93
Table 2.3: Results of neutron activation analysis of 'Edinburgh Clay' standard reference material along with recommended values (Topping and MacKenzie, 1988).	94
Table 2.4: Gamma spectroscopic results of standard used in soil samples analysis ^{210}Pb , ^{134}Cs , ^{137}Cs , and ^{226}Ra .	97
Table 2.5: Results of alpha spectroscopic analyses of standard reference sandstone DL-1a along with certified values (CANMET, 1983).	103
Table 2.6: Results of alpha spectroscopic analyses of HB-granodiorite sample from Craignair quarry, southwest Scotland.	104
Table 3.1: Uranium and thorium concentrations and Th/U concentration ratios of granite and granodiorite samples from different zones of the Criffel pluton, southwest Scotland.	113

Table 3.2: Uranium and thorium concentrations and activity ratios for granitic rock samples from different zones of the Criffel pluton, southwest Scotland.	117
Table 3.3: Uranium and thorium concentrations, concentration and activity ratios for sliced samples (increasing distance from fracture face) in rock section CQ1 from Craignair Quarry, Dalbeattie, southwest Scotland.	118
Table 3.4: REE concentrations for sliced samples (increasing distance from fracture face) in rock section CQ1 from Craignair quarry, Dalbeattie, southwest Scotland. The REE normalising values of chondrite (Bynton, 1984) and REE concentrations for sample HB-056 from the Criffel pluton (Stephens et al., 1985) are also indicated.	119
Table 3.5: Uranium and thorium concentrations, concentration and activity ratios for sliced samples (increasing distance from fracture face) in rock section CQ2 from Craignair Quarry, Dalbeattie, southwest Scotland.	120
Table 3.6: REE concentrations for sliced samples (increasing distance from fracture face) in rock section CQ2 from Craignair quarry, Dalbeattie, southwest Scotland. The REE normalising values of chondrite (Bynton, 1984) is also indicated.	121
Table 3.7: Uranium and thorium concentrations, concentration and activity ratios for sliced samples from MB-granite (increasing distance from rock surface), Kinharvie, southwest Scotland.	122
Table 3.8: REE concentrations for sliced samples (increasing distance from rock surface) in granite core from Kinharvie, southwest Scotland. The REE normalising values of chondrite (Bynton, 1984) and REE concentrations for sample MB-272 from the Criffel pluton (Stephens et al., 1985) are also indicated.	123
Table 3.9: Uranium and thorium concentrations, concentration and activity ratios for sliced samples from CHB-granodiorite (increasing distance from rock surface), Clifton, southwest Scotland.	124

Table 3.10: REE concentrations for sliced samples (increasing distance from rock surface) in granodiorite core from Clifton, southwest Scotland. The REE normalising values of chondrite (Bynton, 1984) is also indicated.	125
Table 3.11: Results of radioactivity survey of U and ^{40}K over a uraniferous vein in Beeswing (Map Ref: 885681), Scotland.	126
Table 3.12: Uranium and thorium concentrations, concentration and activity ratios of vein materials from Beeswing, southwest Scotland.	127
Table 3.13: Uranium and thorium concentrations, Th/U concentration ratios and organic content and ^{210}Pb , ^{226}Ra , ^{134}Cs and ^{137}Cs concentrations of soil samples from location A, Beeswing, southwest Scotland.	128
Table 3.14: Uranium and thorium concentrations, Th/U concentration ratios and organic content and ^{210}Pb , ^{226}Ra , ^{134}Cs and ^{137}Cs concentrations of soil samples from location B, Beeswing, southwest Scotland.	130
Table 3.15: Uranium and thorium concentrations, Th/U concentration ratios and organic content and ^{210}Pb , ^{226}Ra , ^{134}Cs and ^{137}Cs concentrations of soil samples from location C, Beeswing, southwest Scotland.	132
Table 3.16: Uranium and thorium concentrations, concentration and activity ratios of water samples around the Criffel pluton, southwest Scotland.	134
Table 4.1: Mean and modal values and ranges of uranium and thorium concentrations and Th/U concentration ratios of granite and granodiorite samples from different zones of the Criffel pluton, southwest Scotland.	137

List of Figures

	page
Figure 1.1: Location of the Criffel pluton study site and simplified geological map of southwest Scotland.	6
Figure 1.2: Distribution of uranyl-hydroxyl and carbonate complexes plotted against pH for $P_{\text{CO}_2} = 10^{-2}$ atm. and a total U concentration of 10^{-8} M (2.38 ppb) at 25°C (from Langmuir, 1978).	12
Figure 1.3: Distribution of uranyl complexes plotted against pH at 25°C for a total U concentration of 10^{-8} M, in the presence of other ions: F = 0.3 ppm, Cl = 10 ppm, $\text{SO}_4 = 100$ ppm, $\text{PO}_4 = 0.1$ ppm, and $\text{SiO}_2 = 30$ ppm (from Tripathi, 1979).	13
Figure 1.4: Eh-pH diagram in the $\text{UO}_2\text{-CO}_2\text{-H}_2\text{O}$ system at 25°C for $P_{\text{CO}_2} = 10^{-2}$ atm. Uraninite, $\text{UO}_2(\text{c})$, solution boundaries are drawn at 10^{-6} M (0.24 ppm) dissolved uranium species. "H & G" denotes the boundary of the uraninite stability field according to Hostetler and Garrels (1962), (from Langmuir, 1978).	14
Figure 1.5: Typical ranges of $^{234}\text{U}/^{238}\text{U}$ activity ratios and uranium concentrations of waters and rocks (from Gascoyne, 1982).	16
Figure 1.6: The natural radioactive decay series.	17
Figure 1.7: Behaviour of model systems which have been disturbed at various past times. Interpretations of isotopic data indicating the order of magnitude of the interval that has elapsed between events (from Schwarcz et al., 1982).	23
Figure 1.8: Regions of uranium deposition and removal in a plot of $^{234}\text{U}/^{238}\text{U}$ versus $^{230}\text{Th}/^{238}\text{U}$ for whole-rock samples based upon Thiel et al. (1983); Alexander et al. (1989); Scott et al. (1992).	24
Figure 1.9: Schematic diagram showing the major steps in the nuclear fuel cycle and main radioactive waste streams generated which require disposal (from NEA/OECD, 1977).	31

Figure 1.10: Toxicity index of high level waste as a function of time (from NAGRA, 1985).	34
Figure 1.11: Potential critical pathways for human exposure to radiation from radionuclides released from an underground radioactive waste repository.	38
Figure 1.12: Schematic illustration of the multi-barrier system for high level waste (from McKinley, 1989; Chapman and McKinley, 1987).	39
Figure 1.13: Schematic diagram of movement of a redox front along a fracture in the near-field and in the vicinity of a radioactive waste repository (after canister failure and radiolysis of water have occurred).	43
Figure 1.14: Schematic representation of the many possible retardation mechanisms that result from interaction between a rock surface and radionuclides in solution, particulate and colloidal form. 'R' represents the radionuclide species (from McKinley, 1989; Chapman and McKinley, 1987).	44
Figure 1.15: Map of the petrological types of the 5 zones in the Criffel pluton. Letters used are: B, biotite; M, muscovite; H, hornblende; C, clinopyroxene (based on Stephens et al., 1985).	62
Figure 2.1: Location of sampling sites, Criffel pluton, southwest Scotland.	70
Figure 2.2: Location map and simplified map of the Criffel igneous rocks, southwest Scotland. Letters used represent: B, biotite; M, muscovite; H, hornblende; C, clinopyroxene (based on Stephens, 1972 and Stephens et al., 1985).	71
Figure 2.3: Schematic diagram showing the Fe^{2+}/Fe^{3+} redox fronts in the Craignair quarry, resulting from the penetration of oxidising groundwater into the fracture system.	74
Figure 2.4: Sketch showing relation of rock sample from location CQ1 in Craignair quarry, to fracture face and subsequent division of sample into 1-cm slices.	76

Figure 2.5: Sketch showing relation of rock sample from location CQ2 in Craignair quarry, to fracture face and subsequent division of sample into 1-cm slices.	77
Figure 2.6: Sketch of rock sample from location CQ4 in Craignair quarry showing V-shaped fractures containing infilling-minerals of iron-manganese oxyhydroxides.	80
Figure 2.7: Schematic diagram of the Beeswing study site showing the locations of uranium veins, surface transect and soil sections.	86
Figure 2.8: A schematic diagram of the VG PlasmaQuad (PQ1) used in this study (VG Isotopes, 1988).	109
Figure 4.1: Average uranium and thorium concentrations of samples from different zones of the Criffel pluton.	139
Figure 4.2: Average U/Th concentration ratios of samples from different zones of the Criffel pluton.	139
Figure 4.3: Histograms of uranium concentrations for samples from (a) BM, (b) MB, (c) B, (d) HB and (e) CHB zones and (f) Criffel pluton (all samples) (c.f. Table 4.1).	141
Figure 4.4: Histograms of thorium concentrations for samples from (a) BM, (b) MB, (c) B, (d) HB and (e) CHB zones and (f) Criffel pluton (all samples) (c.f. Table 4.1).	142
Figure 4.5: Histograms of Th/U concentration ratios for samples from (a) BM, (b) MB, (c) B, (d) HB and (e) CHB zones and (f) Criffel pluton (all samples) (c.f. Table 4.1).	143
Figure 4.6: Uranium versus thorium concentrations for samples from (a) BM, (b) MB, (c) B, (d) HB and (e) CHB zones and (f) Criffel pluton (all samples).	144
Figure 4.7: Distribution of $^{230}\text{Th}/^{234}\text{U}$ activity ratios for samples from different zones of the pluton.	147
Figure 4.8: Plots of $^{234}\text{U}/^{238}\text{U}$ activity ratio versus $^{230}\text{Th}/^{238}\text{U}$ activity ratio for whole-rock samples from (a) BM, (b) MB, (c) B, (d) HB and (e) CHB zones and (f) Criffel pluton (all samples).	149

Figure 4.9: Plot of uranium concentration (ppm) versus distance from the fracture face for rock section CQ1 from Craignair quarry, Dalbeattie.	157
Figure 4.10: Plot of thorium concentration versus distance from the fracture face for rock section CQ1 from Craignair quarry, Dalbeattie.	157
Figure 4.11: Plot of U/Th concentration ratio versus distance from the fracture face for rock section CQ1 from Craignair quarry, Dalbeattie.	158
Figure 4.12: Plot of $^{234}\text{U}/^{238}\text{U}$ activity ratio versus distance from the fracture face for rock section CQ1 from Craignair quarry, Dalbeattie.	158
Figure 4.13: Plot of $^{230}\text{Th}/^{234}\text{U}$ activity ratio versus distance from the fracture face for rock section CQ1 from Craignair quarry, Dalbeattie.	159
Figure 4.14: Plot of $^{234}\text{U}/^{238}\text{U}$ activity ratio versus $^{230}\text{Th}/^{238}\text{U}$ activity ratio for whole-rock samples from rock section CQ1 from Craignair quarry, Dalbeattie.	159
Figure 4.15: Plot of $^{226}\text{Ra}/^{230}\text{Th}$ activity ratio versus distance from the fracture face for rock section CQ1 from Craignair quarry, Dalbeattie.	160
Figure 4.16: Regions of addition and removal of both uranium and radium in a plot of $^{226}\text{Ra}/^{230}\text{Th}$ activity ratio versus $^{230}\text{Th}/^{234}\text{U}$ activity ratio for whole-rock samples.	160
Figure 4.17: Plot of $^{226}\text{Ra}/^{230}\text{Th}$ activity ratio versus $^{230}\text{Th}/^{234}\text{U}$ activity ratio for sample CQ1 from Craignair quarry, Dalbeattie.	161
Figure 4.18: Plots of REE concentrations versus distance from the fracture face in rock section CQ1 from Craignair quarry, Dalbeattie.	170
Figure 4.19: Plot showing the ratio of REE concentrations in (a) 1-2 cm, (b) 3-4 cm and (c) 5-6 cm sections to concentrations in 8-9 cm section in the reduced rock of section CQ1 from Craignair quarry, Dalbeattie.	173

Figure 4.20: Chondrite-normalised REE patterns for sliced samples in rock section CQ1 from Craignair quarry, Dalbeattie.	175
Figure 4.21: Chondrite-normalised REE patterns for sliced sample at 8-9 cm in the reduced rock of the rock section CQ1 from Craignair quarry and sample HB-056 from the Criffel pluton (Stephens et al., 1985).	176
Figure 4.22: Plot of uranium concentration versus distance from the fracture face for rock section CQ2 from Craignair quarry, Dalbeattie.	179
Figure 4.23: Plot of thorium concentration versus distance from the fracture face for rock section CQ2 from Craignair quarry, Dalbeattie.	179
Figure 4.24: Plot of U/Th concentration ratio versus distance from the fracture face for rock section CQ2 from Craignair quarry, Dalbeattie.	180
Figure 4.25: Plot of $^{234}\text{U}/^{238}\text{U}$ activity ratio versus distance from the fracture face for rock section CQ2 from Craignair quarry, Dalbeattie.	180
Figure 4.26: Plot of $^{230}\text{Th}/^{234}\text{U}$ activity ratio versus distance from the fracture face for rock section CQ2 from Craignair quarry, Dalbeattie.	181
Figure 4.27: Plot of $^{234}\text{U}/^{238}\text{U}$ activity ratio versus $^{230}\text{Th}/^{238}\text{U}$ activity ratio for whole-rock samples from rock section CQ2 from Craignair quarry, Dalbeattie.	181
Figure 4.28: Plot of $^{226}\text{Ra}/^{230}\text{Th}$ activity ratio versus distance from the fracture face for rock section CQ2 from Craignair quarry, Dalbeattie.	182
Figure 4.29: Plot of $^{226}\text{Ra}/^{230}\text{Th}$ activity ratio versus $^{230}\text{Th}/^{234}\text{U}$ activity ratio for sample CQ2 from Craignair quarry, Dalbeattie.	182
Figure 4.30: A diagrammatic sketch showing uranium migration and retardation in fractured crystalline rock.	193

Figure 4.31: Plots of REE concentrations versus distance from the fracture face in rock section CQ2 from Craignair quarry, Dalbeattie.	197
Figure 4.32: Chondrite-normalised REE patterns for sliced samples in rock section CQ2 from Craignair quarry, Dalbeattie.	200
Figure 4.33: Plot of uranium concentration as a function of depth (cm from rock surface) for granite core sample from Kinharvie.	204
Figure 4.34: Plot of thorium concentration as a function of depth (cm from rock surface) for granite core sample from Kinharvie.	204
Figure 4.35: Plot of U/Th concentration ratio as a function of depth (cm from rock surface) for granite core sample from Kinharvie.	205
Figure 4.36: Plot of $^{234}\text{U}/^{238}\text{U}$ activity ratio as a function of depth (cm from rock surface) for granite core sample from Kinharvie.	205
Figure 4.37: Plot of $^{230}\text{Th}/^{234}\text{U}$ activity ratio as a function of depth (cm from rock surface) for granite core sample from Kinharvie.	206
Figure 4.38: Plot of apparent percentage uranium loss versus depth for granite core GR from Kinharvie.	206
Figure 4.39: Plot of $^{234}\text{U}/^{238}\text{U}$ activity ratio versus $^{230}\text{Th}/^{238}\text{U}$ activity ratio for whole-rock samples for granite core from Kinharvie.	207
Figure 4.40: Plot of $^{226}\text{Ra}/^{230}\text{Th}$ activity ratio as a function of depth (cm from rock surface) for granite core sample from Kinharvie.	207
Figure 4.41: Plot of $^{226}\text{Ra}/^{230}\text{Th}$ activity ratio versus $^{230}\text{Th}/^{234}\text{U}$ activity ratio from granite core sample GR from Kinharvie.	208
Figure 4.42: Plots of REE concentrations versus distance from the fracture face in granite core GR from Kinharvie, southwest Scotland.	215

Figure 4.43: Plot showing the ratio of REE concentrations in (a) 1-2 cm, (b) 9-10 cm and (c) 13-14 cm sections to concentrations in 17-18 cm section in the reduced rock of the granite core GR from Kinharvie.	218
Figure 4.44: Chondrite-normalised REE patterns for sliced samples in granite core GR from Kinharvie, southwest Scotland.	220
Figure 4.45 Chondrite-normalised REE patterns for sliced sample at 17-18 cm in the reduced rock of the granite core GR from Kinharvie and sample MB-272 from the Criffel pluton (Stephens et al., 1985).	222
Figure 4.46: Plot of uranium concentration as a function of depth (cm from rock surface) for granodiorite core sample GD from Clifton.	224
Figure 4.47: Plot of thorium concentration as a function of depth (cm from rock surface) for granodiorite core sample GD from Clifton.	224
Figure 4.48: Plot of U/Th concentration ratio as a function of depth (cm from rock surface) for granodiorite core sample GD from Clifton.	225
Figure 4.49: Plot of $^{234}\text{U}/^{238}\text{U}$ activity ratio as a function of depth (cm from rock surface) for granodiorite core sample GD from Clifton.	225
Figure 4.50: Plot of $^{230}\text{Th}/^{234}\text{U}$ activity ratio as a function of depth (cm from rock surface) for granodiorite core sample GD from Clifton.	226
Figure 4.51: Plot of apparent percentage uranium excess/deficiency versus depth for granite core GR from Kinharvie.	226
Figure 4.52: Plot of $^{234}\text{U}/^{238}\text{U}$ activity ratio versus $^{230}\text{Th}/^{238}\text{U}$ activity ratio for whole-rock samples of granodiorite core sample GD from Clifton.	227
Figure 4.53: Plot of $^{226}\text{Ra}/^{230}\text{Th}$ activity ratio as a function of depth (cm from rock surface) for granodiorite core sample GD from Clifton.	227

Figure 4.54: A diagrammatic sketch showing a complex series of redox fronts in granodiorite core GD from Clifton, southwest Scotland.	228
Figure 4.55: Plot of $^{226}\text{Ra}/^{230}\text{Th}$ activity ratio versus $^{230}\text{Th}/^{234}\text{U}$ activity ratio from granodiorite core sample GR from Clifton.	229
Figure 4.56: Plots of REE concentrations versus depth from the weathered rock surface in granodiorite core GD from Clifton, southwest Scotland.	235
Figure 4.57: Chondrite-normalised REE patterns for sliced samples in granodiorite core GD from Clifton, southwest Scotland.	238
Figure 4.58: Uranium and ^{40}K count rates over abandoned quarry at Beeswing, southwest Scotland.	241
Figure 4.59: Plots of uranium and thorium concentrations versus depth for soil cores (i) A, (ii) B and (iii) C from Beeswing. Leaching results for samples from top, middle and bottom sections are indicated.	244
Figure 4.60: Plots of U/Th concentration ratio versus depth for soil cores (i) A, (ii) B and (iii) C from Beeswing.	245
Figure 4.61: Sketch showing distribution of uranium in soil along A-C cross-section, Beeswing.	249
Figure 4.62: Plots of ^{226}Ra concentration profiles for soil cores (i) A, (ii) B and (iii) C from Beeswing.	250
Figure 4.63: Plots of ^{210}Pb concentration profiles for soil cores (i) A, (ii) B and (iii) C from Beeswing.	252
Figure 4.64: Plots of ^{134}Cs and ^{137}Cs concentration profiles for soil cores (i) A, (ii) B and (iii) C from Beeswing.	253
Figure 4.65: Uranium and thorium concentrations of river water samples around the Criffel pluton, southwest Scotland.	257
Figure 4.66: U/Th concentration ratio of river water samples around the Criffel pluton, southwest Scotland.	257

List of plates

	page
Plate 2.1: Photograph of the Craginair quarry study site showing the location from which samples were collected.	73
Plate 2.2: Photograph of the Craginair quarry study site showing the location from which sample CQ2 was collected.	73
Plate 2.3: Photograph of sample CQ1 showing the Fe ²⁺ /Fe ³⁺ redox front about 4.0 cm from the fracture face. Sample collected from about 2 m from the surface.	75
Plate 2.4: Photograph of sample CQ3 showing a thin coating of iron-oxyhydroxides along the fractures. Sample collected from about 20 m from the surface.	79
Plate 2.5: Photograph of sample CQ4 showing V-shaped iron-oxyhydroxides infilling fractures. Sample collected from mid level of the Craginair quarry.	79
Plate 2.6: Photograph showing granite core GR from Kinharvie.	82
Plate 2.7: Photograph of granodiorite core GD from Clifton showing complex fracture system.	83
Plate 2.8: Photograph of portable NaI detector used in locating uranium veins at Beeswing.	84
Plate 2.9: Photograph of the Beeswing study site showing location of uranium veins.	84
Plate 4.1: Matched thin-section (a) and fission track image on plastic film (b). Fission track print showing association of uranium with sphene grain.	152
Plate 4.2: Matched thin-section (a) and fission track image on plastic film (b). Fission track print showing association of uranium with obdurate minerals (altered rock sample but showing unaltered intergrowth sphene).	153

- Plate 4.3: Matched thin-section (a) and fission track image on plastic film (b). Fission track print showing association of uranium along the boundary of biotite minerals. 154
- Plate 4.4: Matched thin-section (a) and fission track image on plastic film (b). Fission track print showing association of uranium with infilling fracture minerals, Fe-Mn oxyhydroxides. 163

Acknowledgements

I wish to thank the following people whose assistance to get this thesis moving and keep it on the rails throughout this work is appreciated and hereby acknowledged:

Prof. M.J. Russell and Dr. A. B. MacKenzie who diligently supervised the entire work and for introducing me to the subject and inspiring a sense of appreciation of the challenges and complexities in a natural analogue study. Their constant advice, suggestions, criticisms and encouragement were of immense help.

Dr. G. D. Couples, Dr. R. Jemielita and Dr. P. McDonald for their advice on the fieldwork.

Dr. W. E. Stephens of St. Andrews University for providing me with the archived powdered rock samples from different zones of the Criffel pluton and his helpful discussions.

Dr. A. N. Whitton for reading the manuscript of the early version of Chapters 1 and 2.

Mr. Henderson who kindly gave permission to sample for soils and rocks for analysis from his land in Beeswing.

Mr. Ward of Tarmac Construction Co. for his permission to collect granite samples from the Craignair quarry, Dalbeattie.

The Forestry Commission for allowing access to the forestry properties in Nithsdale and Castle Douglas districts.

SUMMARY

Technicians of the Department of Geology and Applied Geology and the Scottish Universities Research and Reactor Centre, East Kilbride, for their technical assistance. My special thanks to Mr. R. Morrison for his unending help, Mr. D. Maclean for all photographic work, Mr. Kavanagh for his help in the use of computing facilities, Mr. A. Russell for his assistance in collecting soil and water samples and Messrs. J. Thomson, C. Robertson, J. Morrison, R. MacDonald, J. Gallagher, P. Ainsworth, A. Jones, D. Turner, K. Roberts and M. MacLeod for their assistance in the laboratory analyses.

Mrs. T. M. Shimmiel for performing the rare earth elements analyses for rocks and water samples.

The Government of Malaysia for awarding me financial support for my Ph.D. study at the University of Glasgow. Thanks are due to the Public Services Department (Kuala Lumpur) and Malaysian Students' Department (London and Glasgow) for providing the administration facilities. Also, I wish to thank the Director General of the Nuclear Energy Unit, Malaysia for granting me a study leave.

Finally, my family for their patient, encouragement and continual support. We shared many things together including 'burning the midnight oil' in the course of this thesis. To my wife, Haya and my children Faiz and Farid, I wish to thank you, and promise that it will probably be a long time before I may try another venture like this again. Appropriately, this thesis is dedicated to them.

SUMMARY

This thesis describes a study utilising natural decay series radionuclides and rare earth elements in the granitic rocks of the Criffel pluton, southwest Scotland, in an investigation of processes affecting radionuclide transport and retardation in the environment. The work was performed in the context of a natural analogue study of relevance to radioactive waste disposal on the basis that many of the processes which govern the long term performance of a deep geological repository for radioactive waste also take place and can be characterised in nature. Such an analogue study can play an important role in validating the importance of far-field radionuclide retardation mechanisms in the case of radioactive waste disposal in crystalline bedrock where fracture flow will be the dominant mode of radionuclide transport upon failure of the near field barriers.

Natural decay series analyses were performed on the whole rock samples obtained from different zones of the pluton, giving results consistent with the expected geochemical behaviour of these two elements in igneous rock. Thus, uranium was observed to be highly susceptible to oxidation-induced dissolution and is consequently relatively mobile, whereas thorium exhibited an extremely low solubility and is effectively immobile. The study shows that the Criffel pluton has experienced removal of between 20 and 30 percent of the uranium from the uppermost section of the granite, with a removal probability for uranium dissolution of $1.9 \times 10^{-5} \text{ y}^{-1}$. There is no significant 'whole rock' re-deposition of uranium within the pluton. However, it is evident that matrix diffusion, sorption/scavenging by fracture lining minerals and redox front trapping processes are potentially very important for uranium retardation in the pluton.

All samples from the pluton displayed $^{234}\text{U}/^{238}\text{U}$ ratios about unity, whereas $^{230}\text{Th}/^{234}\text{U}$ ratios were greater than unity. This suggests that the pluton has experienced a recent and rapid removal of uranium from the uppermost section of the granite (i.e. since the end of the last glaciation), whereas thorium has remained relatively immobile. The activity ratio data of a representative granite core in the pluton indicate that the average rate of downwards movement of the weathering front is about 12 m in 10^6 y. This observation suggests that the postulated maximum rate of far-field movement of a repository-related redox front of about 50 m in 10^6 y is a realistic value for use in models.

Concentrations and activity ratios of natural decay series radionuclides were studied in two rock sections that traversed redox fronts and intersecting water-bearing fractures in Craignair quarry in the pluton. Investigation of natural redox fronts in the quarry revealed that both redox sensitive (U) and non-redox sensitive (Ra and REE) elements are subjected to dissolution and re-deposition processes in the vicinity of the front. Uranium concentrations are depleted in the oxidised rock, whereas slight enrichments are observed in the reduced rock close to the redox front. There is also some uranium re-deposition on the oxidised side of the front which would not be expected from a simple thermodynamic viewpoint. The $^{226}\text{Ra}/^{230}\text{Th}$ ratios displayed disequilibrium, reaching a value above unity on the oxidised side of the front but dropping to less than unity in the reduced rock. This situation indicates that radium is readily removed from the reduced rock but is re-deposited in the oxidised rock. Taken together, the radium, REE and uranium distributions indicate that both advection

and diffusion processes control the distribution of radionuclides about the front.

Fission track studies revealed that uranium is associated with fracture-infilling minerals, suggesting uptake by iron-manganese oxyhydroxides, clays and carbonate minerals during fracture flow. Also, uranium mobility apparent in rocks adjacent to fractures implied a depth of matrix diffusion of at least 7 cm. It was also observed that uranium concentrations in fracture-lining minerals increased with depth, suggesting that uptake of uranium by such minerals is not a permanent process.

The rare earth element data reveal a general loss of these elements from the rock section close to the front, but with some re-deposition in the oxidised rock, in association with Fe-Mn oxyhydroxides. This phenomenon indicates that both diffusion and scavenging processes probably control the re-distribution of rare earth elements about the front.

Analyses of uranium and thorium clearly show evidence that a uranium vein at Beeswing on the northern edge of the pluton has been subject to two phases of uranium distribution i.e. (i) long - term leaching with preferential loss of ^{234}U relative to ^{238}U ; and (ii) recent, rapid loss of uranium with a probability of dissolution of uranium from the vein of about $5.2 \times 10^{-5} \text{ y}^{-1}$ (upper limit). Uranium and radium were again observed to be relatively mobile, whereas thorium was found to be effectively immobile. Caesium (^{134}Cs - attributed to Chernobyl fallout; ^{137}Cs - from Chernobyl accident and nuclear weapons testing), is relatively mobile in the soil, while the mobility of lead is extremely low, probably because of strong retention properties of

soil organic matter, clay minerals and iron-manganese sesquioxides. This observation clearly has implications for radioactive waste disposal in the context of far-field movement of soluble nuclides, and highlights the importance of characterising radionuclide retardation by processes related to groundwater flow in soils (i.e. final component of far-field barrier) eg. uptake of radionuclides by organic matter, clay minerals and iron-manganese sesquioxides.

Uranium analyses performed on river waters draining from the pluton clearly show that uranium concentrations in water are about three orders of magnitude less than that of the predicted value from models. This observation thus suggests that the models are conservative.

In conclusion, the study of natural decay series radionuclides and rare earth elements from the Craignair quarry in the Criffel pluton revealed that three distinct retardation processes affect these elements during groundwater transport in the environment, namely scavenging by Fe-Mn oxyhydroxides, redox fronts trapping and matrix diffusion. The study of natural decay series radionuclides and radiocaesium isotopes from Beeswing revealed that these elements are removed from groundwater by complexing with soil organic matter and scavenging by Fe-Mn sesquioxides or sulphides. In the context of radioactive waste disposal, operation of these processes would be of significance in both far-field and near-field transport and retardation of radionuclides released from a repository. The study revealed that the very near surface rocks (weathered zone) and overlying soil act as a potentially important site of deposition and as such constitute the final barrier in the multi-barrier systems for radioactive waste disposal.

DECLARATION

The material presented in this thesis is the result of independent research by the author, undertaken between January 1990 and January 1993, at the Department of Geology and Applied Geology, University of Glasgow and the Scottish Universities Research and Reactor Centre, East Kilbride. Any published or unpublished results of other workers have been given full acknowledgement in the text.

Daud Bin Mohamad

CHAPTER 1

INTRODUCTION

1.1 Overview

This thesis describes a study of natural decay series radionuclides and rare earth elements in the Criffel pluton, southwest Scotland, in the context of a natural analogue study of processes of relevance to radioactive waste disposal. Particular emphasis is placed upon geochemical aspects of migration and retardation processes affecting these species within the bedrock environment. The geochemical processes studied are of relevance to radioactive waste disposal since they are comparable to those that will influence the migration of radionuclides after escape from a repository.

Safe disposal of radioactive waste presents a major challenge to the nuclear power and other industries (eg. phosphate production and rare earth element extraction) and such waste must be managed in a way that will not endanger public health and safety or environmental quality. By far the largest quantity of radioactive waste is produced from the spent fuel rods of nuclear reactors, which may either be disposed of directly or after re-processing to recover unused fissile material. Other industries, however, do produce significant quantities of radioactive waste as a consequence of the concentration of radionuclides during industrial processing. In Malaysia, for instance, thorium wastes are produced as a result of the extraction of rare earth elements from monazite and xenotime minerals which contain substantial amounts of natural uranium and thorium. Such operations result in the production of thorium hydroxide cake (about 2000

tonnes per year) containing thorium (about 14% ThO_2) and a small quantity of uranium (IAEA, 1988). These thorium hydroxide cakes are, at present, stored in drums in a temporary facility, pending a final decision as to whether to continue to store the waste or dispose of it.

Effluent control technologies are employed in nuclear power production and industrial processes to limit the release of radionuclides to the environment, but residual radioactive waste materials from such operations must be controlled for the time within which they could present a hazard. Consequently the nuclear industries in many countries are planning to dispose of high level, long-lived radioactive waste by deep burial in underground repositories using a multiple barrier system to retain the radionuclides in the repository or surrounding rock for a suitable time to allow their decay to non hazardous levels. In such a scheme, the waste, either in the form of unprocessed, spent fuel rods (pellets of UO_2 in zircaloy) or as a borosilicate glass containing reprocessing waste, will be encapsulated in a canister (eg. steel or copper), surrounded by a buffer material (eg. bentonite-clay) and concrete, and placed in a stable part of the geosphere (eg. crystalline rocks) at a depth of 1 km or more. The area hosting such a repository should be one where tectonic disturbance, volcanic activity and deep erosion are unlikely; with rocks which have a low permeability and a high capacity for sorbing dissolved materials and; where topography is suitable for a large engineering operation.

The principal aim of a repository is to isolate the radioactive waste for a sufficiently long time to ensure that in any eventual migration of radionuclides to the biosphere, the concentration levels will be low enough to ensure that there is no unacceptable level of risk to public health and safety or environmental quality (NAGRA, 1985). In all geological disposal

schemes, however, it must be assumed that groundwater will eventually come in contact with the waste and dissolve radionuclides, resulting in their release to the surrounding rock, where many complex variables may affect their migration or retardation. The assessment of the optimum design and overall long-term safety of a repository involves the evaluation of potential mechanisms of failure of the engineered barriers, migration and retardation processes influencing radionuclides in the geosphere and possible disruption scenarios. Such assessments involve the use of complex conceptual and mathematical models to predict these various aspects of repository performance and safety, and large data bases, incorporating theoretical considerations and information from laboratory and field experiments, are required for this purpose. One of the major limitations in such assessments is that the time period over which laboratory experiments can be performed to produce the necessary data is extremely short compared with the time period required for isolation of the waste to ensure its safe disposal. Moreover, the relatively simple conditions that apply to a laboratory experiment are often inadequate to account for the complex physical, chemical and biological conditions that exist in the natural environment.

Many of the processes and phenomena that govern the long-term performance of a deep geological repository for radioactive waste also take place in natural geological systems, and the use of 'natural analogues' has become an important aspect of repository performance and safety assessments. In particular, such studies can give assurance that the most important processes, phenomena and scenarios have been included in the models and can be used to test the models under realistically complex conditions over 'geological' timescales (Chapman et al., 1984). Such analogue studies can provide direct information on the cumulative effects

of transport and retardation processes over timescales commensurate with the half-lives of the radionuclides of concern in waste disposal.

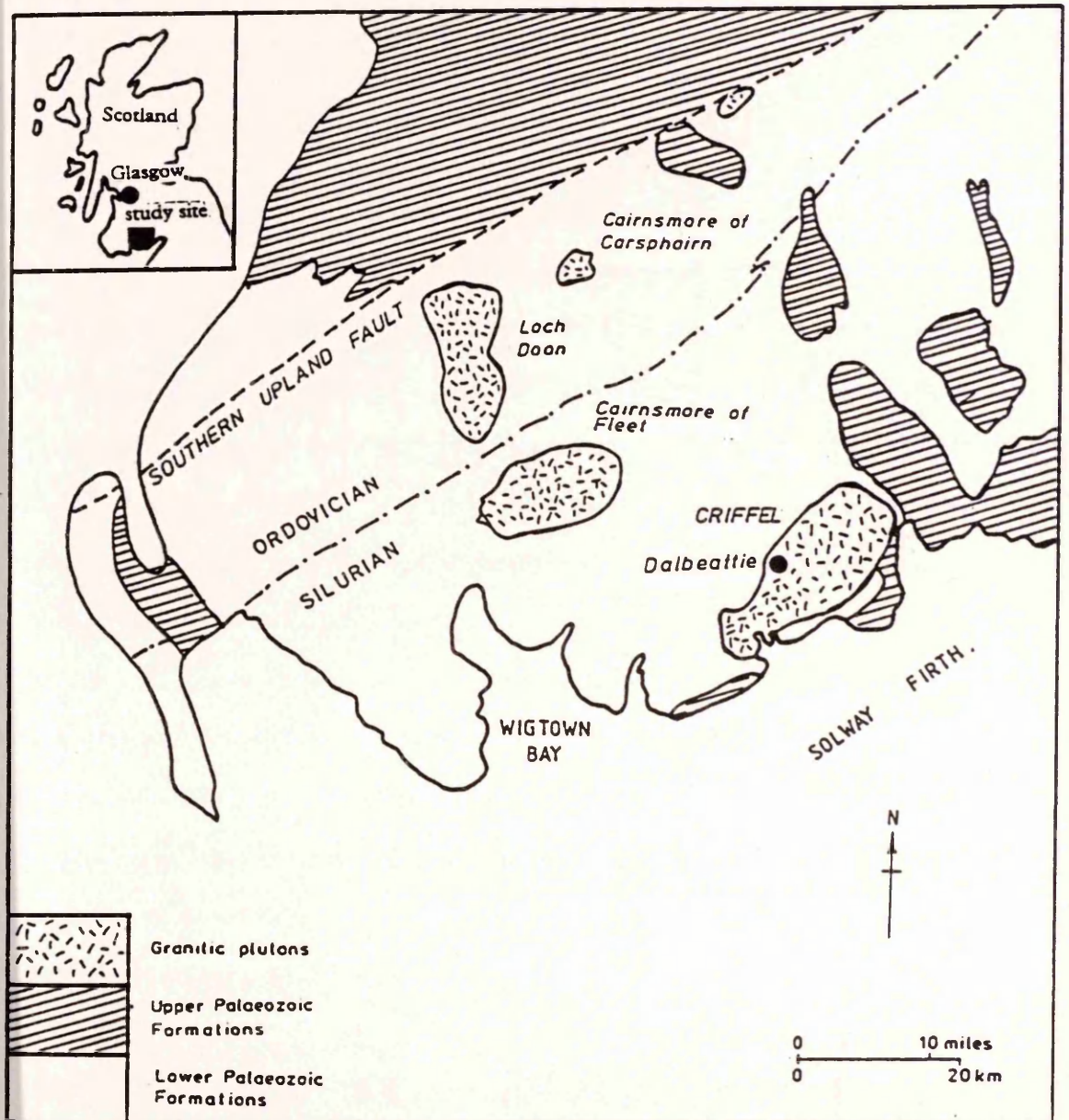
For some of the nuclides in high level waste the obvious analogues are simply non-radioactive isotopes of the same elements, eg. strontium, caesium, iodine and rare earth elements. Technetium and the transuranic elements (notably neptunium, plutonium and americium), however, have no non-radioactive isotopes in nature, therefore suitable chemical analogues are required which exhibit similar physico-chemical properties. For instance, uranium, thorium and rare earth elements can be taken as analogues for plutonium and americium. Plutonium occurs in three valence states, Pu^{5+} , Pu^{4+} and Pu^{3+} , and suitable analogues for these states are U^{6+} , Th^{4+} and rare earth elements (eg. Nd^{3+}) respectively. Similarly Nd^{3+} is an acceptable analogue for Am^{3+} (Chapman and Smellie, 1986). The natural decay series radionuclides are also of direct relevance to radioactive waste disposal since they are actually present in, or will grow in to, high level waste in a repository.

Investigation of radioactive disequilibrium in the natural decay series provides a powerful method for investigating the mechanisms and rates of migration and retardation of these natural radionuclides (eg. fracture flow, sorption and redox front processes) on a geological time scale (Smellie et al., 1986; Come and Chapman, 1987; Alexander et al., 1988; MacKenzie et al., 1991). In addition evidence of the migration or retardation of radionuclides in natural geological systems can be obtained over distances of centimetres to hundreds of metres, and time periods from days up to about 1×10^6 y. Assessment of the radionuclide retention capability of a repository and the surrounding rock is difficult because it depends on complex and interdependent processes which must be envisaged on large scales (> 1

km³), long times (10^5 to 10^7 y), and because some nuclides such as the transuranium elements are normally absent in significant quantities in nature. Such assessment can be satisfactorily tackled by combining laboratory and field experiments, and modelling of natural analogues. Natural analogues are the only means by which very slow mechanisms can be identified and by which long-term predictions of models can be tested (Chapman et al., 1984; Smellie et al., 1986; McKinley, 1989; MacKenzie et al., 1991).

The present study involved an investigation of natural decay series radionuclide disequilibrium, and rare earth element behaviour in the granitic rock of the Criffel pluton in southwest Scotland (Figure 1.1). The results are used in the investigation of processes involved in elemental migration/retardation in the rock. As part of this work detailed studies were carried out on the distribution of radionuclides and rare earth elements at redox fronts associated with water-bearing fracture systems, and of weathered/unweathered granite and granodiorite core samples. Also fission track analysis was carried out to investigate the spatial distribution of uranium and its mode of occurrence in relation to redox fronts and fracture-lining minerals in the pluton. A further aspect of the work involved the investigation of uranium dispersion in the vicinity of a pitchblende vein in an attempt to provide an improved understanding of migration/retardation of uranium in the soils of the study site.

Figure 1.1: Location of the Criffel pluton study site and simplified geological map of southwest Scotland.



1.2 The geochemistry of uranium and thorium

A brief review of uranium and thorium geochemistry is presented in this section since it is of fundamental importance in understanding geosphere transport and retardation of these species as well as natural decay series disequilibrium.

Uranium and thorium are primordial radionuclides which are distributed throughout the Earth and oceans as a function of their geochemical properties. They are members of the actinide series of elements and both exist in the 4+ oxidation state in unweathered igneous rocks and minerals. Their ions have similar radii ($U^{4+} = 1.00\text{\AA}$; $Th^{4+} = 1.05\text{\AA}$) (Katz et al., 1986), and they can consequently substitute extensively for each other in minerals, which explains their geochemical coherence (Rogers and Adams, 1970).

Uranium can show changes from one oxidation state to another under environmental conditions. The possible valence states of uranium are 3+, 4+, 5+ and 6+ (Rogers and Adams, 1970), but only the 4+ and 6+ states are of geological and environmental importance. The transition from the 4+ to 6+ oxidation state occurs at a redox potential within the normal range encountered in geological environments:



$$E_0 = 0.27 \text{ volts (Langmuir, 1978)}$$

Under oxidising conditions uranium can therefore be oxidised to the 6+ oxidation state to form the soluble uranyl ion $(UO_2)^{2+}$ which plays an important role in uranium transport during weathering. Uranium is therefore a mobile element under oxidising conditions, and can be separated

from thorium which exists only in the 4+ state and has extremely low solubility in most natural waters.

Uranium and thorium are relatively highly concentrated in igneous rocks and, in particular, silicic rocks such as granite in which typical concentrations of 1 to 10 ppm uranium and 5 to 40 ppm thorium are observed. These concentrations are up to two orders of magnitude higher than those of basaltic rocks. Although uranium and thorium concentrations increase from basaltic rocks to granitic rocks, the Th/U concentration ratios remain virtually constant, ranging from 3 to 6. The constancy of this value among many different igneous rock types indicates the general lack of fractionation of the two elements during magmatic processes.

In the course of partial melting and fractional crystallisation of magma, uranium and thorium are concentrated in the liquid phase and become incorporated into late crystallising magmas and residual solutions because their large ionic radii preclude their incorporation in early crystallising silicates such as olivine, pyroxenes and plagioclase. It is for this reason, that igneous rocks of granitic composition are strongly enriched in uranium and thorium compared to rocks of basaltic or ultramafic composition.

Uranium and thorium are distributed in three ways in igneous rocks: (i) by direct cation substitution in the silicate lattice of the major rock-forming minerals which have uniformly low uranium and thorium concentrations, of the order of a few ppm or less, (ii) as minor or major components of accessory minerals such as apatite, monazite and xenotime (phosphates); uraninite and thorianite (oxides); zircon, thorite and allanite (silicates); and sphene (titano-silicate), and (iii) by adsorption on the surfaces of lattice

defects or crystal and grain boundaries (Gascoyne, 1982; Faure, 1986).

Uranium and thorium concentrations vary markedly between different sedimentary rocks depending upon the geochemical conditions in the depositional environment. The Th/U concentration ratios of sedimentary rocks are similar to those of igneous rocks, with the exception that sedimentary carbonates have a Th/U concentration ratio of about 0.8 (Faure, 1986). The uranium concentration of carbonate rocks of about 2 ppm results from the fact that uranium occurs in the ocean as the soluble uranyl ion which co-precipitates with calcium carbonate, while thorium is almost exclusively transported bound in insoluble, obdurate detrital minerals or adsorbed on the surface of clay minerals. Uranium is found to be strongly enriched in certain organic sediments, particularly those formed from humic substances, such as coal (10 - 600 ppm).

The primary source of uranium and thorium in the geochemical cycle is the weathering of felsic igneous rocks where they are present almost entirely as U^{4+} and Th^{4+} . During surficial chemical weathering processes uranium is oxidised to soluble uranyl ions, $(UO_2)^{2+}$, whereas thorium exists only in the 4+ state, in compounds generally insoluble in water. The degree of their solubility in a given environment is dependent on a number of geochemical variables, especially the Eh-pH conditions, the availability and concentration of complexing ions, and temperature and pressure (Mason and Moore, 1982). The dominant factor giving rise to the difference in solubility between uranium and thorium however, is the difference in their values of ionic potential, which is defined as the ratio of ionic charge to ionic radius (\AA) and which controls the degree of hydration, hydrolysis, complex formation and particle or surface reactivity of an ion in solution. Table 1.1 shows ionic radii, ionic potentials and general solubility

Table 1.1. Ionic potentials, radii and general solubility characteristics of some selected elements (Henderson, 1982; Mason and Moore, 1982; Greenwood and Earnshaw, 1984).

Ion	Radius (Å)	Ionic Potential	General Solubility Characteristics
Cs ⁺	1.67	0.60	
Na ⁺	1.02	0.98	
Ra ²⁺	1.48	1.35	
Sr ²⁺	1.12	1.69	Generally soluble
Eu ²⁺	1.17	1.71	
Mn ²⁺	0.83	2.41	
Fe ²⁺	0.78	2.56	-----
Co ²⁺	0.745	2.68	
La ³⁺	1.14	2.60	
Ac ³⁺	1.12	2.68	
Zn ²⁺	0.740	2.70	
Ni ²⁺	0.690	2.90	
Ce ³⁺	1.01	2.97	
Nd ³⁺	0.987	3.00	
Sm ³⁺	1.04	3.00	
Am ³⁺	0.98	3.06	
Eu ³⁺	0.947	3.17	
Yb ³⁺	0.86	3.50	
Lu ³⁺	0.85	3.50	
Sb ³⁺	0.76	3.95	Generally insoluble
Th ⁴⁺	0.94	4.25	
Po ⁴⁺	0.94	4.25	
Ru ³⁺	0.68	4.41	
U ⁴⁺	0.89	4.49	
Ce ⁴⁺	0.87	4.60	
Pu ⁴⁺	0.86	4.65	
Fe ³⁺	0.645	4.65	
Co ³⁺	0.61	4.92	
Pb ⁴⁺	0.775	5.16	
Zr ⁴⁺	0.72	5.55	-----
Tc ⁴⁺	0.645	6.20	
Pa ⁵⁺	0.78	6.41	Intermediate solubility
Np ⁵⁺	0.75	6.66	
Pu ⁵⁺	0.74	6.76	
Mn ⁴⁺	0.53	7.55	-----
U ⁶⁺	0.73	8.22	Soluble
Pu ⁶⁺	0.71	8.45	

characteristics for uranium, thorium and other elements of interest in this study.

In oxidising groundwater systems uranium transport occurs mainly as U^{6+} species, commonly as $(UO_2)^{2+}$ in the form of highly stable complexes with ligands such as fluoride $(UO_2F)^+$, phosphate $[UO_2(HPO_4)]^{2-}$, hydroxyl $[UO_2(OH)]^+$ and $[(UO_2)_3(OH)_5]^+$, silicate $[UO_2SiO_3(OH)_3]^+$, sulphate $[(UO_2)(SO_4)]^0$, carbonates $[(UO_2)(CO_3)]^0$; $[(UO_2)(CO_3)_2]^{2-}$; $[(UO_2)(CO_3)_3]^{4-}$ and organic complexes (Garrels and Christ, 1965; Langmuir, 1978). The most significant uranyl complexes in natural waters between pH 4 to 10 are uranyl carbonates and uranyl phosphates (Langmuir, 1978; Tripathi, 1979), as indicated in Figures 1.2, 1.3 and 1.4. Furthermore, Hostetler and Garrels (1962) have shown that uranyl carbonate complexes exhibit considerable stability even under slightly reducing conditions. The formation of such complexes greatly increases the solubility and mobility of uranium in surface and ground waters.

Conversely, in reducing groundwater environments U^{6+} is reduced to U^{4+} and precipitates as uraninite (UO_2) and coffinite $[U(SiO_4)]$ (Langmuir, 1978; Boyle, 1982; Ivanovich and Harmon, 1982), as in sedimentary uranium deposits (Hostetler and Garrels, 1962; Nash et al., 1981; Brookins, 1984).



Moreover, uranium in solution can also be removed by sorptive materials such as zeolite, clay, limonite and organic matter (Dement'yev and Syromyatnikov, 1968; Doi et al., 1975; Andreyev and Chuvachenke, 1964; Milodowski et al., 1990; Lovely et al., 1991). As a result of precipitation and sorption processes, the uranium content of natural waters may decrease

Figure 1.2: Distribution of uranyl-hydroxyl and carbonate complexes plotted against pH for $P_{\text{CO}_2} = 10^{-2}$ atm. and a total U concentration of 10^{-8} M (2.38 ppb) at 25°C (from Langmuir, 1978).

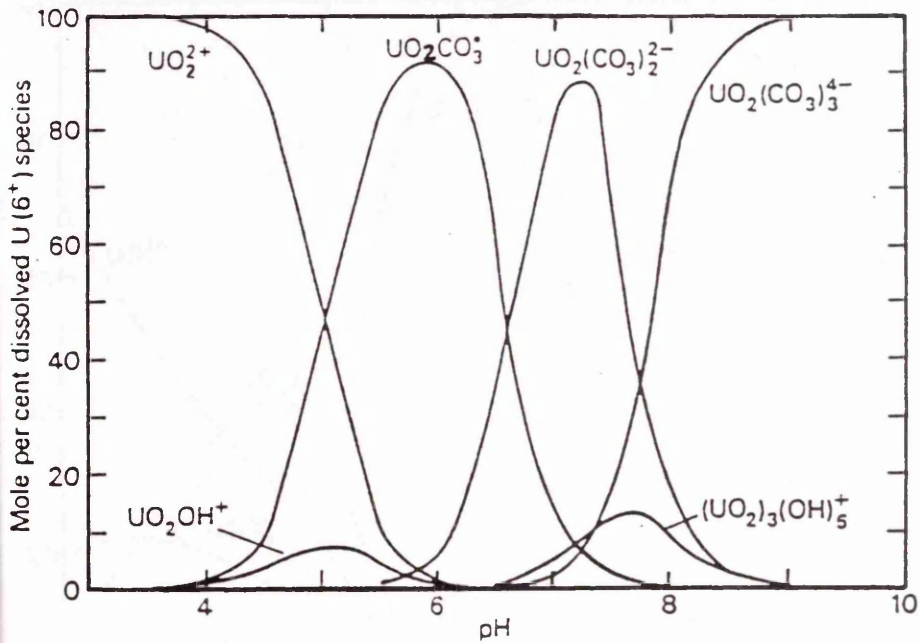


Figure 1.3: Distribution of uranyl complexes plotted against pH at 25°C for a total U concentration of 10^{-8} M, in the presence of other ions: F = 0.3 ppm, Cl = 10 ppm, SO_4 = 100 ppm, PO_4 = 0.1 ppm, and SiO_2 = 30 ppm (from Tripathi, 1979).

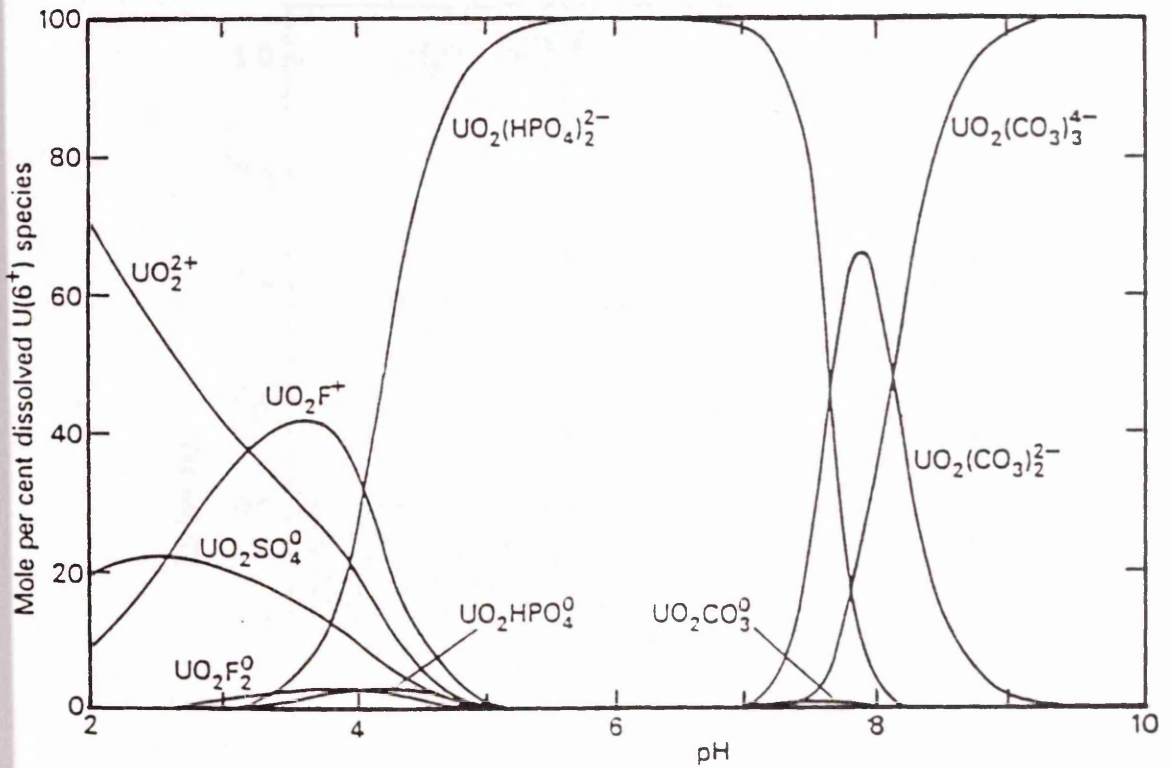
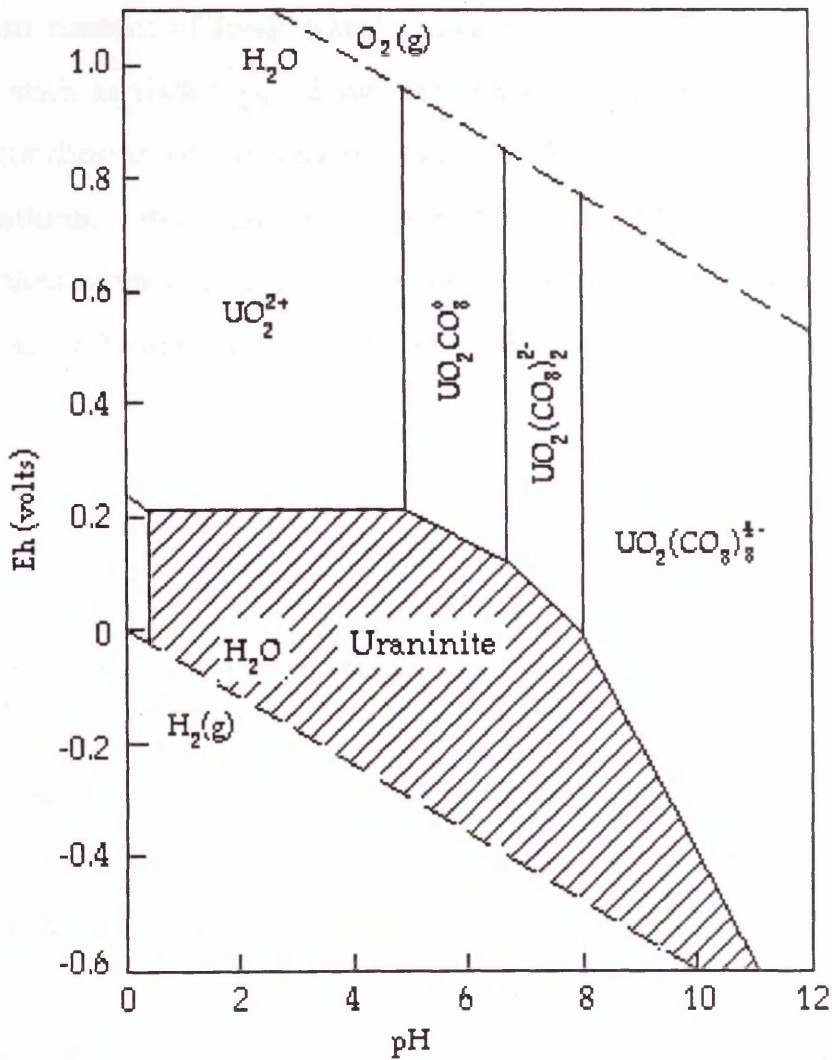


Figure 1.4: Eh-pH diagram in the UO_2 - CO_2 - H_2O system at 25°C for $P_{\text{CO}_2} = 10^{-2}$ atm. Uraninite, UO_2 (c), solution boundaries are drawn at 10^{-6} M (0.24 ppm) dissolved uranium species (Langmuir, 1978).



drastically in response to varying geochemical conditions.

Ranges of uranium concentrations in natural waters of the world have been tabulated by Rogers and Adams (1970). In seawaters, the uranium concentration is almost constant, at 3.2 ppb (Henderson, 1982). However, the uranium content of fresh water is highly variable, depending on local conditions such as rock types, flow rate of water, evaporation and physico-chemical conditions of the environment (Barker and Scott, 1958; Cohen, 1964; Lopatkina, 1964; Langmuir, 1978; Mohamad, 1980; Dominik et al., 1991). Typical ranges of uranium concentrations in rocks and waters in the hydrological cycle are shown in Figure 1.5 (Gascoyne, 1982; Henderson, 1982).

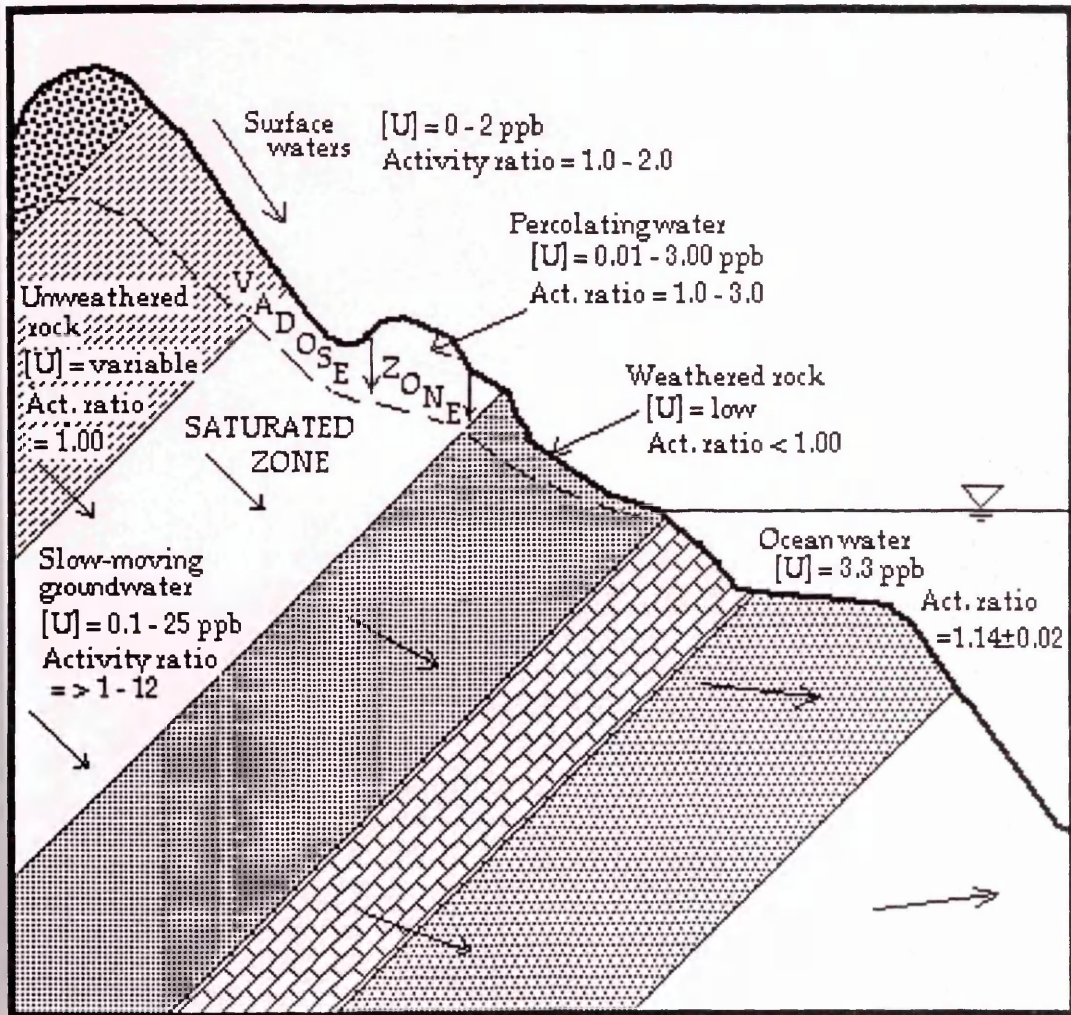
1.3 The Natural Radioactive Decay Series

^{238}U , ^{235}U and ^{232}Th are the parents of the three natural radioactive decay series shown in Figure 1.6. Investigation of the systematics of radioactive disequilibrium within these decay chains provides a powerful method of defining the rates and mechanisms of natural environmental processes. Before describing such studies it is helpful to outline the radioactive decay and growth processes which apply to disequilibrium situations affecting the decay series nuclides in natural systems. The basic equation describing the rate of decay of an unsupported radionuclide is:

$$A_t = A_0 e^{-\lambda t} \quad \dots\dots\dots 1.1$$

where, A_0 is the activity at time zero, A_t is the activity at time t and λ is the decay constant (such that $\lambda = \ln 2 / t_{1/2}$).

Figure 1.5: Typical ranges of $^{234}\text{U}/^{238}\text{U}$ activity ratios and uranium concentrations of waters and rocks (from Gascoyne, 1982).



In the case of a pure fraction of a parent nuclide X that decays to form a daughter nuclide Y, if no atoms of Y are present initially, and closed system conditions apply, the activity of Y at time t is given by:

$$(A_Y)_t = \frac{\lambda_Y}{\lambda_Y - \lambda_X} (A_X)_0 (e^{-\lambda_X t} - e^{-\lambda_Y t}) \quad \dots\dots\dots 1.2$$

In the case of more than two radioactive products in one chain, the solution is given by the Bateman equation (Friedlander et al., 1981).

If $(t_{1/2})_X$ is much greater than $(t_{1/2})_Y$ then λ_X will be much smaller than λ_Y therefore,

$$\lambda_Y - \lambda_X \approx \lambda_Y$$

and $e^{-\lambda_X t} \approx 1$, and for values of t small relative to $(t_{1/2})_X$ A_X will be effectively constant.

Thus, equation 1.2 reduces to:

$$(A_Y)_t = A_X(1 - e^{-\lambda_Y t}) \quad \dots\dots\dots 1.3$$

As t becomes large relative to $(t_{1/2})_X$ the system will come to a condition of radioactive equilibrium, known as secular equilibrium, in which the rate of decay of the daughter is equal to that of its parent:

$$A_Y = A_X \quad \dots\dots\dots 1.4$$

If the half life of the parent radionuclide is only slightly greater than that of

its daughter (i.e. λ_x is slightly less than λ_y), the approximations used above for secular equilibrium do not apply, and as t becomes large relative to $(t_{1/2})_y$ a state of transient equilibrium is reached in which

$$\frac{A_y}{A_x} = \frac{\lambda_y}{\lambda_y - \lambda_x} \dots\dots\dots 15$$

In a geological system which has remained closed for at least 10^6 y, secular equilibrium will be established in the three decay series and the specific activity (Bqkg^{-1}) of all daughter nuclides will be equal to that of the parent member of the chain. Thus, the activity ratio of parent/daughter pairs (eg. $^{234}\text{U}/^{238}\text{U}$, $^{230}\text{Th}/^{234}\text{U}$, $^{226}\text{Ra}/^{230}\text{Th}$) will be unity. Thus we may expect that such equilibrium should obtain in the unweathered rocks of the Criffel pluton, the focus of the present study, which was emplaced $397 \pm 2 \times 10^6$ y ago. Any disequilibrium of natural decay series parent/daughter pairs found here would therefore indicate that rock-water interaction has taken place within the last 1×10^6 y. In contrast, in open systems that are exposed to weathering and groundwater circulation, separation of parent and daughter members in the decay chains can occur by dissolution of soluble nuclides in groundwater. The differences in chemical and physical properties of the various descendants of ^{238}U , ^{235}U and ^{232}Th in the natural decay series (Figure 1.6) give rise to differences in their solubilities; pronounced radioactive disequilibria are consequently observed in natural waters. Uranium (6+), radium and radon are generally soluble, whereas the other decay chain nuclides are highly insoluble. For example, ^{230}Th is much less soluble in normal, neutral groundwaters than is its parent ^{234}U . If the rock is fractured, as in granitic rocks, and groundwater percolates through it, uranium will tend to be preferentially leached from the rock,

with the result that the $^{230}\text{Th}/^{234}\text{U}$ activity ratio will increase above the equilibrium value of unity ($^{230}\text{Th}/^{234}\text{U} > 1$). If the groundwater then encounters varying geochemical conditions (eg. reducing zone) along its flow path, re-deposition of the uranium can occur, resulting in a $^{230}\text{Th}/^{234}\text{U}$ activity ratio in the precipitate below its equilibrium value of unity. Such a $^{230}\text{Th}/^{234}\text{U}$ activity ratio can thus be taken to indicate recent deposition of uranium in a rock. Radioactive disequilibrium in the natural decay series can be used to investigate natural processes such as migration/retardation of nuclides in a bedrock environment. Other established applications of the natural decay series radionuclides include geochronological studies, uranium prospecting techniques, hydrological investigations and marine chemistry studies (Ivanovich and Harmon, 1982; Faure, 1986). These applications lie outside the scope of the present study.

During chemical weathering relatively large scale fractionation of the isotopes ^{238}U and ^{234}U can occur as a result of preferential leaching into solution of ^{234}U relative to ^{238}U . Two mechanisms are assumed to be involved in the enhancement of the $^{234}\text{U}/^{238}\text{U}$ activity ratio in the aqueous phase: (i) direct alpha-recoil of ^{234}Th across the solid/liquid interface when ^{238}U decays close to the surface of a mineral and (ii) preferential leaching of minerals along alpha particle damage tracks produced by the decay of ^{238}U (Fleischer and Raabe, 1978; Fleischer, 1982a; 1982b). Consequently the $^{234}\text{U}/^{238}\text{U}$ activity ratio of natural waters and of secondary uranium-bearing minerals precipitated less than 10^6 y ago is generally greater than unity, whereas that of weathered rocks is generally less than unity (Chalov, 1959; Chalov et al., 1964; Kigoshi, 1971; Cherdyntsev, 1971; Kobashi et al., 1979; Gascoyne, 1982). $^{234}\text{U}/^{238}\text{U}$ activity ratios in groundwater have been observed to vary from 1 to about 10

(Osmond and Cowart, 1976), and the corresponding range in river waters is between 1 and 2 (Thurber, 1965; Cherdyntsev, 1971). Ocean water has a fairly constant $^{234}\text{U}/^{238}\text{U}$ activity ratio of about 1.14 (Thurber, 1962). Typical ranges of $^{234}\text{U}/^{238}\text{U}$ activity ratios of the hydrological cycle are shown in Figure 1.5 (Gascoyne, 1982).

The parents of the two uranium decay series ^{238}U and ^{235}U are chemically equivalent and do not undergo fractionation in normal geochemical processes. Their isotopic abundance ratio ($^{238}\text{U}/^{235}\text{U}$) in naturally occurring minerals is constant at an atomic ratio of 137.5 ± 0.5 , the only known exception to this being in the uranium deposits of Precambrian age at Oklo in Gabon, Africa (IAEA, 1978). The uranium deposits here are significantly depleted in ^{235}U because this isotope was consumed by neutron-induced fission when the deposits became natural fission reactors about 1.8×10^9 y ago (Lancelot et al., 1975; Kuroda, 1982). The isotopic abundance of ^{235}U in the ore mined at Oklo is as low as 0.3% compared to the 0.72% in normal uranium ores or minerals.

Detection of disequilibrium between any parent-daughter nuclide pair in a rock not only shows that migration of one of the nuclides has occurred (and therefore indicates the physical and chemical conditions in the rock) but can also indicate the time interval over which this migration has taken place. For instance, disequilibrium between ^{238}U and ^{234}U indicates differential migration of these isotopes within the last 10^6 y. Any migration prior to this would not be observed today because radioactive equilibrium would have been re-attained. In addition, other daughter-parent activity ratios can be applied to different timescales, eg. $^{230}\text{Th}/^{234}\text{U}$ can show migration within the last 3.5×10^5 y and $^{226}\text{Ra}/^{230}\text{Th}$ within the last 8.0×10^3 y (five half-lives of the daughter nuclide). Schwarcz et al. (1982) have presented qualitative

interpretations of natural decay series disequilibrium data, indicating the order of magnitude of the interval that has elapsed between events based upon the departure of the activity ratio from unity for the pairs $^{234}\text{U}/^{238}\text{U}$, $^{230}\text{Th}/^{234}\text{U}$ and $^{226}\text{Ra}/^{230}\text{Th}$ (Figure 1.7). A highly convenient method of presentation of natural decay series analytical data for rock samples is in the form of a graph plotting one radionuclide activity ratio against another. For example, Latham and Schwarcz (1987a, b, c) have utilised plots of $^{234}\text{U}/^{238}\text{U}$ against $^{230}\text{Th}/^{234}\text{U}$ and $^{226}\text{Ra}/^{230}\text{Th}$ against $^{230}\text{Th}/^{234}\text{U}$ to illustrate the effects of various removal and deposition processes affecting uranium and radium in rocks.

Thiel et al. (1983) demonstrated that different types of uranium mobilisation or deposition can be mathematically modelled using a linear plot of the $^{234}\text{U}/^{238}\text{U}$ activity ratio versus the $^{230}\text{Th}/^{238}\text{U}$ activity ratio for rock samples. This method has been adopted and extended by Scott et al. (1992). In such an approach, it is assumed that the rock initially exists with the natural decay series radionuclides in a state of secular equilibrium, and that its equilibrium is then disturbed by the addition of uranium from groundwater, or removal of uranium to groundwater, either in a single event or in a continuous process. Thorium is assumed to be highly insoluble. The $^{234}\text{U}/^{238}\text{U}$ versus $^{230}\text{Th}/^{238}\text{U}$ plot can be divided into various sectors representing the effects of different uranium deposition or removal processes as shown in Figure 1.8. The different sectors of the graph correspond to (i) a uranium removal area (A) involving either continuous or sudden removal of uranium, and a uranium removal area (A') which can only be attained by samples which have undergone removal of uranium in a single rapid event and cannot be attained by samples subject to continuous removal of uranium, (ii) a uranium deposition sector (B) involving either continuous or sudden deposition of uranium, and a

Figure 1.7: Behaviour of model systems which have been disturbed at various past times. Interpretations of the isotopic data indicating the order of magnitude of the interval that has elapsed between events (from Schwarcz et al., 1982).

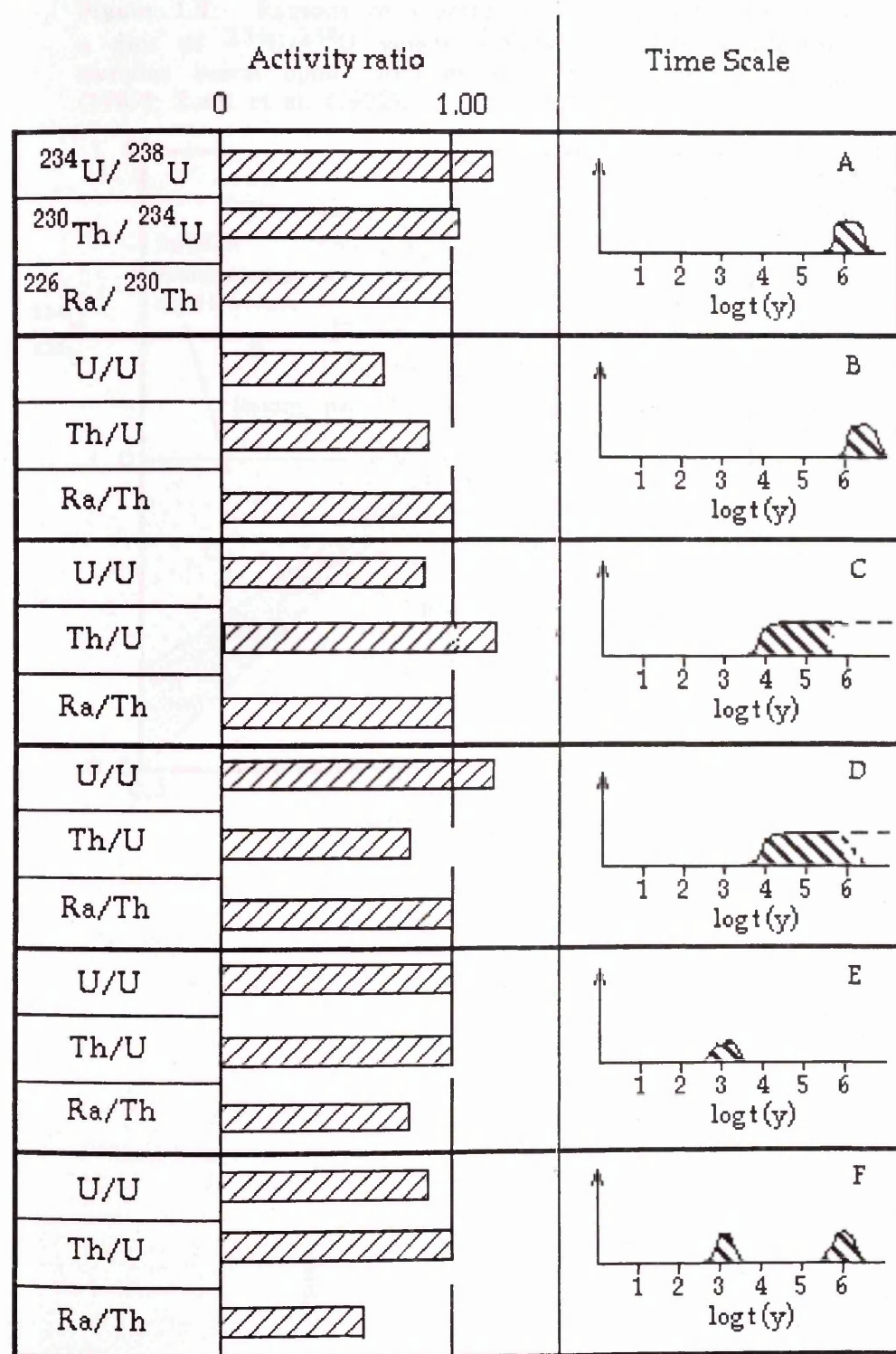
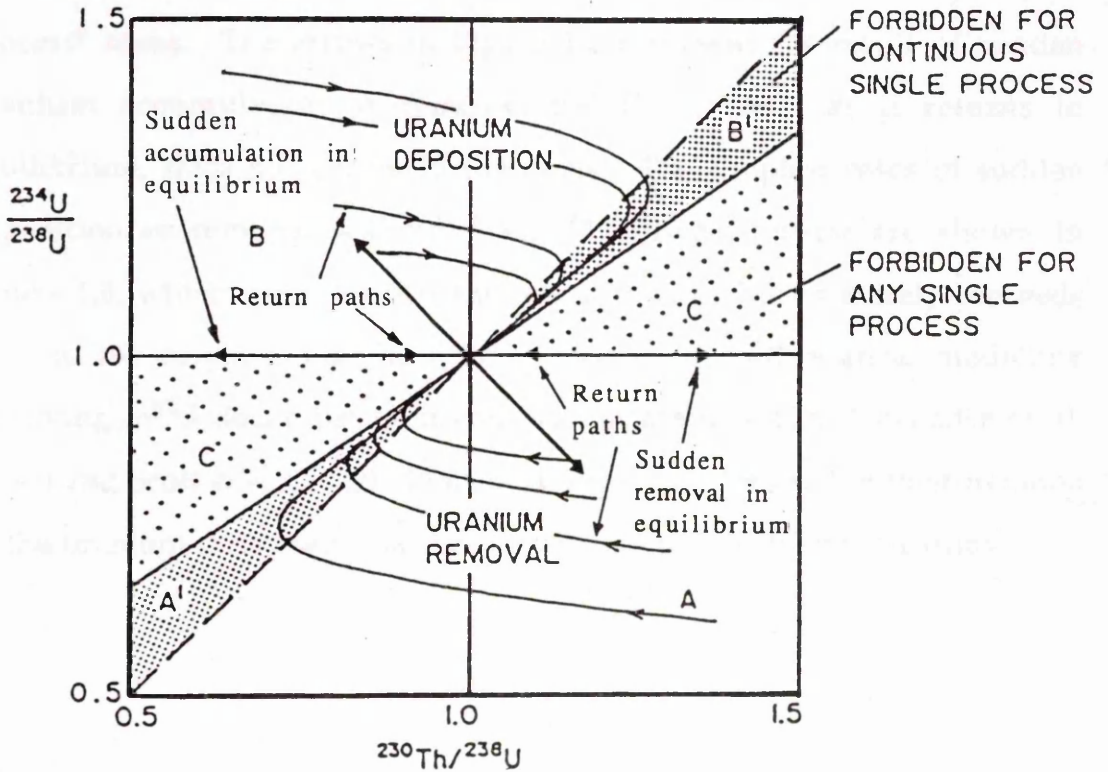


Figure 1.8: Regions of uranium deposition and removal in a plot of $^{234}\text{U}/^{238}\text{U}$ versus $^{230}\text{Th}/^{238}\text{U}$ for whole-rock samples based upon Thiel et al. (1983); Alexander et al. (1989); Scott et al. (1992).



uranium deposition area (B') which can only be attained by samples which have undergone deposition of uranium in a single rapid event and cannot be attained by samples subject to continuous deposition of uranium, and (iii) two regions (C) in the plane which are inaccessible by any single process, and these sectors are consequently classed as "forbidden" or "complex process" areas. The arrows in Figure 1.8 represent the result of sudden uranium accumulation or removal and the system, as it returns to equilibrium, trace out curves in the plane. The simplest cases of sudden deposition or removal without $^{234}\text{U}/^{238}\text{U}$ disequilibrium are shown in Figure 1.8, which indicates that the return to equilibrium merely proceeds back to the origin along the x-axis. Details of mathematical modelling involving ^{238}U decay series disequilibrium are given in Alexander et al. (1989) and Scott et al. (1992). Plots of this type will be used in interpretation of the uranium decay series analysis data from the Criffel pluton study.

1.4 Geochemistry of the rare earth elements

This section presents a brief review of the geochemistry of the rare earth elements of relevance to their geosphere transport and retardation as they can occur as fission products in high level waste and are also used as analogues for trivalent actinides.

The rare earth elements, lanthanum to lutetium (La-Lu), are members of Group IIIA in the periodic table, and all have very similar chemical and physical properties. They generally exist in the 3+ oxidation state, and exhibit systematically decreasing radii with increasing atomic number, from 1.14Å for lanthanum ($z = 57$) to 0.85Å for lutetium ($z = 71$). The ionic

potentials of the rare earth elements consequently show a systematic increase with increasing atomic number, and this affects their geochemical properties, resulting in increasing reactivity with respect to hydrolysis, adsorption and precipitation and a corresponding decrease in solubility with increasing atomic number (Table 1.1). Thus, despite the general similarity in their chemical behaviour, these elements can be fractionated by petrological and mineralogical processes during the formation of igneous rocks, and by weathering processes in open systems. There are two exceptions to the general 3+ oxidation state for the REE, namely cerium and europium, which in addition to the 3+ state can exist in the 4+ and 2+ oxidation states respectively. As a consequence of these changes in oxidation state, cerium and europium can exhibit different solubility characteristic to the other REE as a function of redox potential. Thus Eu^{2+} is generally more soluble, while Ce^{4+} is generally less soluble than the other REE, and this can result in europium and cerium enrichment or depletion in minerals as a result of rock/water interactions. Details of the geochemistry of the rare earth elements are given in Henderson (1984).

In geochemical studies, analytical data for the rare earth elements are normally presented in a graphical form in which the concentrations are normalised to those of the corresponding elements in a chosen reference material, eg. chondrite or shale (Henderson, 1982). The advantages of this approach are that any variation between rare earth elements of odd and even atomic number is eliminated and enrichment or depletion of rare earth elements relative to the reference material is easily seen.

Igneous rocks generally contain several hundred ppm of the rare earth elements, distributed across both the major and accessory minerals (Henderson, 1984). The light rare earth elements, i.e. La-Sm (LREE) are

usually concentrated in plagioclase, K-feldspar, apatite and biotite, whereas pyroxenes, amphiboles and garnet commonly concentrate the heavy group of the rare earth elements, i.e. Eu-Lu (HREE). The ability of amphiboles to fractionate HREE has been shown by Arth and Barker (1976) in dacitic rocks of northern Minnesota. In granitic rocks the REE are mainly concentrated in accessory minerals such as sphene, apatite and monazite, which tend to preferentially concentrate the LREE. Stephens et al. (1985) have investigated the REE distribution in the Criffel pluton and observed a progressive decrease in total REE concentrations towards the centre of the pluton i.e. from granodiorite to granite zones. The REE distribution patterns also correlated strongly with Sr ($^{87}\text{Sr}/^{86}\text{Sr}$) and O isotope data. The LREE/HREE and La/Yb values showed considerable variations over the pluton, with a distinct trend of increasing La/Yb in the granodiorite towards the biotite-bearing granite, followed by a marked drop and continuing decrease in the muscovite-bearing granites. The studies of Stephens and Halliday (1980) and Stephens et al. (1985) led to the presently accepted classification of the zoning of the pluton as described in section 1.7.

In sedimentary rocks, the REE content varies markedly depending upon the composition of the sediment. For instance, in oceanic carbonates and shales clay minerals are usually present in abundance and such sediments consequently have high REE concentrations. The REE concentration patterns in various shales are very similar to each other, being enriched in LREE relative to HREE (Henderson, 1984), and shales have therefore been used for normalising REE concentrations for sediment samples. In contrast, sandstones usually have low REE concentrations due to low REE concentrations in the major constituent minerals of sandstone, eg. quartz. However, in some sandstones, obdurate detrital grains of minerals such as apatite, zircon or monazite, are present in abundance, and sandstones of

this type are rich in REE. In metamorphic rocks, garnet is a very efficient concentrator of the HREE as reported by Schnetzler and Philpotts (1970) for gneissic rocks. In addition, White et al. (1972) have analysed both garnet and pyroxene in eclogite from New Zealand, and found that the heavier REE tend to concentrate more in the garnet.

The rare earth elements occur in high concentrations in several economically important minerals such as bastnaesite (CeFCO_3), monazite [$(\text{Ce,La,Nd,Th})\text{PO}_4$] and cerite [$(\text{Ca,Mg})_2(\text{Ce})_8(\text{SiO}_4)_7 \cdot 3\text{H}_2\text{O}$]. They also occur as trace elements in common rock-forming minerals in which they replace major ions in the crystal structure, and may also reside in inclusions of accessory minerals such as apatite, zircon, xenotime and allanite (Henderson, 1984). Monazite found in Malaysia, for instance, typically consists of 25% Ce_2O_3 , 2% Sm_2O_3 , 2% Y_2O_3 , 27% phosphate, 6% ThO_2 and 0.2% U_3O_8 , whereas xenotime consists of 35% Y_2O_3 , 4% Dy_2O_3 , 4% Yb_2O_3 , 29% phosphate, 0.7% ThO_2 and 1.6% U_3O_8 (Sulaiman, 1991). So it appears that both REE and actinides exist together in these minerals, reflecting their geochemical coherence, and thus strongly supporting the use of REE as analogues for actinides.

During weathering only a very small proportion of the total REE content of the rock goes into solution during rock-water interaction as they have a generally low level of solubility. In general preferential dissolution of the light REE (except Ce which is present in the less soluble 4+ valence state) occurs and this can result in fractionation between the REE during weathering (Fleet, 1984). The small fraction of the REE that is dissolved is highly susceptible to re-deposition in secondary minerals such as iron and manganese oxyhydroxides or adsorption onto clay minerals. For example, a study of altered granodiorite in Victoria, Australia (Nesbitt, 1979) has shown

that REE concentrations were depleted, and fractionation of light and heavy REE was observed as a result of preferential uptake of HREE in the exfoliate and friable zones of vermiculite (alteration product of biotite) and Fe-Ti oxyhydroxides (alteration products of hornblende and biotite), while kaolinite and illite (alteration products of feldspars) may accommodate the LREE. In the marine environment, Elderfield and Greaves (1982) observed fractionation between light and heavy $3+$ REE in seawater from the North Atlantic Ocean where the surface-water was found to be highly enriched in light REE relative to the base of the mixed layer, whereas the HREE were slightly depleted. Fractionation of the heavy and light REE (except Ce) was found to be a maximum at the base of the mixed layer (~100 m depth), indicating that surface removal processes are effective in that zone.

Rare earth elements have been used in a number of natural analogue studies. For example Lei et al. (1986) observed that lanthanum and neodymium are practically immobile in the Morro Do Ferro Th/REE deposit in Brazil, and concluded that this observation gives some assurance that the long-lived isotopes of curium and americium in high level waste would decay in-situ if emplaced under similar conditions to those which exist there. In addition, Krauskopf (1986) has observed low concentrations of lanthanum and neodymium in groundwater and surface water in the vicinity of the Morro do Ferro mineralisation and has concluded that neither americium nor curium would escape from a breached high level radioactive waste repository.

1.5 Radioactive waste disposal

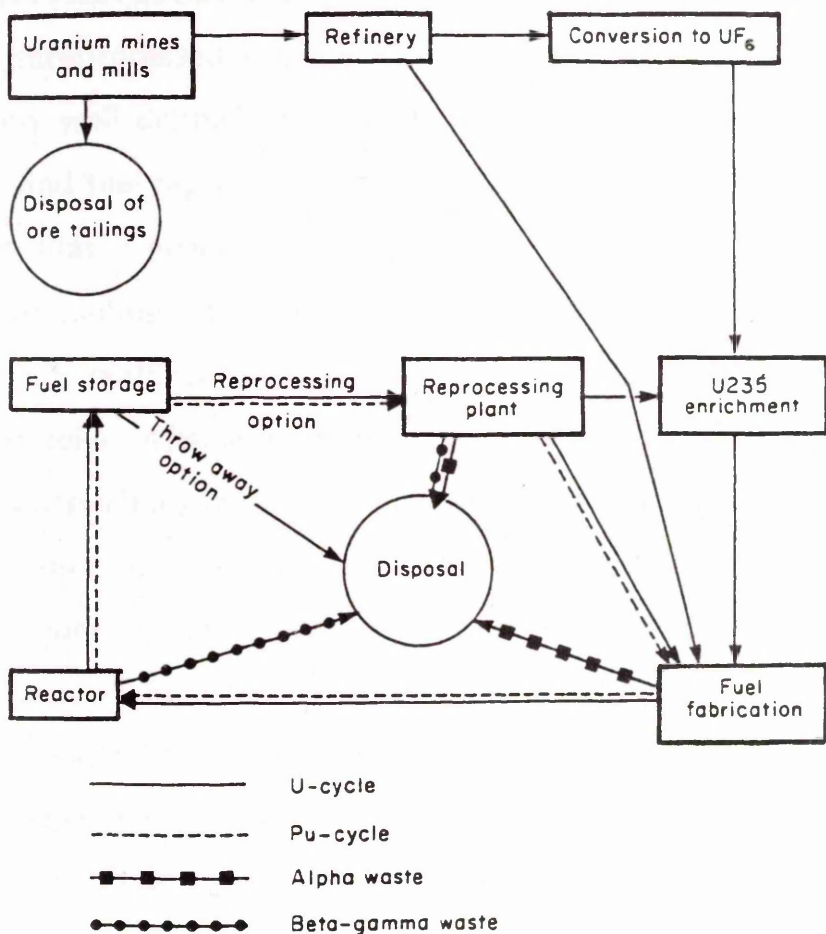
This section presents a general overview of the origin, and types of radioactive wastes and of proposed methods for their disposal. Particular emphasis is placed upon the mined repository option which is the method currently being considered by many countries for the disposal of high level waste.

1.5.1 Origin and types of radioactive wastes

Radioactive waste arises from the use and handling of radioactive materials in nuclear power production, industry, defence, medicine and research activities. The nuclear industry gives rise to the largest quantities of radioactive waste, where it arises at all stages of the nuclear fuel cycle as shown in Figure 1.9. Mining, milling, purification, and fuel fabrication stages produce wastes that are not too difficult to manage because they contain only naturally occurring radionuclides at relatively low levels. By far the major concern of radioactive waste management is therefore connected with irradiated fuel and the highly radioactive wastes that arise from the processing of such material.

There have been many attempts to develop quantitative systems of classification of radioactive wastes according to activity, but the heterogeneous nature of the wastes and their varied origins can make this very difficult. For operational purposes radioactive wastes are generally classified into low (LLW), intermediate (ILW) and high (HLW) level categories, but there is no rigorous, internationally accepted, definition of these levels. In the United Kingdom the LLW/ILW division is at 4 GBq/t

Figure 1.9: Schematic diagram showing the major steps in the nuclear fuel cycle and main radioactive waste streams generated which require disposal (from NEA/OECD, 1977).

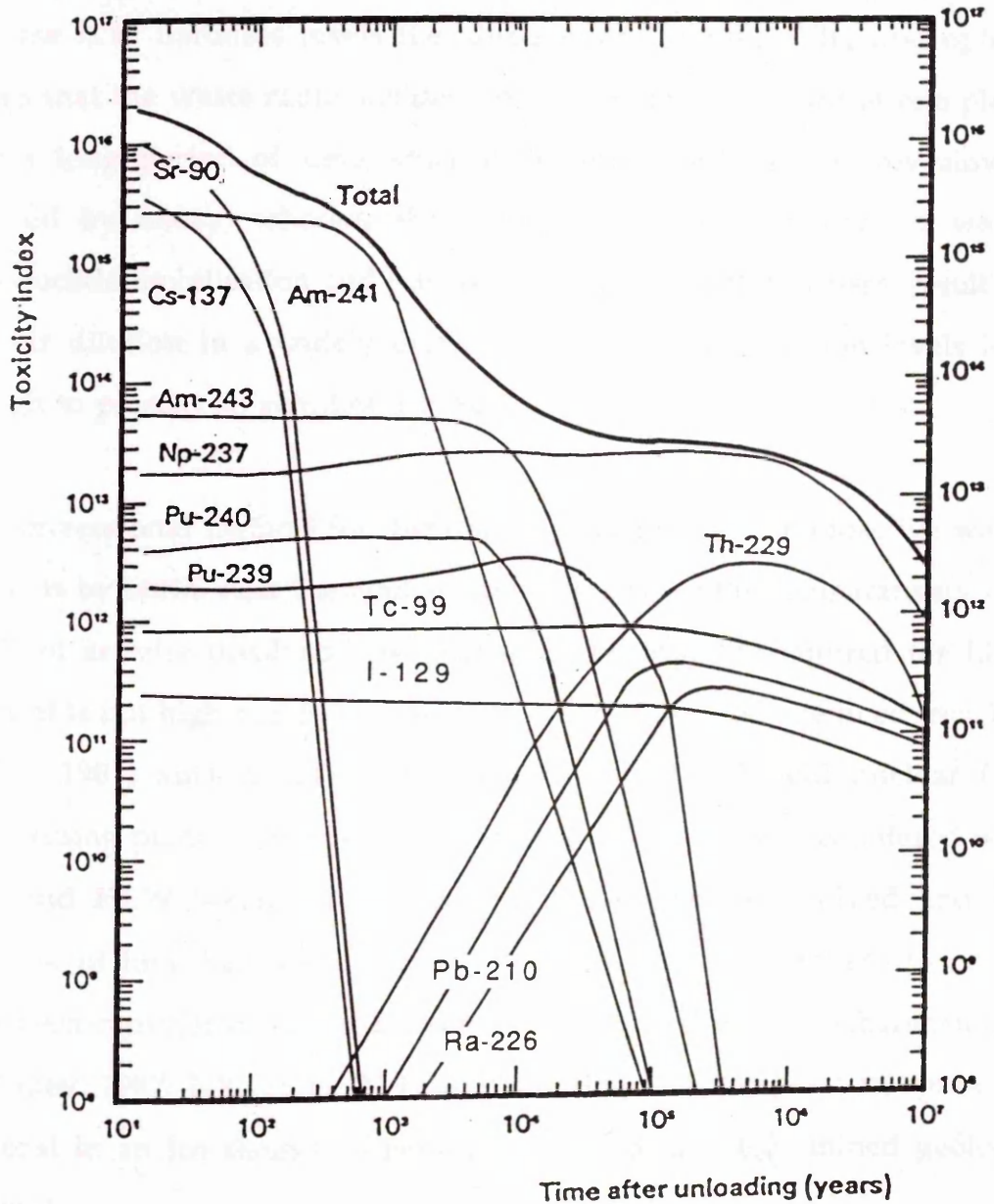


for alpha activity, and 12 GBq/t for beta-gamma activity (Chapman and McKinley, 1987). LLW generally includes material from power stations, hospitals, research laboratories and industry, such as contaminated laboratory clothing and activated plant and equipment. ILW consists of irradiated fuel-cladding, reactor components and chemical process residues. The term HLW is reserved specifically for reprocessed nuclear fuel wastes or spent unprocessed fuel itself. The composition of HLW is therefore relatively well defined, but shows some variation according to the type of reactor and fuel reprocessing involved. The specific activity of this waste is so high that it generates significant heat and special provision has to be made for cooling. Initially, the waste is stored as a liquid in high integrity tanks with multiple cooling systems and located inside massive concrete shielded cells. After a delay of a few decades to allow some of the shorter-lived radionuclides to decay, it is intended that the waste will be vitrified, by incorporation into large glass blocks which will then be encased in stainless steel canisters. Some of the radionuclides of potentially major radiological significance in high level waste are shown in Table 1.2 (Chapman, 1984; Chapman and Smellie, 1986). The actinides are very significant in waste management terms since some have long half-lives such as ^{237}Np (2.04×10^6 y), ^{239}Pu (2.44×10^4 y), ^{243}Am (7.4×10^3 y) and ^{247}Cm (1.64×10^7 y), and many are α -emitters (consequently presenting a potentially high biological hazard). Figure 1.10, which shows the toxicity index (or activity) of various radionuclides in HLW as a function of time after unloading, reveals that the major isotopes of plutonium and americium will decay appreciably within about 10^5 y. A few very long-lived nuclides, such as ^{237}Np , ^{129}I , ^{99}Tc and daughter products of uranium will, however, be present at significant levels of activity for more than 10^6 y. Any safe form of disposal of high level radioactive waste must, therefore, ensure its isolation from the biosphere for at least 10^6 y.

Table 1.2: Some important radionuclides of high-level waste (from Chapman et al., 1984; Chapman and Smellie, 1986).

Element	Isotopes of Interest	Half-life (y)
C	14	5.7×10^3
Ca	41	1.3×10^5
Ni	59	8.0×10^4
Se	79	6.5×10^4
Zr	93	1.5×10^6
Mo	93	3.5×10^3
Tc	99	2.1×10^5
Pd	107	6.5×10^6
Sn	126	1.0×10^5
I	129	1.6×10^7
Cs	135	2.3×10^6
Ra	226	1.6×10^3
Th	229, 230	7.3×10^3 ; 7.5×10^4
Pa	231	3.3×10^4
U	233, 234	1.6×10^5 ; 2.4×10^5
	235, 236	7.0×10^8 ; 2.3×10^7
	238	4.5×10^9
Np	237	2.1×10^6
Pu	239, 242	2.4×10^4 ; 3.8×10^5
Am	241, 243	7.4×10^3

Figure 1.10: Toxicity index of high level waste as a function of time (from NAGRA, 1985).



1.5.2 Methods of disposal

There are two fundamental options available for disposal of radioactive waste: either to keep it in the same place for as long as necessary, (i.e. concentrate and confine), or to allow natural processes to mobilise and disperse it to harmless levels (i.e. disperse and dilute). The first option means that the waste radionuclides remain a potential hazard at one place over a long period of time, since their concentrations are only slowly reduced by decay, whereas the latter option would allow for waste radionuclide mobilization and transportation by natural processes, resulting in their dilution in a widely dispersed form at concentration levels low enough to present no significant hazard.

The conventional method for disposal of solid low level radioactive waste (LLW) is by burial near the land surface. Because of the comparatively low levels of activity involved, the degree of construction required for LLW disposal is not high and it is common practice to use concrete lined trenches (IAEA, 1981) such as at Drigg near the BNFL Sellafield nuclear fuel reprocessing plant. However, more serious problems are encountered with ILW and HLW because of the higher activity levels involved and the presence of long half-life and α -emitting nuclides. A number of options have been considered for disposal of ILW/HLW (IAEA, 1982; Chapman and McKinley, 1987; NEA/OECD, 1984a) including: (a) disposal in space (b) disposal in an ice sheet (c) disposal in the sea, and (d) mined geologic disposal.

By far the greatest effort internationally has been devoted to investigation of (d), the mined repository option since the other options (a-c) listed are considered to be too expensive, to present too great a risk, to be beyond the

present state of technical knowledge or to be politically unacceptable. For instance, deep sea disposal appears to present a safe, practical and economical option for waste disposal but the international aspect of any resultant contamination has rendered this approach politically unacceptable, and treaties banning such disposal are currently in force, eg. the London Dumping Convention of 1975 (NEA/OECD, 1984a). Consequently, geological disposal is the method currently being adopted in all countries where HLW disposal is planned (NEA/OECD, 1984b; WHO, 1982) and a wide range of potential 'host rocks' is being considered for repository development. For instance, salt deposits are being studied by the Federal Republic of Germany; crystalline rock in Switzerland, Sweden, France, Canada and the United Kingdom; tuff in the United States of America; argillaceous rock in Italy, Belgium, France, Switzerland and the United Kingdom (Brookins, 1984; Chapman and McKinley, 1987; USDOE, 1988; NEA/OECD, 1984b).

The following points are generally considered to be of major importance in evaluating the functional requirements of any disposal system for ILW/HLW (Chapman and McKinley, 1987).

- (a) the extremely long periods over which isolation is required
- (b) assurance of low release rates once the required period of isolation is complete ;
- (c) removal of the wastes from the effects of man's activities or catastrophic natural events;
- (d) the technology to implement disposal should be available, and the task should be achievable at reasonable cost;
- (e) it must be possible to model, with an acceptable degree of confidence, those processes which control the long-term performance of the chosen

system.

Proposals for disposal of radioactive waste in underground repositories have attempted to address these points by development of a multi-barrier system in an attempt to guarantee the safe isolation of radioactive wastes from the biosphere. In this concept it is recognised that there are numerous mechanisms by which radionuclides could possibly return to the biosphere, but most of these are of low probability (although they would be catastrophic), eg. earthquakes and volcanoes. By far the most probable transport mechanism leading to return of waste radionuclides to the biosphere would be by groundwater transport (i.e. this is by far the most probable critical pathway as shown in Figure 1.11), and this could present a radiological hazard if: (i) contaminated groundwater entered lakes, streams or rivers, with a radiological impact via fishing, irrigation, agriculture or drinking water, or (ii) groundwater resources were used directly by future generations via deep wells. The multi-barrier concept has been developed to guard the waste from permeating groundwater, and to minimise the quantity and rate of release of radionuclides should water eventually reach the waste. A schematic diagram showing a typical plan of safety barriers (indicating both the near- and far-field zones) in a repository for high-level waste is shown in Figure 1.12. The near-field zone is generally taken to be the repository itself and the zone altered by the presence of the emplaced waste, comprising all the engineered barriers (i.e. waste form, canister and backfill materials) and extends a small way into the host rock itself. On the other hand, the far-field zone (i.e. geologic barriers), which is the most important of the barriers to waste migration, extends through the undisturbed host rock and the surrounding geological formations. In multi-barrier designs, the details of individual barriers may differ from one disposal system to another, but the purposes of the individual barriers

Figure 1.11: Probable critical pathway to the discharge of underground high level waste.

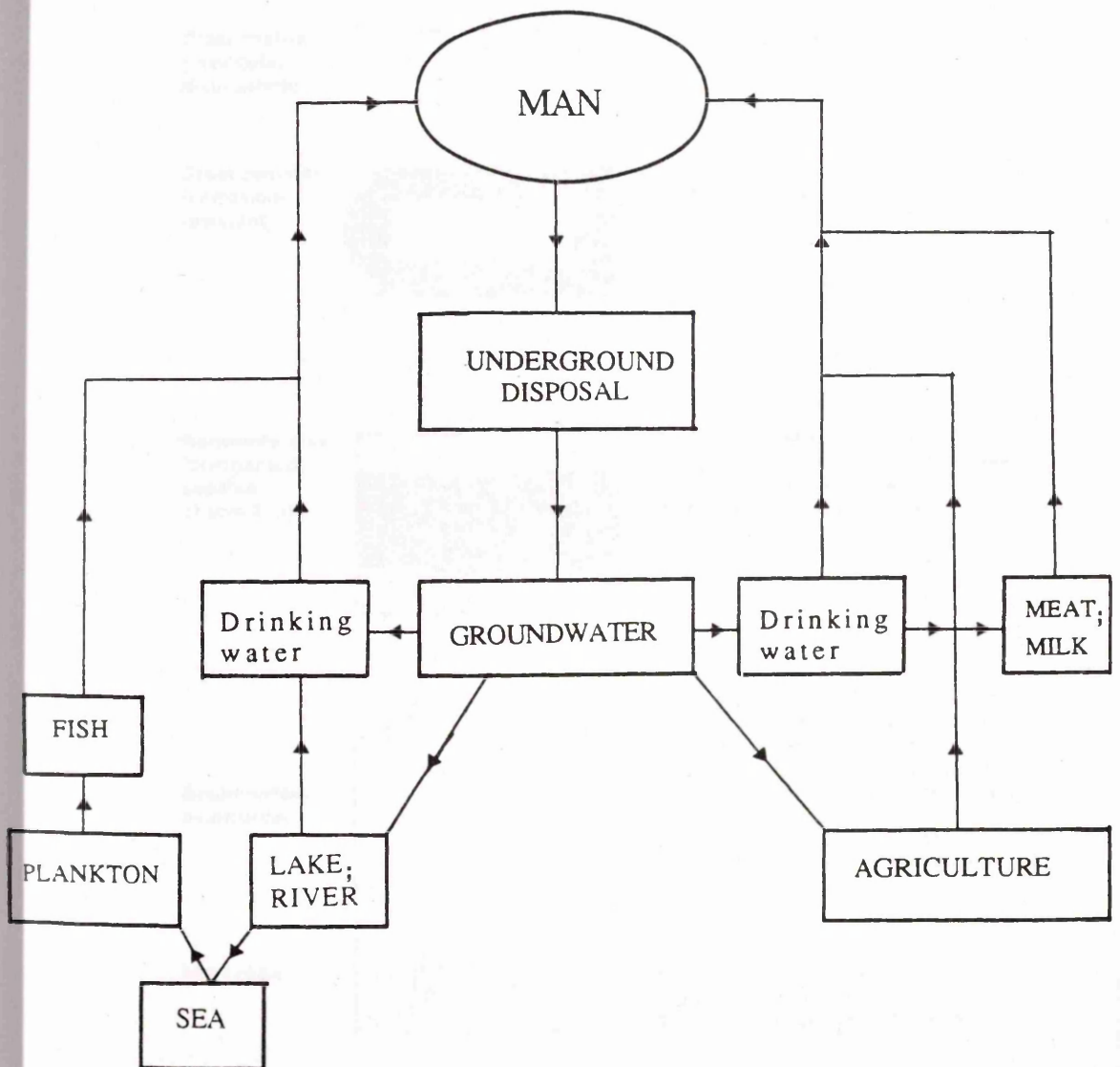


Figure 1.12: Schematic illustration of the multi-barrier system for high level waste (from McKinley, 1989; Chapman and McKinley, 1987).

Glass matrix
(molecular
distribution)



- Restricts release

Steel canister
(corrosion-
resistant)



- Retards water penetration
- Provides favourable chemistry

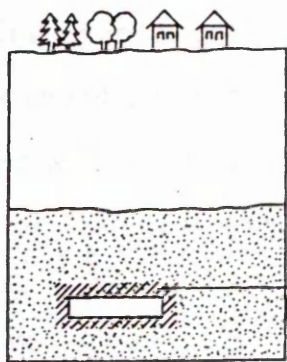
Bentonite-clay
(compacted,
capable
of swelling)



- Restricts water penetration
- Delays commencement of release (diffusion break-through time)
- Restricts release (diffusion)

Sedimentary
overburden

Host rock



Geosphere

- Long water-flow times
- Additional retardation of radioactive material transported in water (sorption, matrix diffusion)
- Long-term stability of hydro-geological conditions in view of climatic and geological changes

Repository zone

- Limited water supply
- Favourable chemistry
- Geological long-term stability

remain basically the same as described below.

(a) The first barrier is the waste package, consisting of the waste form in a container. The waste form is designed to be resistant to leaching by groundwater, the primary agent for transport of radionuclides from the waste to the human environment. For example, in the case of high-level wastes, the waste form could be a special glass matrix of very low solubility containing immobilised radionuclides. Upon the eventual ingress of groundwater, glass degradation would form an extensive suite of secondary minerals which should ideally incorporate radionuclides and form a diffusion barrier.

(b) The second barrier is the container in which the wastes are placed. This is constructed of materials (eg. steel or copper) which are resistant to corrosion in the chemical and physical environment expected in the waste repository. When all the canister materials have been corroded, the corrosion products are expected to have very low permeability and a high retardation/adsorption capacity for many radionuclides. In particular iron oxyhydroxides resulting from corrosion may buffer both pH and redox conditions (ensuring a chemically reducing environment, thus keeping the actinides in their less soluble forms) and strongly sorb many radionuclides, and thus would provide a site for scavenging of radionuclides dissolved from the waste form.

(c) The third barrier consists of backfill material (eg. dry bentonite clay) placed around the waste containers. The backfill initially prevents ingress of water, and bentonite is ideally suited to this purpose, having a high capacity for uptake of water which results in swelling, giving low permeability and sealing fractures in the surrounding structure. After the

waste form has been breached by groundwater, the low permeability and high ion exchange capacity of the bentonite should restrict the rate of release of radionuclides from the repository.

(d) The fourth barrier consists of a concrete structure containing the bentonite, canister and the waste form. The concrete delays ingress of water and eventually, after ingress, gives high pH conditions favouring hydroxide precipitation.

(e) The final barrier is the host rock, the function of which is to provide isolation of the waste and to give long periods of time for transport of escaped radionuclides to the biosphere if the engineered barriers were to eventually fail. In safety and performance assessments pessimistic assumptions are made about the time within which each of the engineered barriers will fail, with the result that the geosphere barrier becomes the key component of the multi-barrier design (McKinley and Hadermann, 1984; NAGRA, 1985).

It is assumed that after closure of a radioactive waste repository water will penetrate zones of the host rock which have been drained during construction, then the backfill, and eventually come into contact with the canister which will begin to corrode. At some point canister failure will occur due to corrosive penetration or mechanical effects eg. due to external hydrostatic pressure or backfill swelling pressure, and finally water will come into contact with the waste itself. The waste will then begin to degrade and radionuclides will be released, either into solution or as particulates or colloids, and begin to migrate through the near-field and far-field and finally into the biosphere. It has been suggested that, following the ingress of groundwater into a repository, radiolytic decomposition of water

could lead to the development of oxidising conditions, initially within the repository but, eventually, encroaching into the far-field especially along water-bearing fractures (Neretnieks and Aslund, 1983a and b). A schematic diagram showing the radiolytic development of oxidising conditions within a repository (near-field) and the extension of the oxidised zone into far-field is shown in Figure 1.13. However, in several disposal concepts the effects of oxidation are assumed to be buffered by the presence of (a) elemental iron in the canister material, and (b) ferrous minerals present in the host rock and the backfill (Hadermann and Rosel, 1985). It is therefore essential to characterise processes involved in far field radionuclide transport and retardation as described below.

Transport of radionuclides in crystalline rock (eg. granite) is assumed to occur predominantly in water bearing discontinuities, eg. fractures and shear zones. In such transport it is assumed for modelling purposes that the two most important retardation mechanisms affecting the radionuclides are 'sorption' on the fracture surface and 'matrix diffusion' into the structure of the rock on either side of the fracture (McKinley, 1989). Dissolved radionuclides will interact with the minerals (eg. chlorite, montmorillonite, iron and manganese oxyhydroxides and sulphides) lining the fracture surface which have high adsorption capacity as reported by Smellie et al. (1986), Alexander et al. (1988) and MacKenzie et al. (1989). Modelling studies (Hadermann and Rosel, 1985) have shown that sorption alone can provide a significant barrier when a discontinuity is massive (eg. wide shear-zone or a large clay-rich channel). Interaction of radionuclides with the mineral surface can be further subdivided into (a) 'reversible' sorption (i.e. ion-exchange, physical sorption), and (b) 'irreversible' deposition (i.e. mineralisation) as shown in Figure 1.14. The effects of (a) are to slow down the rate of movement of radionuclides, whereas (b) will

Figure 1.13: Schematic diagram of movement of a redox front along a fracture in the near-field of a radioactive waste repository (after canister failure and radiolysis of water have occurred).

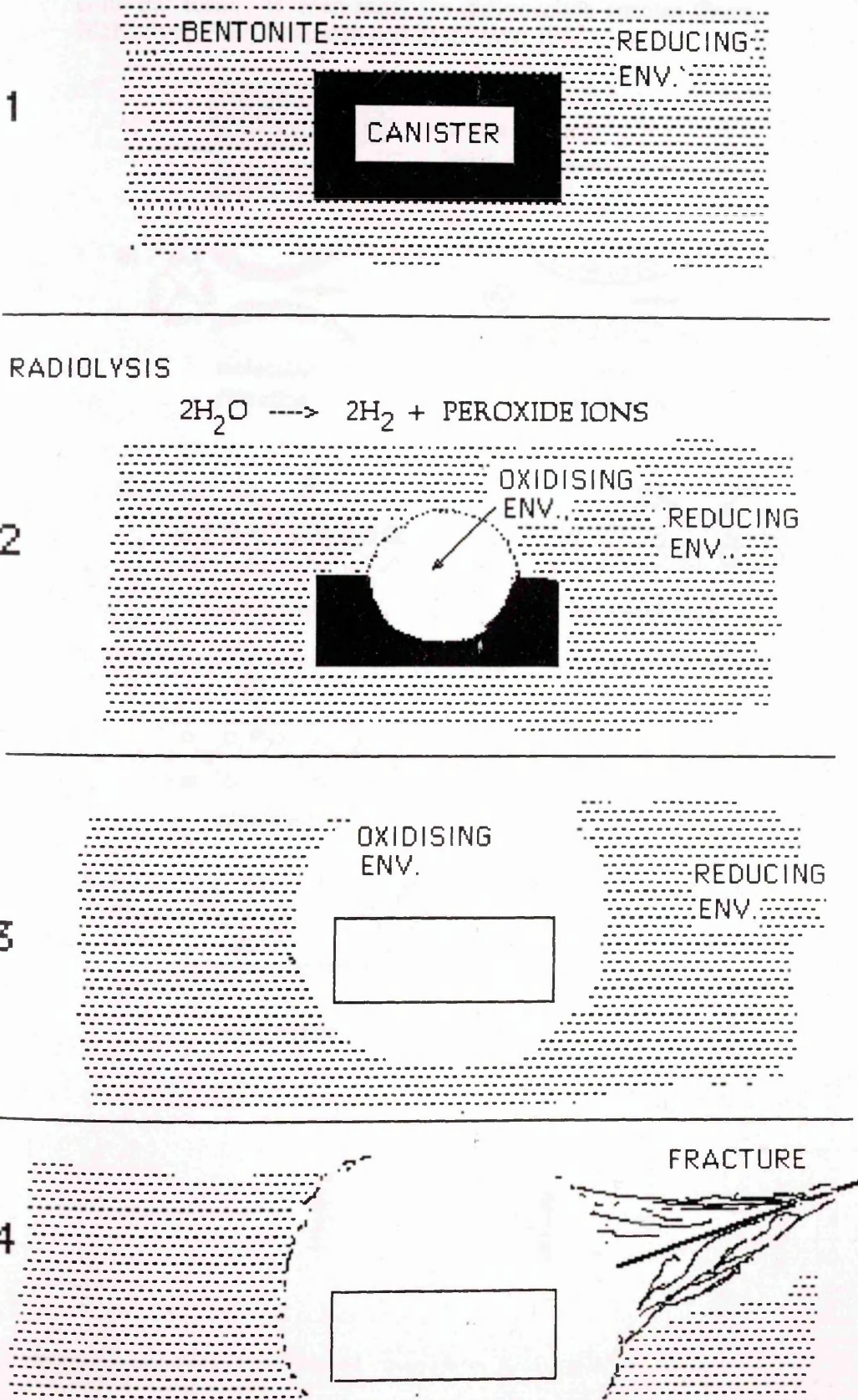
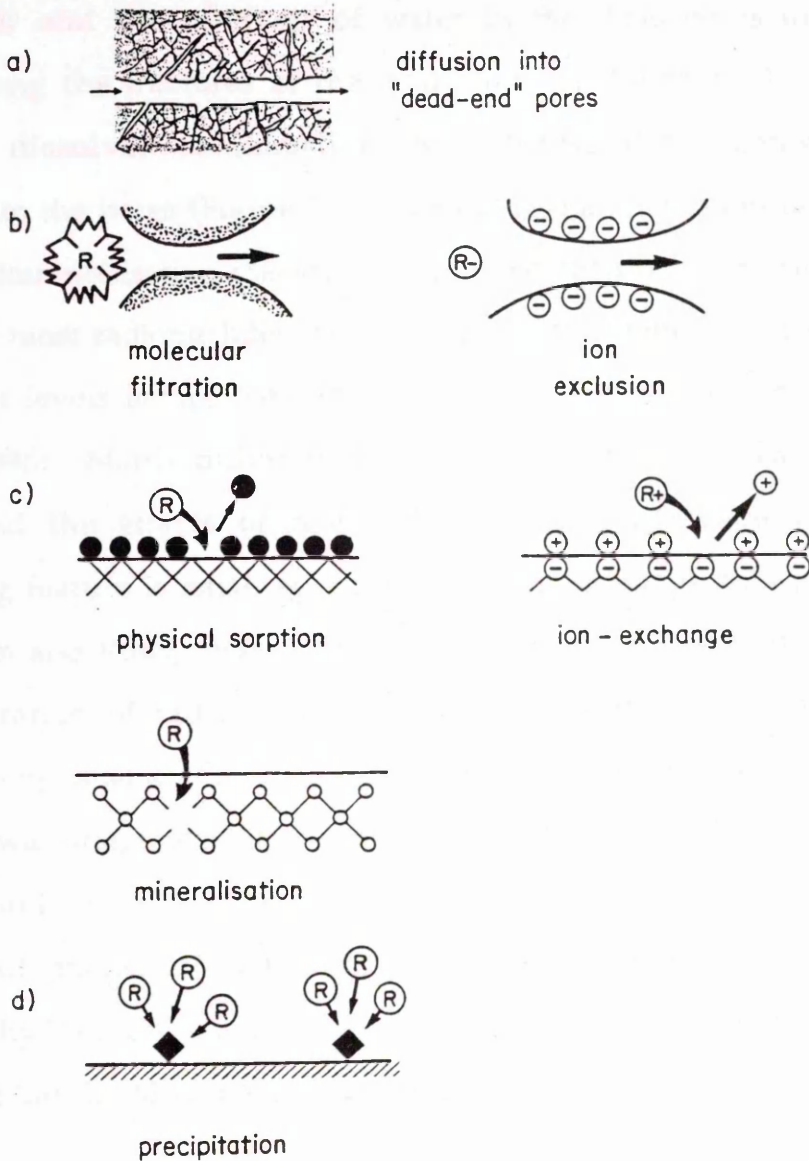


Figure 1.14: Schematic representation of the many possible retardation mechanisms that result from interaction between a rock surface and radionuclides in solution, particulate and colloidal form. 'R' represents the radionuclide species (from McKinley, 1989; Chapman and McKinley, 1987).



give permanent immobilisation.

'Matrix diffusion' (or 'dead-end pore diffusion') is considered to occur when a concentration gradient is established between the fissure groundwater and the reservoir of water in the dead-pores (or microfissures) along the fractures of the main body of the rock. Under such conditions dissolved radionuclides will diffuse down concentration gradients into the pores (Figure 1.14). This is also a retardation rather than permanent immobilisation mechanism but is potentially so efficient that it could cause most radionuclides released from a HLW repository to decay to insignificant levels before they are released to the biosphere (Neretnieks, 1980 and 1986). Matrix diffusion is a key component of far field transport models, and the effects of retardation are greatest when the water transporting feature is small eg. narrow fissures, perhaps only μm across (Hadermann and Rosel, 1985). The potential effects of 'matrix diffusion' to retard migration of radionuclides in fractured granitic rock have been investigated by Smellie et al. (1986), Alexander et al. (1988), and a depth of at least 3 cm was suggested for the extent of migration of radionuclides from fracture fluids into the 'pore-space' within the saturated rock. The efficiency of 'matrix diffusion' depends critically upon the volume of accessible, hydraulically connected 'pore-space' in the rock on each side of the fracture but, in this context, matrix diffusion is still poorly understood at present.

In summary the net effect of the 'sorption' processes described above is to retard the movement of radionuclides released from a repository so that they lag behind the flow of groundwater. The other important process which can cause 'retardation' but does not directly fall into any of the categories above is 'precipitation' which is primarily a function of aqueous

chemistry yet the kinetics of which may be dependent on the availability of particular surfaces. Additionally redox process, a potentially important factor in transport and retardation of radionuclides in the bedrock environment, will be discussed in the next section.

1.6 Natural Analogues

As indicated above the complexity and timescale of processes of relevance to modelling repository performance places considerable uncertainty upon the validity of using theoretical considerations and laboratory based experiments. Consequently there has been extensive development over the last decade of natural analogue studies for use in performance assessments. Such analogue studies can: (a) provide information for input to models, (b) be used to develop (or confirm) conceptual geochemical models and (c) test models. A review of some of the major applications of natural analogue is presented below. Such studies, although related primarily to radioactive waste disposal, can often provide information of fundamental geological importance, for example on aspects of the development of the low-temperature ore deposits (Mohamad et al., 1992).

1.6.1 Analogue studies for the waste form

In this case the main objective of analogue studies is to evaluate the long term stability of the waste form with respect to dissolution as a result of its reaction with permeating groundwater and to determine the leach rate of specific elements.

For waste vitrified in borosilicate glass the analogue can be natural glasses like obsidian or basalt glass. Naturally occurring obsidian and other glasses are, under many terrestrial conditions, stable for up to about 10^7 y (Lutze et al., 1987; Zhou et al., 1987). Supporting evidence for the use of natural glasses as analogues for vitrified waste has been provided by Zhou et al. (1987) who have shown, in laboratory leaching experiments, that both the waste form and natural (basaltic and rhyolitic) glasses exhibit similar corrosion behaviour, forming hydration layers composed dominantly of amorphous material enriched in magnesium that may act as a barrier to further reaction. It was observed that both natural and synthetic glass exhibit comparable corrosion rates averaging about 2×10^{-8} kg m⁻² d⁻¹ (2.5 μ m/1000 y) (Lutze et al. 1987; Heimann, 1987).

The obvious analogue for an unprocessed fuel element is a deposit of the same compound in nature i.e. the common uranium ore mineral uraninite, or the less pure variety pitchblende. The waste form is, however, somewhat different from the natural material in that the waste contains elements not present in the natural mineral and its crystal structure will be partly disorganised by the intense radiation field and hence may be somewhat more soluble. Despite these differences the study of uraninite ore and its surroundings should provide clues as to the behaviour of spent fuel, in particular its stability in a repository environment. At Oklo in Gabon, Africa, a uranium deposit operated as a natural nuclear reactor about 2×10^9 y ago, over a period of 10^5 to 10^6 y (Brookins, 1984), during which time fission products and transuranics were produced. The uraninite ore has survived with little evidence of dissolution over the very long time since the reaction stopped. It is estimated that about 6 to 12 tonnes of ²³⁵U underwent fission, and while the original radionuclides produced have long since disappeared, the stable isotopes such as lead and

bismuth resulting from their decay are readily detectable (Chapman and McKinley, 1987). At several places in the Oklo mine the products of a nuclear fission reaction were generated underground and then remained in a groundwater environment for some 2×10^9 y. Thus studies at the 'Oklo Natural Reactor' site show an ability of the surrounding rocks (i.e. shale and sandstone) to retain fission products, actinides and actinide-daughter products over a time of 10^9 y.

In addition to the Oklo studies uranium behaviour has also been investigated at other major deposits eg. Cigar Lake in Canada, Pocos de Caldas in Brazil and Alligator River in Australia. These ore bodies have been shown to have existed as stable features in a variety of rock types over very long times, eg. (a) Cigar Lake uranium deposit: located in sandstone of age about 1.3×10^9 y (Cramer, 1987); (b) Alligator River uranium deposit: primary mineralisation comprising uraninite veins within^a sheared zone of quartz-diorite-schists of age about 1.6×10^9 y and secondary mineralisation in weathered schists of age greater than 1×10^6 y (Deurden, 1990); and (c) Pocos de Caldas uranium deposit (5×10^7 y): located in alkaline intrusive rock of age about 8×10^7 y (Waber et al., 1990).

The study of the rate of deposition and dissolution of uranium in the natural environment was also carried out within the Pocos de Caldas project which focussed on uranium nodules that occurred on both sides of a redox front in a uranium orebody (MacKenzie et al., 1991). In this study, pitchblende nodules (~2cm and 4cm) were found near the redox front in the reduced rock and growth rates have been established at 1.8 - 2.6 cm in 10^5 y (MacKenzie et al., 1991). The uranium nodules that occurred initially on the reduced side of the front were estimated to undergo dissolution after the redox front has moved and passed them in a time of the order of 10^4 to 10^5

y. On the basis of $^{230}\text{Th}/^{234}\text{U}$ and $^{234}\text{U}/^{238}\text{U}$ disequilibrium considerations Scott et al. (1992) derived ^{238}U removal probabilities of 0.36×10^{-6} and $1.7 \times 10^{-6} \text{ y}^{-1}$ for the reduced and oxidised rock respectively. In addition natural ^{239}Pu , which only occurs in very few places in the world, was also found in a nodule from the reduced rock at Pocos de Caldas. The concentration of plutonium in the nodule was measured as $2.3 \pm 0.7 \times 10^8$ atoms per gram, consistent with a state of secular equilibrium between ^{238}U and ^{239}Pu . Judging from the Pu/U ratio of the nodule we can summarise that the two elements have resided unfractionated in the deposit for the last 10^5 y. The study thus reveals that uranium (plus daughters) and plutonium are chemically stable in the form of a nodule on the reduced side of a redox front in rock for at least 10^5 y which would allow approximately 95% decay of ^{239}Pu in a repository.

A natural analogue study centred upon uranium dissolution has also been carried out on the southern edge of the Criffel pluton at an exposed uranium mineralised vein close to an ancient sea arch known as The Needle's Eye (MacKenzie et al., 1989). The age of the pitchblende vein was reported (Darnley et al., 1962) to be $185 \pm 20 \times 10^6$ y, which is more recent than the age of the pluton of $397 \pm 2 \times 10^6$ y (Halliday et al., 1980). On the basis of $^{230}\text{Th}/^{234}\text{U}$ and $^{234}\text{U}/^{238}\text{U}$ disequilibrium considerations Scott et al. (1991) derived a removal probability of $5.2 \times 10^{-5} \text{ y}^{-1}$ for dissolution of uranium from the vein on the assumption that leaching has been continuous since the end of the last glaciation (about 12000 y ago). On the other hand a uranium removal probability of $4.3 \times 10^{-6} \text{ y}^{-1}$ was estimated on the assumption that leaching has been going on throughout the Quarternary period, perhaps with temporary, short (relative to the ^{230}Th half-life) interruptions due to conditions under the ice-sheet. These estimates thus implied that uranium is being physically removed from the

vein at a rate between 11 and 130 Bq kg⁻¹ y⁻¹. Two mechanisms of uranium dissolution from the vein were identified, namely (a) long term, slow leaching (probably by reducing groundwater) with preferential loss of ²³⁴U relative to ²³⁸U, and (b) rapid, contemporary dissolution by oxidising groundwater (MacKenzie et al., 1991). The uranium in fissure water flowing from the area of the vein was found to be predominantly present (over 90%) in the 6+ oxidation state (Whitton et al., 1992). However, although oxidising water was in contact with the vein, only limited enrichment of uranium was observed in fissure water (1 - 2.4 Bq l⁻¹) suggesting that the weathered vein material is probably relatively stable and forms a protective layer which retards dissolution of the deeper unweathered pitchblende.

1.6.2 Analogue studies for canister materials

In this case, the purpose of analogue studies is to establish rate of corrosion of potential canister materials eg. iron and copper.

Studies of archaeological artefacts have become accepted in analogue investigations for canister materials. Numerous examples of objects manufactured from copper or iron, which were widely used by primitive societies and in ancient civilizations, have been recovered after periods of burial of hundreds to thousands of years and are available for corrosion study. One example of such an analogue study of corrosion processes involved a bronze cannon, with a copper content of 96.3%, salvaged from the Swedish warship "Kronan" which sank in the Baltic Sea in 1676 (Hallberg et al., 1987). The cannon was embedded in a vertical position in the sediment with the top part exposed to oxidising conditions while the

bottom part was buried in reducing sediment (largely illites and montmorillonite) which was moderately well compacted and was thus analogous to the bentonite clay barrier around canisters in a repository system. This study indicated that the rate of loss of copper has been about 4 mg cm^{-2} over a period of some 300 years, resulting in a rate of corrosion of $1.0 \times 10^{-3} \text{ mm y}^{-1}$. Thus copper canisters with 10 cm thick walls for waste disposal should be able to withstand corrosion for more than 10^5 y if they experience a similar rate of corrosion. Additionally the Swedish experimental work on the corrosion behaviour of copper as a canister material for high level radioactive waste has been evaluated and confirmed that copper canisters with walls 10 cm thick would not be breached in 10^5 y at least (KBS, 1983).

Even longer survival times for copper canisters are suggested by studies of native copper deposits. For example, a study of the White Pine copper deposits of northern Michigan (White, 1968) has revealed that the native metal has remained intact during exposure to groundwater for a time of at least $970 \times 10^6 \text{ y}$ (Chaudhuri and Faure, 1967), since the late Precambrian. Native iron does not occur in rocks and the closest analogue for steel canisters are iron meteorites (composed of Fe/Ni alloys), which have been found at or near the Earth's surface and have survived for up to $2 \times 10^4 \text{ y}$ (Chapman and McKinley, 1987).

Preserved Roman iron objects from oxidising environments show corrosion rates between 0.1 and $10 \text{ } \mu\text{m y}^{-1}$ (Chapman and McKinley, 1987), and this suggests that corrosion would not breach thick-walled iron canisters ($\sim 10 \text{ cm}$) for at least 10^3 y . Laboratory studies (Marsh, 1982) of corrosion of iron show compatible results with the data derived from archaeological studies. Moreover, high corrosion rates were observed at the

initial stage, and the rate decreased with time suggesting the formation of a protective layer of corrosion products. The study of uranium migration and retardation in the Cigar Lake deposit (Cramer et al., 1987) has indicated that ferric-oxyhydroxide phases at the clay-ore contact are strongly enriched in uranium, suggesting iron corrosion products can act as effective reducing and scavenging agents. In summary, natural analogue studies relating to the two proposed canister materials i.e copper and iron provide confirmation of their durability under actual environmental conditions over time periods appropriate for HLW disposal.

1.6.3 Analogue studies for bentonite backfill

The main objective of analogue studies of relevance to bentonite backfill is to investigate its stability and to provide information on its capacity to retard radionuclide movement.

Bentonite clay exists in beds as old as mid-Palaeozoic (eg. Kinnekulle bentonite in Sweden) and there is ample evidence for its long-term stability at low temperatures (Smellie and Papp, 1988). However, bentonite can change to illite at temperatures above 100°C, if a sufficient source of K^+ is present (Chapman and McKinley, 1987). Nevertheless, studies of buried, smectite-rich sediments (i.e. closest analogue of bentonite; eg. Gulf zone of United States) have shown that the transformation of bentonite clay to illite is sluggish provided temperatures do not rise far above 100°C (Krauskopf, 1988). The change to illite may not be seriously damaging to a repository, but it would certainly make the clay somewhat more permeable, less expansive and less sorptive. This should not present a problem in the use of bentonite in repositories where the expected temperatures will be kept

below 100°C. As we know that in these conditions the bentonite will remain chemically and physically intact for more than 10⁶ y eg. Sweden and Switzerland (Smellie and Papp, 1988). Moreover natural hydrothermal systems show that even at 100 - 200°C and with a sufficient supply of K⁺, alteration occurs only slowly, in the order of 10⁶ y (Chapman and McKinley, 1987).

A study of elemental migration in the post-glacial sediments of Loch Lomond in West Scotland is of direct relevance to elemental migration in backfill clays (MacKenzie et al., 1983; Hooker et al., 1985). The sediment of Loch Lomond contains a distinct band of material of marine origin in the middle of freshwater sediments which is attributable to the differential rates of changing sea level and isostatic recovery of the land after the last ice age. The marine incursion has been dated to approximately between 6900 and 5400 y ago by ¹⁴C dating (Dickson et al., 1978). The principle of this study is that the marine sediment (and associated pore water) are chemically in disequilibrium with the overlying and underlying freshwater sediment and the dissolution of marine deposited materials provides a source of ions in solution, allowing quantitative characterisation of diffusion processes into freshwater sediment. This diffusion is analogous to that of radionuclides from a waste package into a clay backfill or an argillaceous host rock and can be modelled by techniques used in repository safety assessment given appropriate input data (timescales, sorption constants and porosity). The results of the study showed that, in general, the observed mobility of Br⁻ and I⁻ (effective diffusion coefficient of about 10⁻⁷ cm² s⁻¹) was compatible with laboratory data which were used in modelling studies. It would be expected that diffusion coefficients in bentonite backfill would be lower since it would be more compacted and would have a greater sorption capacity than the Loch Lomond sediments which contain only about 30%

clay.

The investigation of uranium migration and retardation at the Cigar Lake uranium deposit also provides an analogue study of relevance to clay backfill since a clay-rich halo (between 30 and 80% of illite plus kaolinite) surrounds the uranium ore (Cramer et al., 1987). In this case the clay was found to have acted as an important barrier to movement of dissolved radionuclides, as indicated by the presence of enriched uranium, thorium, radium, lead and lanthanides in the first few metres into the clay zone from the contact with the ore.

In Belgium extensive analogue experiments have been performed in the Boom clay which underlies the Mol nuclear research site. This Tertiary plastic clay formation ($\sim 3 \times 10^7$ y) is about 100 m thick and lies between 190 and 300 m below the surface (NEA/OECD, 1984b). The main investigation has concerned the physical, chemical and hydrogeological properties of the clay (via in situ and laboratory experiments). The downward hydraulic gradient was from 1 to 2% across the clay layer, thus indicating a very slow flow rate of water. A trial shaft and experimental underground laboratory have been constructed in the clay at a depth of over 200 m and this provides information on the techniques which will be required in construction of a mined repository in plastic clays as well as data for safety assessments purposes.

1.6.4 Analogue studies for far field radionuclide movement

The main objective of analogue studies for far field radionuclide movement is to investigate processes considered to be of importance in the

context of the geosphere migration of waste radionuclides following the eventual failure of the engineered near-field barriers. During far-field radionuclide transport along hydraulically connected fracture systems radionuclides in solution will be subject to retardation mechanisms such as sorption, matrix diffusion and deposition at redox fronts. Some of the major applications of natural analogue studies in this context are presented below.

Schwarcz et al. (1982) have used natural decay series disequilibrium techniques to study the migration and dispersion of radionuclides in crystalline rocks (i.e. Atikokan granite) in the Canadian Shield. They observed that radium and uranium have migrated on a scale of at least a few centimetres in deep granite (from 0.5 to 1 km depth), over the past few thousands to tens of thousands of years. Thiel et al. (1983) have undertaken similar studies, in conjunction with fission track analysis, of Precambrian consolidated conglomerate sediments in South Africa and found that uranium remobilisation (uranium gain or loss) has occurred on a micron-to metre-scale within the last 10^6 y.

Natural decay series radionuclides have been used to study transport and retardation processes affecting radionuclides in water-bearing fractures in crystalline rocks (Smellie et al., 1986; Alexander et al., 1988). Smellie et al. (1986) noted that uranium migration was observed for distances of the order of 40 cm in Swedish granite on a timescale of 10^6 y, while thorium is practically immobile under the same conditions. Fracture lining-materials, mostly hematite, FeOOH-oxides, chlorite and clay minerals, showed a high affinity for radionuclides, and were strongly enriched in uranium as a result of sorption and/or scavenging processes. A limit of ~3 cm has been suggested (Smellie et al., 1986; Alexander et al., 1988) for the migration of

radionuclides from fracture fluids into the adjacent saturated rock (i.e. matrix diffusion processes) and it has been suggested that this may correspond to a zone of enhanced matrix porosities (Norton and Knapp, 1977; Skagius and Neretnieks, 1982) resulting from earlier hydrothermal activity along the same channels. These studies therefore demonstrated that uranium retardation occurred during fracture flow as a result of adsorption onto fracture-lining materials and matrix diffusion and provided quantitative data for modelling such processes. The low value of thorium observed in the fracture-lining materials suggests that this element has probably been immobile and has retained in its original location in the granite for at least 10^6 y.

A detailed study of uranium migration and retardation in the vicinity of redox fronts was carried out within the Pocos de Caldas Project in Brazil by MacKenzie et al. (1992). The study site consisted of an eroded caldera at an altitude of 1300 - 1600 m that was initially formed some 8×10^7 y ago. Redox fronts with a sharp colour change, marking the Fe^{2+} to Fe^{3+} transition, were observed in the walls of the open cast uranium mine at depths of the order of 100 m below ground surface, with a preferential downward extension of oxidised conditions around major fissures. This pattern is the consequence of the established long-term flow of oxidising groundwater (Holmes et al., 1990). This study demonstrated that the redox fronts act as an effective retardation barrier as indicated by deposition of uranium and other elements on both sides of the front. The deposition of uranium occurs in the reduced rock as a result of the reduction of U^{6+} to U^{4+} , and in the oxidised rock as a result of scavenging by Fe oxides, giving a bimodal distribution about the fronts. Thus, in a HLW repository scenario, development of a redox front (section 1.5.2) would initially lead to the beneficial effect of radionuclide retardation but if such a front were to

penetrate a sufficient distance through the far field, it could result in the undesirable effect of a breakthrough of a pulse of high radionuclide concentration to the near-surface zone. Natural decay series disequilibrium investigations indicated that the general rate of movement of the redox front at Pocos de Caldas is of the order of 2 - 20 m in 10^6 y which is consistent with the rate of regional erosion, although in places the front has been stationary for at least the last million years. This provides support for the proposal by Neretnieks and Aslund (1983a and b) of a rate of far-field movement of repository-related redox fronts of up to 50 m in 10^6 y, for use in far-field transport models. The Pocos de Caldas study additionally revealed that ^{226}Ra , which is not an inherently redox-sensitive element, had moved over distances of the order of 10 m from the reduced to the oxidised rock on a timescale of 10^3 y, suggesting deposition as a result of scavenging from solution by secondary iron oxyhydroxides close to the redox front. The observed deposition of uranium and radium in the oxidised rocks of the Pocos de Caldas studies represents a potentially important radionuclide retardation process which would not be predicted on the basis of purely thermodynamic considerations. Investigation of uranium migration from the Cigar Lake uranium deposit (Cramer et al., 1987) has also indicated that ferric-oxyhydroxide phases in the clay halo are highly effective scavenging uranium from solution.

Natural analogue studies centred upon uranium dispersion and retardation in the far-field environment have also been carried out at Needle's Eye and Broubster in Scotland, Alligator River in Australia and the Oklo uranium deposits in Gabon. The pitchblende veins at The Needle's Eye, which outcrop on the cliff marking the edge of the pluton (Miller and Taylor, 1966; Basham et al., 1989) act as a source of uranium and the study has included an investigation of the dispersion and retardation of uranium in the post-

glacial sediments stretching below the cliff (MacKenzie et al. 1989). There are two main inputs of dissolved uranium into this sediment system, i.e. surface flow of groundwater from the exposures of the mineralisation in the cliff, and upward flow from the bedrock below (MacKenzie et al. 1989). The fixation of uranium in the sediments is controlled by organic matter (humic layers and roots) and uptake on iron and manganese oxides (Basham et al. 1989; MacKenzie et al. 1989). Uranium was found to accumulate at two distinct levels in the sediment profile, i.e. at around 50 cm depth where it was associated with humified organic matter with fixation due to reduction, and between 100-150 cm, where it was located almost exclusively within discrete plant root structures (Basham et al., 1989).

Milodowski et al. (1989) have undertaken a similar study at Broubster in northeast Scotland where the Caithness Middle Old Red Sandstone contains a laminated limestone (lamellae of limestone and siltstone of age 4×10^8 y, enriched in uranium up to 30 ppm) which acts as a source of uranium to groundwater. A peat bog ($\sim 10^4$ y), containing about 0.1 wt.% U (Gallagher et al., 1971; Michie et al., 1972) about 100 m away was observed to act as a sink for the uranium transported by groundwater. This study has shown that uranium is removed from solution by complexing with organic matter, as well as by scavenging by iron-sesquioxides, resulting in the occurrence of anomalously high uranium in the peat bog.

In the Alligator River studies (Duerden, 1990), uranium and thorium were found to concentrate principally in the iron minerals whereas radium concentrated in the clay-quartz phases. The Oklo natural reactor studies (Curtis et al., 1987) have revealed that fission products and transuranic elements were mostly contained in crystalline uraninite within the reactor

zone, i.e. they remained where they were formed. This is evidence that the movement of these elements is restricted, even in the 2×10^9 y since the early Precambrian as demonstrated in Oklo.

Thus observations of fission products and transuranic elements behaviour in and around ore deposits and in the far-field environment give added assurance that long-distance migration of these elements away from spent fuel in a repository will be subject to retardation, and it is reasonable to assume that the waste radionuclides would experience similar processes.

1.7 The Study Area

The Criffel pluton study site is located in a glaciated terrain on the northern side of the Solway Firth, southwest Scotland (Figure 1.1). The pluton measures about 27×10 km and has an elongate shape, with the axis inclining northeast-southwest. Most of the area is upland and exposure of rock is generally very good. The highest peak within the pluton is Criffel (569 m asl) which is found at the eastern end of the pluton.

The main surface water drainage from the area is towards the south, by the Rivers Nith, Urr Water, Kirkgunzeon Lane, Fairgirthlane burn, Southwick burn and Glensone burn which drain into the Solway Firth. The area experiences a temperate climate and about 50% is covered by forest, with the remaining land being used for cattle farming and agriculture. Along the Solway Coast are extensive floodplain and intertidal silt and mud deposits. The salt marsh areas of the floodplain, which are known locally as "Merse" were laid down in the past 10000 y or so upon bedrock comprising Silurian

hornfelsed siltstone faulted against Carboniferous limestone, grits and shales.

The Criffel pluton intruded sedimentary rocks of Lower Palaeozoic age and forms a marked physiographic feature, standing out above the greywacke and shale in which it is emplaced. The geology of the Criffel pluton and the surrounding area is reported in detail by MacGregor (1937 and 1938), Phillips (1956), Stephens (1972), Halliday et al., (1980), Phillips et al (1981), Courrioux (1987) and Craig (1991). Rb-Sr dating has revealed that the pluton was emplaced towards the end of the Caledonian orogeny some $397 \pm 2 \times 10^6$ y ago (Halliday et al., 1980), and was intruded into Ordovician and Silurian greywackes, siltstones and shales. The sediments were deposited along a destructive oceanic margin. They were strongly folded about a NE-SW axis prior to igneous activity. When the foldbelt stabilised the Lower Palaeozoic rocks in the Dalbeattie area were subjected to contact metamorphism and hydrothermal alteration, on intrusion of the Criffel granodiorite. During, and shortly after the emplacement of this granodiorite, large numbers of NW-trending granite porphyry and porphyrite dykes were emplaced in both the intrusion and its surrounding aureole (Phillips, 1956).

A detailed petrological study of the western part of the pluton was first attempted by MacGregor (1937, 1938), who suggested that the quartz-diorite complex found in the hills west of the main pluton may have been formed by the process of granitisation. Phillips (1956), Stephens (1972) and Stephens and Halliday (1980) extended this work and divided the pluton into two main parts comprising a discontinuous outer ring of granodiorite and an asymmetrically placed inner core of granite i.e. the pluton is complex with a margin comprised of more basic rock than the core. Stephens (1972) also demonstrated that steeper gradients in chemical composition occur in the

boundary zone between the granite and granodiorite. Stephens et al. (1985) further refined the description of the pluton, dividing it into five zones on the basis of petrographic studies, rare earth element distributions and Sr and O isotope data. This classification, indicating inner to outer progression is summarised as follows (Figure 1.15): (i) Biotite muscovite granite (BM), (ii) Muscovite biotite granite (MB), (iii) Biotite granite (B), (iv) Hornblende biotite granodiorite (HB), and (v) Clinopyroxene hornblende biotite granodiorite (CHB).

The modes and petrologic ranges in the Criffel pluton for typical granodiorite and granite are shown in Tables 1.3 and 1.4 respectively (Stephens and Halliday, 1980). Sphene and apatite are the common accessory minerals in granodiorite. Xenoliths are common near the outer contact of the granodiorite where it is also well foliated, whereas the granite itself is structurally more isotropic. K-feldspar megacrysts are a feature of the granite and primary muscovite is present only near the centre of the pluton.

There have been many geological investigations and mineral exploration programmes in southwest Scotland since the early part of this century because this area contains several types of mineralisation; and the metal ores of Pb, Zn, Cu, Ni and uranium have been recorded. Details of the uranium mineralisation as well as of the Pb-Zn-Cu and barite veins can be found in Miller and Taylor (1966), Gallagher et al., (1971), Russell (1985), Craig (1991). The exploitation of metalliferous minerals in Scotland came to a standstill in 1953 with the closure of Gasswater barite mine in Ayrshire. Mining at Leadhills, the best-known lead-zinc district in Scotland, continued in a small way after the second world war until 1958, but elsewhere in southwest Scotland there has been negligible recent mining

Figure 1.15: Map of the petrological types of the 5 zones in the Criffel pluton. Letters used are: B, biotite; M, muscovite; H, hornblende; C, clinopyroxene (Based on Stephens et al., 1985).

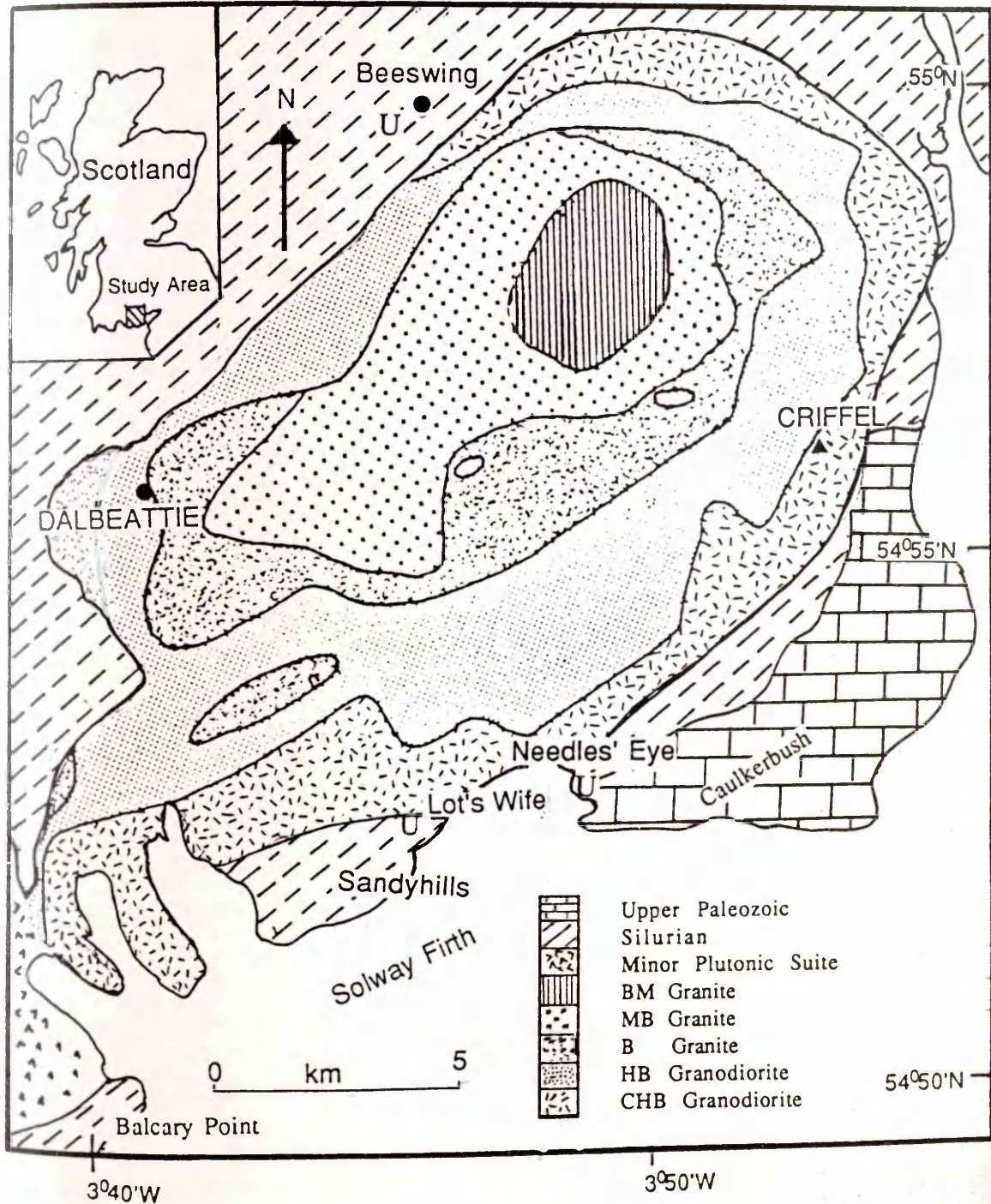


Table 1.3: Modes for typical granite and granodiorite of the Criffel pluton, southwest Scotland (from Stephens and Halliday, 1980).

Mineral	Granite (Sample No. BM/MB-165)	Granodiorite (Sample No: CHB-155)
Quartz	24.0	19.8
Alkali feldspar	30.3	15.0
Plagioclase	39.4	48.1
Biotite	5.0	9.6
Muscovite	0.0	0.0
Hornblende	0.0	6.1
Diopside	0.0	0.4
Magnetite	<0.1	0.5
Sphene	<0.1	0.6

Table 1.4: Petrologic range for typical BM-, MB- and B-granite and HB- and CHB-granodiorite of the Criffell pluton, southwest Scotland (from Stephens and Halliday, 1980).

Sample no.	BM-174	MB-272	B-205	HB-244	CHB-244
SiO ₂	72.00	71.60	68.70	64.70	66.80
TiO ₂	0.01	0.08	0.41	0.45	0.55
Al ₂ O ₃	14.75	15.05	15.74	15.62	14.76
Fe ₂ O ₃	0.49	1.30	1.73	1.80	1.95
FeO	0.30	0.64	0.99	1.66	1.58
MnO	0.02	0.04	0.06	0.05	0.05
MgO	0.43	1.14	1.55	2.45	2.40
CaO	0.68	1.33	1.42	3.97	3.05
Na ₂ O	4.00	4.10	3.80	4.40	4.10
K ₂ O	5.30	4.40	4.80	3.40	3.70
P ₂ O ₅	0.08	0.17	0.25	0.31	0.26
Thornton and Tuttle index	91.66	87.52	84.10	72.76	76.29
Rb (ppm)	259	184	181	121	145
Sr (ppm)	152	338	585	922	648
⁸⁷ Rb/ ⁸⁶ Sr	4.952	1.576	0.8963	0.3805	0.6478
⁸⁷ Sr/ ⁸⁶ Sr	0.73487	0.71538	0.71104	0.70736	0.70929

activity (Gallagher et al., 1971).

In a survey for economic deposits of uranium, Miller and Taylor (1966) located 60 mineralised structures/veins along the southern edge of the Criffel pluton and identified 13 of them as containing visible amounts of pitchblende. The uraniferous veins generally occupy NW faults and outcrop at various localities in the cliffs between Balcary Point and Caulkerbush. The localities showing strong radioactivity are at Portling to Sandyhills Bay, Powbrade Burn, Marbrue Cove, Steps, Lot's Wife and Needle's Eye, with some weakly radioactive sites located at Balcary Point, on the shore south of Rockcliff, at Castle Point and opposite Guther's Isle. Gallagher et al. (1971) have also identified two to three discontinuous uraniferous quartz veins which were exposed in a small quarry near Beeswing, just outside the granodiorite contact. The Beeswing veins occur in hornfelsed Silurian greywackes and the radioactive mineral is mainly uraninite.

Most of the uranium-bearing veins in the cliffs between Balcary Point and Caulkerbush are structurally comparable to, but probably later than, the larger Pb-Zn-Cu and barite deposits further west (Miller and Taylor, 1966; Gallagher et al., 1971). They occupy lines of tectonic disturbance which range from simple parallel-sided open-fissures to brecciated zones a metre or so wide. In open fissures the mineralisation displays a crustified, vuggy texture, but in the brecciated zones it forms a cement between the component fragments of country rock. The dominant gangue minerals in the veins are quartz and dolomite with smaller amounts of calcite and barite. Pitchblende most commonly occurs as colloform bands up to 20 mm in width either adjacent to vein walls or mantling fragments of country rock in vein breccias. It also forms sub-spherical grains up to 5 mm in

diameter within dolomite, and occasionally coats dolomite rhombs (Miller and Taylor, 1966; Basham et al. 1989). The predominant U mineral is pitchblende, which is associated with hydrocarbon, chalcopyrite, native bismuth and hematite in a carbonate-quartz gangue (Darnley et al. 1962). The chemical composition of pitchblende from Sandyhills analysed by Darnley et al. (1962) is as follows : U_3O_8 (82.19%), ThO_2 (0.007%) and Pb (2.17%); and x-ray fluorescence showed: (U) major; (Pb) minor; and (Fe, Y, Dy, Gd, Sm, Zr, Bi, Ce, Mn, Nd, Cu, Er) trace.

Uranium and copper minerals also occur late in the paragenetic sequence in some vein lead-zinc deposits in Scotland (Tyndrum and Inverneil) and in a pyritiferous portion of the lead-zinc vein at Great Laxey in the Isle of Man (Davidson and Bowie, 1951; Darnley et al., 1962; Miller and Taylor, 1966;). The uranium and copper (plus iron) sulphide minerals often occur associated with hydrocarbons. Such is the case too in the 185×10^6 y veins along the southern margin of the Criffel granite though, here, earlier galena and sphalerite appear to be absent (Miller and Taylor, 1966). Instead there is some pyrite and strong developments of hematite. Perhaps bacteriogenic reduction of the U^{6+} and Cu^{2+} complexes is combined with the oxidation of iron sulphide to the hematite, as well as oxidation of the hydrocarbons to CO_2 (Lovely et. al., 1991) and hydrogen to water (Levinson, 1977); the complexes themselves may have been finally delivered to the reducing sites in the last, oxidizing stages of large scale free convection cells some 160×10^6 y after pyrite deposition (Russell, 1983).

Three main features appear to have controlled the localization of the uranium mineralisation in the Criffel area; (i) the aureole of the Criffel granodiorite; (ii) the NE coastal fault; and (iii) the juxtaposition of Carboniferous beds and hornfels along this belt (Miller and Taylor, 1966).

The Criffel uranium veins are remarkably homogeneous both in physical characteristics and mineralogical content. At Needle's Eye the early quartz and main carbonate-quartz phases both occur within a structure which cuts the youngest (L. Carboniferous) rocks in the area. The field evidence implies that both phases are post-Lower Carboniferous but it defines no minimum age. Pitchblende from Step's vein in the Sandyhills area has been dated by the U-Pb method as $185 \pm 20 \times 10^6$ y (U. Triassic to L. Jurassic), whereas the barite deposits are probably Carboniferous, i.e. $\sim 360 \times 10^6$ y (Darnley et al., 1962; Patrick and Russell, 1989). Generally, the Criffel mineralisation is similar to the other uranium deposits in Scotland and the Isle of Man (Gallagher et al., 1971).

1.8 Objectives of the study

The objective of this research is to provide information on the distribution of natural radionuclides and rare earth elements in the environment of the Criffel pluton and to assess the behaviour of these species during geosphere transport in the context of an analogue study of relevance to far-field transport of radionuclides released from an underground repository.

Specific objectives were:

- a. To evaluate variations in the distribution of uranium and thorium and natural decay series disequilibrium in rock samples from different zones of the Criffel pluton in an attempt to define migration and retardation processes affecting uranium in the bedrock environment of the individual zones as well as the entire pluton.

- b. To investigate the distribution and geochemical behaviour of natural decay series radionuclides and rare earth elements about redox

fronts associated with water-bearing fracture systems from Craignair quarry. In this case the aim was to use the data to investigate the mechanisms of migration and retardation (fracture flow, sorption, matrix diffusion and redox front processes) of these species in a water bearing fracture.

c. To assess the spatial distribution of uranium in thin sections of rock from the Craignair quarry by fission track mapping in order to provide information on the mineralogical associations of uranium in the vicinity of the water-bearing fracture and redox front.

d. To investigate the distribution and geochemical behaviour of natural decay series radionuclide and rare earth elements in core samples from surficially weathered granite and granodiorite from Kinharvie and Clifton respectively, in order to evaluate the geochemical behaviour of these elements during weathering, in particular as a result of intensive weathering since the end of the last glacial period 12000 years ago.

e. To investigate the distribution of uranium, ^{210}Pb and ^{226}Ra in soil in the vicinity of the pitchblende vein at Beeswing in an attempt to provide an improved understanding of the migration and geochemical associations of these species in soil.

CHAPTER 2

SAMPLING AND ANALYTICAL METHODS

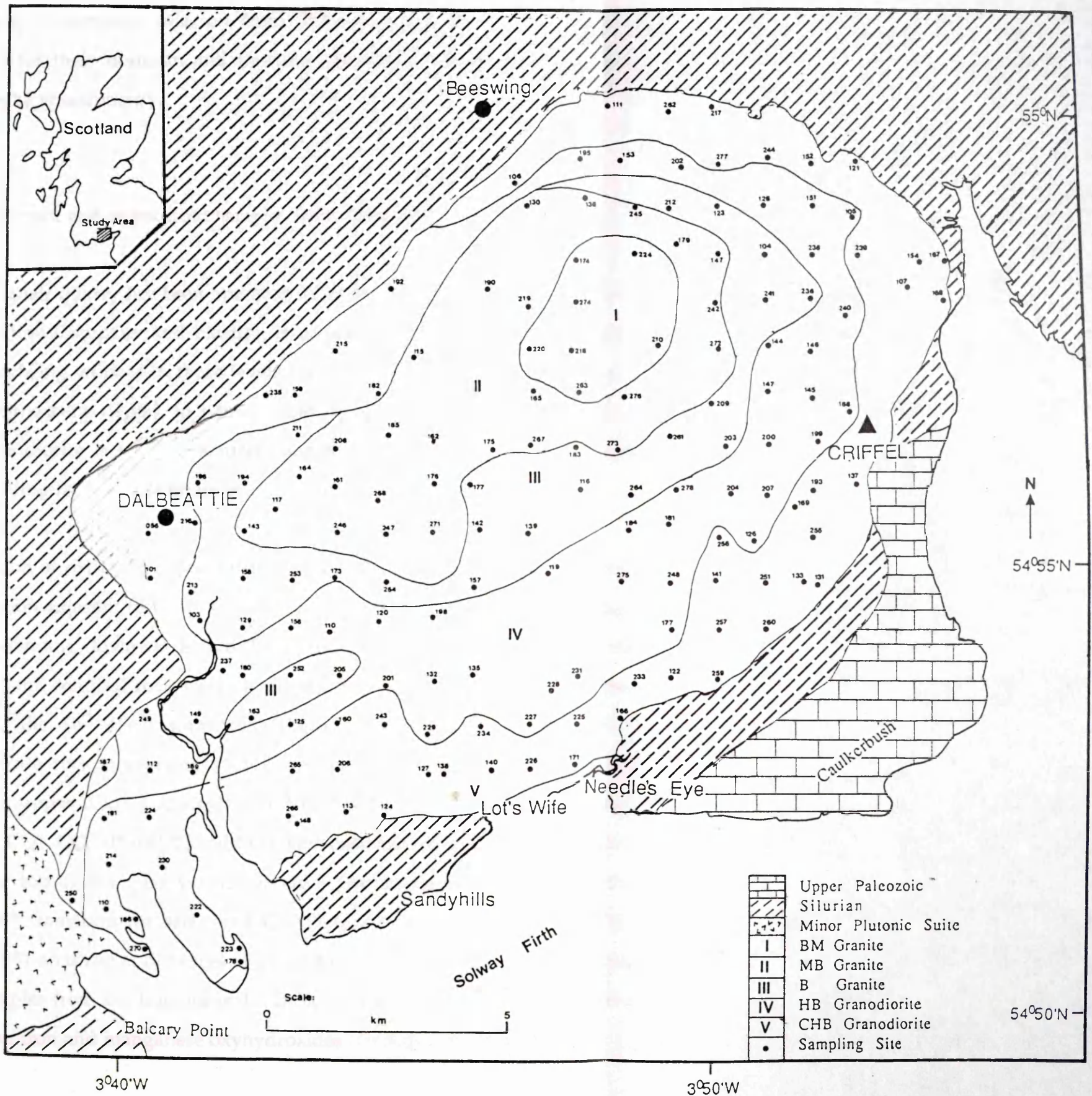
2.1 Summary of samples analysed

Samples of rock, soil and water from the Criffel pluton and adjacent areas were studied during the course of this research. The samples collected comprised: four sections of rock traversing water-bearing fractures from different locations of Craignair quarry; granite and granodiorite samples, including both weathered and unweathered sections, from Kinharvie and Clifton; stream water samples from seven selected streams in the pluton; soil samples from Beeswing. The localities of the sampling sites are shown in Figure 2.1. In addition to the above 169 archived powdered rock samples from different zones of the pluton, provided by Dr. E. Stephens of St. Andrews University, were also used in this study.

2.1.1 Granite and granodiorite samples from different zones of the Criffel pluton

169 rock samples from various zones of the Criffel pluton, which were collected on the basis of the Ordnance Survey one kilometre grid by Dr. E. Stephens in the late 1960s, were used in the present study (Figure 2.2). Only 'fresh looking' samples were collected using a chisel with geological and sledge hammers. A composite sample from a few parts of each exposure was normally taken. In order to remove weathered surfaces the samples were split in the laboratory using a hydraulic press with hardened steel jaws. Only fresh fragments were taken for analysis (Stephens, 1972).

Figure 2.2: Location map and simplified map of the Criffel igneous rocks, southwest Scotland. Letters used represent: B, biotite; M, muscovite; H, hornblende; C, clinopyroxene (Based on Stephens, 1972 and Stephens et al., 1985).



150 of these samples were analysed for their uranium and thorium concentrations using instrumental neutron activation analysis. The remaining 19 samples, selected from different zones of the pluton were analysed for their uranium and thorium concentrations and activity ratios using alpha spectrometry.

2.1.2 Fracture and redox front samples from Craignair quarry, Dalbeattie

The Craignair quarry has been operated for more than 30 years by the Tarmac Construction Company and blasting is usually carried out fortnightly. The quarry is being worked in three levels (upper, middle and lower levels, each of about the same depth), to a total depth of approximately 30 m (Plate 2.1). The granodiorite is highly fractured, and the fractures are normally coated with infilling-fracture materials of iron oxides (hematite).

Penetration of oxidising groundwater down fissures in the rock has resulted in oxidation adjacent to the fissures, giving rise to narrow V-shaped oxidised zones extending downwards into the granite. The redox fronts between the oxidised and reduced rock were clearly visible as a change from red to grey marking the $\text{Fe}^{2+}/\text{Fe}^{3+}$ transition (Figure 2.3). Three sections of HB-granodiorite rock, traversing such water-bearing fractures, were collected from the upper (CQ1 and CQ2) - and middle (CQ3) - level of the quarry. Samples CQ1, CQ2 (Plate 2.2) and CQ3 were collected from about 2, 8 and 20 m from the top of the quarry respectively. The colour change marking the $\text{Fe}^{2+}/\text{Fe}^{3+}$ transition for samples CQ1 (Plate 2.3 and Figure 2.4) and CQ2 (Figure 2.5) occurred at distances of about 4 cm and 1 cm respectively into the rock samples from the fracture wall. In both cases the fracture surface had a coating of iron and manganese oxyhydroxides (FeOOH ; MnOOH), clay

Plate 2.1: Photograph of the Craignair quarry study site showing the location from which samples were collected.



Plate 2.2: Photograph of the Craignair quarry study site showing the location from which sample CQ2 was collected.



Figure 2.3: Schematic diagram showing the $\text{Fe}^{2+}/\text{Fe}^{3+}$ redox fronts in the Craignair quarry, resulting from the penetration of oxidising groundwater into the fracture system.

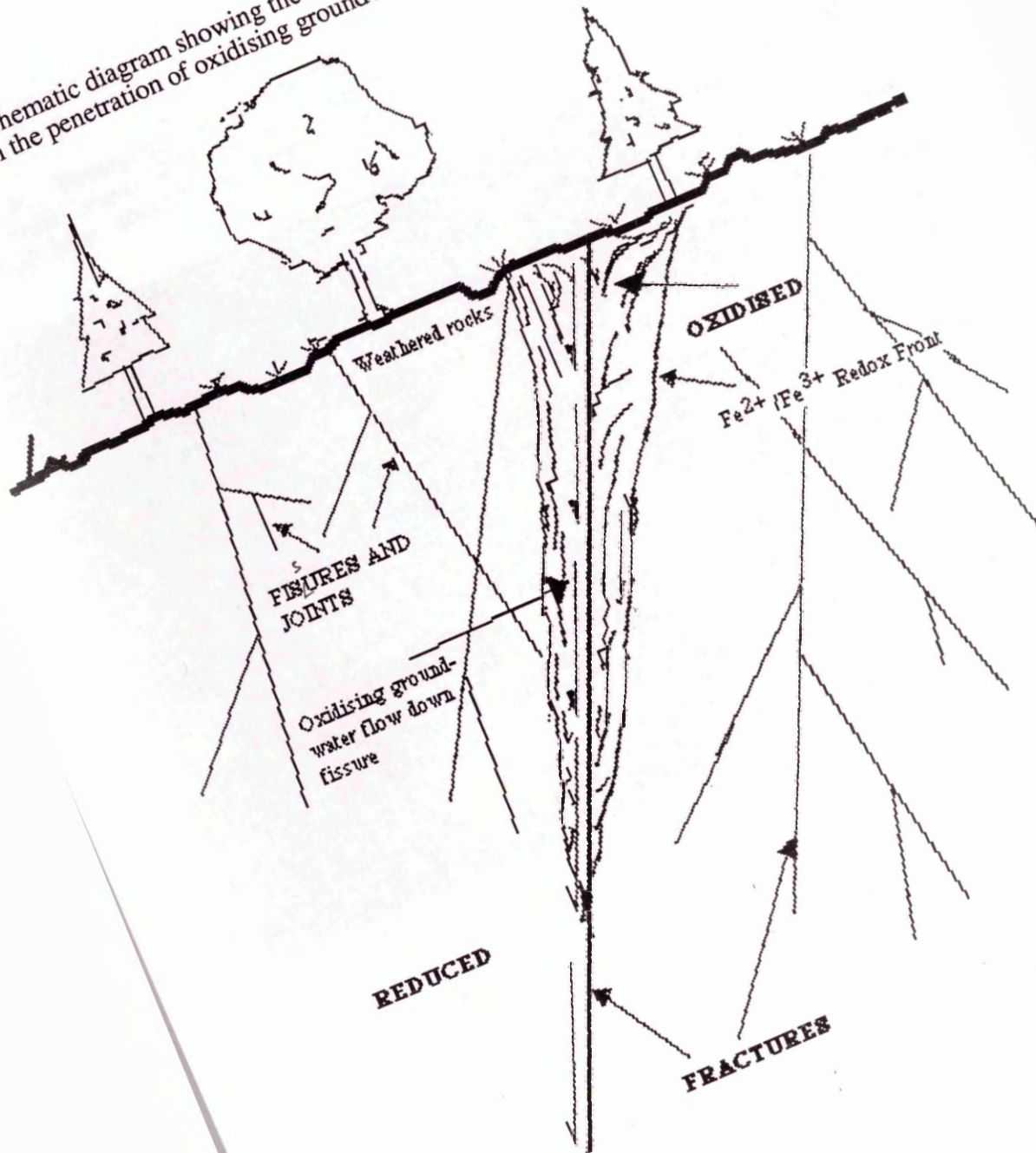


Plate 2.3: Photograph of sample CQ1 showing the $\text{Fe}^{2+}/\text{Fe}^{3+}$ redox front about 4.0 cm from the fracture face. Sample collected from about 2 m from the surface.

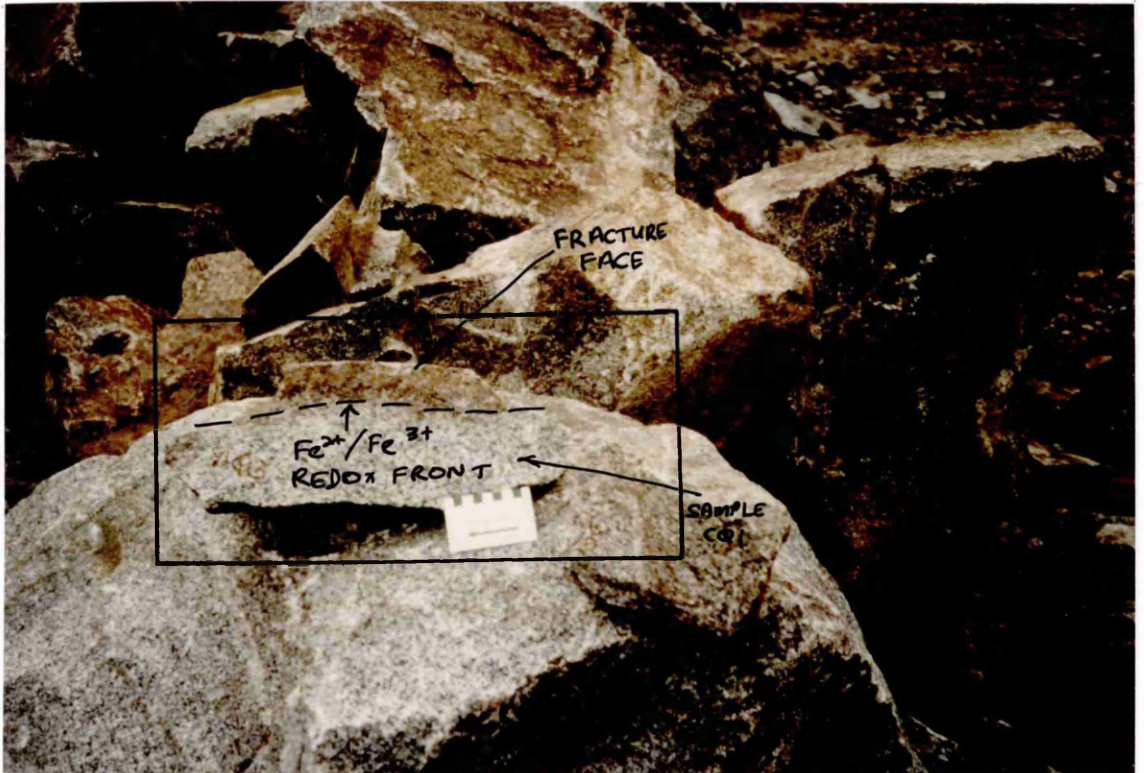


Figure 2.4: Sketch showing relation of rock sample from location CQ1 in Craignair quarry, to fracture face and subsequent division of sample into 1 cm slices.

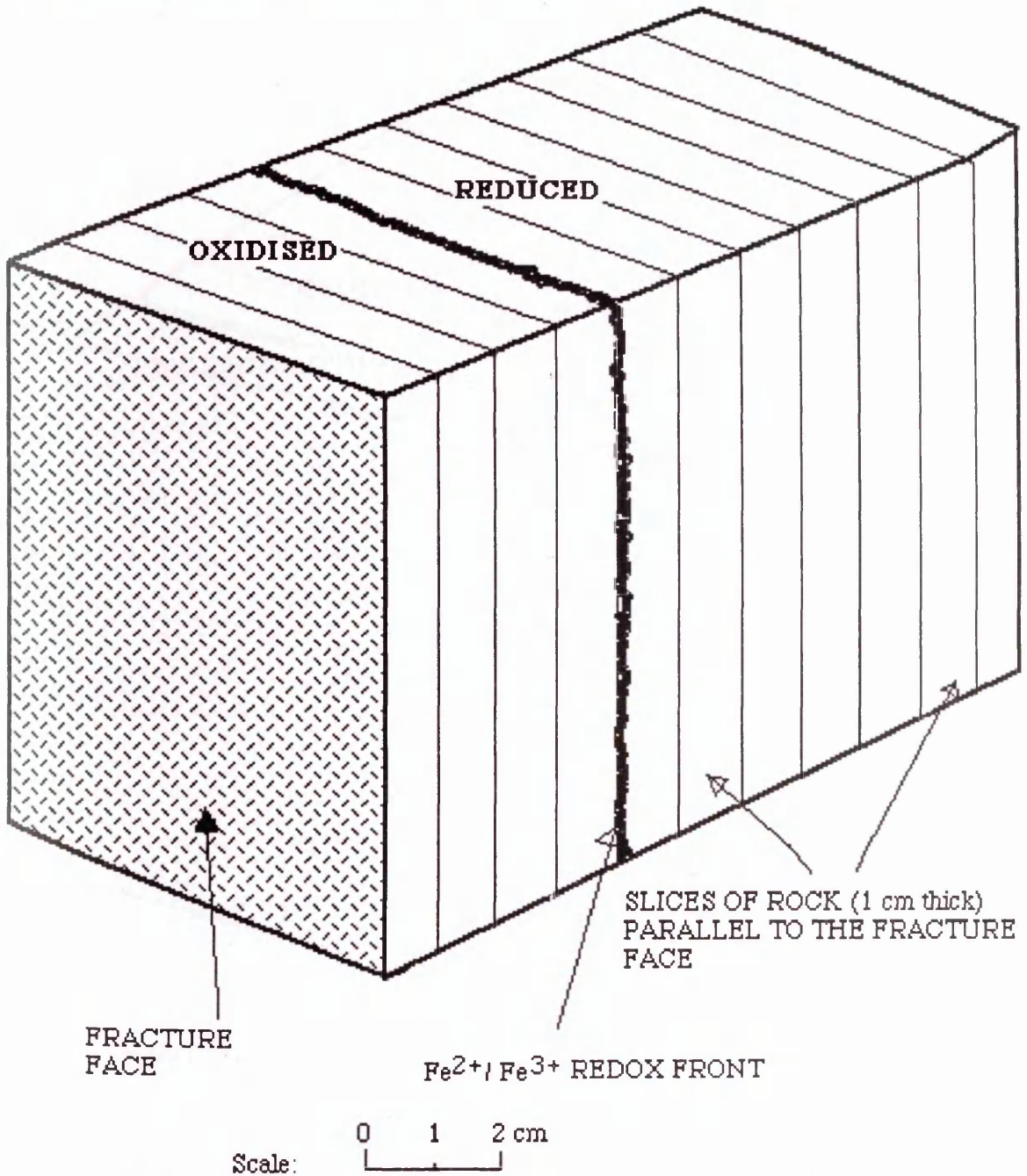
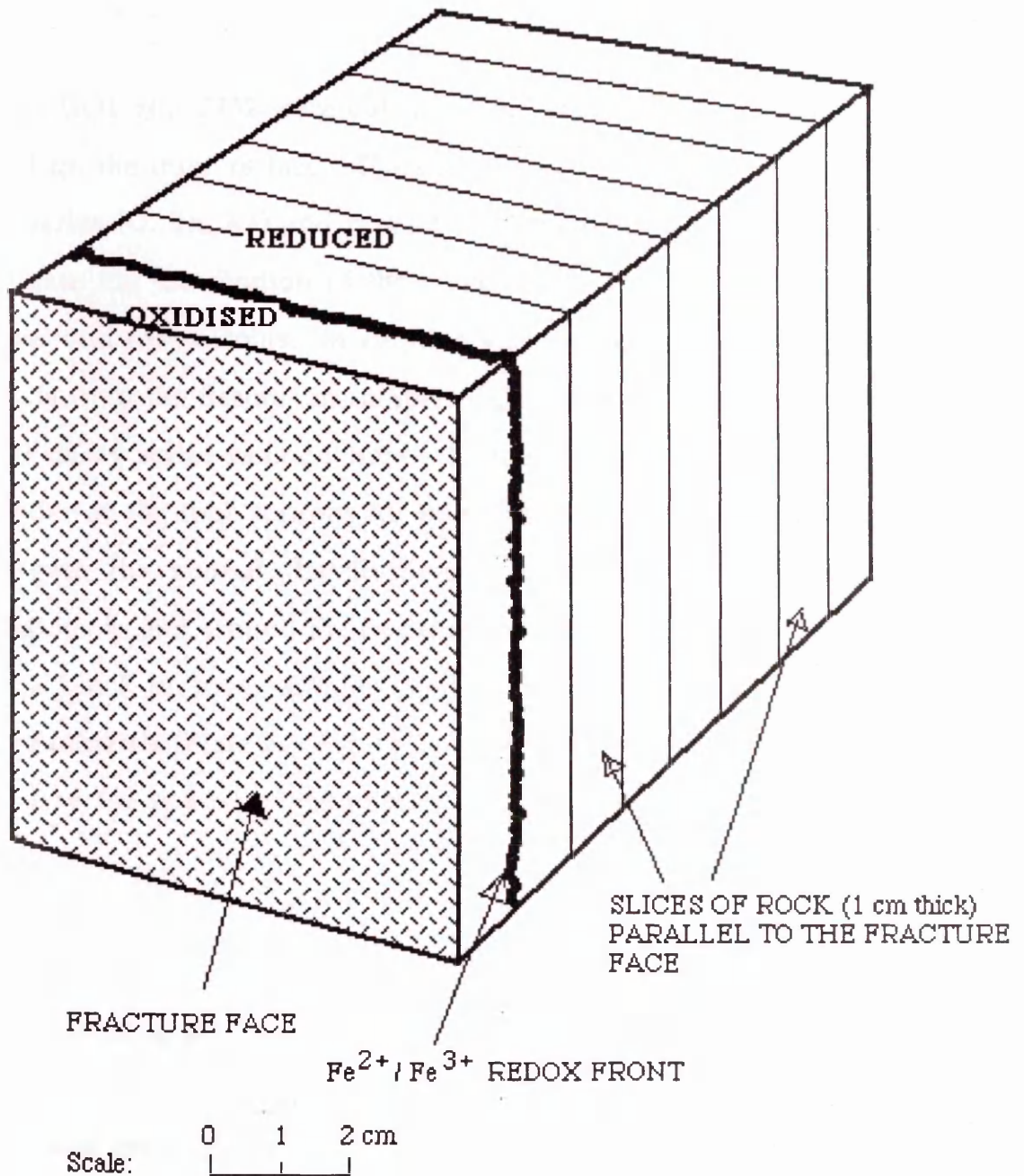


Figure 2.5: Sketch showing relation of rock sample from location CQ2 in Craignair quarry, to fracture face and subsequent division of sample into 1 cm slices.



minerals (determined by the scanning electron microscopy method) and carbonate minerals (reaction with dilute hydrochloric acid). Sample CQ3 was 'fresh looking' and had only a thin coating of iron on the fracture walls (Plate 2.4).

Samples CQ1 and CQ2 were cut into 1 cm slices working away from, and parallel to, the fracture face. The slices of rock were powdered for natural decay series (U, Th, Ra) and rare earth element (REE) analyses in order to investigate the distribution of these species in the rocks in relation to the fractures and redox fronts. In addition surface scrapings of fracture-infilling materials from the fissures in samples CQ1 and CQ2 were also analysed for natural decay series radionuclides. Thin sections were prepared from the remainder of the rock sections for mineralogy and fission track analyses to investigate the spatial distribution of uranium and its mineralogical associations in and around the fractures and redox fronts. In addition to the above a block of rock sample (CQ4) containing V-shaped fractures with infilling-minerals (Plate 2.5; Figure 2.6) was collected from the upper level of the quarry for spatial distribution studies of uranium using fission track analysis.

2.1.3 Weathering profile samples of granite and granodiorite

Granite and granodiorite rock samples were collected from Kinharvie and Clifton respectively (Figure 2.1) in order to investigate the extent of weathering since the last period of glaciation (~12000 y BP). These samples were taken from natural outcrops in the escarpments of the pluton. Blocks of granite (GR) and granodiorite (GD) measuring about 30 cm (l) x 25 cm (w) x 22 cm (h) and 30 cm x 20 cm x 45 cm respectively were extracted from the site

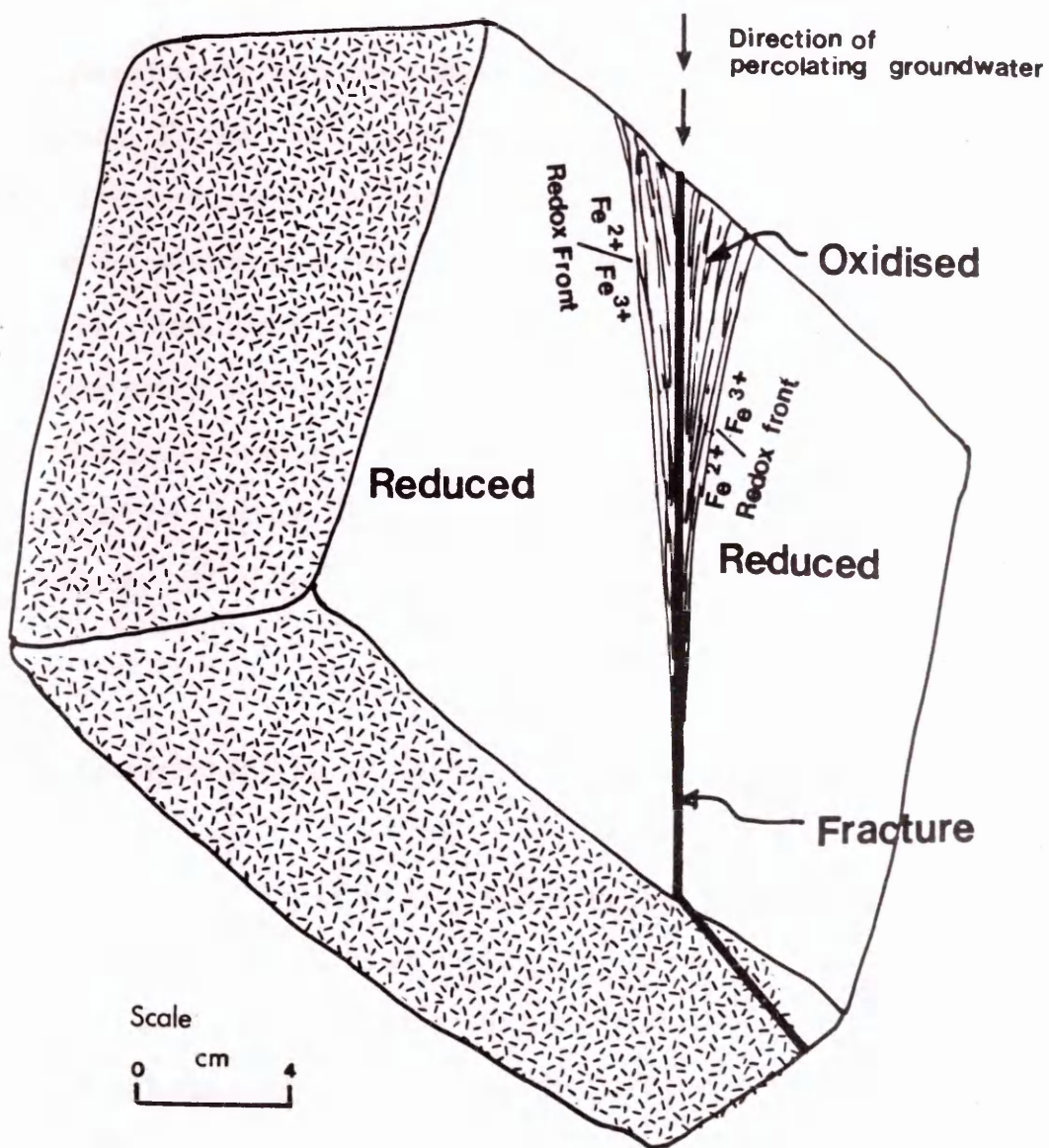
Plate 2.4: Photograph of sample CQ3 showing a thin coating of iron-oxyhydroxides along the fractures. Sample collected from about 20 m from the surface.



Plate 2.5: Photograph of sample CQ4 showing V-shaped iron-oxyhydroxides infilling fractures. Sample collected from mid level of the Craignair quarry.



Figure 2.6: Sketch of rock sample from location CQ4 in Craignair quarry showing V-shaped fractures containing iron-manganese oxyhydroxides.



using a chisel and a sledge hammer. Both samples were fractured, the granodiorite sample particularly so (Plate 2.6), surface alteration (i.e bleaching and friable nature), becoming less intense away from the exposed faces of the samples and from fractures. Fracture-filling materials included iron oxides (hematite) and clay minerals.

Cores were extracted from the samples, working in at 90° to the weathered surface using "Pacera" coring machine with a 51mm (2") diameter diamond drill bit. The cores were sliced into 1 cm thick sections working in from, and parallel to the weathered surface. Twenty four slices of granite (Plate 2.7) and 44 slices of granodiorite were obtained in this way. Eight granite and 12 granodiorite samples were selected and powdered for analyses to investigate the distribution of uranium, thorium, radium and REE in order to establish the extent of penetration of weathering and, by implication, the ingress of water since the end of the last glaciation.

2.1.4 Soil samples and radioactivity survey at Beeswing

A radioactivity survey over an area at Beeswing on the northern edge of the pluton known to contain two to three impersistent uraniferous veins (Gallagher et al., 1971) was carried out in February, 1990. The veins occur in hornfelsed Silurian greywackes and the radioactive mineral is mainly uraninite. During Pleistocene times the area was glaciated, and glacial till and fluvio-glacial deposits of sand and gravel cover much of the bedrock. The location of the veins (i.e. source of uranium) was determined using a portable 2" x 2" NaI gamma detector (Plate 2.8) by traversing along the edge of an abandoned quarry (Kirkcudbright - Sheet 5; map reference: 885681) on a sampling grid of 1 m spacing. The quarry was closed about 50 years ago

Plate 2.6: Photograph showing granite core GR collected from Kinharvie.

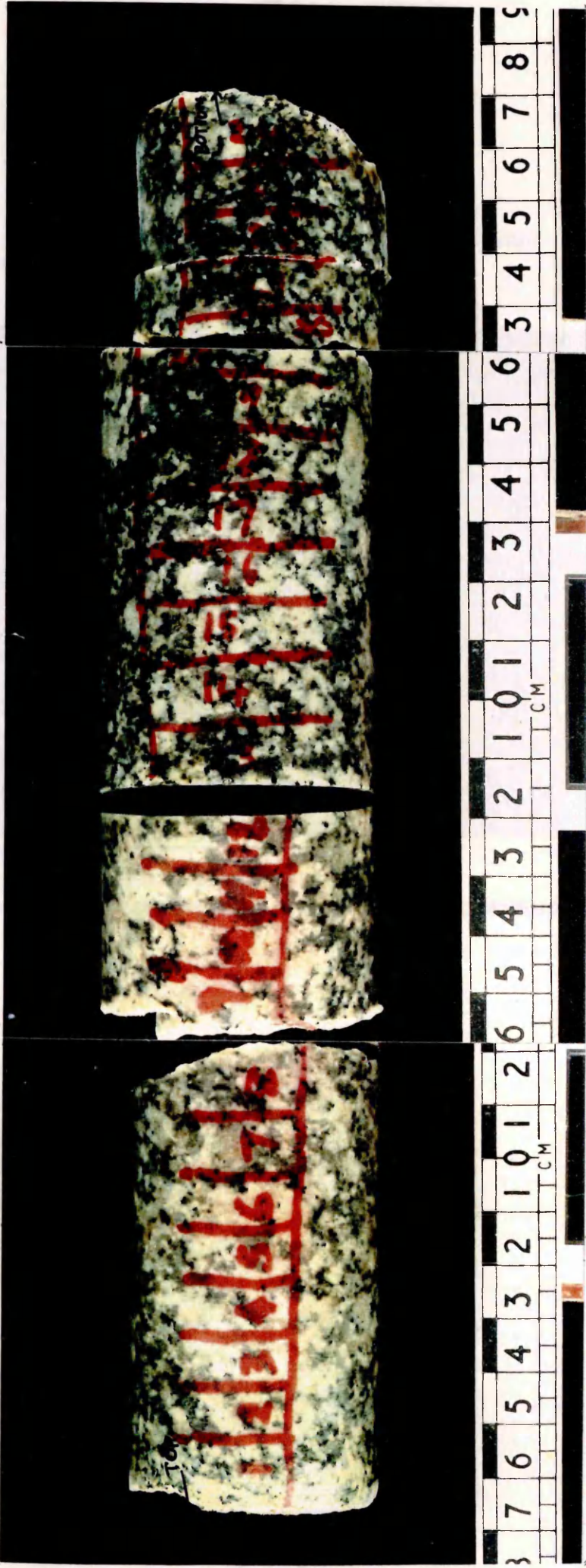


Plate 2.7: Photograph of granodiorite core.GD from Clifton showing complex fracture system.

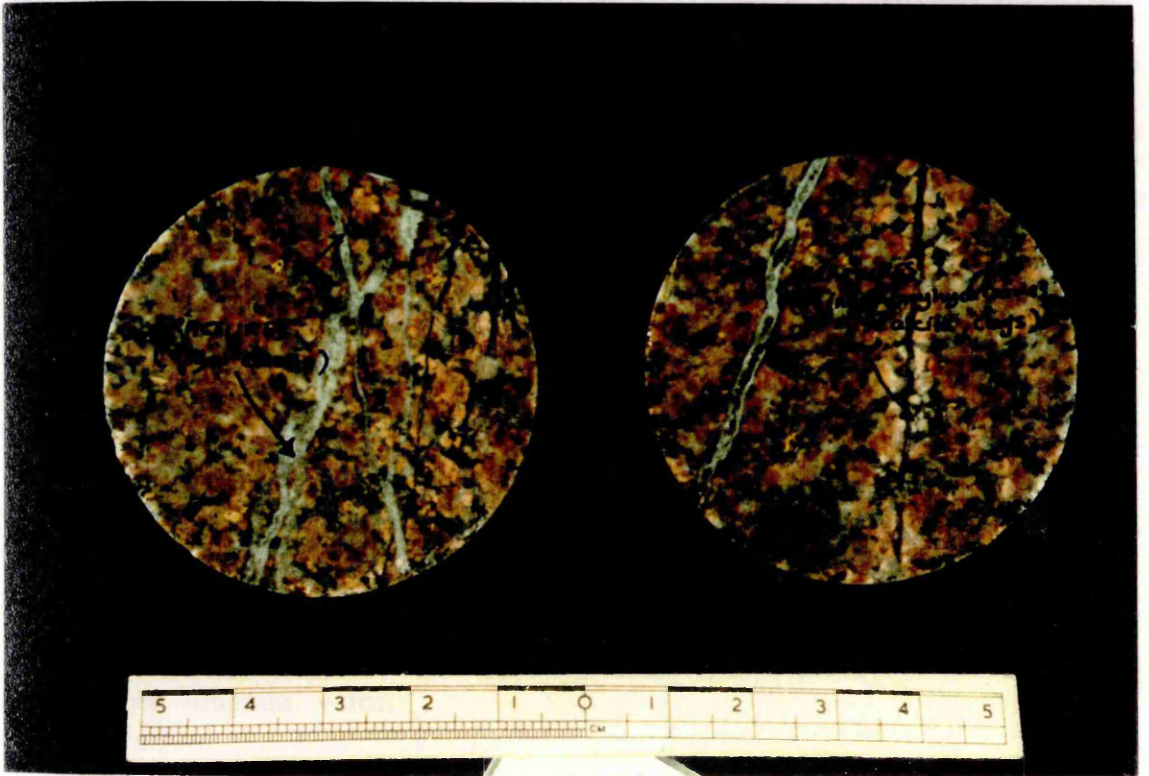


Plate 2.8: Photograph of portable NaI detector used in locating uranium veins at Beeswing.



Plate 2.9: Photograph of the Beeswing study site showing location of uranium veins.



(Henderson, 1991), and was backfilled with quarry spoil, the backfill itself now covered with a peaty silty clay which acts as a potential sink for uranium transported by groundwater flow from the veins (Plate 2.9). This area and its vicinity are grass covered and the fields are used for grazing cattle and sheep.

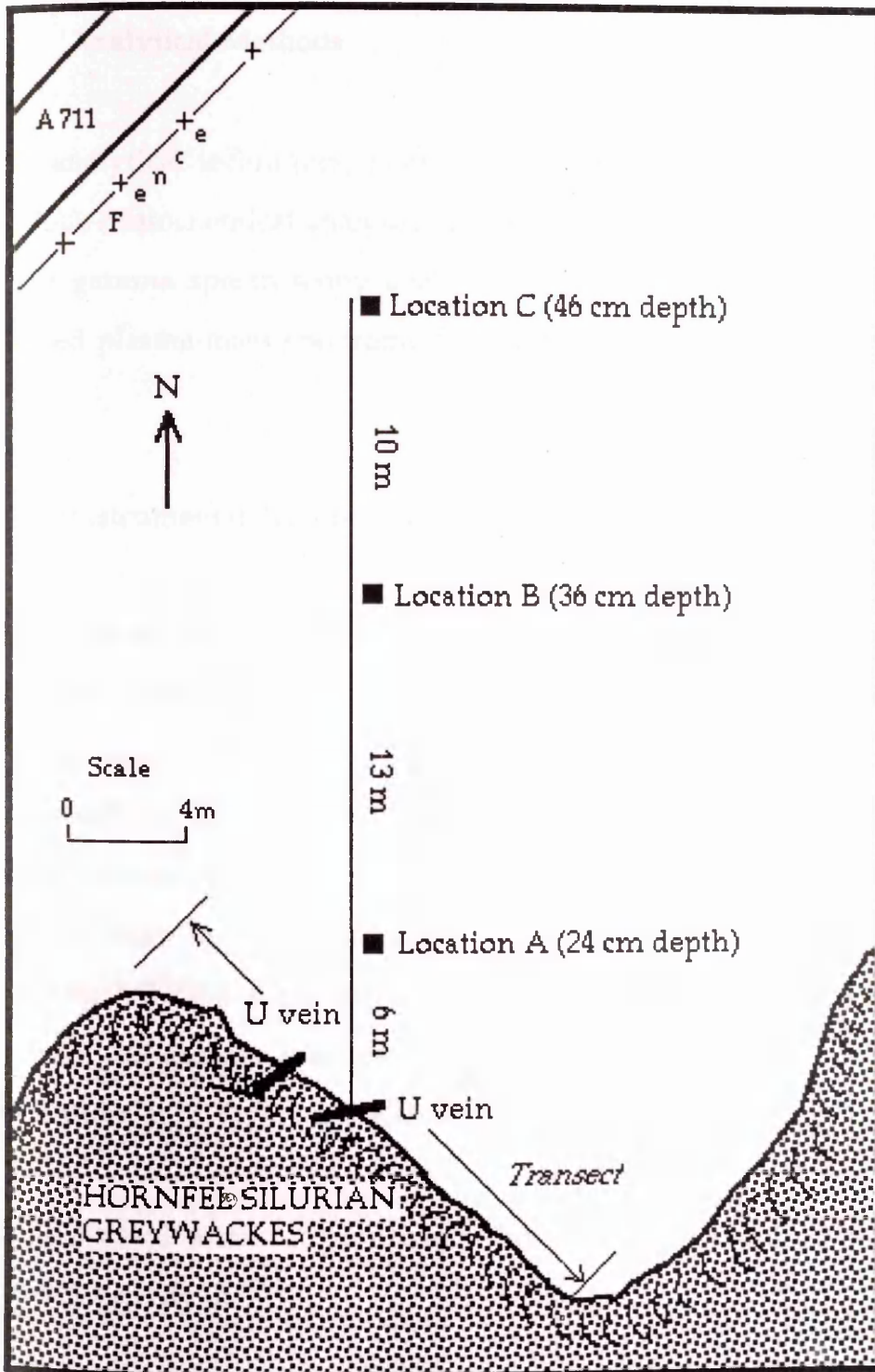
Cores of soil were collected in November 1991 from 3 localities close to the uranium vein at Beeswing. The cores, of lengths 24, 36 and 46 cm, were collected with a hand corer from locations A, B and C respectively shown in Figure 2.7. The cores were sliced into 2 cm thick vertical sections which were transferred to polythene bags and taken back to the laboratory for uranium, thorium, radium, ^{210}Pb , ^{134}Cs and ^{137}Cs analysis.

2.1.5 Stream water samples

One litre samples of stream water were collected in polyethylene bottles from seven locations (Back burn, Fairgirth Lane burn, Southwick burn, Prestonmill burn, Drum burn, Glaisters burn and Kinharvie burn) in November 1991 and April 1992. The sampling locations are shown in Figure 2.1. The water samples were filtered in the laboratory using a $0.2\mu\text{m}$ millipore filter to remove suspended particulates (predominantly silty sand) and were analysed for uranium and thorium by ICP-MS as described in section 2.2.4.

In addition a 20 litre water sample was collected in a polyethylene bottle from Kinharvie burn in November 1991 for analysis of uranium and thorium concentrations and activity ratios. The sample was acidified with 1M nitric acid (~20 ml) in order to prevent precipitation or sorption of cations during storage (Robertson, 1968). Upon return to the laboratory the sample was

Figure 2.7: Schematic diagram of the Beeswing study site showing the location of uranium veins, surface transect and soil sections.



filtered using a Whatman No.1 filter paper to remove suspended sediment.

2.2 Analytical Methods

Five analytical techniques, namely instrumental neutron activation analysis (INAA), radiochemical analyses of uranium and thorium by α -spectrometry, direct gamma spectroscopy analysis, fission track analysis and inductively coupled plasma-mass spectrometry (ICP-MS) were employed in this work.

2.2.1 Instrumental Neutron Activation Analysis

Instrumental neutron activation analysis has been extensively used to measure uranium and thorium concentrations in geological samples (Gordon et al., 1968; Brunfelt and Steiness, 1969; DeSoete et al., 1972; Topping and MacKenzie, 1988). In the present study it was used to quantify the concentrations of uranium and thorium in the granite and granodiorite samples from the different zones of the pluton and in soil samples from Beeswing. Details of the principles and theory underlying neutron activation analysis and gamma spectroscopy can be found in Adams and Dams (1970), Friedlander et al. (1981) and Keller (1988).

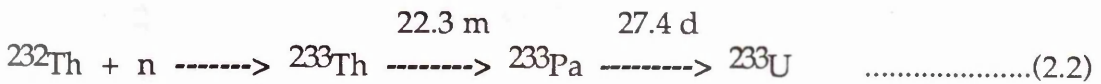
In the present work uranium concentrations were derived by measuring the induced activity of ^{239}Np :



^{239}Np has a half life of 2.35 d and has photopeaks at 277.5 keV (14.1%), 228.2

keV (10.7%) and 210.0 keV (3.4%) (Friedlander et al., 1981). The 277.5 keV photopeak has the highest intensity and is free from any gamma-ray interferences and was, therefore, used for evaluation of the uranium contents of the samples. The 210 keV photopeak was not used since it has the lowest intensity and was not detected in many samples. The 228.2 keV photopeak was not used either since, although it gives high count rates, it has a possible interference from the 229 keV gamma-ray of ^{182}Ta .

Thorium contents of the rock samples were derived by measuring the induced activity of ^{233}Pa :



^{233}Pa has a half-life of 27.4 d and its photopeak at 311.9 keV (intensity 36%) is free from significant interferences (Friedlander et al., 1981).

Uranium and thorium standard solutions were prepared from analytical grade uranyl nitrate $[(\text{UO}_2(\text{NO}_3)_2 \cdot 6\text{H}_2\text{O})]$ and thorium nitrate $[(\text{Th}(\text{NO}_3)_4 \cdot 4\text{H}_2\text{O})]$ respectively and their concentrations, given in Table 2.1, were determined by alpha spectrometry. Uranium and thorium standards were prepared for irradiation by drying 0.1 ml of the standard solutions on 0.2g of acid-washed sand which was then wrapped in aluminium foil. Blank washed sand was also included for the measurement of background uranium and thorium values present in the sand. Reference materials, IAEA Soil-7 (IAEA, 1984) and Edinburgh Clay prepared by the Royal Museum of Scotland (Tate, pers. comm.) were included to evaluate the accuracy of the analysis.

About 0.2 g of each of the finely powdered (250 mesh size fraction) samples

Table 2.1. Results of alpha spectroscopic analyses of uranyl nitrate and thorium nitrate for preparation of uranium and thorium standards for instrumental neutron activation analysis.

Sample No	Uranium (mg l ⁻¹)	Thorium (mg l ⁻¹)
1	13.8 ± 0.5	14.5 ± 0.6
2	14.1 ± 0.5	14.8 ± 0.6
Mean values	13.9 ± 0.5	14.7 ± 0.6

and reference materials was weighed and wrapped in aluminium foil (12 x 12 mm). Small variations occur in the neutron flux experienced by individual samples, standard and reference materials, during the irradiation. In order to compensate for this, flux monitors of Specpure iron wires weighing about 0.02 g were attached to all samples and standards. Each sample, standard and reference material was again wrapped in aluminium foil, to hold the flux monitors and as a secondary containment in case of rupture of the first aluminium layer. The sample identification code was marked on the aluminium foil. Batches of 12 samples, washed sand, uranium and thorium standards and reference materials, were packed together for irradiation in a boron carbide tube in order to minimise activation by thermal neutrons (Brunfelt and Steiness, 1969; Hanna and Al-Shahristani, 1977).

All irradiations were performed in the central vertical stringer (cvs) of the UTR-300 nuclear reactor of the Scottish Universities Research and Reactor Centre (SURRC) for six hours at a neutron flux of $3 \times 10^{12} \text{ n cm}^{-2} \text{ sec}^{-1}$. The samples were left to 'cool' for a period of four days before processing to allow decay of short-lived nuclides such as ^{24}Na , ^{28}Al and ^{42}K , so that they were radiologically safe to handle. They were then unwrapped behind lead shielding, transferred to labelled polythene bags and stored behind lead prior to counting. A high resolution intrinsic Ge gamma-ray detector (EG and G Ortec GAMMA-X; 80 cm³ active volume, resolution 1.8 keV at 663 keV) was used for uranium and thorium determinations and a smaller Ge(Li) detector (25 cm³ active volume, resolution 1.9 keV at 663 keV) was used for determining the induced activities in the flux monitors. The gamma spectroscopy system comprised an EG & G 918 ADCAM multichannel buffer interfaced with a computer, and spectra were analysed by the Ortec software package MINIGAM 2. All samples, standards and reference materials were held on a perspex sample holder during γ - spectroscopy analysis to give a

highly reproducible geometry at a height of 2 cm above the detector with a suitable dead time (< 10%). In order to minimise background, 4" Pb shielding was used and only the sample which was being counted was in the counting room. Counting times of samples varied between 1 and 3 hours to give suitable counting statistics.

Neutron flux variations were corrected for by assuming that the specific activity induced in the flux monitor for each sample is proportional to the neutron fluence that it experienced. The iron wires were counted in a standard geometry and in each case the ^{59}Fe count rate was calculated at a defined reference time. The observed gamma spectroscopy results for both uranium and thorium were, during subsequent computer based calculations, normalised to an average flux based upon the flux monitor results.

The element concentrations were calculated using the SURRC neutron activation analysis programme NAA (Harris, 1989) which takes the output file from the Ortec MINIGAM 2 programme directly from disc and performs a conventional activation analysis calculation based upon the following equation (Adams and Dams, 1970; Friedlander et al., 1981):

$$\frac{\text{Weight of X in sample}}{\text{Weight of X in standard}} = \frac{\text{Count rate of Y in sample}}{\text{Count rate of Y in standard}} \dots\dots\dots(2.3)$$



where, X = element of interest

Y = isotope of element produced by activation

This programme decay corrects observed count rates to a defined reference time and allows for decay during counting. Apriori errors to allow for uncertainties in counting geometry (2%), weights and systematic errors due

to flux variations, are included in calculation of the overall analytical uncertainties. The final results are expressed as concentrations in "ppm". The results for analysis of the IAEA Soil-7 and Edinburgh Clay standard reference materials are given in Tables 2.2 and 2.3 respectively, and show a generally satisfactory accuracy and precision for the method.

2.2.2 Direct gamma spectroscopy analysis

Direct gamma spectroscopy analysis can be applied to the determination of specific activities of gamma-emitting radionuclides in geological and environmental materials without chemical processing of the samples (MacKenzie et al., 1979; MacKenzie and Scott, 1982; Smellie et al., 1986; BenShaban, 1989). The technique was adopted in this study for the analysis of ^{226}Ra in rock samples from the Craignair Quarry, Dalbeattie and also for the analysis of ^{226}Ra , ^{137}Cs , ^{134}Cs and ^{210}Pb in soil samples from Beeswing. The high resolution Ge detector with 4" Pb shielding described above for INAA was used for analysis of the radionuclides and spectra were analysed using the EG and G Ortec software package, MINIGAM 2, as described above. The photopeaks used for analysis of ^{210}Pb , ^{226}Ra , ^{134}Cs , and ^{137}Cs were 47 keV, 59.9 keV, 186 and 609 keV, 604 keV and 662 keV, respectively (Adams and Dams, 1970).

Two types of calibration of the detector were carried out for direct γ -spectroscopy analysis of radionuclides, namely energy calibration and detection efficiency calibration. The energy calibration was regularly performed using a standard sealed solid source of ^{226}Ra . Under normal circumstances the detector was highly stable and showed negligible drift of peak positions over a long period of time. The detection efficiency

Table 2.2. Results of neutron activation analysis of IAEA standard reference material Soil-7 along with certified values (IAEA, 1984).

	Uranium (ppm)	Thorium (ppm)
Certified values	2.6 ± 0.2	8.2 ± 1.3
Observed values		
1	2.3 ± 0.1	6.5 ± 0.4
2	3.0 ± 0.2	7.3 ± 0.4
3	3.0 ± 0.3	7.6 ± 0.3
4	2.8 ± 0.4	7.1 ± 0.7
5	2.5 ± 0.1	6.7 ± 0.5
6	3.0 ± 0.2	7.5 ± 0.4
7	2.9 ± 0.2	6.5 ± 0.4
8	3.5 ± 0.2	7.7 ± 0.2
9	2.5 ± 0.2	7.5 ± 0.5
10	2.2 ± 0.2	6.5 ± 0.3
11	2.7 ± 0.2	7.5 ± 0.6
12	2.8 ± 0.1	6.6 ± 0.4
13	2.3 ± 0.2	6.8 ± 0.5
14	2.9 ± 0.2	6.8 ± 0.6
15	2.9 ± 0.2	7.9 ± 0.6
Avg.	2.7 ± 0.2	7.1 ± 0.5

Table 2.3. Results of neutron activation analysis of 'Edinburgh Clay' standard reference material along with recommended values (Topping and MacKenzie, 1988).

	Uranium (ppm)	Thorium (ppm)
Recommended values	3.4	12.8
Observed values		
1	3.0 ± 0.2	9.9 ± 0.5
2	3.7 ± 0.2	10.1 ± 0.5
3	3.8 ± 0.3	10.8 ± 0.4
4	3.7 ± 0.4	10.5 ± 0.7
5	3.3 ± 0.2	10.8 ± 0.7
Avg.	3.5 ± 0.3	10.4 ± 0.6

calibration for rock samples was carried out using the standard reference material DL-1a (CANMET, 1983) while for soils, standards were prepared by dropwise addition of known activities of standard solutions of ^{210}Pb , ^{226}Ra , ^{134}Cs and ^{137}Cs to materials which resembled the sample composition.

About 20g of each of the finely powdered rock samples from Craignair quarry, Dalbeattie and standard reference material DL-1a (CANMET, 1983) were weighed into polythene containers and wrapped with cling film. They were then placed directly on the top face of the Ge detector, giving a highly reproducible geometry and low dead time ($< 0.1\%$), and counted for at least four days to give suitable counting statistics. Longer counting times of up to seven days were normally employed for samples with low activity. The specific activity of the radionuclides in the sample were calculated using the equation:

$$\text{Activity} = \frac{A}{B} \times C \quad \text{Bqkg}^{-1} \quad \dots\dots\dots (2.4)$$

where,

- A = cps/g of sample
- B = cps/g of standard
- C = activity of the radionuclide in the standard (Bq kg⁻¹)

Wet weights of the soil samples from Beeswing were recorded after which they were dried in an oven at about 100°C ; the dry weights being recorded after drying. The samples were pounded using a mortar and pestle after which sub-samples of about 0.2 g were weighed and ashed in a furnace at 500°C for about three hours, with the weight loss on ignition being taken as the organic content. The organic content of the soil samples range between

about 30% (top layer) and 5% (bottom layer), with most values being about 15%. These data were used to prepare appropriate mixtures of organic (cellulose) and inorganic (SiO_2) components to resemble the sample composition for use in efficiency calibration of the detector. The standards were prepared by dropwise addition of known activities of ^{210}Pb , ^{226}Ra , ^{134}Cs and ^{137}Cs tracers to the appropriate mixture of cellulose and SiO_2 (Table 2.4). About 8 g of each of the samples and standards were weighed and counted in the same geometry, and from the observed counting rates the energy-detection efficiency relationship was found. The activities of ^{210}Pb , ^{226}Ra , ^{134}Cs and ^{137}Cs in the samples were calculated using equation 2.4.

2.2.3 Radiochemical analysis of uranium and thorium

2.2.3.1 Whole rock analysis

Determination of uranium and thorium concentrations and activity ratios in rock samples entails four major steps: dissolution, co-precipitation, separation and α -spectrometry analysis. In the present study the natural decay series analyses were based upon methods described by Bacon and Rosholt (1982), MacKenzie et al., (1986), Smellie et al., (1986) and Alexander and Shimmiel (1990). Full details are provided below. All samples were ground to a fine powder (250 mesh) using a Tema mill for about 5 minutes. Two sets of samples were weighed (about 0.5g each) into teflon digestion vessels. To the first set of samples about 3 ml aqua regia, 1ml 40% hydrofluoric acid and a known quantity of $^{232}\text{U}/^{228}\text{Th}$ spike were added. The second set of samples was treated identically excepting the $^{232}\text{U}/^{228}\text{Th}$ spike, to allow the measurement of actual $^{228}\text{Th}/^{232}\text{Th}$ activity ratios in the samples.

Table 2.4: Activities of ^{210}Pb , ^{226}Ra , ^{134}Cs and ^{137}Cs tracers in standard solution used in soil analysis.

Isotopes	Activity (Bq/0.1 ml)	Date
^{210}Pb	6.31	22.10.90
^{226}Ra	2.27	14.3.91
^{134}Cs	186.48	16.3.89
^{137}Cs	1.0	1.11.87

The digestion vessels were sealed with tight fitting screw-on lids and the samples were then digested in a microwave oven at maximum power in a fume cupboard for 5 minutes after which they were left to cool for about 1 hour (Alexander and Shimmield, 1990). The samples were then transferred to PTFE beakers and evaporated to dryness on a hot plate. Further aqua regia plus 40% hydrofluoric acid digestions were performed on a hot plate in a fume cupboard until total dissolution was obtained, after which the samples were then evaporated to dryness, re-dissolved in 6M hydrochloric acid and transferred into plastic centrifuge tubes.

Uranium and thorium were scavenged from solution by dropwise addition of ammonium hydroxide to the sample solutions to precipitate $\text{Fe}(\text{OH})_3$ using the natural iron in the sample as a carrier. The $\text{Fe}(\text{OH})_3$ precipitate was separated from the supernatant liquid by centrifuging and decanting. The precipitate was then re-dissolved in 9M hydrochloric acid and the iron extracted with di-isopropyl ether.

To separate uranium from thorium the sample was passed through a 6 cm x 1 cm² column of anion exchange resin (Bio Rad AG1-X8, 100 - 200 mesh chloride form) preconditioned with 2 x 15 ml (1M) and 2 x 15 ml (9M) portions of hydrochloric acid. Uranium and iron are strongly held by the resin under these conditions whereas thorium, radium and the alkali and alkaline earth elements pass through. The resin was washed with 40 ml of 9M hydrochloric acid and the combined hydrochloric acid washings were kept for thorium analysis as described below. Uranium was eluted from the resin with 1M hydrochloric acid (4 x 30 ml) and the solution was evaporated to dryness. The residue was re-dissolved in 9M hydrochloric acid and a second anion exchange purification was carried out as described above. The uranium solution was evaporated to dryness and re-dissolved in 9M

hydrochloric acid for a further iron extraction using di-isopropyl ether. About 2 ml of 5% (w/v) NaHSO₄ solution was added to the uranium solution which was evaporated to dryness, and then re-dissolved in 10% (w/v) (NH₄)₂SO₄ solution for uranium electrodeposition.

The thorium solution was evaporated to a volume of about 25ml and then co-precipitation of thorium was performed by addition of concentrated ammonia solution to precipitate Al(OH)₃, using the natural aluminium in the sample as a carrier. It is essential at this stage to remove all Cl⁻ from the sample to avoid formation of uncharged ThCl₄. The precipitate was washed thoroughly with distilled deionised water and shaken vigorously to totally disaggregate it and avoid physical trapping of Cl⁻. The sample was then centrifuged, the aqueous washings discarded and the precipitate containing the thorium re-dissolved in 8M nitric acid. The thorium co-precipitation with Al(OH)₃ and washing were repeated after which the precipitate was re-dissolved in 8M nitric acid and the solution was passed through a Bio Rad AG1-X8 anion exchange column, preconditioned with 2 x 15ml (1M) and 2 x 15ml (8M) nitric acid. Thorium, in the form of [Th(NO₃)₆]²⁻, is strongly held by the resin under these conditions. Elution of thorium was carried out by passing 9M hydrochloric acid (6 x 25ml) through the column. About 2ml of 5% (w/v) NaHSO₄ solution was added to the thorium solution which was then evaporated to dryness after which it was re-dissolved in 10% (w/v) Na₂SO₄ solution for electrodeposition.

If the uranium or thorium residue (i.e. after addition of NaHSO₄ and evaporation to dryness) appeared brown in colour, it was boiled to dryness under reflux with about 5 ml of aqua regia to remove organic materials that may have been derived from the sample or decomposed resin.

Uranium and thorium were electrodeposited from the solutions described above onto 2.5 cm diameter stainless steel discs (planchettes) based upon the method described by Hallberg et al. (1960). Electrolysis was carried out for about 2.5 hours at a voltage of 10 to 15 V and a current of 1.8 Amps, using an electrolysis cell consisting of a cylindrical perspex body, 6 cm in diameter and 10 cm in depth with a screw fitted to a brass base which acts as a sink for the heat produced during the plating process. A platinum wire was used as the anode and the stainless steel disc as the cathode. The plating cell was sealed by use of a teflon coated rubber ring fitted between the cell body and the planchette. At the end of the deposition the solution was made alkaline by adding about 1 ml of concentrated ammonia solution to prevent re-dissolution of the uranium or thorium when the current was switched off. The source was then removed, rinsed with distilled water and acetone and dried on a hot plate. Counting of samples was carried out using a Canberra Quad Alpha alpha spectrometer under high vacuum (10^{-1} mbar), with a counting efficiency of about 30%. Counting times of the samples varied between three and seven days to give suitable counting statistics.

A blank experiment was carried out with all chemicals and resin used in the uranium and thorium analyses for the samples. The results showed that uranium and thorium were undetectable.

The uranium and thorium concentrations and the activity ratios ($^{234}\text{U}/^{238}\text{U}$; $^{230}\text{Th}/^{234}\text{U}$; $^{230}\text{Th}/^{238}\text{U}$) of the samples were determined from the alpha spectra using the following equations.

Specific activity (S.A) of uranium or thorium:

$$\text{Specific activity (dpm g}^{-1}\text{)} = \frac{N_{\text{sample}}}{N_{\text{spike}}} \times \frac{A_{\text{spike}}}{w_s} \dots\dots\dots(2.5)$$

- where, N_{sample} = observed count rate of U or Th isotope in sample (cts)
- N_{spike} = observed count rate of U or Th in spike (cts)
- A_{spike} = spike activity constant of ^{232}U or ^{228}Th (dpm)
- w_s = weight of sample (g)

Concentrations of uranium and thorium in ppm were calculated as follows:

$$\begin{aligned} \text{U concentration} &= (\text{S. A.}) \text{ of } ^{238}\text{U} \times 1.34 \text{ (ppm)} \\ \text{Th concentration} &= (\text{S. A.}) \text{ of } ^{232}\text{Th} \times 4.12 \text{ (ppm)} \end{aligned}$$

The uncertainties were calculated as follows:

% Uncertainties of S.A = $[(\% \text{ uncertainty } N_{\text{sample}})^2 + (\% \text{ uncertainty } N_{\text{spike}})^2]^{1/2} + 1\%$
 Assuming 1% uncertainty for spike calibration and negligible uncertainty for mass.

$$\text{The \% uncertainty for each isotope} = \frac{(N)^{1/2}}{N} \times 100\%$$

where, N = observed activity of respective isotope (cts.)
 therefore,

$$\text{Error} = (\text{S.A}) \times \% \text{ uncertainty of (S. A)}$$

Activity ratio (A.R) of uranium and thorium isotopes were calculated as follows:

$$\text{Activity Ratio (A.R)} = \frac{N_A}{N_B} \dots\dots\dots(26)$$

- where,
- N_A = observed count rate of isotope A (cts).
- N_B = observed count rate of isotope B (cts).

The uncertainties for A.R:

% uncertainty of A. R. = $[(\% \text{ uncertainty of isotope A})^2 + (\% \text{ uncertainty of isotope B})^2]^{1/2}$
therefore,

$$\text{Error} = (\text{A.R}) \times \% \text{ uncertainty of A. R.}$$

The accuracy of the technique was evaluated by analysis of the standard reference material DL-1a from the Canadian Centre for Mineral and Energy Technology, Ottawa. The certified (CANMET, 1983) and experimentally derived values shown in Table 2.5, indicate a satisfactory level of accuracy for the procedure. The precision of the method was evaluated by analysing triplicate fresh rock sample (collected from Craignair quarry, Dalbeattie) and the results, given in Table 2.6., show a satisfactory level of consistency.

2.2.3.2 Soil leaching analysis

Three soil samples (top, middle and bottom of the cores) were taken from locations A, B and C at Beeswing (Figure 2.7) to investigate the geochemical association of uranium and thorium (i.e. leachable and resistate forms). Two sets of samples were weighed (about 0.5g each) in a beaker, and boiled under reflux with about 50 ml aqua regia on a hot plate at a medium setting for about three days. Additional aqua regia was added to the samples as necessary to maintain the volume. The samples were left to cool for one day and separation of the residue and supernatant liquid was carried out by centrifuging and decanting. A known quantity of $^{232}\text{U}/^{228}\text{Th}$ spike was added to the supernatant liquid from the first set of samples. About 3 mls aqua regia, 1 ml 40% hydrofluoric acid and a known quantity of $^{232}\text{U}/^{228}\text{Th}$ spike were added to the residue portion in a teflon digestion vessel. The second set of samples were treated identically, but without addition of

Table 2.5. Results of alpha spectroscopic analyses of standard reference sandstone DL-1a along with certified values (CANMET, 1983).

	^{238}U (BqKg $^{-1}$)	^{234}U (BqKg $^{-1}$)	^{230}Th (BqKg $^{-1}$)
Observed values	1380 \pm 27	1399 \pm 26	1398 \pm 33
Certified values	1400	1400	1400

DL-1a: Canadian Centre for Mineral and Energy Technology
Standard Reference Material (sandstone) - CANMET.

Table 2.6. Uranium and thorium analysis of HB-granodiorite sample from Craignair Quarry, Dalbeattie, southwest Scotland.

Sample No	U ppm	Th ppm	Th/U	$^{234}\text{U}/^{238}\text{U}$ Ad. ratio	$^{230}\text{Th}/^{234}\text{U}$ Ad. ratio	$^{230}\text{Th}/^{238}\text{U}$ Ad. ratio	$^{226}\text{Ra}/^{230}\text{Th}$ Ad. ratio
1	4.7 ± 0.2	14.9 ± 1.0	3.2 ± 0.3	1.00 ± 0.03	1.27 ± 0.06	1.27 ± 0.06	1.08 ± 0.05
2	4.6 ± 0.2	14.1 ± 1.0	3.1 ± 0.2	1.00 ± 0.04	1.32 ± 0.07	1.32 ± 0.07	1.06 ± 0.06
3	4.5 ± 0.2	14.0 ± 1.0	3.1 ± 0.2	1.02 ± 0.03	1.26 ± 0.06	1.29 ± 0.07	1.07 ± 0.06
Avg.	4.6 ± 0.2	14.3 ± 1.0	3.1 ± 0.2	1.00 ± 0.03	1.28 ± 0.06	1.29 ± 0.07	1.07 ± 0.06

$^{232}\text{U}/^{228}\text{Th}$ spike, to allow measurement of actual $^{228}\text{Th}/^{232}\text{Th}$ activity ratios of the samples. The rest of the procedure, i.e. dissolution, coprecipitation, separation, electroplating and α -spectrometry analysis, were carried out as described above.

2.2.3.3 Water analysis

1 ml of iron chloride solution (~40 mg of iron) and a known quantity of $^{232}\text{U}/^{228}\text{Th}$ spike were added to the 20 litre volume of filtered water sample from Kinharvie burn. The resulting solution was shaken to allow the $^{232}\text{U}/^{228}\text{Th}$ tracer to equilibrate with the uranium and thorium in the sample, after which ammonium hydroxide was added to produce a brown precipitate of $\text{Fe}(\text{OH})_3$ which scavenged the uranium and thorium from solution (Gascoyne, 1979). After the precipitate had settled the floc was separated from the supernatant liquid by decanting and centrifuging. The hydroxide precipitate was dissolved in 9M hydrochloric acid (~25 ml) and iron was extracted into di-isopropyl ether. Further treatment, i.e separation, plating and α -spectrometry analysis of the sample, was carried out as described above.

2.2.4 Fission track analysis

The feasibility of uranium determination using induced fission tracks in a suitable detector was first demonstrated by Price and Walker (1963). Since then many applications of the technique have been reported, especially in the study of the geochemistry of uranium in various rock types and individual

minerals (Kleeman and Lovering, 1967; Hashimoto, 1971; Thiel et al., 1972; Grauert et al., 1974; Basham, 1981; Guthrie, 1989) and in dating of minerals (Wagner, 1968; Poupeau, 1981; Hurford and Green, 1982; Yim et al., 1985).

Induced nuclear fission comes about when heavy nuclei are bombarded by neutrons, which, as uncharged particles, experience no repulsion from the target nucleus. ^{235}U fission can be induced by exposure to thermal neutrons (≤ 0.025 eV), whereas ^{238}U and ^{232}Th undergo fission when irradiated by epithermal (0.025 to 1 keV) and fast neutrons (> 1 keV) (Friedlander et al., 1981). Irradiation in the present work thus used thermal neutrons to selectively induce fission of ^{235}U in the absence of ^{232}Th fission. The fission fragments produced in this way move in various directions, leaving tracks of damage on an atomic scale in the material through which they pass. The tracks can be preserved in many non-conductive solid materials (eg. muscovite, polycarbonate and many plastic materials) and they can be enlarged to microscopically visible dimensions by etching with a suitable reagent.

Fission track mapping is an established technique in the study of uranium migration during weathering (Tieh et al., 1980; Guthrie and Kleeman, 1986). In the present work a fission track mapping technique based upon Fleischer (1966) was used to investigate the distribution of uranium about the redox fronts associated with water-bearing fractures in the granodiorite samples from Craignair quarry. In particular the spatial distribution of uranium was investigated in: (i) weathering-resistant accessory minerals (resistate uranium); (ii) grain boundaries of major minerals, particularly biotite (intergranular uranium); (iii) infilling fractures, where it is associated with Fe-OOH and Mn-OOH; and (iv) weathered feldspar and biotite (i.e. sericite and chlorite). The "uranium maps" were used to provide complementary

information to the natural decay series analyses with regard to the migration and retardation of uranium about the redox fronts.

Determination of the spatial distribution of uranium in rock samples using fission track analysis involves four steps: sample preparation, irradiation, etching and analysis. In the present study thin sections of each of the granodiorite samples from Craignair quarry were cleaned with distilled water and a 1mm thick polycarbonate plastic sheet of comparable size was placed on the surface of the section and taped in place. The sample identification code was marked on both section and plastic detector so that the fission tracks of uranium produced in the detector could accurately be matched with the mineral distribution in the rock section simply by superimposing the respective section and detector.

The sections and detectors were placed in a plastic container and irradiations (with a neutron fluence of 6×10^{15} neutrons per square centimetre) were carried out in the thermal column of the SURRC UTR 300 reactor. After irradiation the samples were left to cool for about four weeks to allow the decay of nuclides such as ^{24}Na and ^{42}K so that they were radiologically safe to handle. The plastic detectors were subsequently removed from the thin sections and etched with 6N NaOH for 1.5 hours at 40°C to enlarge the fission tracks to microscopically visible sizes (Fleisher, 1966). The plastic detectors were superimposed on the thin sections to allow microscopic comparison of the fission track distribution with the mineralogy of the rock.

2.2.5 Inductively coupled plasma - mass spectrometry (ICP-MS)

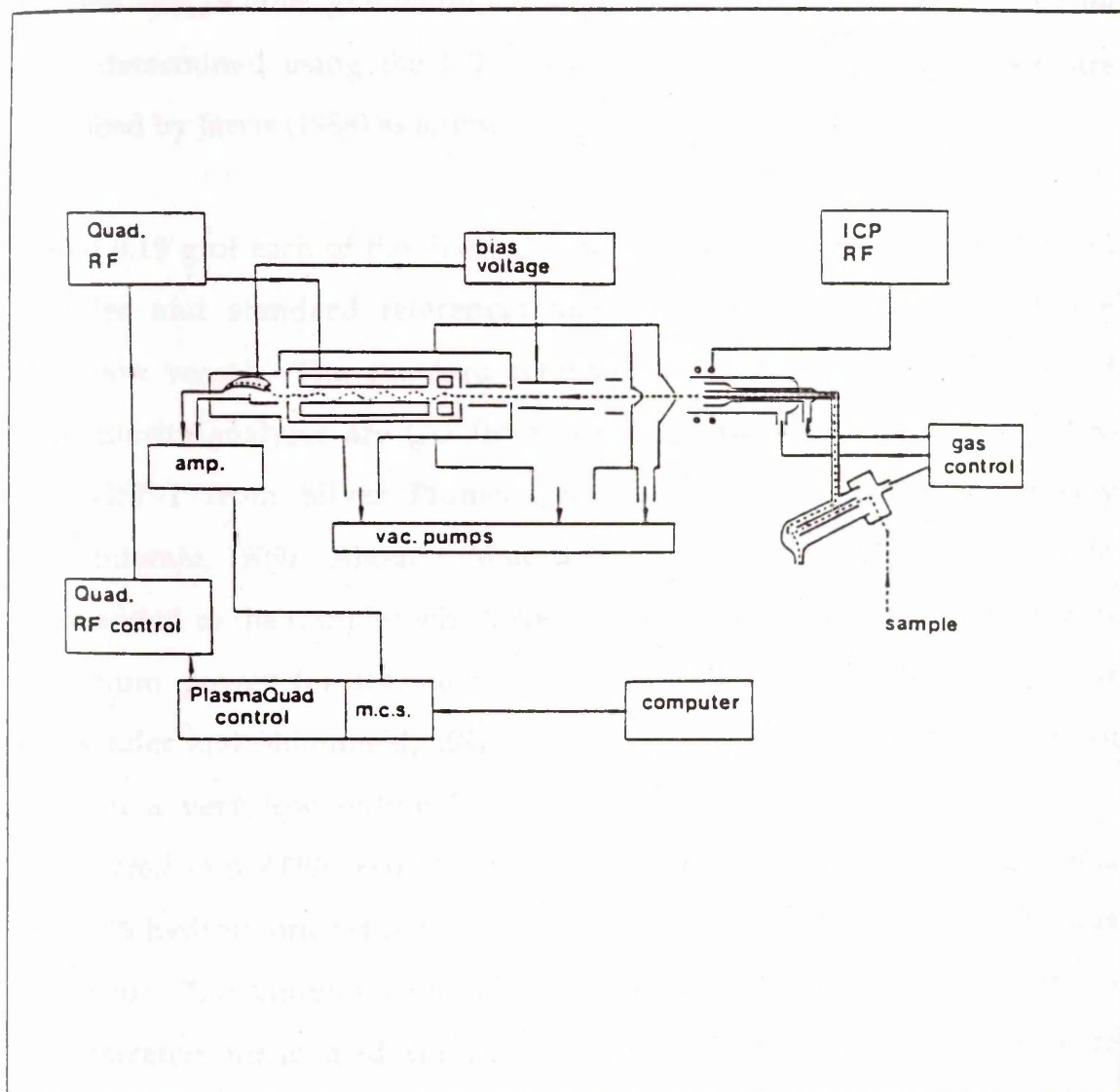
Inductively couple plasma-mass spectrometry was developed about ten years

ago and can be used to determine major, minor, trace and ultra-trace elemental concentrations in a single sample. The technique is capable of routinely determining more than 65 elements with precision of 2 to 5%. Some of the applications of ICP-MS in the geological and environmental sciences are: petrogenetic studies of orebodies (Hall and Plant, 1992); rare earth element (REE) patterns in sediments (Roelands and Deblonde, 1992); analysis of ostracod shells to reconstruct ancient lake environments (Holmes et al., 1992); the study of potential effects of acid rain on soils (Beauchemin et al., 1992); and analysis of uranium in marine sediment pore water (Toole et al., 1990).

Figure 2.8 shows a schematic diagram of an ICP-MS. The principles of operation of such an instrument are described in detail in Riddle et al., (1988), Date and Gray (1989), Hall (1989) and Jarvis et al. (1990, 1991). They can be summarised as follows: The ICP-MS employs an Ar plasma to produce (M^+) ions which are extracted via a series of vacuum stages into a mass spectrometer for analysis. The plasma is generated from radio-frequency (RF) magnetic fields induced by a copper coil which is wound around the top of the glass torch of the ICP. The plasma gives very high temperatures of 6000 - 10000° K resulting in efficient atomisation and consequently very small chemical interferences.

The sample is first nebulised to form a fine aerosol and is then introduced into the ICP torch. The aerosol is transported into the centre of the ICP (usually only 1 - 2% of the sprayed solution reaches the ICP) where it rapidly undergoes desolvation, vaporisation to molecular level and dissociation into atoms, some of which are ionised. The ions are extracted from the plasma into a mass spectrometer and measured using an ion detector. This process of mass selection is rapid and the instrument is able to obtain a spectrum for

Figure 2.8: A schematic diagram of the VG PlasmaQuad (PQ1) used in this study (VG Isotopes, 1988).



the entire mass range from ${}^7\text{Li}$ to ${}^{238}\text{U}$ in about 1 minute (Jarvis and Jarvis, 1992).

In the present study REE concentrations in 8 granite and 12 granodiorite core samples and 19 other granodiorite samples from Craginair Quarry, Dalbeattie were determined using the ICP-MS technique based upon the procedure described by Jarvis (1988) as follows:

About 0.15 g of each of the finely powdered (250 mesh size fraction, $4.0\ \mu\text{m}$) samples and standard references materials was weighed into a teflon digestion vessel. The standard reference materials used for granite and granodiorite analyses are G-2 from Westerly Granite, Rhode Island (USA) and GSP-1 from Silver Plume Quarry, Colorado (USA), respectively (Govindaraju, 1989). About 3 ml aqua regia and 1 ml 40% hydrofluoric acid were added to the samples which were then digested in a microwave oven at maximum power for five minutes and left to cool for about one hour (Alexander and Shimmiel, 1990). The samples were then heated on a hot plate at a very low setting for about seven days after which they were transferred into PTFE beakers and evaporated to dryness. More aqua regia and 40% hydrofluoric acid were added as necessary until total dissolution was obtained. The samples were heated to dryness and re-dissolved twice in concentrated nitric acid (Primar grade) and finally the residues were dissolved in 100 ml 2% nitric acid (Primar grade), and clear solutions were obtained. The final solutions were made in dilute nitric acid because most elements are stable in solution in nitric acid and it is also the preferred acid matrix for ICP-MS analyses, since it avoids the addition of excess chloride which can cause severe interference for some elements (Totland et al., 1992). The total dissolved solid (TDS) content was kept to less than $2000\ \mu\text{g l}^{-1}$ TDS

(0.2%) in order to minimise signal loss due to cone blockage in the ICP-MS (Jarvis, 1988; Jarvis et al., 1991; Williams and Gray, 1988). The samples were stored in polypropylene bottles and kept in a refrigerator prior to REE analysis.

The REE analyses were performed using a Plasmaquad ICP-MS (Model PQ1 from VG Isotopes). To 10 ml of each of the samples, reference material and standard solutions, 100 μ l (100 ppm) ^{115}In , 100 μ l (10 ppm Ru) and 100 μ l (10 ppm Re) were added and the solutions were analysed directly by the ICP-MS. ^{115}In was used as an internal standard to correct for instrument drift during runs; both Ru and Re were used as internal standards for the REE analysis of the rock samples. Spectra were analysed and concentrations calculated using standard VG software.

CHAPTER 3

RESULTS

The results of analyses of various types of sample (i.e. rock, soil and water) from the Criffel pluton and adjacent areas performed during the course of this research are presented in Tables 3.1 to 3.16. The concentrations of natural decay series radionuclides in rock samples determined by the α -spectroscopy method are given in ppm, while ^{210}Pb , ^{137}Cs , ^{134}Cs and ^{226}Ra in soil samples measured by ^{the} direct γ spectroscopy technique are given in Bq kg^{-1} . Rare earth elements (determined by ICP-MS) and uranium and thorium (measured by INAA technique) concentrations in rock samples are given in ppm, whereas uranium and thorium concentrations in water samples (determined by ICP-MS) are given in ppb. The errors shown with each analysis are from the counting statistics as follows: the natural decay series radionuclide - mostly within $\pm 5\%$; ^{210}Pb , ^{137}Cs , ^{134}Cs and ^{226}Ra - mostly within $\pm 10\%$; uranium and thorium concentrations determined by INAA method mostly below $\pm 15\%$.

Table 3.1: Uranium and thorium concentrations of granite and granodiorite samples from Criffel Pluton, southwest Scotland.

No	Code	Uranium (ppm)	Thorium (ppm)	Th/U
BM-granite				
1	174	2.9 ± 0.4	8.6 ± 0.7	3.0 ± 0.4
2	221	2.5 ± 0.4	8.2 ± 0.7	3.3 ± 0.6
3	274*	4.7 ± 0.1	11.5 ± 0.4	2.5 ± 0.1
4	220	3.3 ± 0.4	7.4 ± 0.9	2.2 ± 0.3
5	218	4.2 ± 0.4	7.1 ± 0.9	1.7 ± 0.2
6	263	5.0 ± 0.5	10.0 ± 0.7	2.0 ± 0.2
7	210*	3.8 ± 0.1	10.7 ± 0.4	2.8 ± 0.1
MB-granite				
8	246*	2.9 ± 0.1	14.5 ± 0.7	5.0 ± 0.3
9	130	6.0 ± 0.4	18.7 ± 0.5	3.1 ± 0.2
10	136	2.5 ± 0.4	10.8 ± 1.8	4.3 ± 0.9
11	245	3.2 ± 0.4	14.1 ± 2.0	4.4 ± 0.8
12	179	2.4 ± 0.4	14.7 ± 1.6	6.1 ± 1.2
13	197	4.6 ± 0.3	16.4 ± 0.9	3.6 ± 0.3
14	242	2.8 ± 0.4	9.4 ± 1.0	3.4 ± 0.6
15	272*	4.6 ± 0.1	14.0 ± 0.4	3.0 ± 0.1
16	276	4.2 ± 0.4	10.0 ± 0.4	2.4 ± 0.2
17	273	2.3 ± 0.5	11.0 ± 1.5	4.8 ± 1.2
18	165	4.0 ± 0.6	14.8 ± 1.6	3.7 ± 0.6
19	267	4.8 ± 0.4	11.5 ± 1.1	2.4 ± 0.3
20	219*	7.8 ± 0.2	12.8 ± 0.8	1.6 ± 0.1
21	190	3.4 ± 0.6	11.5 ± 2.1	3.4 ± 0.8
22	175	3.2 ± 0.4	14.8 ± 1.2	4.6 ± 0.7
23	115	4.3 ± 0.4	12.8 ± 0.9	3.0 ± 0.3
24	162*	5.0 ± 0.1	12.8 ± 0.4	2.6 ± 0.1
25	185	3.2 ± 0.3	12.2 ± 0.9	3.8 ± 0.4
26	176	2.8 ± 0.3	14.7 ± 0.4	5.3 ± 0.6
27	271	3.0 ± 0.3	15.5 ± 0.8	5.2 ± 0.5
28	268	3.2 ± 0.6	10.0 ± 0.8	3.1 ± 0.6
29	247	2.3 ± 0.3	14.5 ± 0.8	6.3 ± 0.9
30	208	2.2 ± 0.4	11.1 ± 1.7	5.1 ± 1.2
31	161	2.5 ± 0.5	13.6 ± 2.0	5.4 ± 1.3
32	246	3.0 ± 0.5	10.1 ± 1.6	3.4 ± 0.7
33	164	3.2 ± 0.5	14.1 ± 2.0	4.4 ± 0.9
34	143	3.2 ± 0.8	13.7 ± 2.0	4.3 ± 1.2
35	117	3.7 ± 0.5	14.0 ± 1.6	3.8 ± 0.6

B-granite

36	212	4.9 ± 0.5	12.4 ± 1.2	2.5 ± 0.3
37	123	3.2 ± 0.5	10.9 ± 1.4	3.4 ± 0.6
38	104	5.2 ± 0.5	12.5 ± 0.7	2.4 ± 0.2
39	241	4.7 ± 0.7	15.7 ± 1.6	3.3 ± 0.6
40	236	5.2 ± 0.5	13.2 ± 1.3	2.5 ± 0.3
41	209	3.5 ± 0.5	11.6 ± 1.2	3.3 ± 0.6
42	203	5.7 ± 0.8	15.4 ± 1.5	2.7 ± 0.4
43	261	5.2 ± 0.4	9.2 ± 1.0	1.8 ± 0.2
44	264	5.9 ± 0.9	20.1 ± 2.0	3.4 ± 0.6
45	183	4.0 ± 0.5	12.5 ± 1.6	3.1 ± 0.5
46	116	2.3 ± 0.6	9.7 ± 1.0	4.2 ± 1.0
47	139*	3.2 ± 0.1	14.8 ± 0.4	4.6 ± 0.2
48	177	4.3 ± 0.7	19.1 ± 2.0	4.4 ± 0.2
49	142	5.3 ± 0.9	15.2 ± 1.5	2.9 ± 0.5
50	157	5.7 ± 0.9	11.6 ± 2.0	2.1 ± 0.4
51	254	5.2 ± 0.8	11.5 ± 1.1	2.2 ± 0.4
52	173	7.5 ± 0.6	14.9 ± 0.9	2.0 ± 0.2
53	253	4.1 ± 0.8	15.3 ± 2.0	3.7 ± 0.7
54	158*	4.6 ± 0.1	15.2 ± 0.4	3.3 ± 0.1
55	129	5.2 ± 0.7	12.2 ± 1.2	2.4 ± 0.4
56	103	5.6 ± 0.5	11.5 ± 0.8	2.1 ± 0.4
57	213	4.5 ± 0.6	13.1 ± 2.0	2.9 ± 0.5
58	196	4.5 ± 0.7	13.2 ± 2.0	2.9 ± 0.5
59	194	6.4 ± 0.6	11.9 ± 0.7	1.9 ± 0.2
60	211	4.8 ± 0.9	14.3 ± 1.9	3.0 ± 0.2
61	205*	3.9 ± 0.1	18.9 ± 0.8	4.9 ± 0.2
62	163	4.1 ± 0.3	19.3 ± 1.3	4.7 ± 0.2
63	252	5.2 ± 0.4	13.3 ± 0.9	2.6 ± 0.2
64	187	4.0 ± 0.3	10.0 ± 0.7	2.5 ± 0.3

HB-granodiorite

65	195	4.0 ± 0.7	12.3 ± 2.0	3.1 ± 0.3
66	128	4.4 ± 0.9	14.3 ± 1.4	3.3 ± 0.3
67	151	3.4 ± 0.6	16.4 ± 1.9	4.8 ± 0.5
68	146	3.9 ± 0.4	17.3 ± 1.7	4.4 ± 0.4
69	144*	3.2 ± 0.1	15.2 ± 0.4	4.7 ± 0.2
70	200*	4.0 ± 0.1	15.2 ± 0.4	3.8 ± 0.1
71	199	5.3 ± 0.5	14.9 ± 1.0	2.8 ± 0.3
72	126	4.0 ± 0.4	14.5 ± 0.6	3.6 ± 0.3
73	181	3.7 ± 0.1	11.1 ± 0.5	3.0 ± 0.2
74	184*	4.0 ± 0.1	16.5 ± 0.8	4.1 ± 0.1
75	248	2.8 ± 0.1	10.6 ± 0.4	3.8 ± 0.3
76	172	3.0 ± 0.3	10.8 ± 0.5	3.6 ± 0.3
77	231	5.3 ± 0.4	19.6 ± 0.8	3.7 ± 0.2
78	228	7.1 ± 0.5	24.8 ± 0.9	3.5 ± 0.3
79	227	4.6 ± 0.4	22.1 ± 0.9	4.8 ± 0.5
80	135*	3.8 ± 0.1	15.7 ± 0.8	4.1 ± 0.2

81	132	5.2 ± 0.5	23.6 ± 0.9	4.5 ± 0.4
82	229	7.8 ± 0.6	20.5 ± 1.2	2.6 ± 0.3
83	056*	6.2 ± 0.2	14.8 ± 0.4	2.4 ± 0.1
84	235	5.8 ± 0.5	12.0 ± 0.9	2.1 ± 0.3
85	159	7.8 ± 0.5	13.6 ± 0.7	1.7 ± 0.1
86	215	4.8 ± 0.3	14.4 ± 0.9	3.0 ± 0.3
87	192	8.0 ± 0.6	12.4 ± 0.7	1.6 ± 0.1
88	153	3.6 ± 0.6	9.4 ± 0.7	2.6 ± 0.4
89	202	3.1 ± 0.3	10.8 ± 0.8	3.5 ± 0.3
90	105	3.9 ± 0.5	11.1 ± 0.9	2.9 ± 0.4
91	238	3.3 ± 0.2	9.0 ± 0.7	2.7 ± 0.3
92	240	4.2 ± 0.3	12.2 ± 1.1	2.9 ± 0.4
93	147	2.7 ± 0.3	8.5 ± 1.0	3.2 ± 0.4
94	145	5.6 ± 0.4	11.5 ± 0.8	2.1 ± 0.2
95	188	4.0 ± 0.5	12.9 ± 1.1	3.2 ± 0.5
96	204	4.5 ± 0.4	12.0 ± 1.0	2.7 ± 0.4
97	207	3.5 ± 0.2	7.3 ± 0.5	2.1 ± 0.2
98	278	3.2 ± 0.3	9.1 ± 0.7	2.8 ± 0.2
99	275	3.9 ± 0.3	9.7 ± 0.5	2.5 ± 0.2
100	119	5.1 ± 0.4	10.0 ± 0.6	2.0 ± 0.1
101	198	2.0 ± 0.1	10.3 ± 1.1	5.2 ± 0.6
102	201	3.5 ± 0.3	11.9 ± 1.2	3.4 ± 0.4
103	120	3.7 ± 0.3	12.1 ± 1.2	3.3 ± 0.4
104	118	4.0 ± 0.4	17.5 ± 1.7	4.3 ± 0.6
105	156	5.7 ± 0.5	14.1 ± 1.4	2.5 ± 0.4
106	125	3.6 ± 0.3	14.7 ± 1.3	4.1 ± 0.5
107	180	3.9 ± 0.4	14.3 ± 1.4	3.7 ± 0.4
108	237	2.6 ± 0.2	10.9 ± 1.1	4.2 ± 0.5
109	149	2.0 ± 0.2	6.9 ± 0.8	3.5 ± 0.2
110	189	3.1 ± 0.3	9.2 ± 0.9	3.0 ± 0.3
111	112	4.0 ± 0.4	17.0 ± 1.6	4.3 ± 0.6
112	249	2.7 ± 0.2	11.7 ± 1.2	4.3 ± 0.5
113	250	4.1 ± 0.4	19.6 ± 2.0	4.8 ± 0.4
114	101	3.0 ± 0.3	9.2 ± 0.8	3.1 ± 0.4
115	216	3.5 ± 0.3	10.3 ± 0.9	3.0 ± 0.3
116	182	7.0 ± 0.4	12.7 ± 0.7	1.8 ± 0.1

CHB-granodiorite

117	262	5.2 ± 0.6	10.1 ± 1.8	1.9 ± 0.4
118	244*	3.0 ± 0.1	14.8 ± 0.4	4.9 ± 0.1
119	154	3.2 ± 0.3	17.3 ± 1.8	5.4 ± 0.6
120	168	2.4 ± 0.3	9.9 ± 1.0	4.1 ± 0.5
121	137	4.2 ± 0.3	17.8 ± 0.9	4.2 ± 0.4
122	193	3.0 ± 0.4	15.1 ± 0.8	5.0 ± 0.7
123	169	2.2 ± 0.1	10.0 ± 0.4	4.6 ± 0.3
124	131	4.1 ± 0.3	11.3 ± 0.5	2.8 ± 0.2
125	133	4.5 ± 0.2	12.5 ± 0.5	2.8 ± 0.2
126	251	6.2 ± 0.4	11.4 ± 0.5	1.8 ± 0.1
127	256	3.2 ± 0.2	10.0 ± 0.5	3.1 ± 0.2

128	141	3.3 ± 0.2	14.8 ± 0.7	4.5 ± 0.3
129	260	3.5 ± 0.3	11.8 ± 0.5	3.4 ± 0.2
130	257	5.5 ± 0.3	15.3 ± 0.6	2.8 ± 0.2
131	259*	2.3 ± 0.1	13.2 ± 0.4	5.7 ± 0.2
132	122*	3.1 ± 0.1	13.2 ± 0.4	4.3 ± 0.2
133	233	4.7 ± 0.4	19.5 ± 0.8	4.1 ± 0.4
134	166	4.7 ± 0.4	16.1 ± 1.0	3.4 ± 0.4
135	225	5.1 ± 0.4	20.6 ± 0.7	4.0 ± 0.3
136	171	3.3 ± 0.3	19.0 ± 1.0	5.8 ± 0.6
137	226	4.0 ± 0.2	19.0 ± 0.8	4.8 ± 0.5
138	140	3.9 ± 0.2	19.4 ± 0.8	4.9 ± 0.5
139	234	5.8 ± 0.7	24.7 ± 1.0	4.3 ± 0.5
140	138	5.8 ± 0.3	20.6 ± 0.8	3.6 ± 0.4
141	127	5.6 ± 0.3	20.1 ± 0.8	3.6 ± 0.3
142	160	5.4 ± 0.8	15.2 ± 0.6	2.8 ± 0.2
143	206*	2.6 ± 0.1	14.0 ± 0.4	5.4 ± 0.3
144	113	5.9 ± 0.6	22.8 ± 0.9	3.9 ± 0.3
145	266	5.6 ± 0.7	19.5 ± 0.8	3.5 ± 0.3
146	148	5.4 ± 0.6	19.3 ± 0.8	3.6 ± 0.4
147	230*	4.3 ± 0.1	15.7 ± 0.4	3.7 ± 0.2
148	186	3.4 ± 0.3	19.2 ± 1.5	5.6 ± 0.7
149	106	3.5 ± 0.3	10.8 ± 0.8	3.1 ± 0.4
150	111	2.9 ± 0.3	8.0 ± 0.8	2.8 ± 0.4
151	217	3.0 ± 0.4	7.8 ± 1.0	2.6 ± 0.3
152	277	3.3 ± 0.3	10.5 ± 1.0	3.2 ± 0.5
153	152	2.8 ± 0.3	14.8 ± 1.4	5.3 ± 0.6
154	121	5.2 ± 0.3	9.3 ± 0.5	1.8 ± 0.1
155	239	4.5 ± 0.3	7.7 ± 0.4	1.7 ± 0.1
156	107	3.1 ± 0.3	7.4 ± 0.4	2.4 ± 0.1
157	167	2.4 ± 0.2	13.7 ± 0.9	5.7 ± 0.4
158	255	2.6 ± 0.3	11.4 ± 1.3	4.4 ± 0.6
159	124	2.4 ± 0.3	14.1 ± 1.7	5.9 ± 0.7
160	265	3.8 ± 0.4	11.9 ± 1.2	3.1 ± 0.5
161	223	3.5 ± 0.3	11.8 ± 1.8	3.4 ± 0.5
162	178	2.2 ± 0.2	9.6 ± 1.1	4.4 ± 0.6
163	222	3.6 ± 0.4	13.9 ± 1.5	3.9 ± 0.6
164	224	6.8 ± 0.4	23.8 ± 1.8	3.5 ± 0.3
165	270	2.7 ± 0.3	12.5 ± 1.4	4.6 ± 0.6
166	110	3.2 ± 0.4	11.5 ± 1.4	3.6 ± 0.5
167	214	2.7 ± 0.3	13.5 ± 1.6	5.0 ± 0.8
168	191	2.5 ± 0.2	11.0 ± 1.0	4.4 ± 0.5
169	243	5.6 ± 0.4	22.7 ± 2.0	4.1 ± 0.5
AVERAGE		4.1 ± 0.4	13.6 ± 1.2	3.3 ± 0.4

Note: * analysed by α - spectrometry

Table 3.2: Uranium and thorium concentrations and activity ratios for granitic rock samples from the Criffel pluton, southwest Scotland.

Smple No.	U (ppm)	Th (ppm)	$^{234}\text{U}/^{238}\text{U}$ Act. Ratio	$^{230}\text{Th}/^{234}\text{U}$ Act. Ratio	$^{230}\text{Th}/^{238}\text{U}$ Act. Ratio
BM-274	4.7±0.1	11.5±0.4	1.04±0.03	1.36±0.04	1.41±0.04
BM-210	3.8±0.1	10.7±0.4	1.02±0.06	1.13±0.05	1.15±0.06
MB-246	2.9±0.1	14.5±0.7	1.03±0.04	1.38±0.07	1.42±0.07
MB-272	4.6±0.1	14.0±0.4	1.10±0.04	1.62±0.06	1.78±0.06
MB-162	5.0±0.1	12.8±0.4	0.97±0.04	1.24±0.02	1.20±0.03
MB-219	7.8±0.2	12.8±0.8	1.03±0.04	1.11±0.05	1.14±0.05
B-205	3.9±0.1	18.9±0.8	1.03±0.05	1.26±0.06	1.30±0.07
B-139	3.2±0.1	14.8±0.4	1.07±0.04	1.29±0.02	1.38±0.05
B-158	4.6±0.1	15.2±0.4	0.92±0.03	1.11±0.04	1.02±0.04
HB-184	4.0±0.1	16.5±0.8	0.96±0.06	1.14±0.06	1.09±0.07
HB-056	6.2±0.2	14.8±0.4	0.98±0.06	1.04±0.05	1.02±0.05
HB-144	3.2±0.1	15.2±0.4	1.01±0.07	1.19±0.04	1.20±0.04
HB-200	4.0±0.1	15.2±0.4	0.98±0.03	1.08±0.04	1.06±0.04
HB-135	3.8±0.1	15.7±0.8	0.98±0.04	1.45±0.06	1.42±0.06
CHB-206	2.6±0.1	14.0±0.4	0.93±0.04	1.59±0.06	1.48±0.05
CHB-244	3.0±0.1	14.8±0.4	1.00±0.05	1.47±0.07	1.47±0.07
CHB-122	3.1±0.1	13.2±0.4	1.04±0.03	1.15±0.04	1.20±0.04
CHB-259	2.3±0.1	13.2±0.4	1.04±0.05	1.19±0.05	1.24±0.05
CHB-230	4.3±0.1	15.7±0.4	1.01±0.03	1.23±0.04	1.24±0.04

Note:

1. BM - Biotite Muscovite Granite
2. MB - Muscovite Biotite Granite
3. B - Biotite Granite
4. HB - Hornblende Biotite Granodiorite
5. CHB - Clinopyroxene Hornblende Biotite Granodiorite

Table 3.3. Uranium and thorium concentrations, concentration ratios and activity ratios for sliced samples (increasing distance from fracture face) in rock section CQ1 from Craignair Quarry, Dalbeattie, southwest Scotland.

No.	Dis (cm)	U (ppm)	Th (ppm)	U/Th Con. ratio	$^{234}\text{U}/^{238}\text{U}$ Act. ratio	$^{230}\text{Th}/^{234}\text{U}$ Act. ratio	$^{230}\text{Th}/^{238}\text{U}$ Act. ratio	$^{226}\text{Ra}/^{230}\text{Th}$ Act. ratio
0	0	11.0±0.1	ND	-	1.73±0.04	1.53±0.06	2.64±0.11	-
1	0-1	3.1±0.1	14.6±0.8	0.21±0.013	1.12±0.04	1.43±0.06	1.62±0.10	0.96±0.21
2	1-2	3.0±0.1	14.2±0.5	0.21±0.010	1.16±0.03	1.93±0.08	2.24±0.09	0.71±0.21
3	2-3	3.2±0.2	16.6±0.7	0.19±0.014	1.12±0.03	1.45±0.05	1.62±0.06	0.83±0.19
4	3-4	3.6±0.1	15.9±0.7	0.23±0.012	1.09±0.03	1.40±0.05	1.52±0.06	0.95±0.23
5	4-5	4.1±0.1	15.0±0.5	0.27±0.011	1.10±0.03	1.40±0.05	1.54±0.05	0.99±0.23
6	5-6	4.1±0.1	14.7±0.4	0.28±0.010	1.12±0.03	1.20±0.05	1.34±0.05	1.01±0.28
7	6-7	3.6±0.1	13.6±0.4	0.26±0.011	1.09±0.04	1.38±0.06	1.50±0.06	0.56±0.26
8	7-8	3.7±0.1	15.0±0.6	0.24±0.012	0.99±0.03	1.47±0.06	1.43±0.06	0.81±0.24
9	8-9	3.7±0.1	14.1±0.5	0.30±0.013	1.01±0.03	1.27±0.05	1.29±0.05	0.81±0.30
10	9-10	3.7±0.1	14.6±0.1	0.25±0.011	0.98±0.03	1.28±0.05	1.25±0.06	0.70±0.25
11	10-11	3.7±0.1	14.1±0.5	0.25±0.011	0.97±0.03	1.31±0.05	1.28±0.05	0.85±0.25

Table 3.4: REE concentrations for sliced samples (increasing distance from fracture face) in rock section CQ1 from Craignair quarry, Dalbeattie, southwest Scotland. The REE normalising values for chondrite (Bynton, 1984) and REE concentrations for sample HB-056 from the Criffell pluton (Stephens et al., 1985) are also indicated.

No	Dist. (cm)	La	Ce	Pr	Nd	Sm	Eu (ppm)	Gd	Tb	Dy	Ho	Er	Yb	Lu
1	0 - 1	43.42	83.30	8.44	27.39	4.52	1.39	3.55	0.41	1.96	0.31	0.91	0.78	0.11
2	1 - 2	48.65	98.90	9.67	31.54	5.23	1.61	3.91	0.47	1.84	0.26	0.78	0.64	0.09
3	2 - 3	35.02	77.32	8.57	28.4e	5.12	1.47	3.45	0.43	1.89	0.30	0.86	0.76	0.12
4	3 - 4	31.70	66.31	7.22	24.34	4.25	1.20	2.58	0.35	1.59	0.26	0.76	0.68	0.11
5	4 - 5	33.47	79.50	7.19	23.79	3.89	1.02	2.58	0.32	1.39	0.22	0.65	0.57	0.09
6	5 - 6	24.83	65.28	5.48	18.36	3.04	0.76	1.98	0.24	1.09	0.17	0.52	0.48	0.07
7	6 - 7	28.53	63.18	6.34	20.89	3.46	0.99	2.21	0.30	1.39	0.23	0.68	0.60	0.09
8	7 - 8	42.61	87.73	9.15	29.97	4.97	1.37	3.12	0.45	1.90	0.31	0.86	0.73	0.12
9	8 - 9	46.17	90.29	9.28	34.65	4.85	1.36	3.28	0.45	2.01	0.31	0.93	0.76	0.11
10	9 - 10	42.39	87.20	9.08	30.81	4.93	1.41	3.17	0.44	2.00	0.32	0.91	0.76	0.11
11	10 - 11	35.53	77.08	8.38	29.06	4.79	1.36	3.05	0.44	1.98	0.32	0.91	0.76	0.11
HB-056		38.30	72.00		28.80	6.15	1.07		0.28				0.90	0.11
Chondrite														
Normali- sing values		0.3100	0.8080	0.1220	0.6000	0.1950	0.0735	0.2590	0.0474	0.3220	0.0718	0.2100	0.2090	0.0322

Table 3.5: Uranium and thorium concentrations, concentration ratios and activity ratios for sliced samples (increasing distance from fracture face) in rock section CQ2 from Craignair Quarry, Dalbeattie, Scotland.

No.	Dist. (cm)	U (ppm)	Th (ppm)	U/Th Conc. Ratio	$^{234}\text{U}/^{238}\text{U}$ Act. Ratio	$^{230}\text{Th}/^{238}\text{U}$ Act. Ratio	$^{230}\text{Th}/^{234}\text{U}$ Act. Ratio	$^{226}\text{Ra}/^{230}\text{Th}$ Act. Ratio
0	0	162±5	13.6±2.4	11.9± 2.13	0.64±0.02	0.16±0.01	0.24±0.02	-
1	0-1	3.5±0.1	11.5±0.5	0.30± 0.016	0.95±0.03	1.08±0.04	1.14±0.04	1.18±0.06
2	1-2	5.3±0.2	13.4±0.5	0.39± 0.015	0.95±0.03	1.12±0.03	1.18±0.04	1.01±0.03
3	2-3	4.9±0.1	14.1±0.5	0.35± 0.014	0.96±0.02	1.40±0.04	1.46±0.04	0.80±0.03
4	3-4	4.9±0.2	13.5±0.3	0.36± 0.015	0.95±0.03	1.17±0.02	1.23±0.03	0.94±0.03
5	4-5	4.8±0.2	12.9±0.5	0.37± 0.015	1.00±0.03	1.08±0.04	1.08±0.04	1.03±0.04
6	5-6	4.9±0.2	11.7±0.4	0.42± 0.022	0.98±0.03	1.05±0.03	1.07±0.03	0.90±0.03
7	6-7	4.8±0.1	13.1±0.5	0.37± 0.015	0.87±0.02	1.00±0.03	1.15±0.04	0.96±0.04
8	7-8	4.7±0.2	11.8±0.4	0.40± 0.021	0.93±0.04	1.12±0.04	1.20±0.04	0.89±0.04

Table 3.6: REE concentrations for sliced samples (increasing distance from fracture face) in rock section CQ2 from Craignair quarry, Dalbeattie, southwest Scotland. The REE normalising values for chondrite (Bynston, 1984) are also indicated.

No. Dist.(cm)	La	Ce	Pr	Nd	Sm	Eu	Gd	Tb	Dy	Ho	Er	Yb	Lu
1 0-1	21.72	47.38	5.48	18.97	3.33	0.98	2.07	0.30	1.39	0.24	0.69	0.60	0.09
2 1-2	35.93	74.92	8.17	57.34	4.38	1.22	3.20	0.51	2.18	0.31	0.92	0.71	0.12
3 2-3	29.90	59.12	6.28	20.76	3.61	0.97	2.36	0.35	1.52	0.24	0.66	0.51	0.08
4 3-4	24.87	58.13	5.20	53.00	2.74	0.79	2.36	0.35	1.52	0.17	0.61	0.42	0.06
5 4-5	39.09	72.96	8.20	67.86	4.54	1.37	3.36	0.49	2.16	0.26	0.86	0.59	0.09
6 5-6	31.06	62.64	7.02	23.89	4.31	1.31	2.62	0.37	1.64	0.27	0.71	0.62	0.09
7 6-7	27.55	59.06	6.50	21.07	4.11	0.81	2.69	0.43	1.88	0.32	0.85	0.79	0.12
8 7-8	22.86	49.81	5.18	17.55	3.52	0.78	2.38	0.36	1.66	0.28	0.75	0.70	0.10
Chondrite Normalising values	0.310	0.808	0.122	0.600	0.195	0.074	0.259	0.047	0.322	0.72	0.210	0.209	0.02

Table 3.7: Uranium and thorium concentrations, concentration ratios and activity ratios for sliced samples from MB-granite (increasing distance from rock surface), Kinharvie, southwest Scotland.

No	Dist. U (cm)	U (ppm)	Th (ppm)	$^{234}\text{U}/^{238}\text{U}$ Act. ratio	$^{230}\text{Th}/^{234}\text{U}$ Act. ratio	$^{230}\text{Th}/^{238}\text{U}$ Act. ratio	$^{226}\text{Ra}/^{230}\text{Th}$ Act. ratio	U/Th Conc. ratio
1	0-1	3.3 ± 0.1	15.4 ± 1.2	1.06 ± 0.03	1.16 ± 0.08	1.23 ± 0.09	1.45 ± 0.37	0.217 ± 0.018
2	1-2	3.0 ± 0.1	13.4 ± 1.6	1.02 ± 0.03	1.15 ± 0.12	1.17 ± 0.11	1.26 ± 0.26	0.222 ± 0.027
3	2-3	3.3 ± 0.1	14.2 ± 0.7	1.01 ± 0.03	1.10 ± 0.05	1.11 ± 0.05	1.24 ± 0.30	0.233 ± 0.014
6	5-6	3.8 ± 0.1	16.7 ± 0.7	0.99 ± 0.03	1.04 ± 0.05	1.03 ± 0.05	1.18 ± 0.20	0.227 ± 0.021
10	9-10	4.3 ± 0.2	18.0 ± 1.0	0.98 ± 0.04	1.04 ± 0.06	1.02 ± 0.06	0.98 ± 0.16	0.238 ± 0.017
14	13-14	4.0 ± 0.2	18.5 ± 1.2	0.96 ± 0.04	1.23 ± 0.04	1.18 ± 0.09	1.03 ± 0.37	0.217 ± 0.018
18	17-18	5.1 ± 0.2	18.8 ± 0.7	0.99 ± 0.04	1.01 ± 0.05	1.00 ± 0.05	0.99 ± 0.22	0.270 ± 0.015
23	22-23	4.9 ± 0.3	18.7 ± 1.0	0.96 ± 0.03	1.08 ± 0.06	1.04 ± 0.06	0.90 ± 0.26	0.263 ± 0.021

Table 3.8: REE concentrations for sliced samples (increasing distance from rock surface) in granite core GR from Kinharvie, southwest Scotland. The REE normalising values for chondrite (Bynston, 1984) and REE concentrations for sample MB-272 from the Criffell pluton (Stephens et al., 1985) are also indicated.

No.	Dist (cm)	La	Ce	Pr	Nd	Sm	Eu	Gd	Tb	Dy	Ho	Er	Yb	Lu
1	0-1	37.640	78.780	8.310	27.860	4.930	1.440	3.270	0.430	1.87	0.290	0.820	0.670	0.090
2	1-2	37.290	76.110	7.920	26.780	4.700	1.350	3.080	0.390	1.81	0.270	0.760	0.650	0.090
3	2-3	20.510	47.470	4.890	15.840	3.280	0.680	2.005	0.324	1.346	0.227	0.627	0.561	0.108
6	5-6	19.780	44.926	4.260	13.967	2.999	0.949	1.933	0.267	1.244	0.211	0.584	0.523	0.088
10	9-10	15.452	33.347	3.517	11.976	2.377	0.562	1.571	0.222	1.085	0.173	0.508	0.435	0.065
14	13-14	36.592	76.411	7.977	32.241	5.211	0.951	3.687	0.514	2.441	0.396	1.079	0.961	0.140
18	17-18	32.741	66.390	6.984	23.221	4.396	0.888	3.061	0.426	2.011	0.331	0.895	0.822	0.116
23	22-23	23.380	50.239	5.323	18.082	3.520	0.745	2.413	0.342	1.588	0.263	0.757	0.706	0.101
MB-272		31.300	56.500	-	22.400	4.460	0.840	-	0.300				0.820	0.140
Chondrite		0.310	0.808	0.122	0.600	0.195	0.074	0.259	0.047	0.322	0.72	0.210	0.209	0.02
Normalising values														

Table 3.9: Uranium and thorium concentrations, concentration ratios and activity ratios for sliced samples from CHB-granodiorite (increasing distance from rock surface), Clifton, southwest Scotland.

No	Dist. (cm)	U (ppm)	Th (ppm)	U/Th Con. ratio	$^{234}\text{U}/^{238}\text{U}$ Act. ratio	$^{230}\text{Th}/^{234}\text{U}$ Act. ratio	$^{230}\text{Th}/^{238}\text{U}$ Act. ratio	$^{226}\text{Ra}/^{230}\text{Th}$ Act. ratio
1	0-1	2.8 ± 0.1	9.9 ± 0.5	0.278 ± 0.017	1.10 ± 0.04	1.04 ± 0.06	1.14 ± 0.07	1.33 ± 0.08
2	1-2	2.6 ± 0.1	9.7 ± 0.5	0.270 ± 0.017	1.02 ± 0.04	2.10 ± 0.08	2.14 ± 0.11	0.71 ± 0.04
3	2-3	3.3 ± 0.1	17.5 ± 1.1	0.189 ± 0.013	0.99 ± 0.04	2.86 ± 0.18	2.82 ± 0.17	0.48 ± 0.03
6	5-6	3.5 ± 0.1	14.9 ± 1.0	0.233 ± 0.017	0.99 ± 0.04	1.27 ± 0.10	1.27 ± 0.10	0.93 ± 0.08
10	9-10	2.8 ± 0.1	13.6 ± 1.1	0.204 ± 0.018	1.01 ± 0.04	1.21 ± 0.12	1.22 ± 0.12	1.37 ± 0.15
15	14-15	2.9 ± 0.1	12.0 ± 0.7	0.244 ± 0.016	0.98 ± 0.04	0.94 ± 0.08	0.90 ± 0.08	1.25 ± 0.10
20	19-20	6.7 ± 0.2	15.3 ± 0.8	0.435 ± 0.026	0.94 ± 0.03	1.04 ± 0.06	0.98 ± 0.05	1.04 ± 0.11
26	25-26	3.4 ± 0.1	36.8 ± 1.9	0.093 ± 0.006	1.05 ± 0.04	2.29 ± 0.15	2.40 ± 0.16	0.53 ± 0.04
30	29-30	3.7 ± 0.1	12.5 ± 0.7	0.294 ± 0.018	1.08 ± 0.04	1.04 ± 0.06	1.13 ± 0.07	0.88 ± 0.07
35	34-35	3.5 ± 0.1	15.7 ± 0.7	0.222 ± 0.012	1.04 ± 0.03	1.04 ± 0.06	1.09 ± 0.06	0.95 ± 0.06
40	39-40	3.3 ± 0.1	18.1 ± 1.6	0.182 ± 0.017	0.97 ± 0.04	2.25 ± 0.17	2.20 ± 0.17	0.48 ± 0.04
44	43-44	3.0 ± 0.1	11.2 ± 1.1	0.270 ± 0.028	1.15 ± 0.03	1.05 ± 0.09	1.18 ± 0.10	1.17 ± 0.12

Table 3.10: REE concentrations for sliced samples (increasing distance from rock surface) in granodiorite core GD from Clifton, southwest Scotland. The REE normalising values for chondrite (Bynston, 1984) are also indicated.

No.	Dist (cm)	La	Ce	Pr	Nd	Sm	Eu	Gd	Tb	Dy	Ho	Er	Yb	Lu
1	0-1	26.23	54.97	5.68	19.71	3.60	1.08	2.44	0.29	1.49	0.24	0.66	0.58	0.07
2	1-2	13.69	28.29	3.74	13.23	2.80	0.93	1.66	0.19	0.95	0.15	0.46	0.39	0.06
3	2-3	42.00	88.43	9.41	30.45	5.25	1.48	3.79	0.45	2.05	0.31	0.90	0.71	0.11
6	5-6	42.00	88.43	9.41	30.45	5.25	1.48	3.79	0.45	2.05	0.31	0.90	0.71	0.11
10	9-10	24.60	54.48	6.19	20.78	3.73	1.07	2.58	0.30	1.39	0.20	0.58	0.49	0.07
15	14-15	13.31	27.44	3.97	14.52	3.01	0.91	1.83	0.25	1.16	0.18	0.50	0.46	0.06
20	19-20	44.08	88.20	8.97	29.11	4.77	1.35	3.70	0.42	1.96	0.29	0.85	0.68	0.09
26	25-26	55.04	317.17	10.77	34.65	5.66	1.55	6.59	0.53	2.42	0.38	1.13	0.94	0.14
30	29-30	36.02	81.89	7.83	25.88	4.47	1.33	3.53	0.40	1.97	0.33	0.89	0.75	0.11
35	34-35	37.74	73.55	7.80	24.95	4.27	1.19	3.15	0.39	1.63	0.26	0.73	0.61	0.11
40	39-40	45.08	93.11	9.00	29.36	4.82	1.38	3.81	0.44	2.07	0.30	0.88	0.74	0.11
44	43-44	36.29	81.04	8.01	26.76	4.85	1.43	3.09	0.40	1.79	0.28	0.77	0.64	0.08
Chondrite Normalising values		0.310	0.808	0.122	0.600	0.195	0.074	0.259	0.047	0.322	0.72	0.210	0.209	0.02

Table 3.11: Results of radioactivity survey of U and ^{40}K over a uraniferous vein at Beeswing (Map Ref. 885681), Scotland (c.f. Figure 2.7).

Distance (m)	U (cpm)	^{40}K (cpm)	Remarks
0	2678	284	
2	2736	224	
3	3150	322	
4	3134	220	
5	3570	312	
6	4430	510	Location of small vein
7	3114	350	
8	2470	272	
9	5040	512	
9.5	21470	1346	Location of main vein
10	3326	226	
11	2338	52	
12	672	44	
13	602	70	
14	772	54	
15	588	60	
16	874	60	
17	718	40	

Table 3.12: Uranium and thorium concentrations, concentration ratios and activity ratios of bulk uranium vein material from Beeswing, southwest Scotland.

Uranium (ppm)	Thorium (ppm)	U/Th Conc.ratio	$^{234}\text{U}/^{238}\text{U}$ Act. ratio	$^{230}\text{Th}/^{234}\text{U}$ Act. ratio	$^{230}\text{Th}/^{238}\text{U}$ Act.ratio	$^{226}\text{Ra}/^{230}\text{Th}$ Act.ratio	$^{210}\text{Pb}/^{226}\text{Ra}$ Act.ratio
66.8±1.1	10.9±0.4	6.13±0.25	0.94±0.01	1.62±0.06	1.52±0.06	1.50±0.05	1.38±0.03

Table 3.13: Uranium and thorium concentrations, Th/U concentration ratios, organic content and ^{210}Pb , ^{226}Ra , ^{134}Cs and ^{137}Cs concentrations of soil samples from location A, Beeswing, southwest Scotland.

No	Depth (cm)	% organic content	U (ppm) (a)	Th (ppm) (a)	U/Th	U (Solution) (ppm) (b)	U (Residue) (ppm) (b)	^{238}U (Bq/kg) (b)	^{234}U (Bq/kg) (b)	$^{234}\text{U}/^{238}\text{U}$ Act. ratio (b)	$^{226}\text{Ra}/^{234}\text{U}$ Act. ratio (b) and (c)	$^{226}\text{Ra}/^{238}\text{U}$ Act. ratio (b) and (c)
1	0-2	25.1	3.4 ± 0.2	4.9 ± 0.4	0.69 ± 0.07	2.80 ± 0.10	0.90 ± 0.10	35 \pm 1	36 \pm 1	1.02 ± 0.04	3.12 ± 0.94	3.21 ± 0.95
2	2-4	18.8	2.5 ± 0.2	4.8 ± 0.4	0.52 ± 0.06							
3	4-6	8.8	3.1 ± 0.2	6.4 ± 0.5	0.48 ± 0.05							
4	6-8	6.2	2.3 ± 0.2	6.7 ± 0.5	0.34 ± 0.04							
5	8-10	4.9	2.3 ± 0.2	6.9 ± 0.6	0.33 ± 0.05							
6	10-12	4.0	3.0 ± 0.2	8.1 ± 0.6	0.37 ± 0.04	2.5 ± 0.10	1.00 ± 0.10	31 \pm 1	32 \pm 1	1.04 ± 0.04	2.15 ± 0.74	2.24 ± 0.77
7	12-14	4.0	3.1 ± 0.2	7.5 ± 0.6	0.41 ± 0.04							
8	14-16	4.9	3.0 ± 0.2	6.6 ± 0.5	0.46 ± 0.04							
9	16-18	3.4	2.3 ± 0.2	4.9 ± 0.4	0.47 ± 0.04							
10	18-20	4.2	4.5 ± 0.3	7.8 ± 0.6	0.58 ± 0.05							
11	20-22	3.7	5.2 ± 0.3	8.0 ± 0.6	0.65 ± 0.06							
12	22-24	4.4	5.8 ± 0.3	8.0 ± 0.9	0.73 ± 0.06	5.7 ± 0.20	1.00 ± 0.10	71 \pm 2	79 \pm 2	1.12 ± 0.05	2.38 ± 0.45	2.65 ± 0.50

Note: i. (a) determined by INAA
 ii. (b) determined by alpha-spectrometry
 iii. (c) determined by direct gamma spectrometry
 iv. Solution: supernatant liquid from leaching of soil
 v. Residue: residue portion of soil from leaching of soil

(Cont. Table 3.13)

No	Depth (cm)	210pb (Bq/kg) (c)	226Ra Bq/kg (c)	137Cs Bq/kg (c)	134Cs Bq/kg (c)	210pb/226Ra Act. ratio
1	0-2	117.9±8.1	112.3±33.8	498.2±33.2	387.2±43.9	1.05±0.32
2	2-4	81.5±8.8	92.4±28.8	397.5±25.8	267.8±46.1	0.88±0.29
3	4-6	49.3±12.6	84.4±35.6	79.8±9.2		0.58±0.25
4	6-8	45.3±8.1		39.4±9.62		
5	8-10	20.0±6.7				
6	10-12	38.5±6.6	69.9±25.1			0.55±0.20
7	12-14	37.6±8.5	69.7±34.1			0.54±0.21
8	14-16	57.1±11.1	83.7±36.2	42.9±6.3		0.68±0.30
9	16-18	53.8±10.9	110.4±37.5	28.6±8.2		0.49±0.19
10	18-20	51.4±8.4	195.0±56.8			0.26±0.08
11	20-22	64.1±12.8	173.0±41.7			0.37±0.11
12	22-24	50.0±9.4	188.0±35.7			0.27±0.07

Table 3.14. Uranium and thorium concentrations, Th/U concentration ratios, organic content and ^{210}Pb , ^{226}Ra , ^{134}Cs and ^{137}Cs concentrations of soil samples from location B, Beeswing, southwest Scotland.

No	Depth (cm)	% organic material (g)	U (ppm) (a)	Th (ppm) (a)	U/Th	U (ppm) (Solution) (b)	U (ppm) (Residue) (b)	$^{234}\text{U}/^{238}\text{U}$ (Solution) (b)	$^{234}\text{U}/^{238}\text{U}$ (Residue) (b)	^{234}U Bq/kg (b)	^{238}U Bq/kg (b)
1	0-2	33.5	3.0±0.3	4.4±0.8	0.68±0.10	2.4±0.10	0.23±0.03	1.02±0.05	1.02±0.05	29±1	30±1
2	2-4	25.6	2.9±0.3	4.7±0.6	0.62±0.14						
3	4-6	21.6	3.2±0.3	5.4±0.7	0.59±0.14						
4	6-8	18.8	2.9±0.2	6.5±0.9	0.45±0.07						
5	8-10	16.3	2.5±0.2	6.0±0.8	0.42±0.06						
6	10-12	14.2	2.8±0.2	5.4±0.5	0.52±0.07						
7	12-14	14.8	2.9±0.3	6.6±0.7	0.44±0.06						
8	14-16	13.8	2.5±0.2	3.7±0.6	0.68±0.11						
9	16-18	14.1	2.8±0.3	5.7±0.7	0.49±0.07	2.9±0.20	1.20±0.03	1.06±0.03	1.02±0.06	36±1	38±1
10	18-20	16.2	3.4±0.3	7.5±0.8	0.45±0.06						
11	20-22	13.3	4.4±0.4	7.1±0.7	0.62±0.10						
12	22-24	11.7	4.4±0.4	7.0±1.0	0.63±0.10						
13	24-26	10.7	5.8±0.4	7.0±0.7	0.83±0.10						
14	26-28	10.7	5.0±0.4	5.1±0.6	0.98±0.14						
15	28-30	10.7	6.9±0.5	5.2±0.7	1.33±0.20						
16	30-32	11.9	6.0±0.4	7.0±0.9	0.86±0.12						
17	32-34	10.9	7.5±0.4	7.8±0.7	0.96±0.10						
18	34-36	10.9	6.1±0.4	5.4±0.6	1.13±0.14	4.9±0.20	1.10±0.04	1.06±0.04	1.02±0.03	61±2	64±2

- Note: i. (a) determined by INAA
 ii. (b) determined by alpha-spectrometry
 iii. (c) determined by direct gamma spectrometry
 iv. Solution: supernatant liquid from leaching of soil
 v. Residue: residue portion of soil from leaching of soil

(Cont. Table 3.14)

No	Depth (cm)	^{210}Pb Bq/kg (c)	^{226}Ra Bq/kg (c)	^{137}Cs Bq/kg (c)	$^{210}\text{Pb}/^{226}\text{Ra}$ (c)	$^{226}\text{Ra}/^{234}\text{U}$ (b) and (c)	$^{226}\text{Ra}/^{238}\text{U}$ (b) and (c)
1	0-2	129.7±10.6	97.1±33.6	598.9±40.5	1.34±0.47	3.19±1.10	3.26±1.02
2	2-4	83.8±8.7	117.8±38.8	303.4±21.4	0.71±0.24		
3	4-6	75.1±11.6	123.8±43.2	92.8±8.5	0.61±0.23		
4	6-8	61.8±6.5	82.1±29.1		0.75±0.27		
5	8-10	56.6±5.9	137.6±37.2	27.7±3.8	0.41±0.11		
6	10-12	36.1±7.4	107.0±36.9	28.5±6.7	0.34±0.13		
7	12-14	36.3±5.6	113.2±21.5		0.32±0.07		
8	14-16	32.3±6.8		28.5±4.2			
9	16-18	38.3±7.3	92.2±25.1	28.8±5.0	0.42±0.13		2.56±0.70
10	18-20	50.6±5.9	92.0±26.9	27.9±8.4	0.55±0.17	2.41±0.66	
11	20-22						
12	22-24	46.4±5.7	119.9±28.5		0.39±0.10		
13	24-26						
14	26-28	44.9±3.5	109.8±24.9		0.41±0.09		
15	28-30						
16	30-32						
17	32-34						
18	34-36		109.8±24.9			1.70±0.38	1.80±0.41

Table 3.15: Uranium and thorium concentrations, Th/U concentration ratios, organic content and ^{210}Pb , ^{226}Ra , ^{134}Cs and ^{137}Cs concentrations of soil samples from location C, Beeswing, southwest Scotland.

No	Depth (cm)	% organic material	U (ppm) (a)	Th (ppm) (a)	Th/U	U (ppm) (Solution) (b)	U (ppm) (Residue) (b)	$^{234}\text{U}/^{238}\text{U}$ (Residue) (b)	$^{234}\text{U}/^{238}\text{U}$ (Solution) (b)	^{234}U Bq/kg (b)	^{238}U Bq/kg (b)
1	0-2	33.4	4.6 ± 0.3	6.1 ± 0.6	0.75 ± 0.08	2.60±0.10	2.00±0.08	1.02±0.03	0.97±0.04	32±1	31±1
2	2-4	29.4	4.3 ± 0.3	6.5 ± 0.5	0.66 ± 0.08						
3	4-6	20.8	3.9 ± 0.3	5.7 ± 0.3	0.68 ± 0.09						
4	6-8	18.7	3.6 ± 0.3	6.6 ± 0.5	0.55 ± 0.05						
5	8-10	16.5	4.2 ± 0.3	8.3 ± 0.8	0.51 ± 0.05						
6	10-12	16.7	4.8 ± 0.4	9.9 ± 0.9	0.49 ± 0.06						
7	12-14	15.8	4.5 ± 0.3	8.0 ± 0.6	0.56±0.06						
8	14-16	13.6	4.3 ± 0.3	7.5 ± 0.9	0.57 ± 0.07						
9	16-18	12.5	4.3 ± 0.3	9.8 ± 0.7	0.44 ± 0.04						
10	18-20	12.3	4.2 ± 0.4	9.3 ± 0.9	0.45 ± 0.04						
11	20-22	11.9	3.8 ± 0.3	8.1 ± 0.6	0.47 ± 0.05						
12	22-24	13.0	3.4 ± 0.3	8.5 ± 0.5	0.40 ± 0.05	2.50±0.10	1.50±0.05	0.91±0.05	1.04±0.05	31±1	32±1
13	24-26	11.2	3.7 ± 0.3	8.8 ± 0.6	0.42 ± 0.05						
14	26-28	9.1	3.8 ± 0.3	7.4 ± 0.7	0.51 ± 0.05						
15	28-30	8.8	3.6 ± 0.2	7.3 ± 0.6	0.49 ± 0.06						
16	30-32	9.0	3.8 ± 0.3	8.6 ± 1.0	0.44 ± 0.04						
17	32-34	9.6	3.4 ± 0.2	8.4 ± 0.6	0.41 ± 0.04						
18	34-36	9.7	3.5 ± 0.3	7.6 ± 0.7	0.46 ± 0.05						
19	36-38	9.6	4.0 ± 0.3	10.6 ± 0.7	0.38 ± 0.04						
20	38-40	8.1	2.4 ± 0.2	8.2 ± 0.8	0.29 ± 0.03						
21	40-42	7.3	2.5 ± 0.2	6.6 ± 0.5	0.38±0.04						
22	42-44	8.1	3.3 ± 0.3	8.2 ± 0.8	0.40 ± 0.04						
23	44-46	6.7	3.0 ± 0.3	8.9 ± 0.9	0.34 ± 0.04	2.00±0.10	1.10±0.05	0.93±0.06	1.06±0.05	25±1	26±1

Note: i. (a) determined by INAA

ii. (b) determined by alpha-spectrometry

iii. (c) determined by direct gamma spectrometry

iv. Solution: supernatant liquid from leaching of soil

v. Residue: residue portion of soil from leaching of soil

(Cont. Table 3.15)

No	Depth (cm)	^{210}Pb Bq/kg	^{226}Ra Bq/kg	^{134}Cs Bq/kg	^{137}Cs Bq/kg	$^{210}\text{Pb}/^{226}\text{Ra}$ Act. ratio	$^{226}\text{Ra}/^{234}\text{U}$	$^{226}\text{Ra}/^{238}\text{U}$
1	0-2	103.3±12.1	91.5± 35.5	794.5±75.7	744.3±130.1	1.13±0.45	3.55±1.38	3.45±1.35
2	2-4	86.3±15.1	93.4±47.5	113.7±48.2	174.2±15.4	0.92±0.44		
3	4-6	73.2±14.3	108.3±32.9		98.8±8.6	0.68±0.24		
4	6-8	68.3± 7.6	129.5±35.6		78.6±8.5	0.53±0.15		
5	8-10	61.6± 5.2			13.0±2.4			
6	10-12	62.9± 6.2	158.8±39.0		31.7±8.2	0.40±0.15		
7	12-14	21.4± 8.2	66.9±21.9		23.1±4.7	0.32±0.15		
8	14-16	46.8± 6.8	87.1±23.4		21.8±3.9	0.54±0.16		
9	16-18							
10	18-20							
11	20-22	48.6±5.1	93.4±24.3		13.8±3.3	0.52±0.14		
12	22-24	49.0±4.9	92.1±25.9		29.4±3.4	0.53±0.15	2.85±0.80	2.96±0.82
13	24-26							
14	26-28	36.5±6.6						
15	28-30							
16	30-32							
17	32-34							
18	34-36	52.6±7.2	102.0±30.0		21.3.8	0.52±0.17		
19	36-38							
20	38-40	30.7±7.1						
21	40-42							
22	42-44	42.6±8.1	83.7±22.7		12.7±3.3	0.51±0.16	3.17±0.86	3.38±0.88

Table 3.16: Uranium and thorium concentrations and concentration and activity ratios of stream water samples around the Criffel pluton, southwest Scotland.

Location	Nov. 1991			April 1992		
	U (ppb)	Th (ppb)	U/Th	U (ppb)	Th (ppb)	U/Th
Back burn	0.512	0.082	6.3	0.654	0.059	11.1
Fairgirth lane burn	0.765	0.056	14.3	1.305	0.111	11.8
Southwick burn	0.048	0.016	3.0	0.109	0.012	9.1
Prestonmill burn	0.047	0.013	3.6	0.097	ND	-
Drum burn	0.046	0.013	3.6	0.087	0.009	9.7
Glaisters burn	0.517	0.033	16.7	0.830	0.042	19.6
Kinharvie burn	0.438	0.052	8.3	1.256	0.068	18.5

Uranium concentration:

Maximum value	1.305 ppb
Minimum value	0.046 ppb
Mean value	0.437 ppb

	U (ppb)	$^{234}\text{U}/^{238}\text{U}$	^{230}Th
Kinharvie burn (*)	0.657 ± 0.030	1.22 ± 0.03	ND

Note: (i) All samples were analysed by ICP-MS, except sample marked (*).

(ii) ND - not detected.

(iii) (*) - determined by alpha spectrometry method.

CHAPTER 4

DISCUSSION AND CONCLUSION

In discussion of the results, the various aspects of the work will be considered as follows: (i) uranium and thorium concentrations and distributions and natural decay series disequilibrium in the different zones of the Criffel pluton; (ii) natural decay series radionuclide and REE behaviour in fissures and at redox fronts in rock sections from Craignair quarry, Dalbeattie; (iii) natural decay series radionuclide and REE distributions in granite and granodiorite cores from outcrops subject to post-glacial weathering; (iv) uranium transport/retardation and geochemical associations and the distribution of ^{210}Pb , ^{226}Ra , ^{134}Cs and ^{137}Cs in soil from the vicinity of the uranium mineralised vein at Beeswing; (v) uranium and thorium studies in stream water around the Criffel pluton; (vi) general conclusions.

4.1 Uranium and thorium concentrations and distributions and natural decay series disequilibrium in the different zones of the Criffel pluton.

As described in detail in section 1.7, the Criffel pluton consists of an upland area reaching an elevation of 569 m with a gradation from Biotite-Muscovite (BM) granite at the centre of the pluton, through concentric Muscovite-Biotite (MB) granite, Biotite (B) granite and Hornblende-Biotite (HB) granodiorite zones to an outer section of Clinopyroxene-Hornblende-Biotite (CHB) granodiorite. This area was heavily glaciated with the most recent period of glaciation ending about 12000 years ago. It has been estimated that around 10 m of rock was removed from the summit of the

pluton and perhaps up to 30 m from the lower areas around it by ice action during the last glaciation (Jardine, 1966; Jardine, 1993). The glacial erosion would have removed the surficial, weathered rock from the pluton, leaving an exposed surface of fresh rock and it is reasonable to assume that intense weathering of the newly exposed rock surface started when the ice retreated. Under such conditions it is likely that uranium could be preferentially dissolved relative to thorium and that natural decay series disequilibrium in the near-surface rock of the pluton would develop rapidly. The possibility must also be considered, however, that some weathering occurred as a result of percolating water in the rock below the ice cover or that the rock retains a residual signature of much older (10^5 y time-scale) disequilibrium.

The uranium and thorium contents of the 169 archived samples analysed are given in Table 3.1 and the sampling locations are shown in Figure 2.2. The average uranium and thorium concentrations and their maximum and minimum values and Th/U concentration ratios for different zones of the Criffel pluton are given in Table 4.1. An examination of Table 4.1 and Figure 4.1 reveals that both uranium and thorium concentrations in the samples from different zones of the pluton do vary to a certain extent. For instance, the BM- and B-zones have a lower average uranium content than the other zones. The B-zone has a distinct maximum with a systematic decrease thereafter towards the edge of the pluton. Uranium is apparently enriched in the B-granite zone (4.8 ppm U) compared to the other zones in the pluton (Table 4.1 and Figure 4.1), suggesting that more uranium probably occurs in crystal inclusions such as zircons within biotite, as well as along grain boundaries of biotite (i.e. intergranular uranium), in addition to uranium that is present in accessory minerals such as sphene, monazite and apatite. In the case of thorium concentrations there is a distinct minimum for the BM-zone with a suggestion of a slight increase

Table 4.1: Mean and modal values and ranges of uranium and thorium concentrations and Th/U concentration ratios of granite and granodiorite samples from different zones of the Criffell pluton, southwest Scotland.

	BM-granite	MB-granite	B-granite	HB-grano-diorite	CHB-grano-diorite	All
No. of samples (n)	7	28	29	52	53	169
Uranium (ppm)						
Mean values	3.8 ± 0.4	3.6 ± 0.4	4.8 ± 0.6	4.3 ± 0.4	3.9 ± 0.4	4.1 ± 0.4
Range	2.5 - 5.0	2.2 - 7.8	2.3 - 5.7	2.0 - 8.0	2.2 - 6.8	2.0 - 8.0
Modal values		3	5	3 and 5	3 and 5.5	3
Distribution /trend	no obvious trend	assymetric dist. about mode, tailing to higher values	slightly assymet. distribution	slight tail to higher values	bimodal distribution	very few values above 5.5 ppm

Table 4.1 (cont.)

Thorium (ppm)							
Mean values	9.8 ± 0.6	13.1 ± 0.4	13.7 ± 0.4	13.4 ± 1.1	14.7 ± 1.1	13.6 ± 1.2	
Range	7.1 - 14.5	9.4 - 18.7	9.2 - 20.1	6.9 - 24.8	7.4 - 24.7	6.9 - 24.8	
Modal values		14 or 11	11 and 15	no distinct mode	11, 13-14, 19 dominant	11 and 14	
Distribution /trend	no obvious trend	Irregular dist.	Bimodal?	broad bimodal dist.	Irregular dist.	bimodal about 11, 14	
Th/U							
Mean values	2.7 ± 0.3	3.7 ± 0.5	2.8 ± 0.4	3.1 ± 0.4	3.7 ± 0.5	3.3 ± 0.4	
Range	1.7 - 3.3	1.6 - 6.3	1.8 - 4.9	1.6 - 4.8	1.7 - 5.9	1.6 - 6.3	
Modal values		3	2.5	3	4	3	
Distribution /trend	no obvious trend	assymetric	possibly bimodal	relatively symmetrical	possibly bimodal	slightly tail towards higher value	

Figure 4.1: Average uranium and thorium concentrations of samples from different zones of the Criffel pluton (from centre to the edge of the pluton).

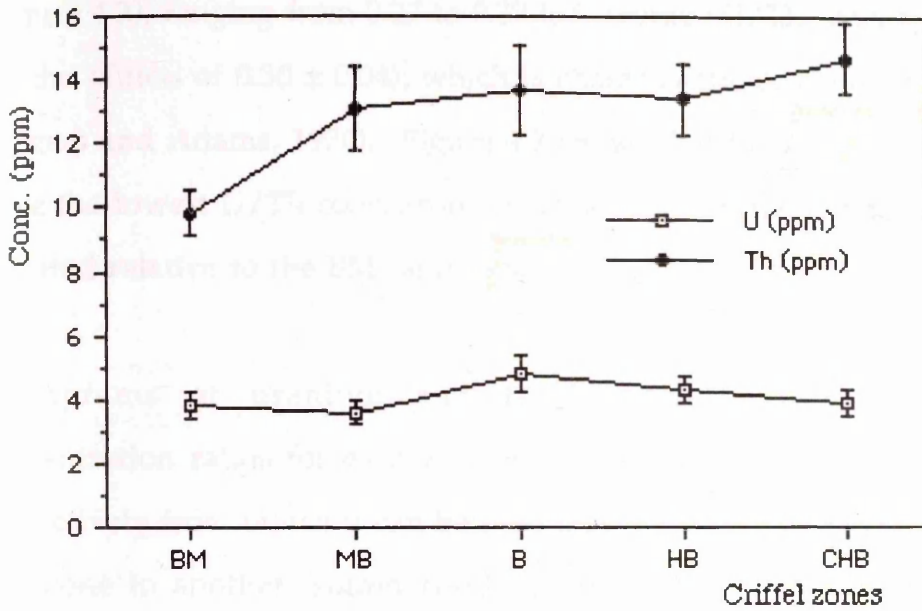
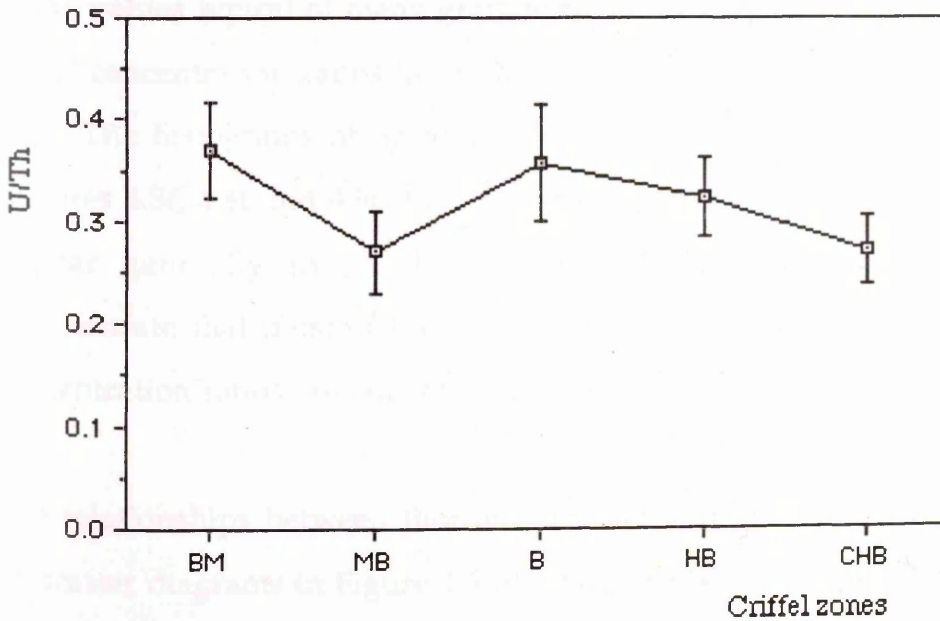


Figure 4.2: Average U/Th concentration ratios of samples from different zones of the Criffel pluton (from centre to the edge of the pluton).



Note:

- BM : Biotite-muscovite granite zone
- MB : Muscovite-biotite granite zone
- B : Biotite zone
- HB : Hornblende-biotite granodiorite zone
- CHB: Clinopyroxene-hornblende-biotite zone

from MB^{granite}-zone towards the edge of the pluton (Figure 4.1). The plot of U/Th concentration ratios shows relatively constant values for all zones (Figure 4.2), ranging from 0.27 to 0.37 (c.f. average U/Th concentration ratio for the pluton of 0.30 ± 0.04), which is characteristic of many granitic rocks (Rogers and Adams, 1970). Figure 4.2 shows that the MB^{granite}- and CHB^{granodiorite}-zones have the lowest U/Th concentration ratios and that the HB-zone is slightly elevated relative to the BM- and B^{granite}-zones.

Histograms of uranium and thorium concentrations and Th/U concentration ratios for each zone are depicted in Figures 4.3, 4.4 and 4.5 respectively from which it can be seen that the values do vary slightly from one zone to another (summarised in Table 4.1). Uranium values for the pluton in general range from 2.0 to 7.8 ppm (average value is 4.1 ± 0.4 ppm) and the thorium values from 6.9 to 24.8 ppm (average value is 13.6 ± 1.2 ppm), values typical of many granitic rocks (Rogers and Adams, 1970). The Th/U concentration ratios lie in the range 1.6 to 6.3 (average value is 3.3 ± 0.4). The histograms of uranium, thorium and Th/U concentration ratios (Figures 4.3f, 4.4f and 4.5f) for the complete set of samples from the pluton appear generally to be skewed towards higher values. They also demonstrate that most of the values obtained for each element and Th/U concentration ratios are clustered closely around their average values.

The relationships between thorium and uranium for each zone are shown on scatter diagrams in Figure 4.6 in which the best fitting straight lines and the correlation coefficients are indicated. An examination of Figure 4.6 indicates that there is no relationship between uranium and thorium in the B-zone ($r = 0.10$) but a weak positive correlation in the MB ($r = 0.35$) and HB ($r = 0.48$) - zones and a slightly stronger correlation in BM ($r = 0.52$) and CHB ($r = 0.59$) - zones. A t-test of uranium and thorium for each zone indicates

Figure 4.3: Histograms of uranium concentrations for samples from (a) BM-granite, (b) MB-granite, (c) B-granite, (d) HB-granodiorite, (e) CHB-granodiorite and (f) Criffel pluton (all samples) (c.f. Table 4.1).

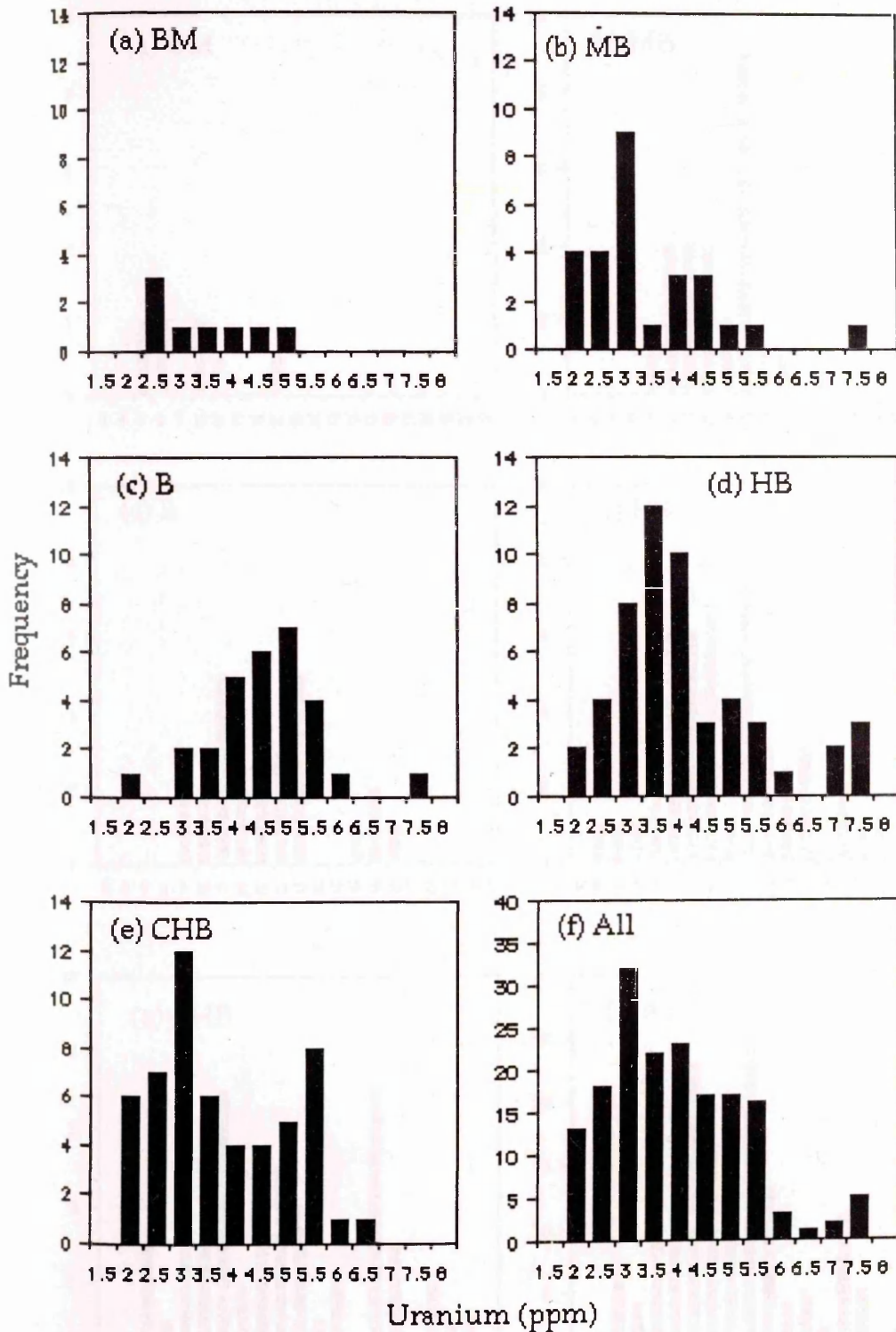


Figure 4.4: Histograms of thorium concentrations for samples from (a) BM-granite, (b) MB-granite, (c) B-granite, (d) HB-granodiorite, (e) CHB-granodiorite and (f) Criffel pluton (all samples) (c.f. Table 4.1).

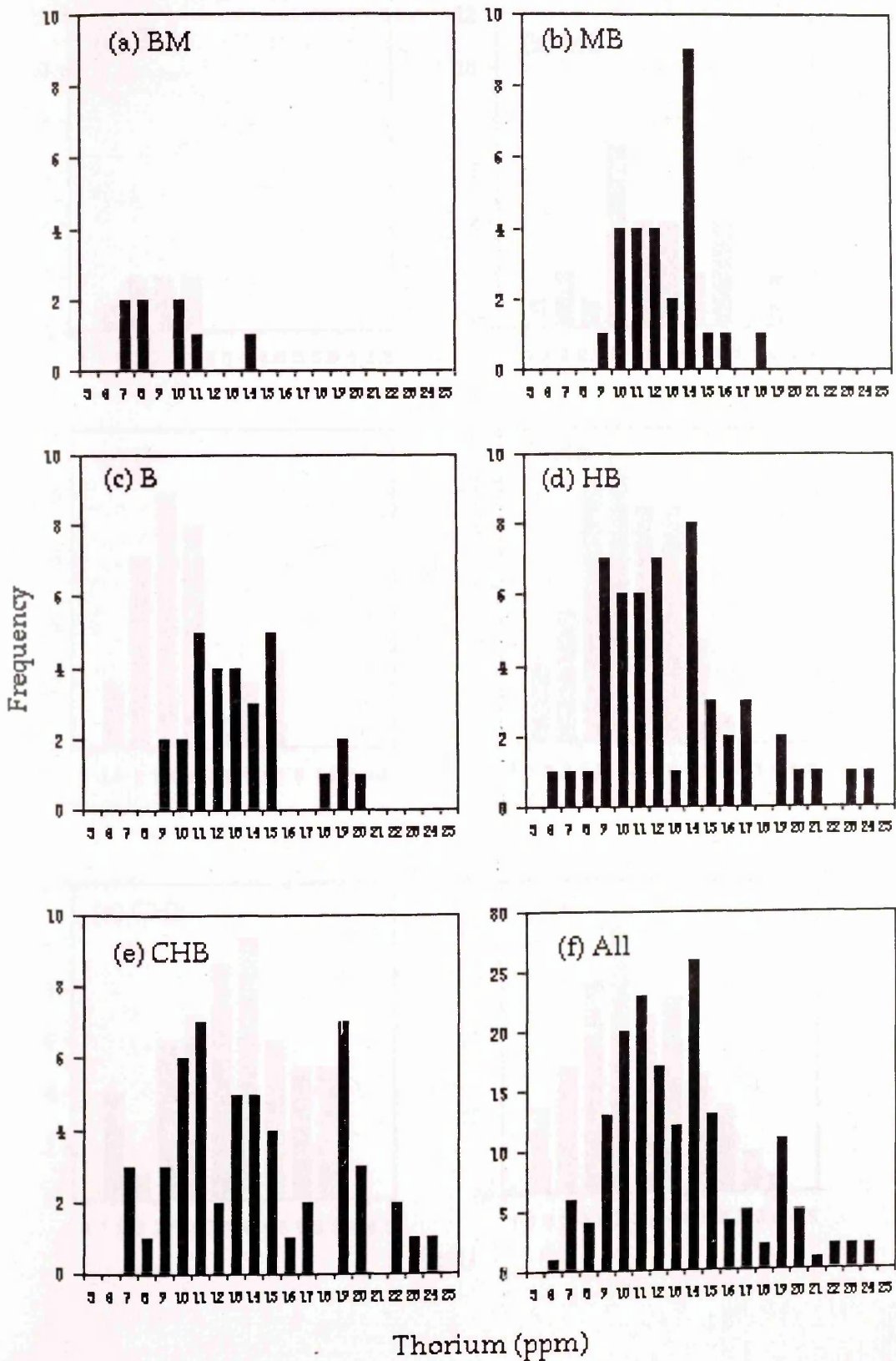


Figure 4.5: Histograms of Th/U concentration ratios for samples from (a) BM-granite, (b) MB-granite, (c) B-granite, (d) HB-granodiorite, (e) CHB-granodiorite zones and (f) Criffel pluton (all samples) (c.f. Table 4.4).

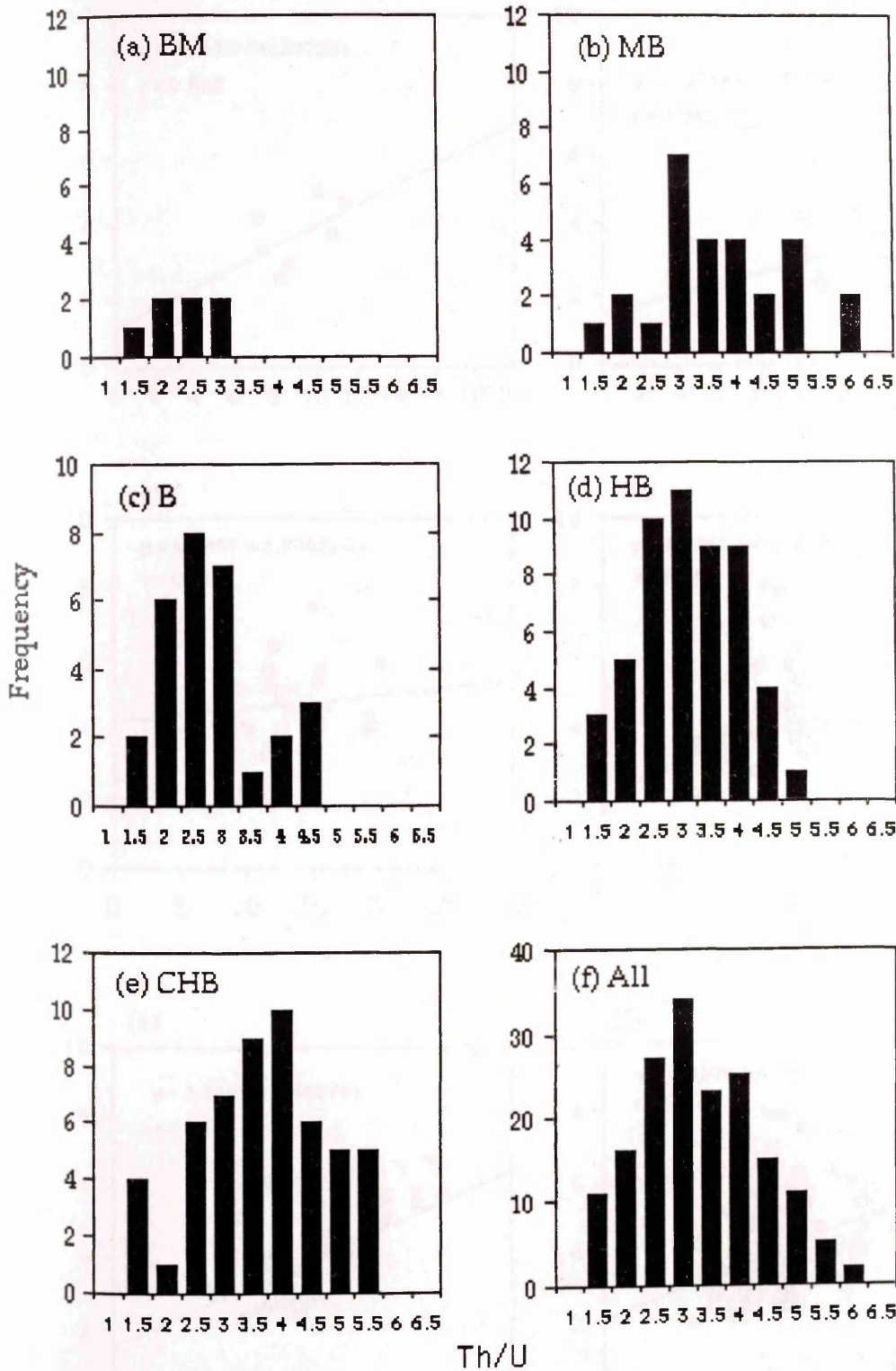
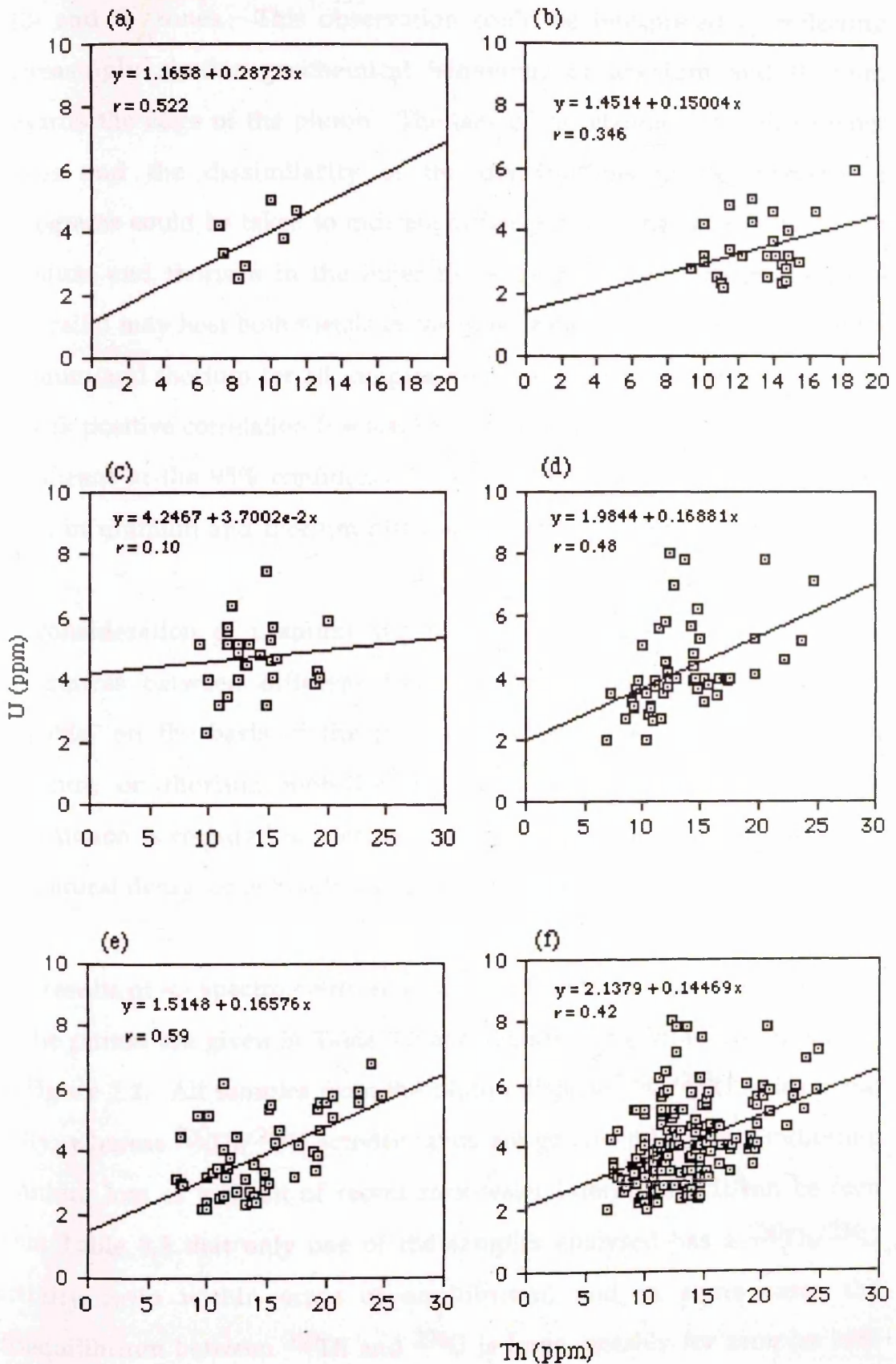


Figure 4.6: Uranium versus thorium concentrations for samples from (a) BM-granite, (b) MB-granite, (c) B-granite, (d) HB-granodiorite, (e) CHB-granodiorite and (f) Criffel pluton (all samples).



that the results for both HB- and CHB-^{granodiorite} zones are significant at the 95% confidence level ($P < 0.05$) whereas the values are not significant in the BM, MB- and B-^{granite} zones. This observation could be interpreted as reflecting increasingly similar geochemical behaviour of uranium and thorium towards the edge of the pluton. The lack of correlation in the three inner zones and the dissimilarity of the distributions in the preceding histograms could be taken to indicate different mineralogical associations of uranium and thorium in the inner three zones, while perhaps the same mineral(s) may host both metals in the outer zones. The overall data set for uranium and thorium for all samples from the pluton (Figure 4.6f) suggests a weak positive correlation ($r = 0.42$) and a t-test indicates that the results are significant at the 95% confidence level ($P < 0.05$), indicating a systematic trend in uranium and thorium distributions in the pluton as a whole.

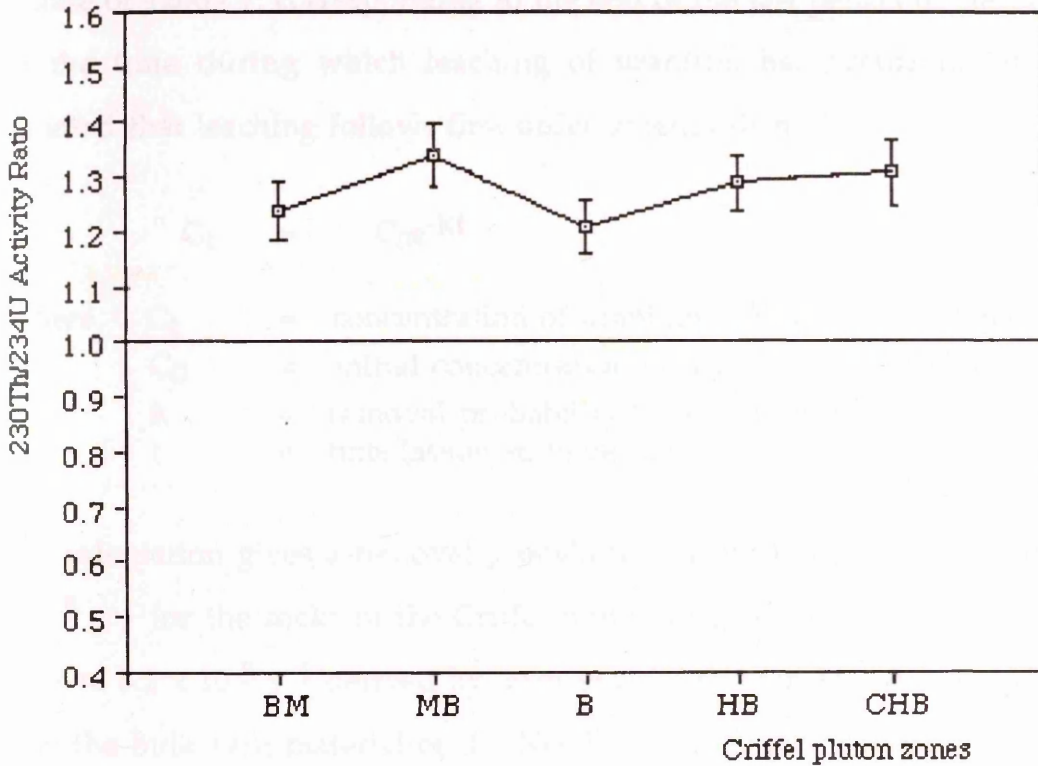
So consideration of uranium and thorium concentrations reveals some differences between different zones in the pluton, although it is not possible, on the basis of the present data, to draw conclusions about uranium or thorium mobility, loss and re-deposition. Additional information is required to identify such processes and this is provided by the natural decay series results as discussed below.

The results of α -spectrometric analyses of 19 samples from different zones of the pluton are given in Table 3.2 and the sampling locations are shown in Figure 2.2. All samples from the pluton display $^{234}\text{U}/^{238}\text{U}$ ratios about unity, whereas $^{230}\text{Th}/^{234}\text{U}$ activity ratios are greater than unity, indicating uranium loss as a result of recent rock-water interaction. It can be seen from Table 3.2 that only one of the samples analysed has a $^{230}\text{Th}/^{234}\text{U}$ activity ratio within error of equilibrium, and in some cases the disequilibrium between ^{230}Th and ^{234}U is large, notably for samples MB-

272 (1.62), HB-135 (1.45), CHB-206 (1.59) and CHB-244 (1.47). The $^{230}\text{Th}/^{234}\text{U}$ data could be taken to indicate that the minerals in the MB-^{granite} HB- and CHB-^{granodiorite} zones are more susceptible to uranium loss than the other two zones but, when uncertainties are considered, it is apparent that the average values of the $^{230}\text{Th}/^{234}\text{U}$ activity ratio (Figure 4.7) for samples from different zones of the pluton are effectively constant (i.e. BM-granite = 1.24 ± 0.05 ; MB-granite = 1.34 ± 0.06 ; B-granite = 1.22 ± 0.05 ; HB-granodiorite = 1.28 ± 0.06 ; and CHB-granodiorite = 1.32 ± 0.07). This observation reveals that approximately 30% of the uranium has been lost from the surface rocks in the MB-^{granite} HB- and CHB-^{granodiorite} zones of the pluton and that less uranium has been removed from the B- and BM-^{granite} zones; here the average loss of uranium is about 22% and 24% respectively. Thorium has apparently remained immobile. The fact that in all cases the $^{234}\text{U}/^{238}\text{U}$ activity ratio is within error of unity while the $^{230}\text{Th}/^{234}\text{U}$ activity ratios are systematically greater than unity demonstrates rapid removal of uranium (i.e. bulk dissolution of minerals with equal removal of ^{234}U and ^{238}U). These observations indicate that effectively all of the samples have undergone significant, recent uranium loss, i.e. they should be regarded as weathered, rather than fresh, samples. This is an important observation, which highlights the difficulty in collecting fresh geological samples and suggests that the potential effects of weathering should be considered in any similar geochemical study.

If the original uranium content before weathering is assumed to be about 5 mg kg^{-1} and uranium loss is estimated at about 1 mg kg^{-1} (20% loss) from the surface of the pluton in the last 12000 years, the resulting regional loss of uranium from the rock to depths of 1 cm, 10 cm and 20 cm over the total extent of

Figure 4.7: Distribution of $^{230}\text{Th}/^{234}\text{U}$ activity ratios for samples from different zones of the Criffell pluton (from centre to the edge of the pluton).



Note:

BM: Biotite-muscovite granite

MB: Muscovite-biotite granite

B: Biotite granite

HB: Hornblende-biotite granodiorite

CHB: Clinopyroxene-hornblende-biotite granodiorite

the pluton (27 x 10 km) is estimated to be 6.2×10^6 g (7.4×10^{12} Bq), 6.2×10^7 g (7.4×10^{13} Bq) and 1.24×10^8 g (7.4×10^{14} Bq) respectively (assuming that the density of granite is about 2650 kg m^{-3}). On this basis, values for the probability of uranium removal by dissolution can be derived by assuming a value of 12000 y, corresponding to the end of the last period of glaciation, for the time during which leaching of uranium has occurred. If it is assumed that leaching follows first order kinetics then,

$$C_t = C_0 e^{-kt}$$

where C_t = concentration of uranium at time $t = 4.00 \text{ mg kg}^{-1}$
 C_0 = initial concentration of uranium = 5.00 mg kg^{-1}
 k = removal probability for uranium (y^{-1})
 t = time (assumed to be 12000 y in this case)

This calculation gives a removal probability for uranium dissolution of $1.9 \times 10^{-5} \text{ y}^{-1}$ for the rocks of the Criffel pluton in general, comparable to the value of $5.2 \times 10^{-5} \text{ y}^{-1}$ derived by Scott et al. (1991) for uranium dissolution from the bulk vein material of the Needle's Eye mineralisation.

The uranium and thorium isotopic data for each zone of the pluton are presented in a plot of the $^{234}\text{U}/^{238}\text{U}$ activity ratio against the $^{230}\text{Th}/^{238}\text{U}$ activity ratio in Figure 4.8. An examination of Figure 4.8 reveals that these plots show similar patterns for all zones, with almost all samples lying on or close to the $^{234}\text{U}/^{238}\text{U} = 1.00$ line in positions to be expected from recent, rapid dissolution of uranium from the pluton without fractionation. This interpretation is more clearly illustrated in Figure 4.8f (i.e. for all samples from the pluton) where the positions of data points with respect to the $^{234}\text{U}/^{238}\text{U}$ activity ratios generally lie close to unity (average value of $^{234}\text{U}/^{238}\text{U}$ is 1.01 ± 0.05) while $^{230}\text{Th}/^{238}\text{U}$ activity ratios are greater than unity.

Figure 4.8: Plots of $^{234}\text{U}/^{238}\text{U}$ activity ratio versus $^{230}\text{Th}/^{238}\text{U}$ activity ratio for whole-rock samples from (a) BM, (b) MB, (c) B, (d) HB and CHB zones and (f) Criffel pluton (all samples).

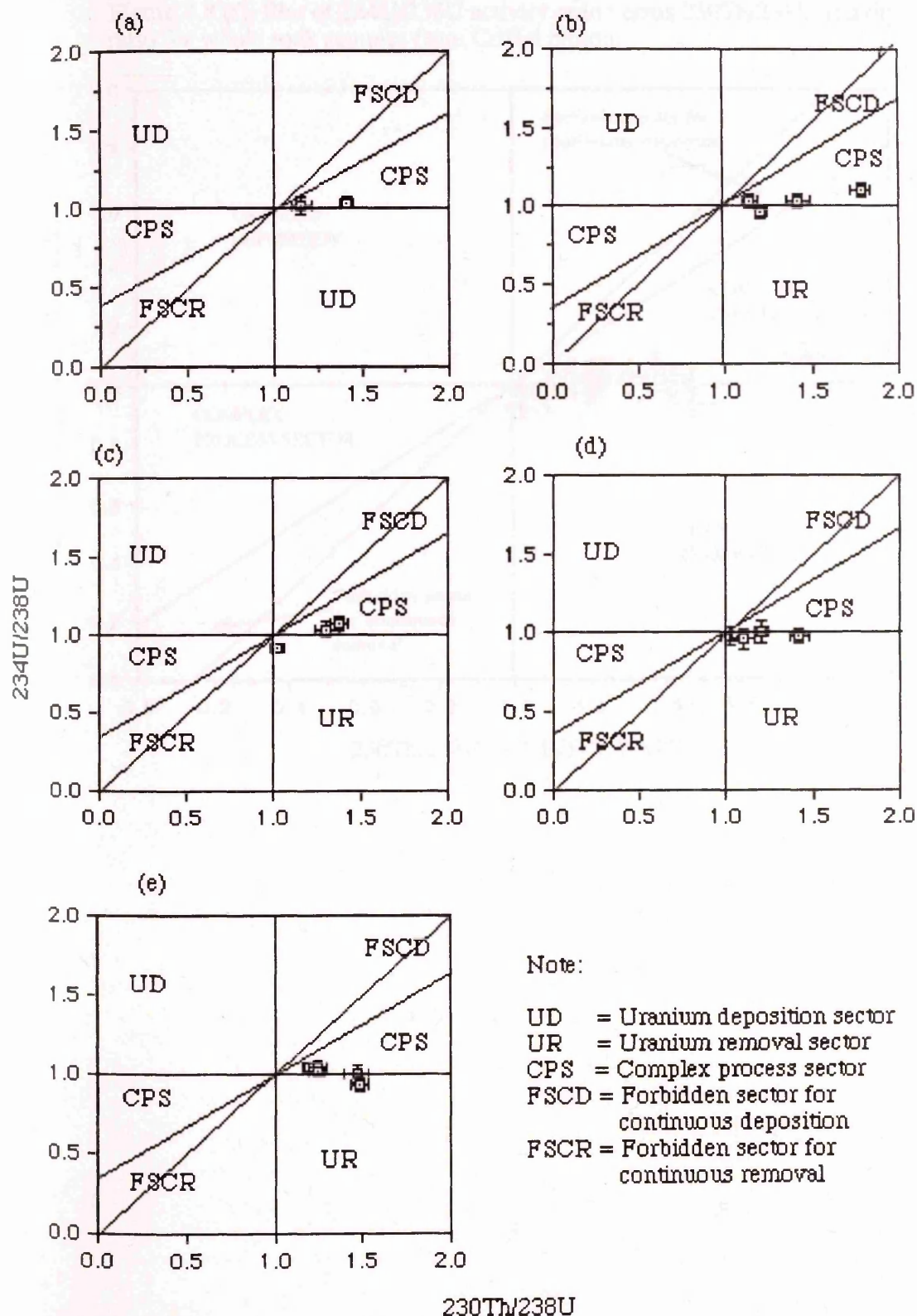
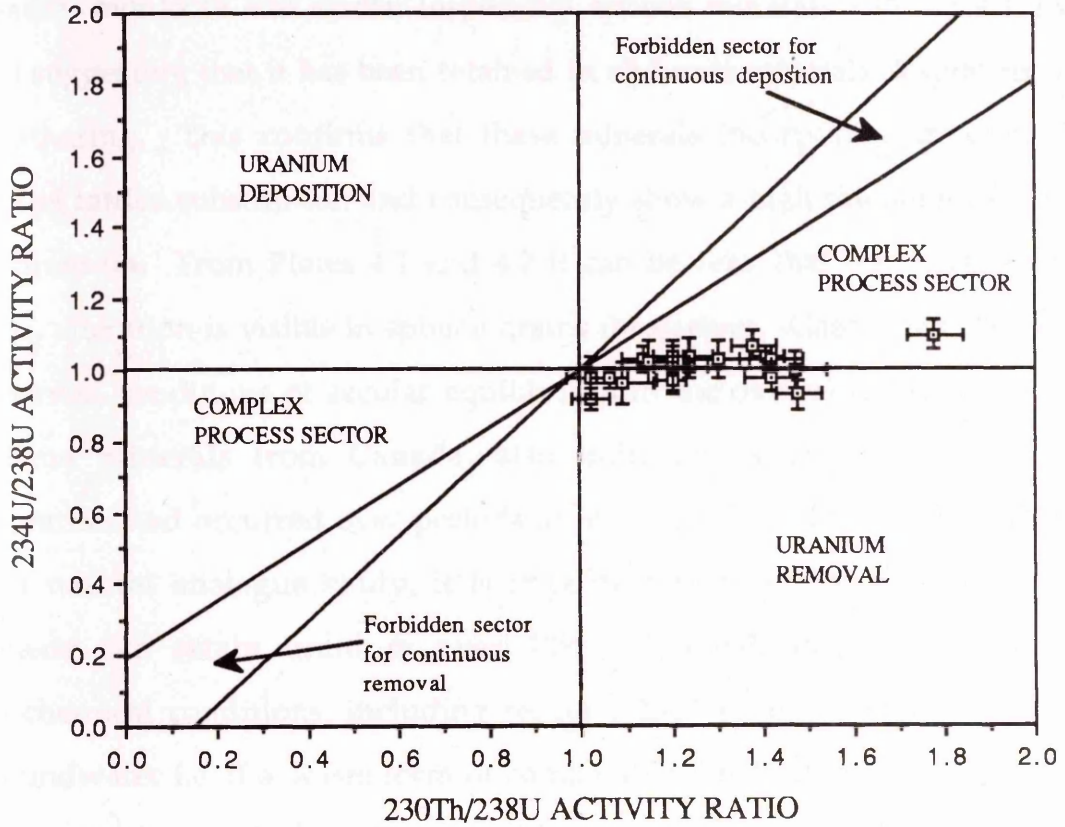


Figure 4.8 (f): Plot of $^{234}\text{U}/^{238}\text{U}$ activity ratio versus $^{230}\text{Th}/^{238}\text{U}$ activity ratio for whole rock samples from Criffel pluton.



Fission track studies of samples from the HB-granodiorite zone from Craignair quarry indicate that uranium is mainly distributed in two ways. Firstly, it is found in association with accessory minerals such as sphene, apatite, monazite and zircon (especially sphene minerals - Plates 4.1 and 4.2) suggesting that it has been retained in obdurate minerals despite recent weathering. This confirms that these minerals incorporate uranium by crystal lattice substitution and consequently show a high retention capacity of uranium. From Plates 4.1 and 4.2 it can be seen that no, or relatively little, alteration is visible in sphene grains themselves. Gascoyne (1986) has observed conditions of secular equilibrium in the natural decay series for sphene minerals from Canada, also indicating that no radionuclide migration had occurred over periods of at least 10^6 y. Thus in the context of a natural analogue study, it is important to note that a mineral like sphene can retain uranium over 10^6 y timescale under a variety of geochemical conditions, including recent (12000 y) exposure to oxidising groundwater i.e. if a waste form of comparable durability can be produced then retention for 10^4 to 10^6 y would be obtained. Secondly, uranium is found distributed along crystal boundaries of biotite or at boundaries of crystal inclusions, such as zircons, within biotite (Plate 4.3).

The 'whole-rock' depletion of uranium observed in the samples of the Criffel pluton may be attributed to the following mechanisms: (i) a significant proportion of the whole grains of the obdurate minerals may be removed during weathering, and (ii) interstitial uranium is probably lost from altered biotite ^{grain boundaries} and feldspar ~~edges~~ and their associated alteration products (chlorite and clay minerals).

In summary, analyses clearly indicate uranium losses from all parts of the pluton whereas thorium is retained; consistent with the expected

Plate 4.1: Matched thin-section (a) and fission track image on plastic film (b). Fission track print showing association of uranium with sphene grain.

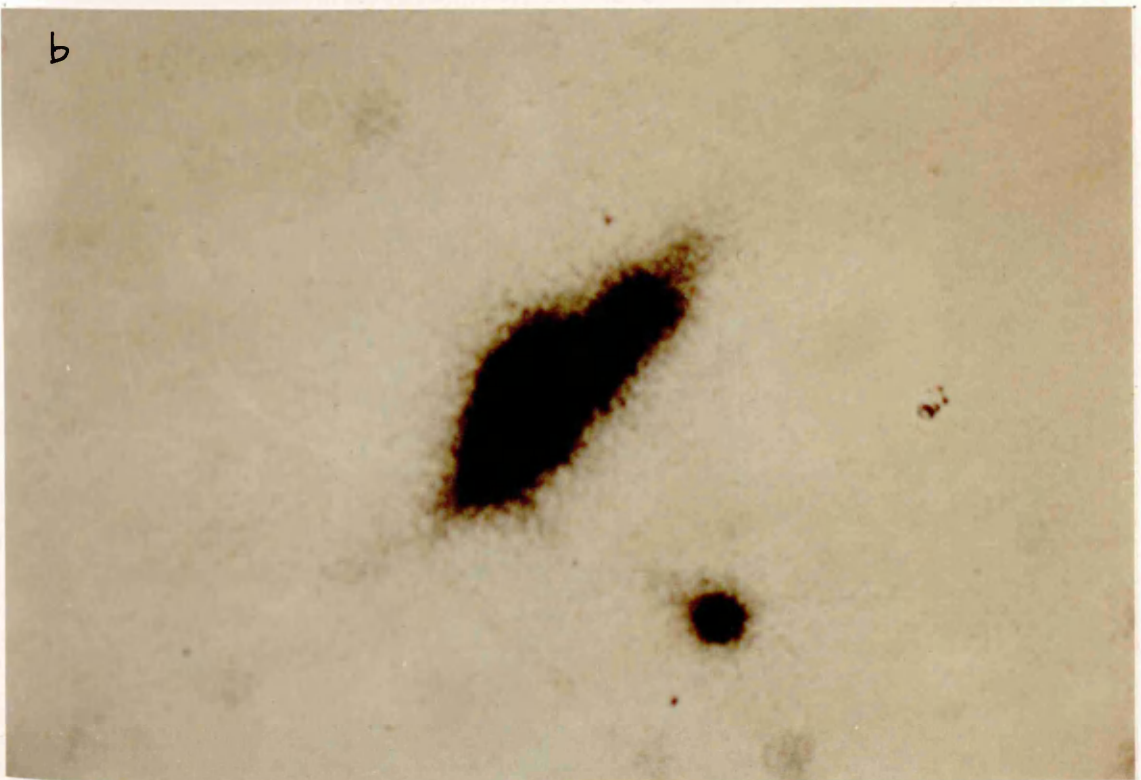
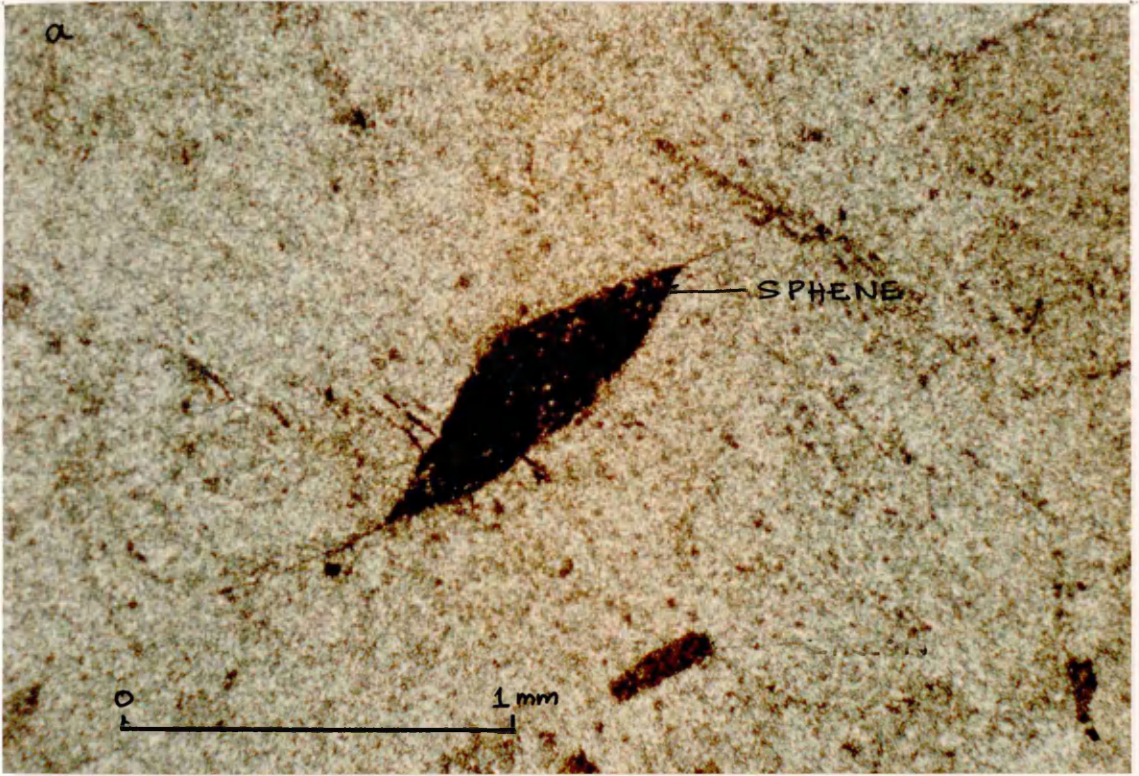


Plate 4.2: Matched thin-section (a) and fission track image on plastic film (b). Fission track print showing association of uranium with sphene (altered granite sample but showing unaltered obdurate minerals).

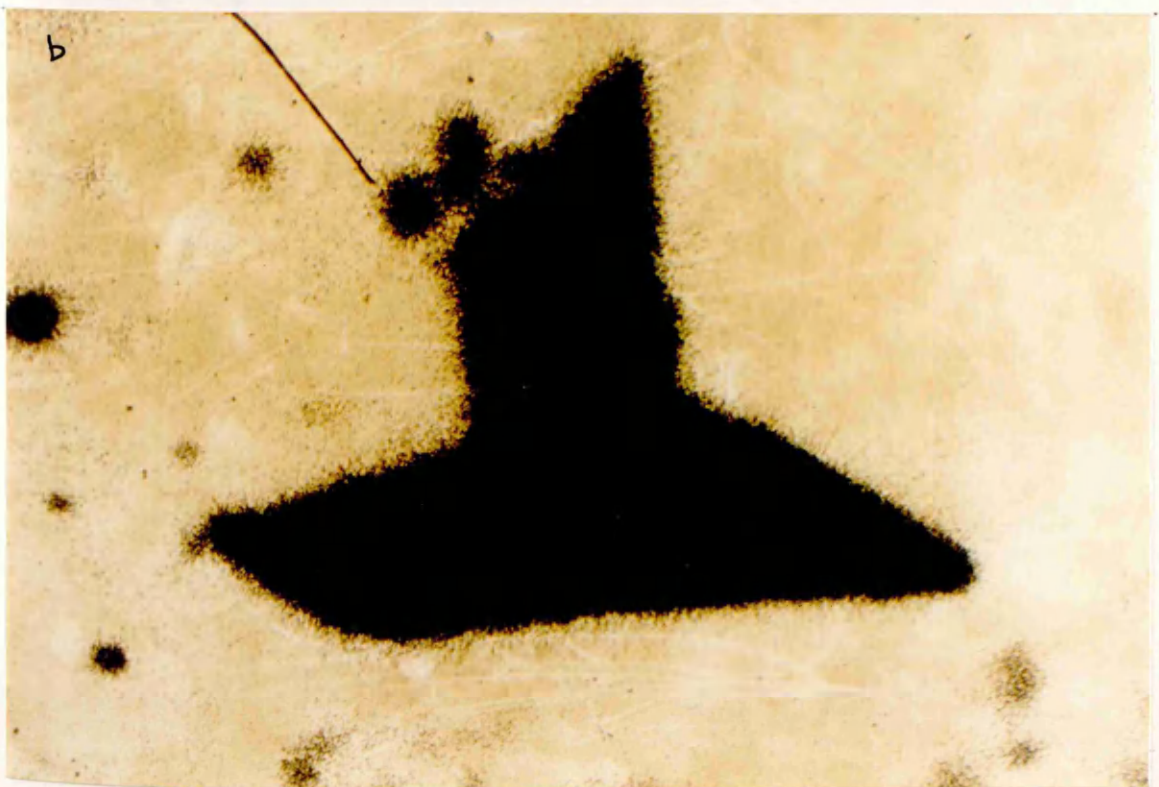
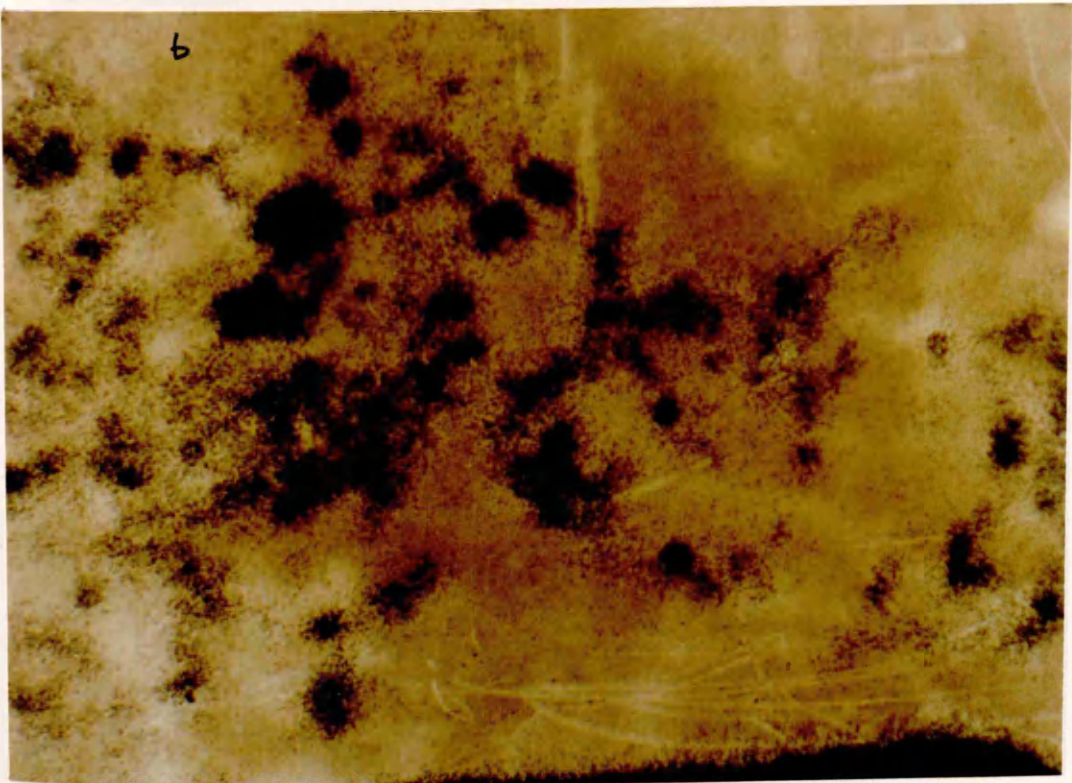
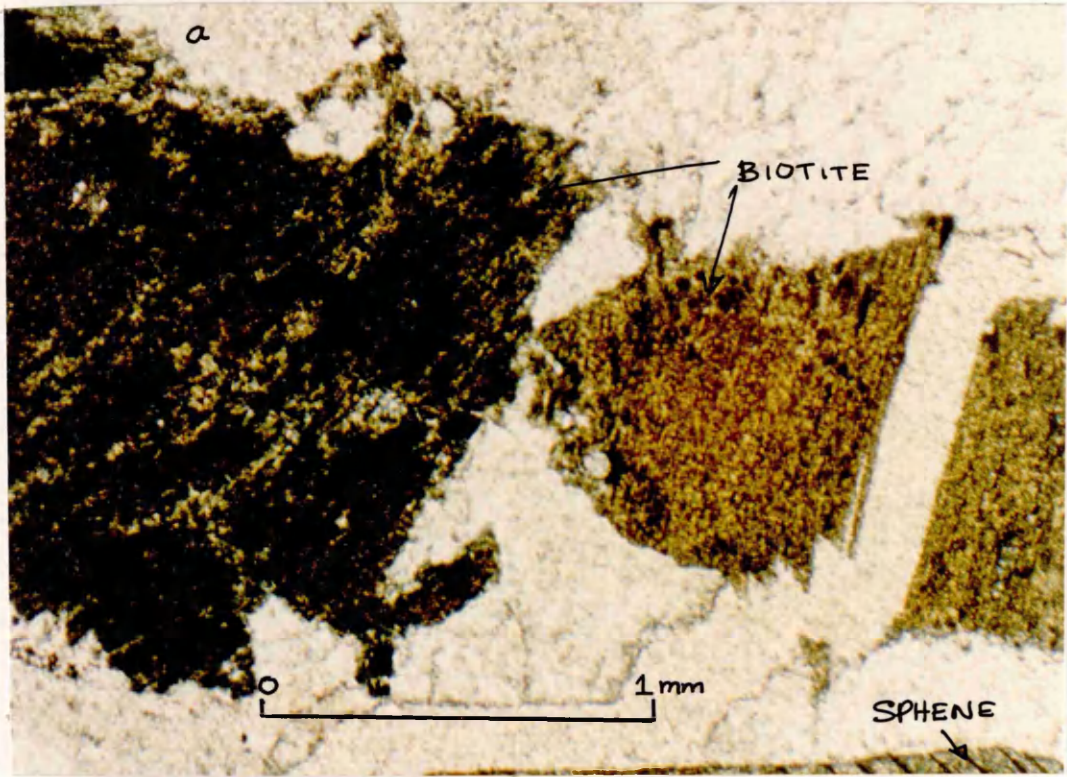


Plate 4.3: Matched thin-section (a) and fission track image on plastic film (b). Fission track print showing association of uranium with biotite (tracks around biotite minerals).



geochemical behaviour of these two elements in igneous rock i.e. uranium is susceptible to oxidation-induced dissolution and is, consequently, relatively mobile, whereas thorium is effectively immobile. The isotopic results also reveal the loss of uranium relative to ^{230}Th and show that the uranium loss has been rapid, and the time was insufficient to allow the development of detectable disequilibrium between ^{234}U and ^{238}U .

So we can say that the ^{surface part of the}pluton has lost between 20 and 30% of its uranium over the last 12000 y. The similarity between observed uranium behaviour in the different zones of the pluton suggests that there is no significant 'whole-rock' re-deposition within any zone. Thus this suggests that the whole-rock structure of the pluton presents a negligible barrier to uranium migration on a scale of 10 km over a time of about 12000 y. Thus the only probable sites of retardation of uranium would appear to be in fractures and at redox fronts. This point will be rejoined in detail in sections 4.2 and 4.3. This observation clearly has implications for radioactive waste disposal in the context of far-field movement of soluble nuclides, and highlights the importance of characterising radionuclide retardation by processes related to fissure flow (eg. sorption, matrix diffusion and advection), redox fronts and groundwater flow vectors.

4.2 Natural decay series radionuclide and REE behaviour in fissures and at redox fronts in rock sections from Craignair quarry, Dalbeattie

4.2.1 CQ1 rock section studies

4.2.1.1 Natural decay series studies

The concentrations and activity ratios of natural decay series radionuclides in samples from rock section CQ1, which was obtained approximately 2m from the top of the quarry in the HB-granodiorite zone, are given in Table 3.3. The redox front in this section of rock was visually obvious as a clearly defined, sharp colour change marking the transition from Fe^{2+} to Fe^{3+} at a distance of 4 cm into the rock from the fracture wall as shown in Fig. 2.4. Full details of the sample and the quarry are provided in section 2.1.1. Plots of U and Th concentrations, U/Th concentration ratios, $^{234}\text{U}/^{238}\text{U}$, $^{230}\text{Th}/^{234}\text{U}$ and $^{226}\text{Ra}/^{230}\text{Th}$ activity ratios versus distance from the fracture face, $^{234}\text{U}/^{238}\text{U}$ activity ratios versus $^{230}\text{Th}/^{238}\text{U}$ activity ratios and $^{226}\text{Ra}/^{230}\text{Th}$ activity ratios versus $^{230}\text{Th}/^{234}\text{U}$ activity ratios are shown in Figures 4.9 to 4.15 and 4.17.

The plot of uranium concentration against distance for section CQ1 (Figure 4.9) shows that uranium is strongly enriched at the fracture (11 ppm relative to a mean value of 4.3 ppm for the HB-granodiorite), indicative of uptake in the iron- and manganese-oxyhydroxides, carbonates and clay fracture-lining minerals. This suggests that uranium, which is leached from the bulk rock, is partially re-deposited on fracture-lining minerals during groundwater transport. Uranium accumulates either by sorption or co-precipitation, with iron-oxyhydroxides which are recognised as good

Figure 4.9: Plot of uranium concentration versus distance from the fracture face for rock section CQ1 from Craignair quarry, Dalbeattie.

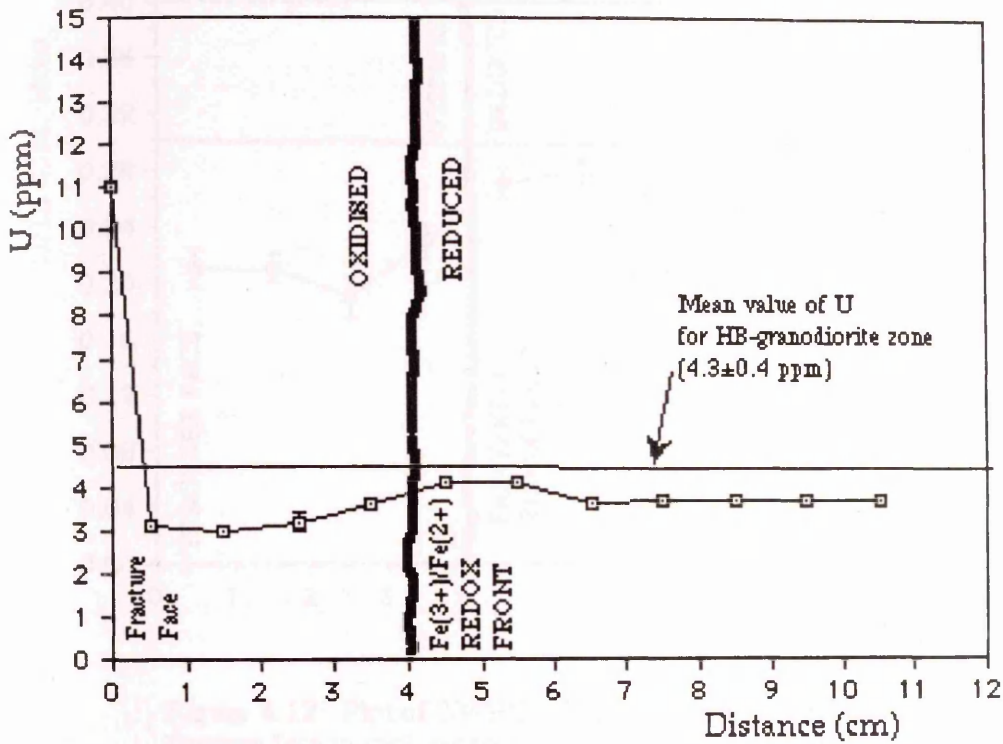


Figure 4.10: Plot of thorium concentration versus distance from the fracture face for rock section CQ1 from Craignair quarry, Dalbeattie.

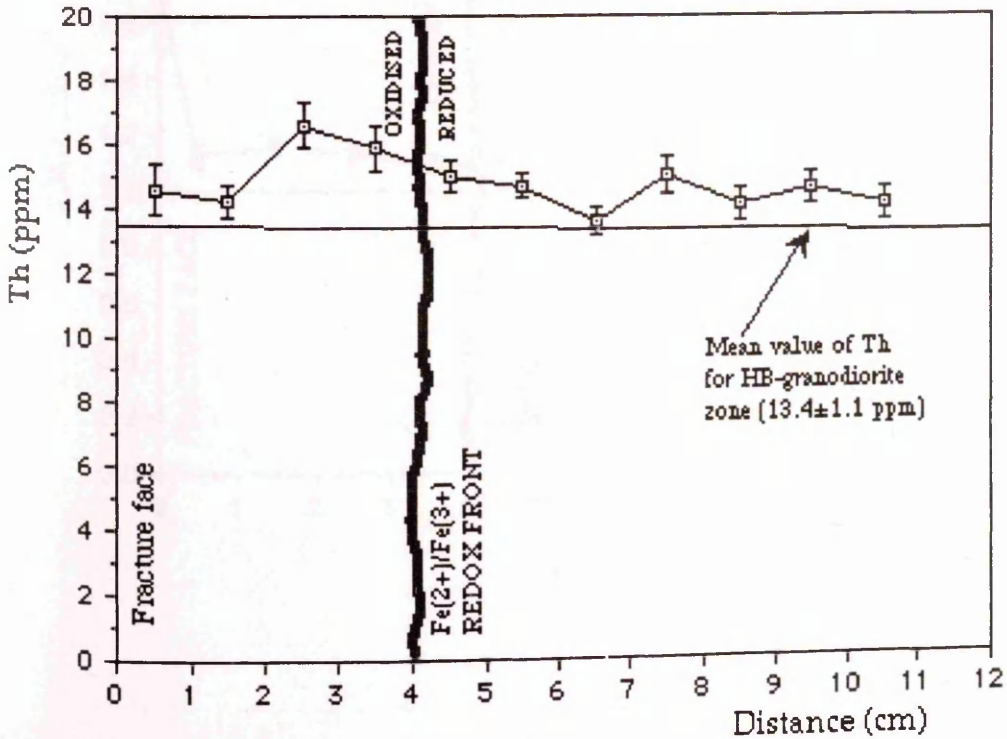


Figure 4.11: Plot of U/Th concentration ratio versus distance from the fracture face in rock section CQ1 from Craignair quarry, Dalbeattie

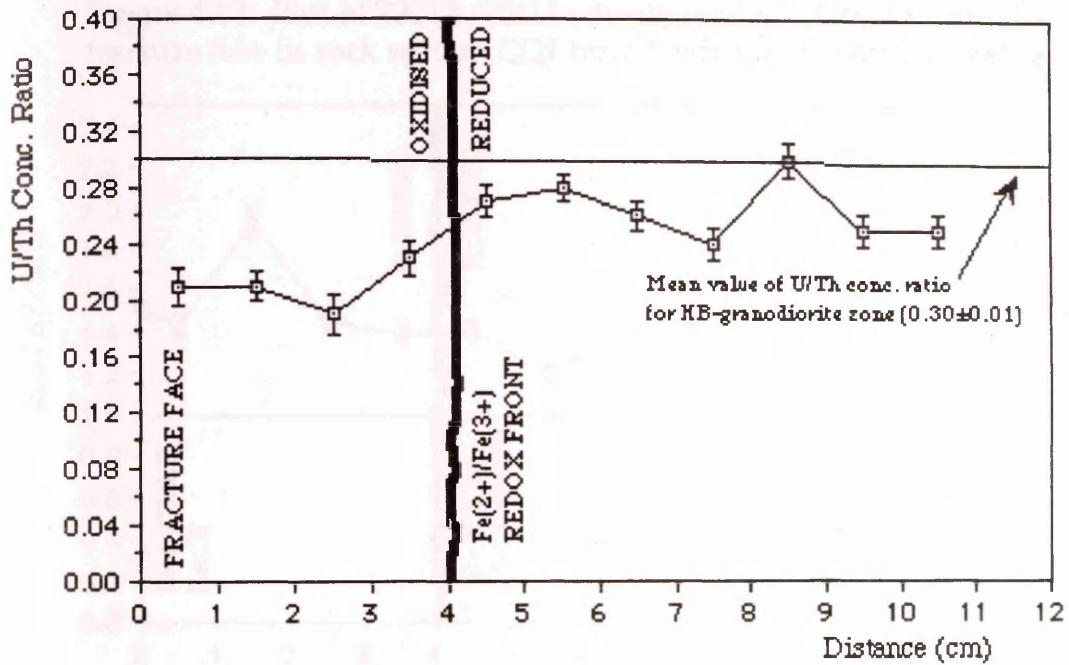


Figure 4.12: Plot of $^{234}\text{U}/^{238}\text{U}$ activity ratio versus distance from the fracture face in rock section CQ1 from Craignair quarry, Dalbeattie

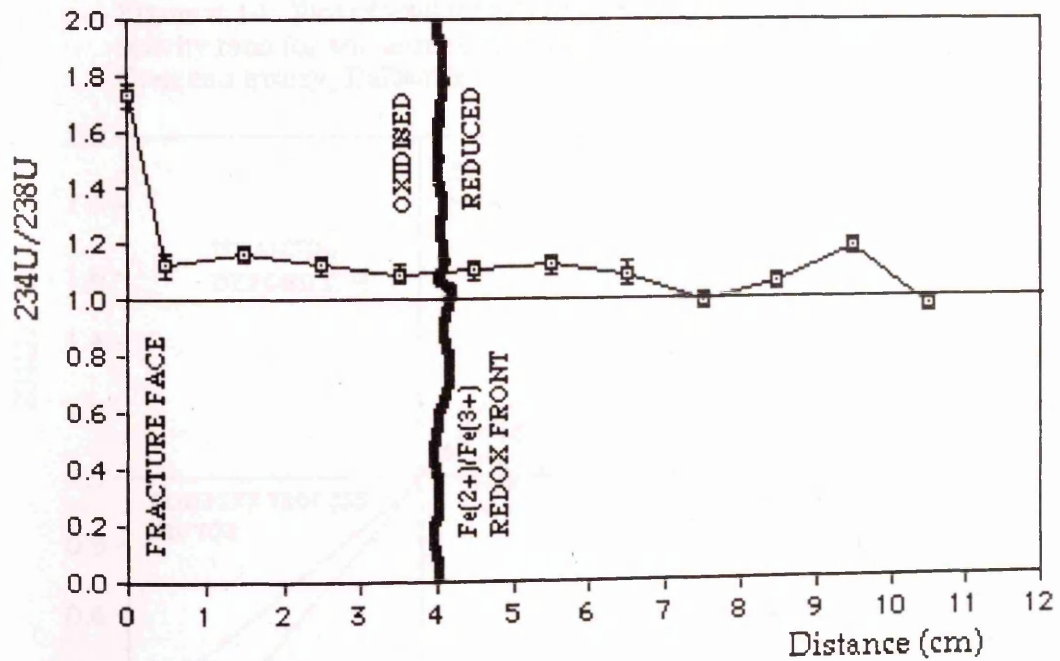


Figure 4.13: Plot of $^{230}\text{Th}/^{234}\text{U}$ activity ratio vs distance from the fracture face in rock section CQ1 from Craignair quarry, Dalbeattie

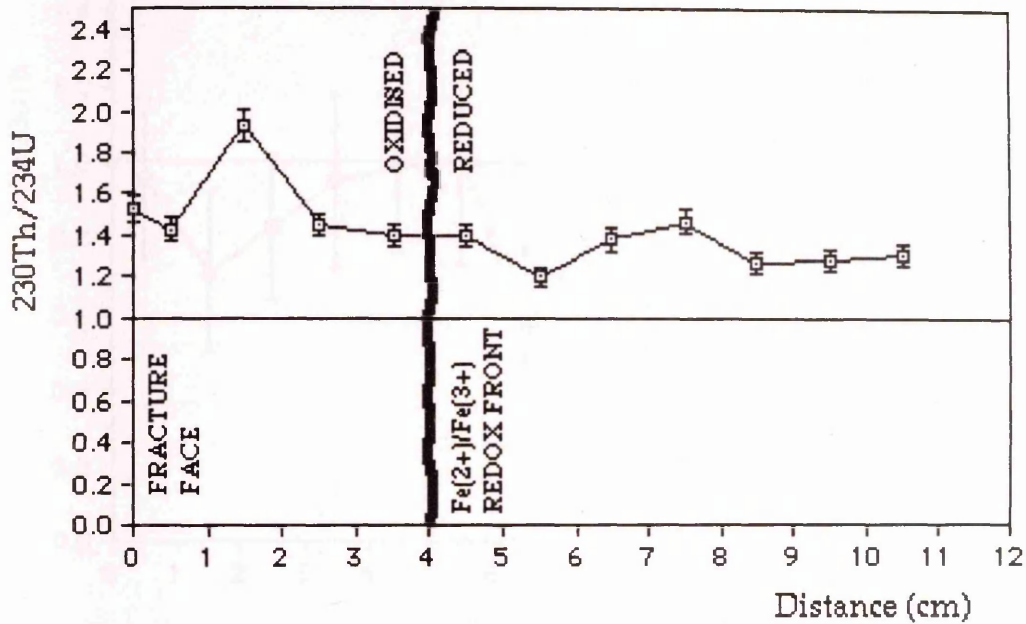


Figure 4.14: Plot of $^{234}\text{U}/^{238}\text{U}$ activity ratio versus $^{230}\text{Th}/^{238}\text{U}$ activity ratio for whole-rock samples from rock section CQ1 from Craignair quarry, Dalbeattie.

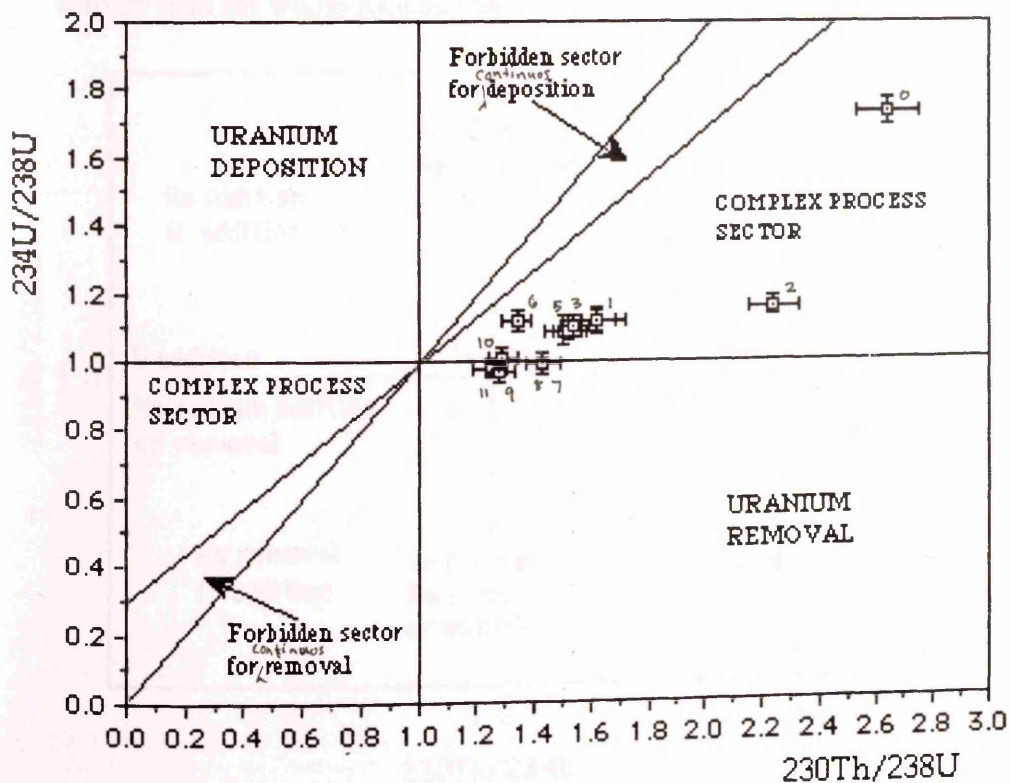


Figure 4.15: Plot of $^{226}\text{Ra}/^{230}\text{Th}$ activity ratio versus distance from the fracture face in rock section CQ1 from Craignair quarry, Dalbeattie.

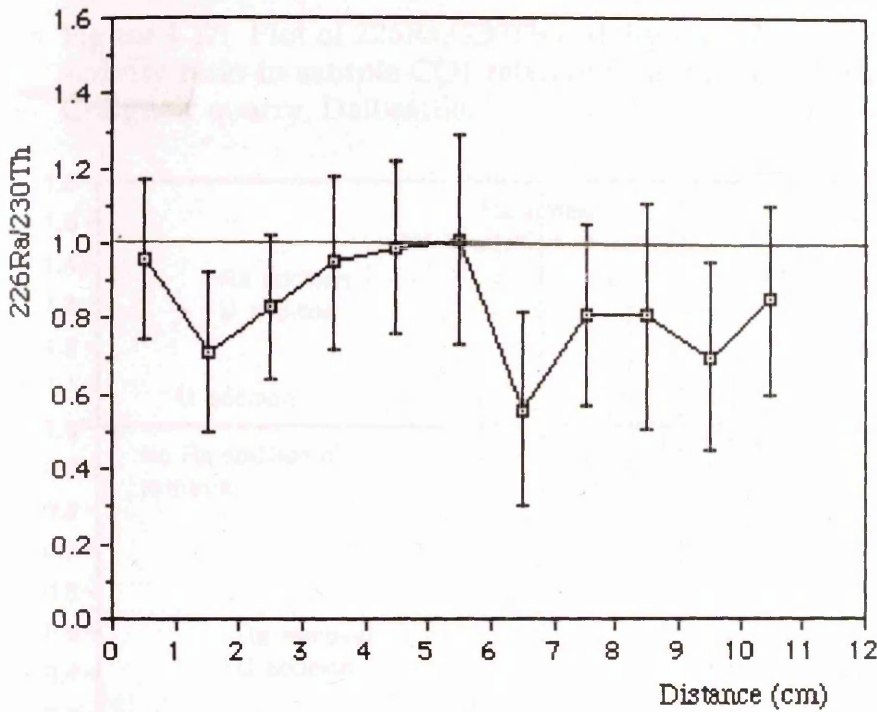


Figure 4.16: Regions of addition and removal of both uranium and radium in a plot of $^{226}\text{Ra}/^{230}\text{Th}$ activity ratio versus $^{230}\text{Th}/^{234}\text{U}$ activity ratio for whole-rock samples.

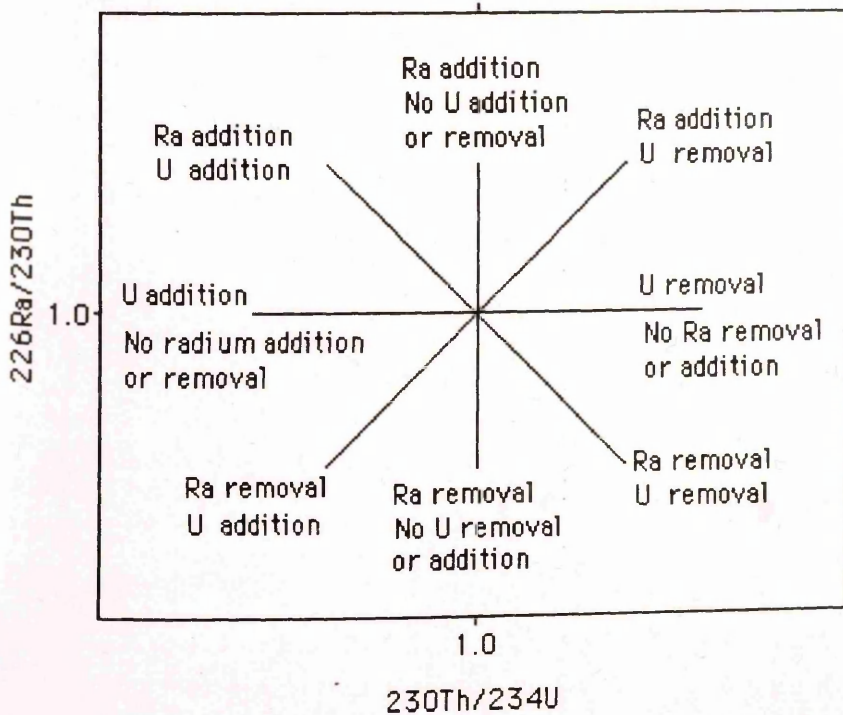
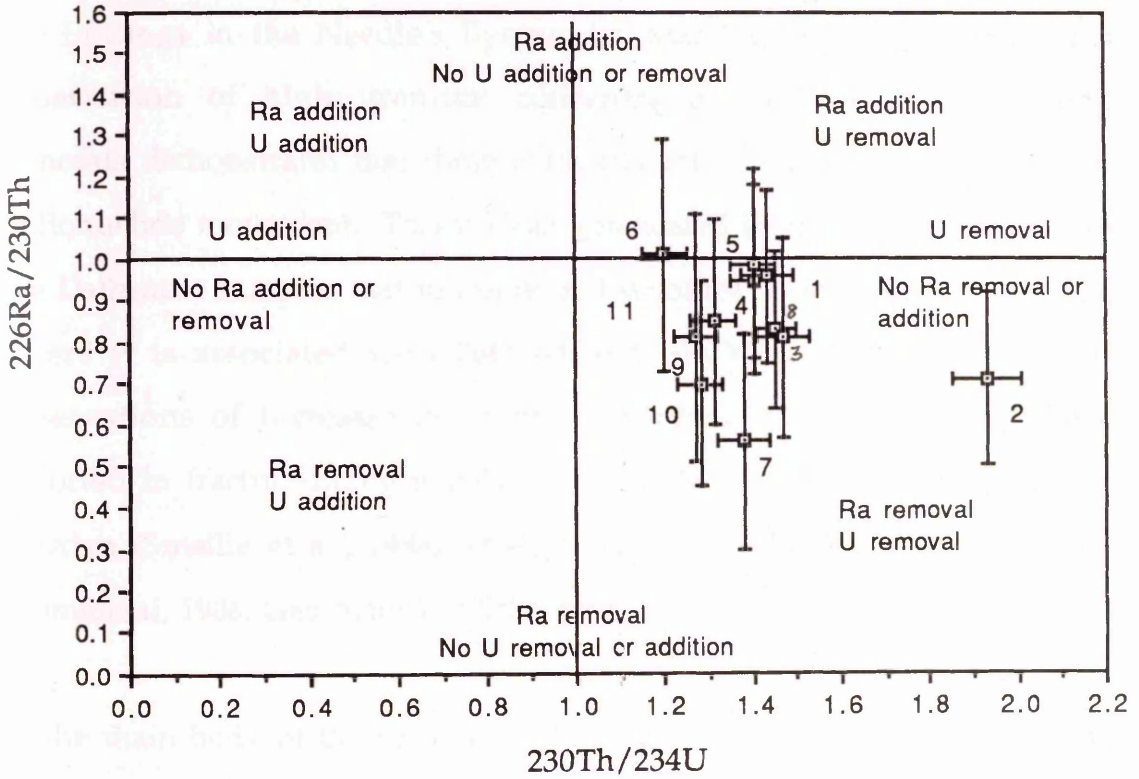


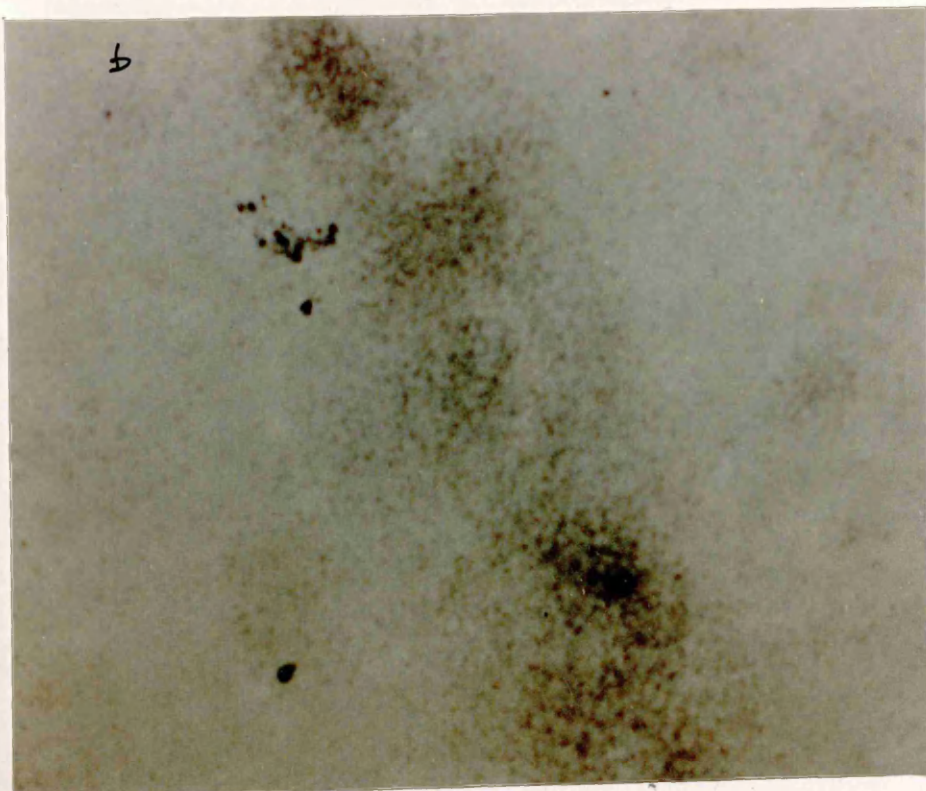
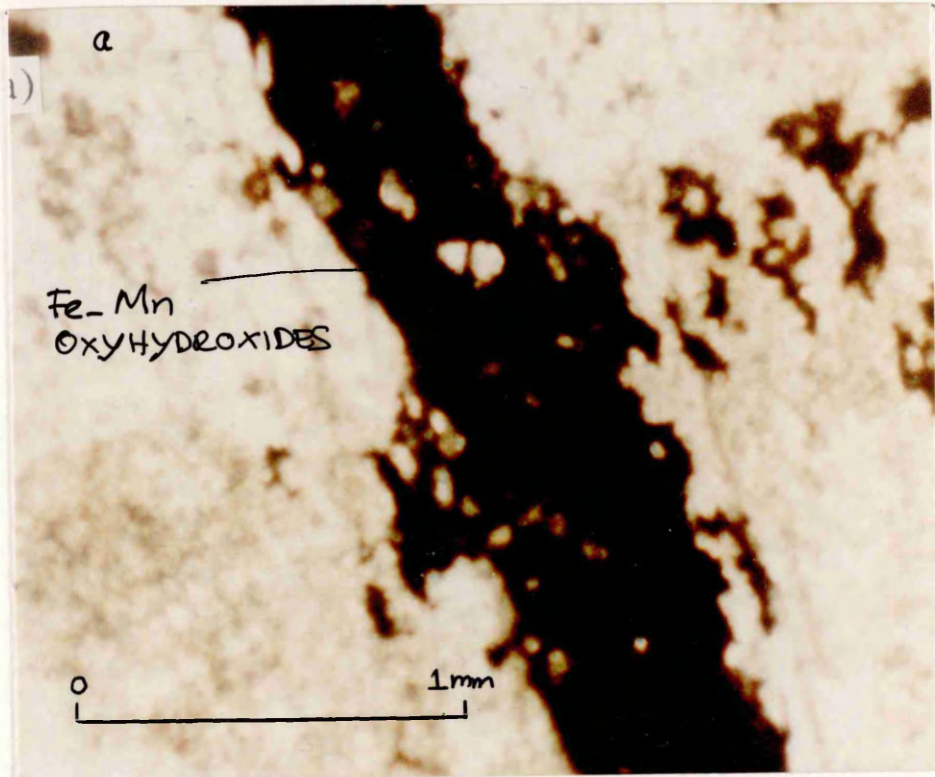
Figure 4.17: Plot of $^{226}\text{Ra}/^{230}\text{Th}$ activity ratio versus $^{230}\text{Th}/^{234}\text{U}$ activity ratio in sample CQ1 relative to secular equilibrium (the axes), Craignair quarry, Dalbeattie.



scavengers of trace metals in geological systems (Means et al., 1978; Kroom et al., 1980). Similarly clay minerals are well known for their high ion exchange capacity (Grim, 1962). In addition the presence of carbonate minerals in fracture-infillings suggested that these minerals act as sites for uranium retardation during fissure flow of groundwater, consistent with the findings in the Needle's Eye study (MacKenzie et al., 1991). This observation of high uranium concentrations in the fracture-lining minerals demonstrates that these materials act as a retardation barrier for radionuclide movement. This is clearly indicated by fission track studies of the Dalbeattie samples that uranium is distributed in infillings in fractures, where it is associated with FeOOH and MnOOH (Plate 4.4). Similar observations of increases in uranium marginal to fractures have been reported in fracture-lining materials of granite from Kråkemåla granite in Sweden (Smellie et al., 1986) and the Eye-Dashaw Lakes pluton, Canada (Kamaneni, 1986; Gascoyne and Schwarcz, 1986).

In the main body of the rock, away from the fracture and the redox front, uranium concentrations are generally depleted in both the oxidised (~3.0 ppm) and reduced (~3.7 ppm) portions. The uranium concentration in the reduced rock close to the front exhibits a weak maximum of 4.1 ppm, but is still depleted relative to the mean concentration of 4.3 ppm of uranium in the HB-granodiorite zone. This observation is consistent with a general dissolution and removal of uranium from the portion of rock adjacent to the fracture with partial re-deposition in the reduced rock close to the front. The intensity of uranium enrichment at the redox front is probably related to the volume of rock through which the groundwater has passed before reaching the front: the weak enhancement observed here, giving no net enrichment relative to the surrounding rock, is consistent with the recent

Plate 4.4: Matched thin-section (a) and fission track image on plastic film (b). Fission track print showing association of uranium with infilling fracture minerals, Fe-Mn oxyhydroxides.



development of this redox front system and, the relatively small volume of rock being traversed by the groundwater. The uranium concentrations thus suggest that there has been general removal of uranium from the rock adjacent to the fractures but that the redox front acts as a retardation barrier for uranium.

In contrast to uranium, thorium has a rather different distribution throughout the section (Figure 4.10), with concentrations ranging between 13.6 and 16.6 ppm relative to a mean concentration of thorium in the HB-granodiorite of 13.4 ppm. Thorium is thus generally enriched in this section, consistent with its highly immobile behaviour. Thorium was undetectable in the fracture-surface scraping sample, again consistent with negligible groundwater concentrations and the high degree of immobility.

The plot of U/Th concentration ratios against distance from the fissure (Figure 4.11) again suggests that U has been removed from the whole rock section, with some re-deposition on the reduced side of the front. Retardation of this type is of potential importance in far-field radionuclide transport but the efficiency of such retardation has not been established. In the present case a mass balance was calculated by comparison of the uranium concentration in the fracture-lining minerals and in the 4-6 cm rock section (showing slight uranium enrichment of 4.1 ppm) with the 7-10 cm section (showing constant uranium concentration value of 3.7 ppm). In each case, the area involved is about 100 cm^2 and the total mass of uranium in unit volume of rock was calculated (assuming a density of 2.65 g cm^{-3}). On this basis the amount of uranium being retarded along the flow path in unit area can be estimated to be about $0.0156 \mu\text{g cm}^{-2}$ and $0.0007 \mu\text{g cm}^{-2}$ at the fracture surface and at the redox front respectively in this rock section. These results therefore indicate that uranium retardation

in the fracture-lining minerals is relatively more efficient than at the redox front. However, the amount of uranium being deposited in the fracture-lining minerals and at the redox front (4-6 cm section) are calculated to be 4.2 mg and 184.0 mg respectively in the rock section. It is apparent that the amount of uranium deposited in the fracture is an order of magnitude less than that deposited at the redox front since the fracture comprises only a very thin layer while the redox front involved a relatively large volume of rock.

Further information on the processes associated with the redox front and fracture flow is provided by the isotopic analyses of natural decay series radionuclides. Plots of $^{234}\text{U}/^{238}\text{U}$ and $^{230}\text{Th}/^{234}\text{U}$ activity ratios over the length of the rock section are shown in Figures 4.12 and 4.13 respectively. The $^{234}\text{U}/^{238}\text{U}$ ratios exhibit disequilibrium from the fracture to a depth of 7 cm into the rock with a maximum value of 1.73 at the fracture-surface. These results reveal that uranium has been recently (relative to the ^{234}U half-life of 2.5×10^5 y) deposited in all samples over a distance of 7 cm into the rock from the fracture, indicating that there must be interconnected porosity in the rock over at least this distance to allow this degree of uranium re-distribution. This suggests that diffusive transport of species in solution in groundwater can take place over this distance, an observation of direct significance for matrix diffusion modelling. A similar conclusion was reached in a study of granite cores from Sweden, in which a limit of about 3 centimetres was suggested for the extent of radionuclide migration into saturated rocks via matrix diffusion (Smellie et al., 1986).

In conjunction with the uranium concentration results the $^{234}\text{U}/^{238}\text{U}$ activity ratio data indicate that while dissolution of uranium has occurred as the result of interaction of oxidising water with the rock, re-deposition

has also taken place in both the reduced rock and the oxidised rock. The similarity of the $^{234}\text{U}/^{238}\text{U}$ values from 1 to 7 cm section suggests that the deposition of uranium has taken place at approximately the same time throughout this section of rock and this is consistent with the suggestion of the process being post-glacial. If it is assumed that the observed $^{234}\text{U}/^{238}\text{U}$ activity ratio of 1.73 for the fracture-lining minerals is equal to that of groundwater and that addition of uranium to rock initially in secular equilibrium has generated the whole rock activity ratio values of 1.11, then the 'excess' uranium deposited throughout the 1-7 cm section can readily be calculated as 0.003 mg cm^{-2} . This represents a total deposition of 525 mg (0.75 mg cm^{-3}) in the 7 cm section of rock adjacent to the fracture.

The plot of the $^{230}\text{Th}/^{234}\text{U}$ activity ratios against distance is shown in Figure 4.13 from which it can be seen that the values for all of the samples are greater than unity, indicating a substantial loss of ^{234}U relative to ^{230}Th throughout the rock. This observation once more indicates that there must be interconnected porosity in the rock system to allow migration of uranium from the rock. As with the $^{234}\text{U}/^{238}\text{U}$ data, the $^{230}\text{Th}/^{234}\text{U}$ results suggest that at least 7 centimetres of rock is available for matrix diffusion. This observation thus suggests that the weathering front has probably penetrated to at least this far but the $\text{Fe}^{2+}/\text{Fe}^{3+}$ is observed at 4 cm. Thus the redox gradient extends over a significant area of rock or else there is a kinetic control of Fe^{2+} oxidation i.e. the Eh conditions have increased but an insufficient time has elapsed for the oxidation reaction to occur. The front is therefore more extensive than it appears. The $^{230}\text{Th}/^{234}\text{U}$ activity ratio for the fracture surface minerals sample, however, has a value of 1.53, revealing that the coatings must have been deposited a long time ago on a 10^6 y timescale (since ^{230}Th had come to

equilibrium with ^{234}U), but there has been recent loss of uranium (eg. from an old fracture-lining, perhaps formed under reducing conditions, with recent ingress of oxidising water). In contrast, the $^{234}\text{U}/^{238}\text{U}$ data indicate deposition of uranium at the fracture surface. So the system is complex.

The uranium and thorium isotopic data for rock section CQ1 are summarised in a plot of $^{234}\text{U}/^{238}\text{U}$ activity ratios against $^{230}\text{Th}/^{238}\text{U}$ activity ratios in Fig. 4.14. Four of the samples (8, 9, 10 and 11) just lie in the uranium removal sector of the diagram and have $^{234}\text{U}/^{238}\text{U}$ ratios that are generally close to unity. These ratios could be taken to indicate removal of uranium at near isotopic equilibrium. The remainder plot in positions for which complex processes are responsible. The high $^{234}\text{U}/^{238}\text{U}$ activity ratio for the surface-lining minerals (sample 0) reveals that the re-deposited uranium had been dissolved in a relatively slow non-equilibrium process eg. under reducing conditions. The following general trends can be observed in the positions of the samples in this plot: (i) The samples closest to the fracture generally lie furthest from the (1,1) equilibrium position, consistent with the effects of oxidising groundwater spreading out from the fracture with time, (ii) all of the samples from the oxidised rock (samples 1-5, including the fracture surface, i.e. sample 0) lie in the complex process sector indicating both uranium removal and deposition, (iii) the samples from the reduced rock close to the front (samples 6-7) lie in the complex process sector closer to equilibrium, and (iv) the samples from the reduced rock, beyond the front (samples 8-11) lie, within error, of the rapid, equilibrium uranium removal line indicating that even at this distance from the fracture these samples have probably been affected by the advancing redox front. Thus this observation indicates that at least 11 cm of the rock is available for matrix diffusion.

With the exception of samples 5 and 6, the $^{226}\text{Ra}/^{230}\text{Th}$ activity ratios (Figure 4.15) are less than unity, suggesting general removal of ^{226}Ra from the rock section and indicating migration of ^{226}Ra over distances of up to 5 cm or more. In general loss of radium is observed from the reduced rock beyond 6 centimetres from the fracture. This observation suggests that the redox front extended further into the rock than is indicated merely by the $\text{Fe}^{2+}/\text{Fe}^{3+}$ colour change at 4 centimetres from the fracture. This is also consistent with the $^{234}\text{U}/^{238}\text{U}$ and $^{230}\text{Th}/^{234}\text{U}$ activity ratio data. On this basis the average rate of movement of the redox front into the rock is estimated to be about 7 cm in 12000 y or 5.8 m in 10^6 y, but it is expected much faster along fractures.

Uranium and radium deposition and removal can be illustrated using a plot of $^{226}\text{Ra}/^{230}\text{Th}$ activity ratios versus $^{230}\text{Th}/^{234}\text{U}$ activity ratios and this diagram can be divided into four sectors representing the effects of uranium and radium addition or removal processes as shown in Figure 4.16. In such an approach it is assumed that the rock initially exists with the natural decay series radionuclides in a state of secular equilibrium and that it is then disturbed by the addition of uranium and radium from groundwater, or removal of uranium and radium to groundwater. Thorium is assumed to be highly immobile. The plot of $^{226}\text{Ra}/^{230}\text{Th}$ versus $^{230}\text{Th}/^{234}\text{U}$ for samples from rock section CQ1 is shown in Figure 4.17 which reveals the samples either lying in positions indicative of net uranium and radium loss (2, 3, 7, 8, 9, 10 and 11), or uranium loss without radium loss (1, 4, 5 and 6), providing confirmation of the net removal of these nuclides by the ingress of oxidising groundwater.

4.2.1.2 Rare earth element studies of rock section CQ1

In addition to the natural radionuclide studies described above, samples from rock section CQ1 were also analysed for rare earth elements. The results of these analyses and chondrite normalised values are given in Table 3.4. The following discussion of this work describes the behaviour of REE in the rock section and these results are compared with the uranium and thorium distribution patterns in an attempt to provide more information on the processes occurring at the redox front.

All of the plots of REE concentrations against distance from the fracture surface (Figures 4.18a to m) exhibit generally similar trends, with maxima in the oxidised rock near the fracture and in the reduced rock from about 9 to 11 cm away, and lower values generally occurring in the section from 3 to 7 cm. This observation suggests a general removal of the REE from the rock close to the front and possibly partial re-deposition in the oxidised rock via scavenging by iron-manganese oxyhydroxides. In general, loss of REE is observed from the reduced rock up to 6.5 cm and this observation suggests that the redox front has probably extended further into the reduced rock than is indicated by the $\text{Fe}^{2+}/\text{Fe}^{3+}$ colour change at 4.0 cm from the fracture, consistent with the conclusion derived above on the basis of the natural decay series data. Again, this suggests an average rate of movement of the redox front of about about 6.5 cm in 12000 y or 5.4 m in 10^6 y.

Comparison of the uranium and thorium data with those of the REE data indicates: (i) there is a slight uranium maximum over the area where the REE minima occur ; (ii) thorium maxima occur over the same areas as the

Figure 4.18: Plots of REE concentrations versus distance from the fracture face in rock section CQ1 from Craignair quarry, Dalbeattie.

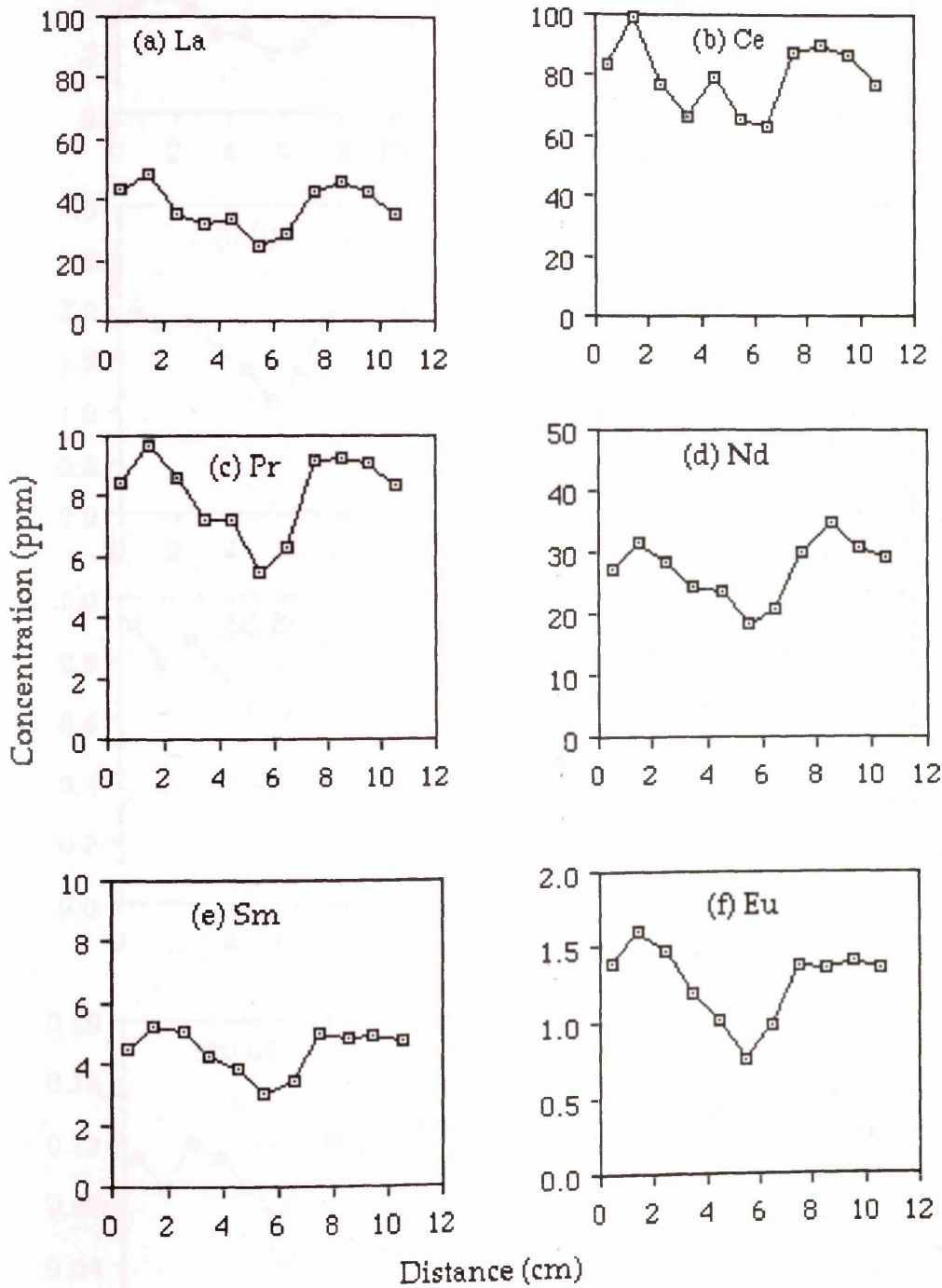
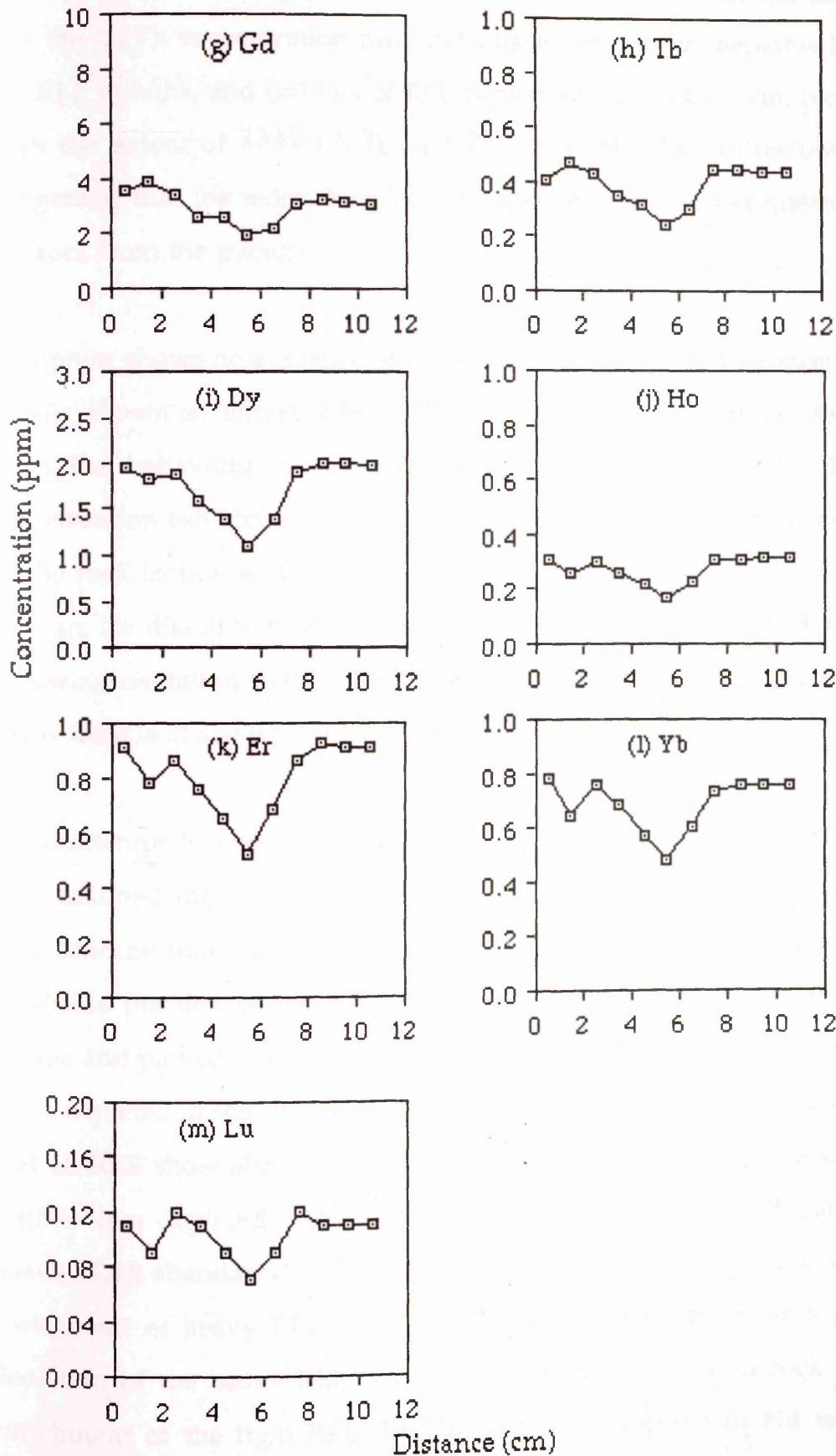


Fig. 4.18 (Cont.)

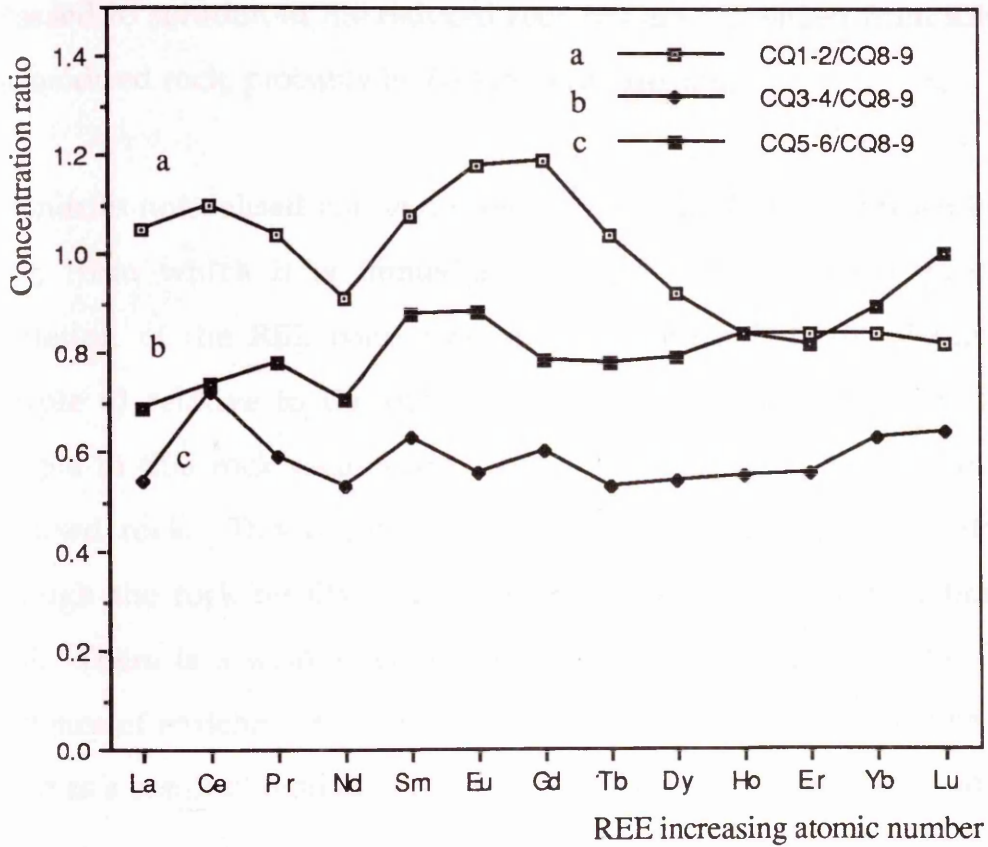


REE maxima, indicating geochemical coherence between thorium and REE; (iii) the U/Th concentration ratio exhibits maxima over the same area as the REE minima, and (iv) loss of REE is observed up to 6 - 7 cm, consistent with the extent of $^{234}\text{U}/^{238}\text{U}$ and $^{230}\text{Th}/^{234}\text{U}$ disequilibrium, thus suggesting that the redox front has probably encroached that distance into the rock from the fracture.

Europium shows no evidence of redox induced effects in the concentration profile shown in Figure 4.18f and does not exhibit any major deviation from the behaviour of the other REE in this rock section. The Ce concentration exhibits a slight enrichment relative to other REE in sample 5 of the rock section at 4 - 5 cm from the fracture. Thus, if this is taken to indicate Ce dissolution on the reduced side of the front and re-deposition following oxidation to Ce^{4+} in the oxidised side, it again suggests that the redox front is at about 6 cm from the fracture.

In an attempt to identify possible dissolution and re-deposition effects, it was assumed that the 8-9 cm section represented unaltered rock and the REE concentrations in the 1-2 cm and 3-4 cm (oxidised rock) and 5-6 cm (probable position of weathering front) were divided by those of 8-9 cm section and plotted in Figure 4.19. It is clear from Figure 4.19 that section 5-6 cm is depleted in the REE relative to the reduced rock at 8-9 cm section and that all REE show about the same degree of depletion, except Ce which is slightly less depleted. The 3 - 4 cm section shows a similar pattern of relative REE abundance to those observed for the 5 - 6 cm section and slight enrichment of heavy REE (Dy-Lu). The 1-2 cm section shows a general depletion of the heavy REE (Dy-Lu) relative to the reduced rock and an enrichment of the light REE (La-Tb) with the exception of Nd which is slightly depleted. This observation suggests that the REE have been lost

Figure 4.19: Plot showing the ratio of REE concentrations in (a) 1-2 cm, (b) 3-4 cm and (c) 5-6 cm sections to concentrations in 8-9 cm section (assumed unaltered) in the reduced rock of the rock section CQ1 from Craignair quarry, Dalbeattie.



from the reduced rock; the light REE are partially re-deposited in the oxidised rock while the heavy REE are probably partially re-deposited nearer the front. This is a significant observation since the REE (except Eu and Ce) are not inherently redox-sensitive elements. This suggests that REE are released to solution in the reduced rock but are scavenged from solution in the oxidised rock, probably by Fe-Mn oxyhydroxides.

Chondrite normalised concentration plots for the REE are shown in Figure 4.20, from which it is immediately obvious that there is pronounced depletion of the REE concentrations in samples 5, 6 and 7 (minima in sample 6) relative to the other samples. However, the trends for each sample in this rock section are generally similar both in the reduced and oxidised rock. This observation implies that passage of the redox front through the rock results in dissolution but with little fractionation of the REE. There is a weak effect evident on the redox-sensitive REE Ce, with evidence of enrichment of Ce in sample 5 (Figure 4.18b), suggesting fixation of Ce as a result of oxidation of Ce to the 4+ oxidation state at this location.

As discussed in section 1.4, Stephens et al. (1985) used REE distributions in their classification of the zones of the Criffel pluton. The REE data for sample 9 of rock section CQ1 from Craignair quarry are compared with those of Stephens et al. (1985) for sample HB-056 (Table 3.4) which was located near the quarry in Figure 4.21. The chondrite-normalised concentration data are found to be almost comparable although the concentrations of the REE in the data from this study are generally higher (except Sm and Yb) than those of Stephens et al. (1985).

In summary the REE data reveal a general loss of these elements from the rock close to the front, but with some re-deposition in the oxidised zone.

Figure 4.20: Chondrite-normalised REE patterns for sliced samples in rock section CQ1 from Craignair quarry, Dalbeattie.

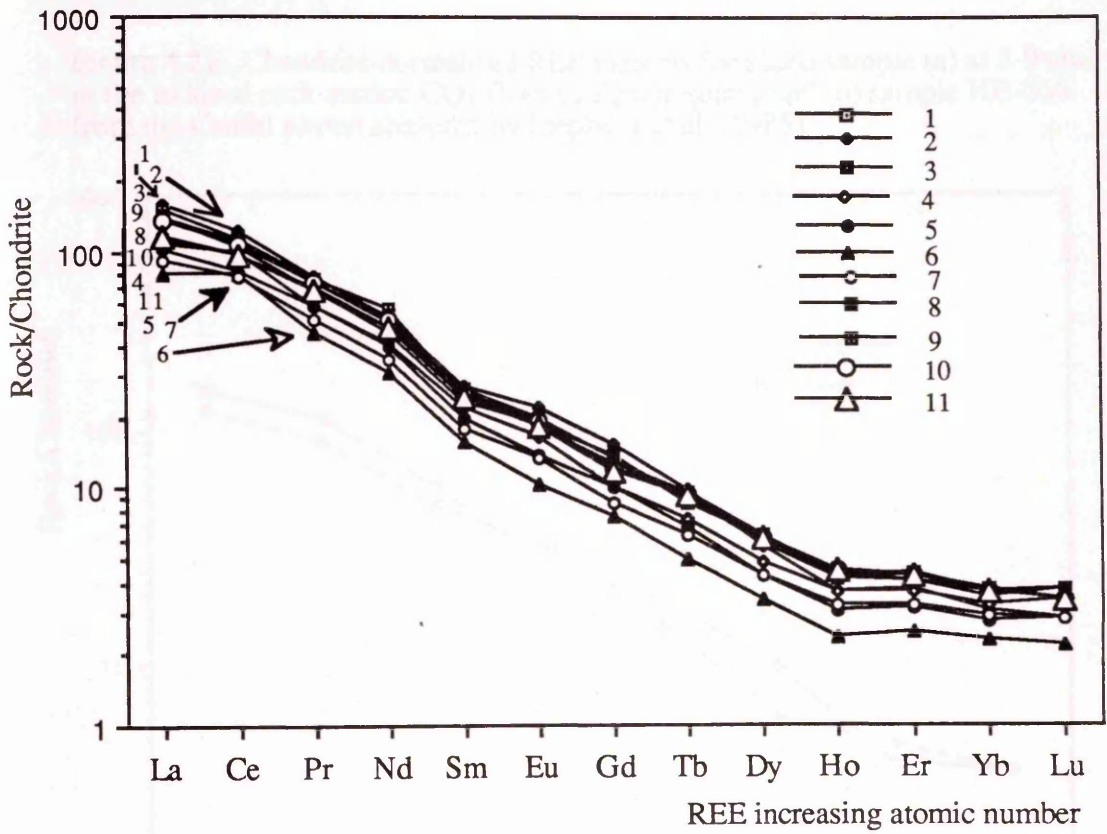
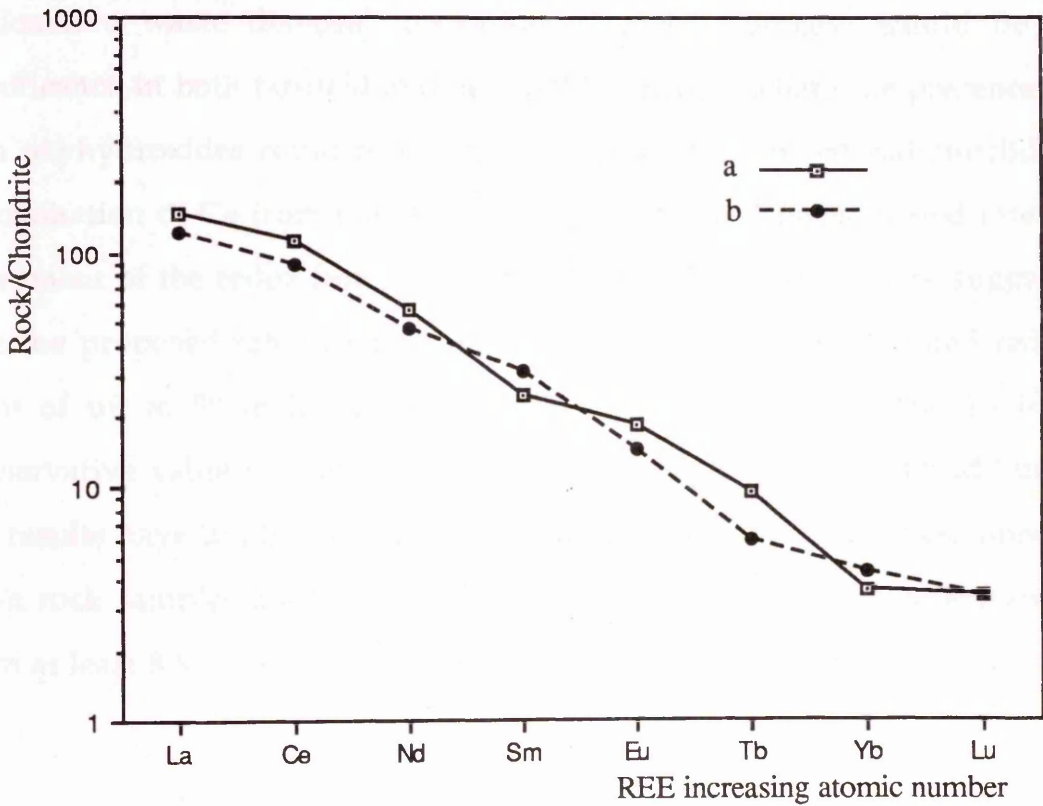


Figure 4.21: Chondrite-normalised REE patterns for sliced sample (a) at 8-9 cm in the reduced rock section CQ1 from Craignair quarry and (b) sample HB-056 from the Criffel pluton analysed by Stephens et al. (1985).



This observation is important for two reasons: firstly, the REE, apart from Ce and Eu, which are non-redox sensitive elements (i.e. they are invariably in 3+ oxidation state) are partially dissolved in oxidising groundwater and; secondly the apparent re-deposition of REE in the oxidised rock represents a potentially important radionuclide retardation process. In the context of radioactive waste disposal, operation of such a process would be of significance in both far-field and near-field transport where the presence of iron oxyhydroxides could result in scavenging of dissolved radionuclides. Fractionation of Ce from the other REE is observed. The estimated rate of movement of the redox front of up to 5.2 m in 10^6 y derived here suggests that the proposed rate of far-field movement of a repository-related redox front of up to 50 m in 10^6 y (Neretneiks and Aslund, 1983a, b) is a conservative value for inclusion in far-field transport models. In addition, the results have implications for sampling of rocks for REE studies, since if fresh rock samples are to be obtained, in this case they must be extracted from at least 8-9 cm from the nearest fractures.

4.2.2 CQ2 rock section studies

4.2.2.1 Natural decay series studies

The results for natural decay series radionuclide analyses of samples from rock section CQ2 collected from the HB-granodiorite zone approximately 8 m from the top of the Craignair quarry are given in Table 3.5. The $\text{Fe}^{2+}/\text{Fe}^{3+}$ redox front in this section of rock is visually obvious as a clearly defined, sharp colour change from red to grey at a distance of about 1 cm into the rock from the fracture wall as shown in Figure 2.5. Relative to section CQ1 the redox front in section CQ2 has therefore extended a smaller distance into the rock (i.e the front is more recent assuming similar permeability). The natural decay series analytical data were treated similarly to those for section CQ1, and plots are shown in Figures 4.22 to 4.29.

The plot of uranium concentration against distance for section CQ2 (Figure 4.22) shows that uranium is strongly enriched (162 ppm relative to a mean of 4.3 ppm in the HB-granodiorite) in fracture-surface scrapings of iron- and manganese- oxyhydroxides and clay minerals. The pronounced increase of uranium concentrations in fracture-surface scrapings by 1-2 orders of magnitude relative to the rest of the samples again illustrates that the uranium, which has been leached from the rock, is partially re-deposited on fracture-lining minerals during groundwater transport. The uranium concentration in the fracture-lining minerals from CQ2 is an order of magnitude greater than that for CQ1, providing evidence of uranium precipitation during downward flows of the oxidising groundwater. The amount of uranium deposited on fracture-lining

Figure 4.22: Plot of uranium concentration versus distance from the fracture face in rock section from Craignair quarry, Dalbeattie.

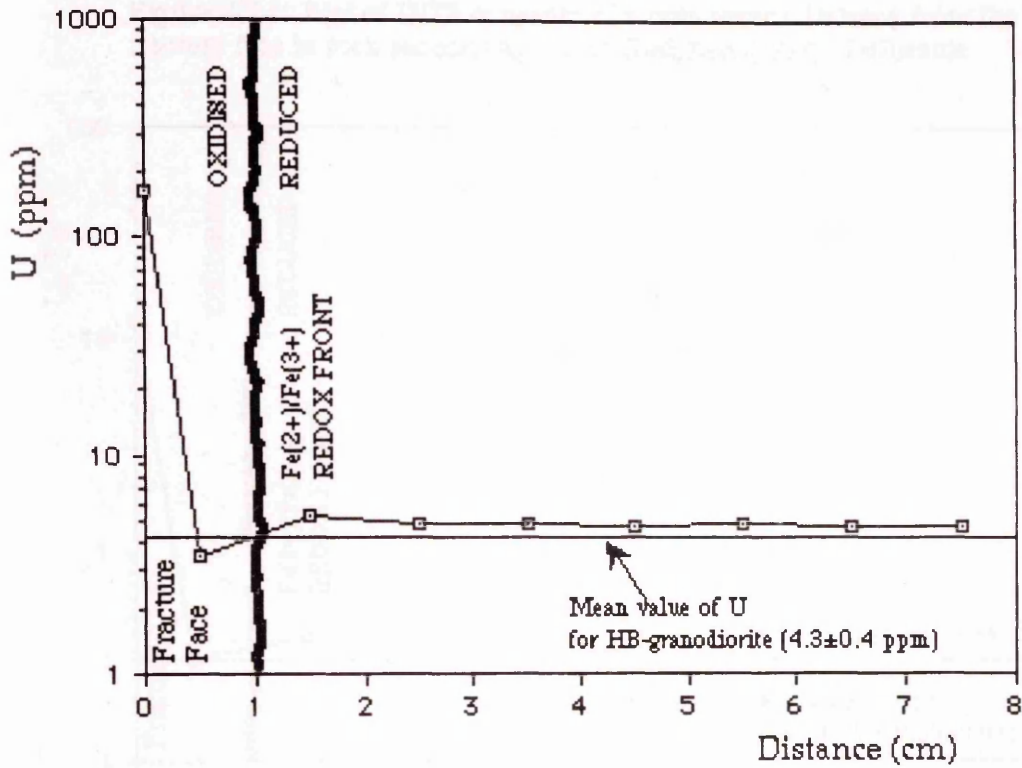


Figure 4.23: Plot of thorium concentration versus distance from the fracture face in rock section CQ2 from Craignair quarry, Dalbeattie.

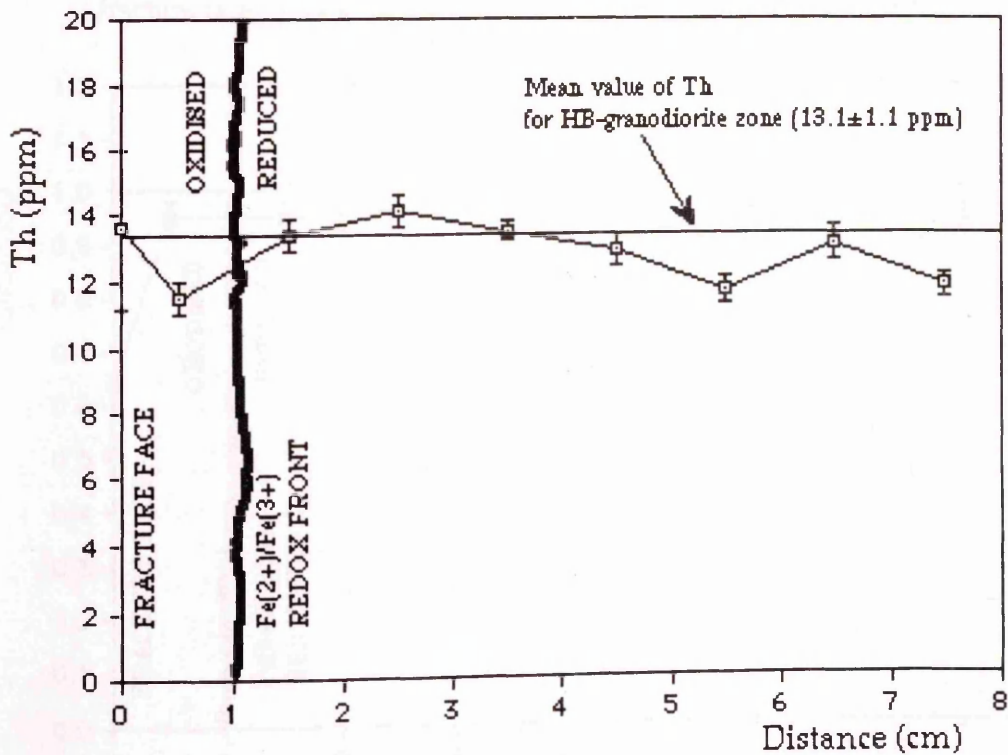


Figure 4.24: Plot of U/Th concentration ratio versus distance from the fracture face in rock section CQ2 from Craignair quarry, Dalbeattie.

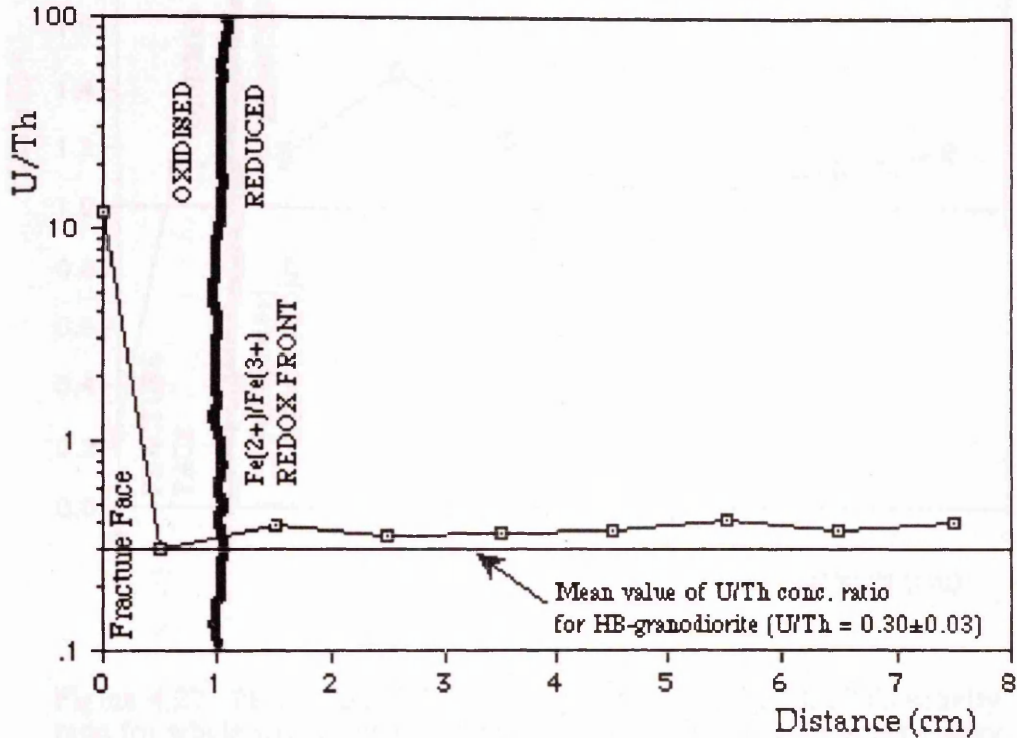


Figure 4.25: Plot of $^{234}\text{U}/^{238}\text{U}$ activity ratio versus distance from the fracture face in rock section CQ2 from Craignair quarry, Dalbeattie

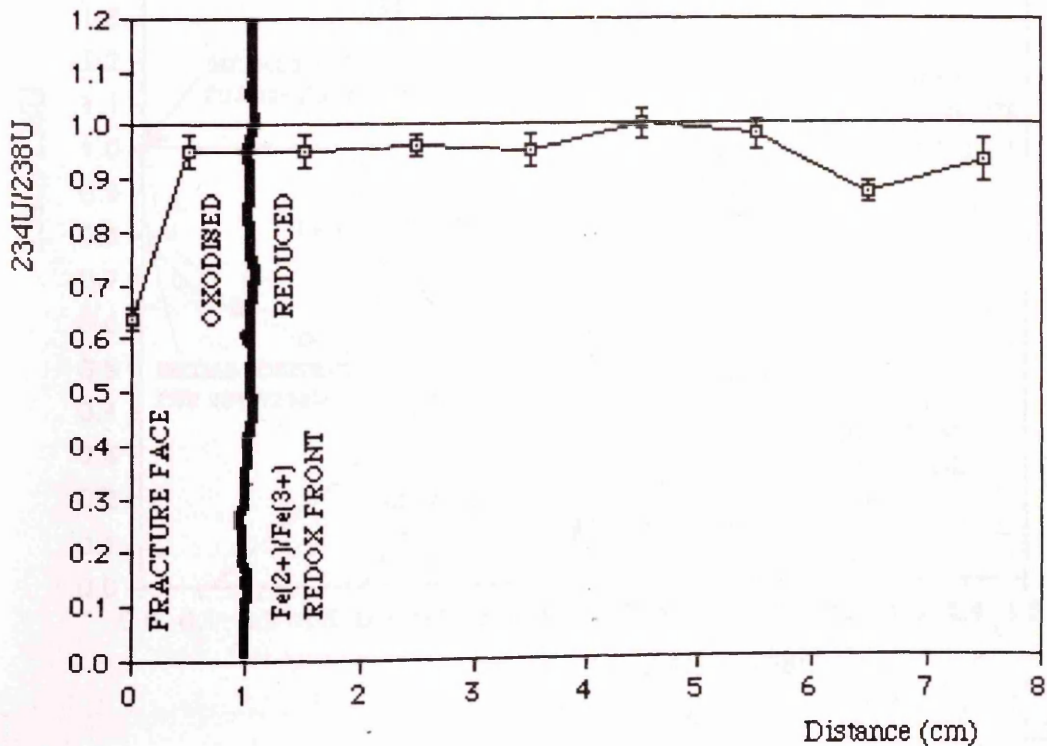


Figure 4.26: Plot of $^{230}\text{Th}/^{234}\text{U}$ activity ratio versus distance from the fracture face in rock section CQ2 from Craignair quarry, Dalbeattie.

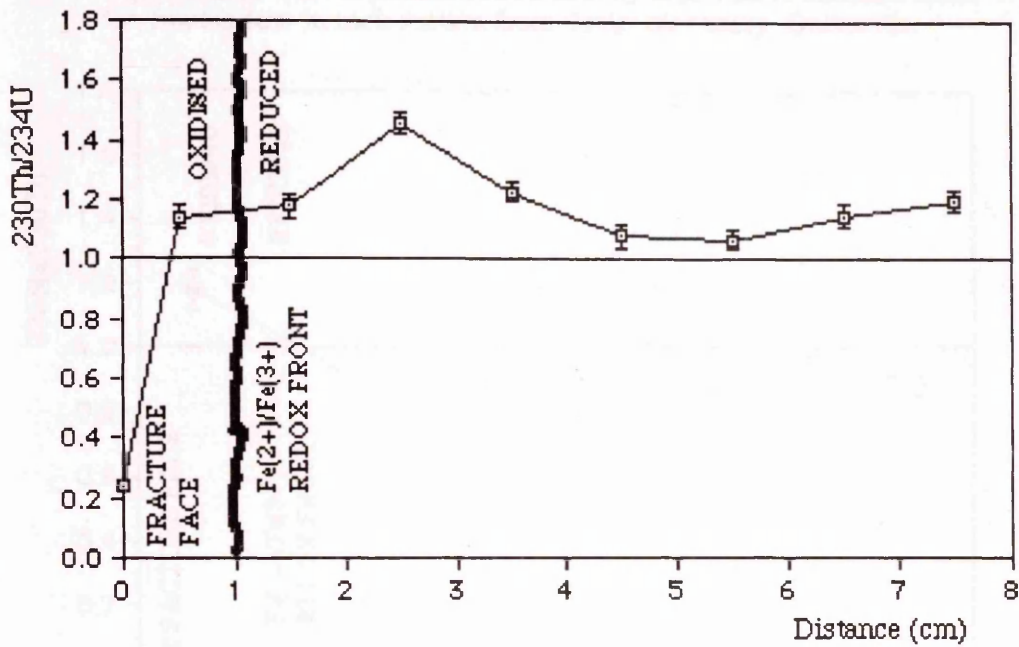


Figure 4.27: Plot of $^{234}\text{U}/^{238}\text{U}$ activity ratio versus $^{230}\text{Th}/^{238}\text{U}$ activity ratio for whole-rock samples from rock section CQ2 from Craignair quarry, Dalbeattie.

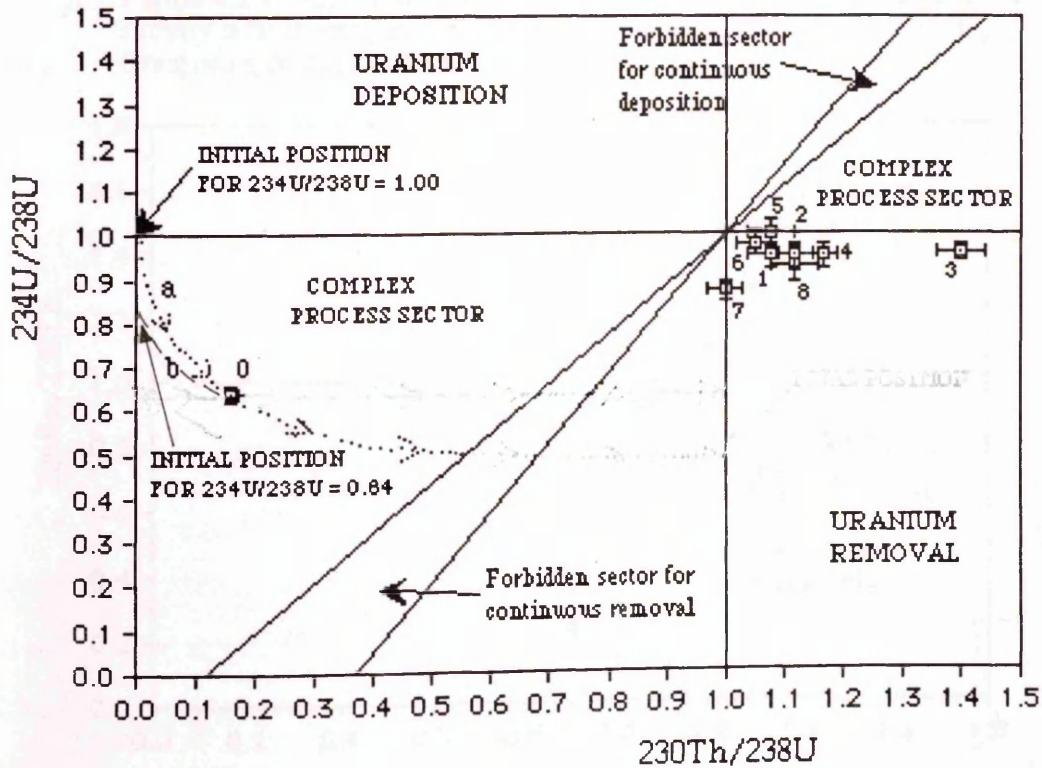


Figure 4.28: Plot of $^{226}\text{Ra}/^{230}\text{Th}$ activity ratio versus distance from the fracture face in rock section from Craignair quarry, Dalbeattie.

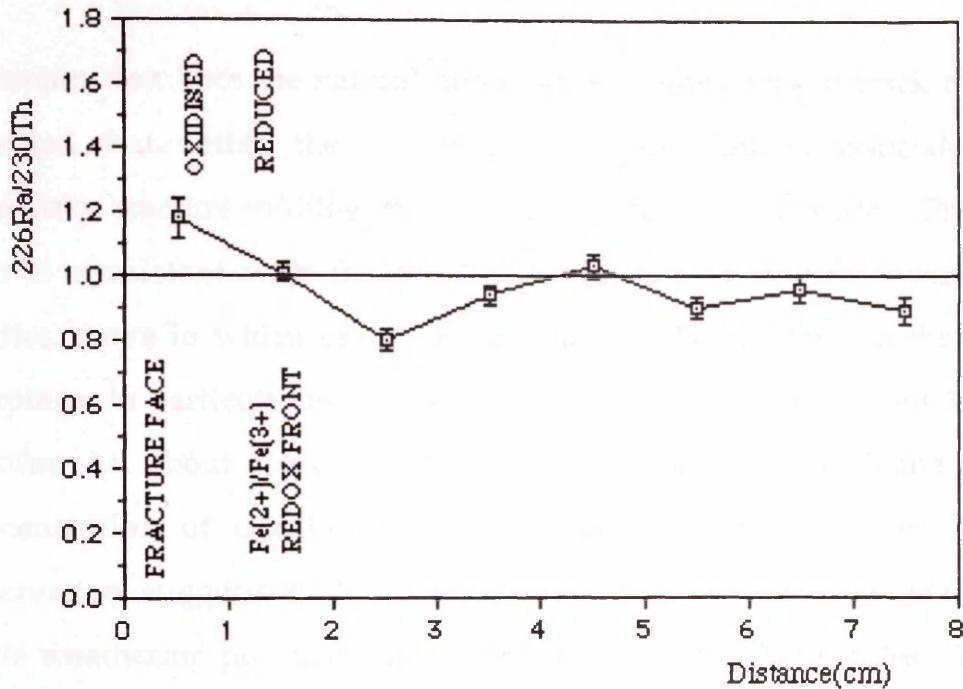
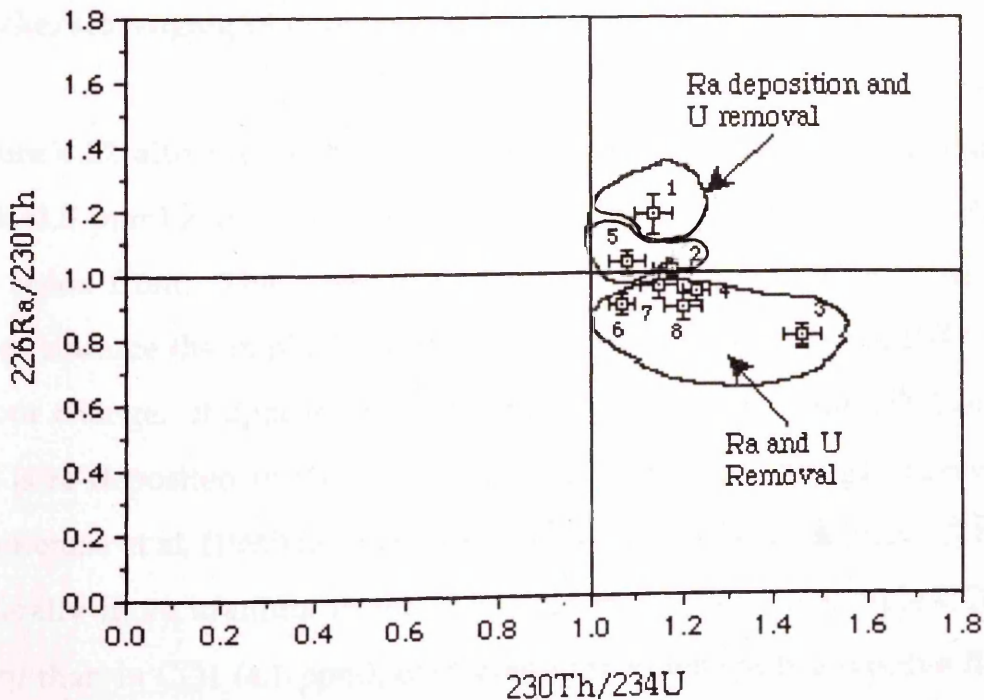


Figure 4.29: Plot of $^{226}\text{Ra}/^{230}\text{Th}$ activity ratio versus $^{230}\text{Th}/^{234}\text{U}$ activity ratio in sample CQ2 relative to secular equilibrium (the axes), Craignair quarry, Dalbeattie.



minerals can be estimated here to be $0.0296 \text{ mg cm}^{-2}$ which is about a factor of two higher than the corresponding estimate for section CQ1 ($0.0156 \text{ mg cm}^{-2}$).

In conjunction with the natural decay series studies, fission track mapping revealed that within the area of fractures uranium is associated with secondary fracture-infilling minerals of Fe-Mn oxyhydroxides (Plate 4.4). This is consistent with the conclusion derived by natural decay series studies above in which uranium was found to be enriched in the surface scrapings, in particular for the section CQ2, which contains about 162 ppm uranium i.e. about 1 order of magnitude greater than that of the average concentration of uranium in the HB-zone of about 4.3 ppm. This observation suggests that the surface-active amorphous iron-manganese oxide weathering products have a high affinity for radionuclides. Thus, in the context of radioactive waste disposal, operation of such a process would obviously be of significance in both far-field and near-field transport; the presence of iron-manganese oxyhydroxides could result in intense uptake/scavenging of dissolved radionuclides.

Figure 4.22 also reveals that uranium is slightly depleted in the oxidised rock (3.5 ppm) and slightly enriched in the reduced rock (5.3 ppm) close to the redox front. This observation suggests that the uranium distribution here reinforces the implied position of the redox front from the $\text{Fe}^{2+}/\text{Fe}^{3+}$ colour change. It appears that uranium is removed from the oxidised rock but is re-deposited in the reduced rock close to the front, as observed by MacKenzie et al. (1992) in redox fronts at Pocos de Caldas in Brazil. There is generally more uranium in the rock close to the front in sample CQ2 (5.3 ppm) than in CQ1 (4.1 ppm), consistent with downwards advective flow of

water in the fracture and lateral diffusive penetration of oxidising conditions into the rock with associated transport of uranium. As with the rock section CQ1, a mass balance calculation was also carried out for section CQ2. On the basis of the uranium concentration at the redox front (5.3 ppm) in the rock section CQ2 and the average value for the HB-granodiorite zone (4.3 ppm), the amount of uranium being retarded at the front can be estimated to be $0.0032 \mu\text{g cm}^{-2}$ which is about a factor of five higher than the corresponding estimate for section CQ1 ($0.0007 \mu\text{g cm}^{-2}$). In the reduced rock away from the redox front the uranium concentration is relatively constant at about 5 ppm which is slightly higher than the mean concentration of uranium of 4.3 ppm in the HB-granodiorite zone, possibly indicating that uranium has been re-deposited throughout this section of reduced rock or that the 'average' result represents samples that have experienced uranium loss as described in section 4.1. On the whole, the uranium concentration data in section CQ2 revealed that uranium is removed of from the oxidised rock and re-deposited in the reduced rock where enrichment is observed to be most pronounced close to the front.

In contrast to uranium, thorium is relatively uniformly distributed throughout the section (Figure 4.23), with concentrations ranging between 11.5 and 13.6 ppm; similar to the mean thorium concentration in the HB-granodiorite of 13.4 ppm. These results are, once more, force the conclusion that a significant degree of mobility of uranium and effective immobility of thorium. There is, however, a higher ^{232}Th concentration in the CQ2 fracture material than CQ1, probably because of the presence of some country rock minerals in the CQ2 fracture scrapings.

The trend in the plot of the U/Th concentration ratio against distance (Figure 4.24) again indicates U enrichment (0.37) in the reduced portion of

the rock section; slightly higher than the mean U/Th concentration ratio in the HB-zone of 0.30. These data are, therefore, entirely consistent with dissolution and removal of uranium from the oxidised rock and re-deposition in the reduced rock close to the front. Again, this observation indicates that the uranium distribution supports the implied position of the redox front from the $\text{Fe}^{2+}/\text{Fe}^{3+}$ colour change. In addition, the plot shows that U/Th concentration ratios for all of the samples in the reduced rock are greater than that of the 'average' U/Th concentration ratio for the HB-zone, suggesting that either uranium has probably been lost from the 'average' samples or uranium has been deposited in the reduced portion of the rock section.

Plots of the $^{234}\text{U}/^{238}\text{U}$ and $^{230}\text{Th}/^{234}\text{U}$ activity ratios for the rock section CQ2 are shown in Figures 4.25 and 4.26 respectively. Figure 4.25 shows that the $^{234}\text{U}/^{238}\text{U}$ activity ratio 0.64 is very low for the fracture-lining minerals. As uranium precipitated from solution is isotopically homogeneous, initially deposited ^{234}U and ^{238}U will not undergo fractionation. Thus the original population of atoms of ^{234}U would have to be substantially replaced to produce this ratio. The value of 0.64 for the $^{234}\text{U}/^{238}\text{U}$ activity ratio requires that at least 40% of the ^{234}U atoms produced by decay of ^{238}U are being preferentially lost to the aqueous phase. Thus it can be inferred that uranium must be present at this location as a thin coating on the surface of fracture materials. This low value also indicates that the rate of bulk dissolution of uranium must be low relative to the rate of preferential recoil loss of ^{234}U , but the ^{234}U atoms ejected must clearly remain in solution for a sufficient length of time to ensure their total removal from this environment. On the assumption of an initial unity value for the $^{234}\text{U}/^{238}\text{U}$ activity ratio and 50% loss of ^{234}U atoms formed in situ and also no ^{238}U loss other than by

decay, a lower age limit can be estimated for uranium in the fracture-lining minerals as follows:

	A	=	$A_0 e^{-\lambda t}$
where,	A	=	activity of uranium at time $t = 0.64$
	A_0	=	initial activity of uranium $t_0 = 0.50$
	$\lambda_{234\text{U}}$	=	$2.8 \times 10^{-6} \text{ y}^{-1}$
	t	=	time for uranium deposited in the lining material (i.e. giving minimum age)

This calculation gives a minimum age limit of 4.6×10^5 y for uranium in the fracture-lining minerals for rock section CQ2.

Similar observations of pronounced deficiency of ^{234}U have been reported in fracture-fillings at 170 m depth from the Eye-Dashaw Lake pluton in Canada (Gascoyne and Schwarcz, 1986) and in the proximity of the Needle's Eye mineralisation on the southern edge of the Criffel pluton (MacKenzie et al., 1989). Similarly in uranium mineral deposits at Pocos de Caldas in Brazil (MacKenzie et al., 1992) and in red beds (Hoffmann, 1991) very low values have again been observed. Thus, there is considerable evidence that uranium deposited from groundwater can remain in situ for times approaching 10^6 y. This is clearly an important point for radioactive waste considerations in that uranium, probably deposited only as a very thin layer in association with secondary iron minerals, has remained immobile despite being in contact with groundwater for $10^5 - 10^6$ y. This provides support for the concept that massive steel containers will provide long-term stability for the waste form. However recoil loss is clearly efficient under these conditions and effects of this type must be considered in any sequential decay in radioactive waste. This observation reveals that the disequilibrium in the uranium decay series is a consequence of both 'old'

and 'post glacial' processes.

Figure 4.25 also shows that $^{234}\text{U}/^{238}\text{U}$ disequilibrium exists, with values less than unity, within the 3.5 cm section of rock closest to the fracture surface - evidence that preferential loss of ^{234}U has occurred. This observation suggests that the rock must be permeable over a distance of at least 3.5 cm to allow this degree of uranium re-distribution; again carrying the implication that at least this volume of rock will be available for matrix diffusion. In contrast the $^{234}\text{U}/^{238}\text{U}$ activity ratios for the corresponding positions in section CQ1 exhibit disequilibrium, with values greater than unity - evidence that deposition of ^{234}U has occurred. Further into the rock from the fracture, samples 5 and 6 attain equilibrium between ^{234}U and ^{238}U , but samples 7 and 8 again show $^{234}\text{U}/^{238}\text{U}$ activity ratios of less than unity, possibly indicating the influence of another fissure deeper in the rockbody. This is parallel to visual observation at the site of weathering in all directions around a complex series of fractures that are interconnected in three dimensions.

The plot of $^{230}\text{Th}/^{234}\text{U}$ ratio against distance is shown in Figure 4.26, from which it can be seen that, with one exception (surface scrapings sample), the $^{230}\text{Th}/^{234}\text{U}$ ratios are greater than unity. These values are particularly significant since they reflect a substantial depletion of ^{234}U relative to ^{230}Th , suggesting that uranium loss has occurred throughout the rock, not just from the oxidised section. This observation shows that there is net loss of uranium from the rock with only partial retardation in the fracture and at the redox front. The fracture lining sample has a very low value for the $^{234}\text{U}/^{238}\text{U}$ activity ratio as described above, suggesting ancient uranium deposition. On the other hand the low $^{230}\text{Th}/^{234}\text{U}$ value suggests

relatively recent uranium deposition. These observations mean that this is a system in which an ancient precipitate of uranium in the fracture has been recently perturbed by an ingress of oxidising water, probably since the last period of glaciation. It can be concluded that uranium has been dissolved and re-deposited without ^{230}Th but with a $^{234}\text{U}/^{238}\text{U}$ activity ratio of 0.64 and subsequent ingrowth (in situ growth of daughter ^{230}Th as an oxide) of ^{230}Th . From these assumptions it is possible to calculate a maximum possible age of uranium deposition as follows:

$$\begin{aligned} A_{\text{Th}} &= A_{\text{U}} (1 - e^{-\lambda_{230\text{Th}} t}) \\ 0.16 &= 1 - e^{-\lambda_{230\text{Th}} t} \\ t &= 1.8 \times 10^4 \text{ y} \end{aligned}$$

where,

$$\begin{aligned} A_{\text{Th}} &= \text{activity of } ^{230}\text{Th} \\ A_{\text{U}} &= \text{activity of } ^{238}\text{U} \\ \lambda_{230\text{Th}} &= 9.2 \times 10^{-6} \text{ y}^{-1} \\ t &= \text{time for uranium deposited in the fracture-lining minerals (i.e. giving maximum age).} \end{aligned}$$

This calculation gives a maximum age limit of 1.8×10^4 y for uranium in the fracture-lining minerals for rock section CQ2.

The uranium and thorium isotopic data for section CQ2 are summarised in a plot of $^{234}\text{U}/^{238}\text{U}$ activity ratios against $^{230}\text{Th}/^{238}\text{U}$ activity ratios in Figure 4.27. It can be seen that sample 0 (surface scraping minerals) lies in the complex process zone of the diagram whereas the rest of the samples all plot in positions that correspond to uranium loss from the rock; either non-equilibrium loss as in samples 1, 2, 3, 4, 7 and 8 (i.e. with preferential loss of ^{234}U which involves a longer timescale); or recent, rapid loss as in samples 5 and 6 from a system in which the $^{234}\text{U}/^{238}\text{U}$ activity ratio was

initially less than unity. The $^{234}\text{U}/^{238}\text{U}$ data for samples closest to the major fracture (samples 1, 2, 3 and 4) as well as the minor fracture (sample 8) generally lie furthest from the (1,1) equilibrium position, indicating the effects of the oxidising groundwater spreading out from the fracture with time. The samples from the reduced rock (samples 5 and 6) lie close to the $^{234}\text{U}/^{238}\text{U}$ unity line, which could be taken to represent recent, rapid processes with near equilibrium removal of uranium. Whereas the position of sample 7 indicates preferential loss of ^{234}U probably resulting from α -recoil. Sample 0 shows a strikingly low $^{234}\text{U}/^{238}\text{U}$ activity ratio of 0.64 and $^{230}\text{Th}/^{238}\text{U}$ activity ratio of 0.16, suggesting two possibilities for the routes for uranium deposition in the fracture-lining minerals: firstly, if the uranium represented by sample that was deposited with $^{234}\text{U}/^{238}\text{U} = 1.00$ and no ^{230}Th the route described on the plot would be along path 'a' (Figure 4.27), and ; secondly, if the uranium was deposited with $^{234}\text{U}/^{238}\text{U} = 0.64$ and no ^{230}Th the route described on the plot would be along path 'b' (Figure 4.27). However, the classical assumptions of initial secular equilibrium do not apply to fracture-lining samples, so the use of a normal Thiel's plot as described in section 1.3 is probably inappropriate.

The $^{226}\text{Ra}/^{230}\text{Th}$ activity ratios display disequilibrium (Figure 4.28) reaching a maximum value of 1.18 on the oxidised side of the front, indicating deposition of ^{226}Ra in the oxidised rock. But the drop to 0.8 in the reduced rock close to the front, suggests a removal of ^{226}Ra . These results, indicating that ^{226}Ra is removed from the reduced rock but is re-deposited in the oxidised rock, are consistent with the observations of MacKenzie et al. (1992) in the more mature and developed redox fronts at Pocos de Caldas in Brazil. This is significant for two reasons: firstly, radium migration is in the opposite direction to that of uranium (i.e. removal from oxidised rock and re-deposition in reduced rock) at the front,

suggesting that the control of radionuclide movement at the front is by diffusive transport driven by concentration gradients which develop in groundwater at or near the front; secondly, radium is not an inherently redox-sensitive element (i.e. it is always restricted to the 2+ oxidation state) and it is present in groundwaters at concentrations that are many orders of magnitude lower than any solubility limitation level. This suggests that radium is released to solution in the reduced rock but is scavenged from solution in the oxidised rock. Either the $\text{Fe}^{2+}/\text{Fe}^{3+}$ and $\text{Mn}^{2+}/\text{Mn}^{4+}$ systems or the $\text{S}^{2-}/\text{SO}_4^{2-}$ system could be invoked to explain this observation via scavenging of ^{226}Ra by iron-manganese oxyhydroxides or the formation of secondary sulphates (from sulphides) in the oxidised rock.

The $^{226}\text{Ra}/^{230}\text{Th}$ activity ratio versus $^{230}\text{Th}/^{234}\text{U}$ activity ratio diagram for samples from rock section CQ2 rock section is shown in Figure 4.29. Interpretation of the results is based upon the diagram portrayed in Figure 4.16. Figure 4.29 reveals that samples 3, 4, 6, 7 and 8 lie in the radium/uranium removal sector whereas samples 2 and 5 lie in positions corresponding to uranium loss without accompanying removal of radium.

In conclusion deposition of uranium in sections CQ1 and CQ2 occurs in the reduced rock as a result of the reduction of U^{6+} to U^{4+} . This observation demonstrates that the redox fronts act as an effective retardation barrier as indicated by deposition of uranium on the reduced side of the fronts. Similarly, uranium enrichment have been reported for the reduced side of the more developed, matured and large-scale redox fronts at Pocos de Caldas in Brazil although here the enrichment is more extensive (MacKenzie et al., 1992). Thus, in a HLW repository scenario, development of redox fronts would be expected to lead to retardation of radionuclides

released from a repository.

The above observations i.e. enrichment/deposition of uranium in the reduced rock close to the fronts have wider significance, including parallels with formation of low-temperature mineral deposits (Maynard, 1983), viz, redox controlled roll-front uranium deposition. These deposits are usually formed either by lateral groundwater flow that oxidises a mildly reduced, uranium-bearing sandstone aquifer, or by downward-percolating, oxidising ground waters invading somewhat reduced, uranium-rich crystalline rock, dissolving uranium in its path and re-precipitating it on the reduced side of the slowly migrating redox 'barrier' (Nash et al., 1981). For instance, the uranium mineralisation at Pocos de Caldas is richest at the strongly developed redox fronts. These are formed as downward-percolating, oxidising ground waters invade somewhat reduced, uranium-rich phonolites. Groundwater can percolate to depth in crystalline terrains where the horizontal deviatoric stress is high (Russell, 1988; Russell and Skauli, 1991). Even in terrains where it is held near the surface in horizontal joints, groundwater can gravitate to depth when vertical fractures are rejuvenated or where recent drilling provides such an opportunity (Pine and Batchelor, 1984).

Although, as demonstrated above, some of the uranium is caught in the redox fronts, a proportion is presumably carried down mega-joints where their walls are oxidised. The geometry of the fracture-associated redox fronts is that of an extremely acute arrow pointing downwards, and we can imagine that, at least along significantly permeable structures, the point of that arrow would eventually follow the shape of the flow lines of open convection systems. Thus, it seems feasible to assume that this study provides us with a microcosm of the process that, under appropriate

conditions, can lead to precipitation of uranium and other redox-sensitive elements at the discharge points of large-scale hydrothermal convection cells where sulphides, hydrocarbons or even hydrogen act as the electron donors for redeposition, a process likely to involve bacteria (Loveley et al., 1991). Although the uranium will eventually leak through in a small proportion of those natural hydrothermal systems where the source rocks have a relatively high oxidation state in the first place, it appears from both radiogenic age dating and structural studies that it would take at least 100×10^6 y for the leading edge of such a front to move through the rocks and back to the surface, by this time a benign addition to the uppermost crust (Mohamad et al., 1992).

In summary the isotope results reveal that the processes operating at the redox front are more complex than merely the simple transport of uranium from oxidised to reduced rock. The fracture samples give evidence of 'old' process of uranium deposition whereas the redox front results suggest recent process that have taken place since the end of the last period of glaciation (12000 y BP). A simple model is thus proposed to explain the distribution pattern and migration processes of uranium during fracture flow, and at the redox front, in the Craignair quarry as well as in the Criffel pluton as a whole, based upon isotopic data from analyses of samples CQ1 and CQ2 (Figure 4.30). The model basically delineates four major stages involved in the dissolution, transportation and retardation of uranium during fracture flow as follows: (i) slow, non-equilibrium uranium loss over long time periods, (ii) mobilisation of uranium in groundwater by surface and subsurface weathering, (iii) transportation of uranium by penetration of oxidising groundwater down fissures and, (iv) uptake of uranium on fracture-lining minerals by iron- and manganese-oxyhydroxides, clays and carbonate minerals during transportation and

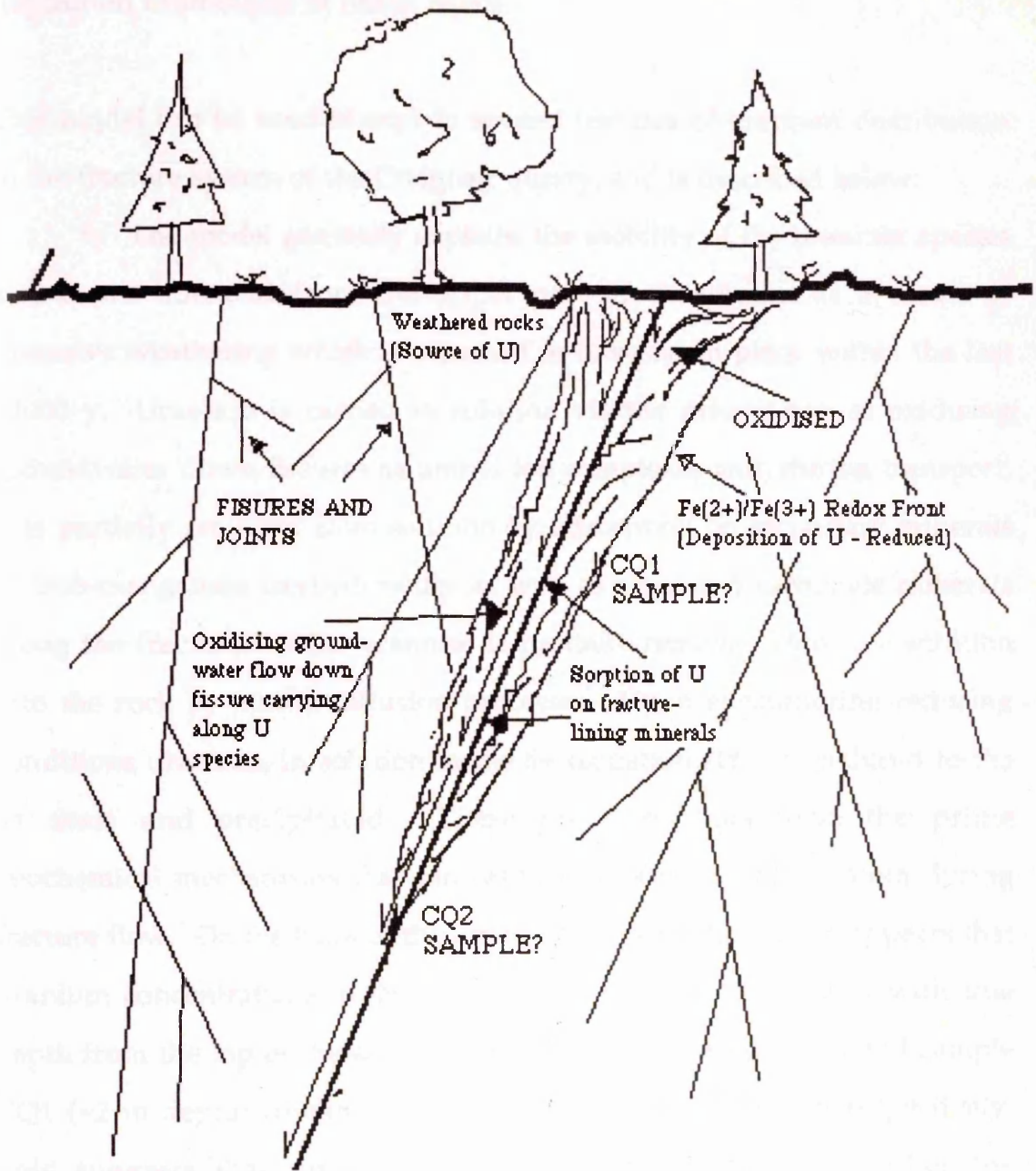


Figure 4.30: A diagrammatic sketch showing uranium migration and retardation in fractures crystalline rock.

deposition of uranium at redox fronts.

This model can be used to explain several features of uranium distribution in the fracture system of the Craignair quarry, and is described below:

i. The model generally explains the mobility of the uranium species which are liberated from the upper part of the pluton as a result of intensive weathering which is assumed to have taken place within the last 12000 y. Uranium is carried in solution via the penetration of oxidising groundwater down fissures as uranyl ion complexes and, during transport, it is partially removed from solution by adsorption on secondary minerals of iron-manganese oxyhydroxides as well as clays and carbonate minerals along the fractures. Also uranium is partially removed from the solution into the rock by matrix diffusion processes. Upon encountering reducing conditions uranium, in solution in the 6+ oxidation state, is reduced to the 4+ state and precipitated. These processes thus form the prime geochemical mechanisms that can result in retardation of uranium during fracture flow. On the basis of the limited data presented here it appears that uranium concentrations in the surface scraping material increase with true depth from the top of the quarry i.e sample CQ2 (~ 8 m depth) and sample CQ1 (~2 m depth) contain 162 ppm and 11 ppm of uranium respectively. This suggests that uptake of uranium is not permanent; either the movement of uranium down fissures is as a result of a series of precipitation/dissolution processes that occurred extensively in the last 12000 y, or an old 'stable' system (probably reduced) has recently been disturbed by ingress of oxidising water. However, the pronounced deficiency of ^{234}U relative to ^{238}U for surface scrapings material suggests preferential loss of ^{234}U as a result of α -recoil, implying that dissolution and transport processes affecting uranium have been operating here on a 10^5 y timescale. In this case, uranium has experienced a slow, non-

equilibrium loss over a long time period to give bulk rock that is slightly depleted in ^{234}U . Following this re-deposition in other areas has either given (a) slightly enhanced ^{234}U (as in section CQ1) or (b) thin deposits which lose ^{234}U very efficiently giving $^{234}\text{U}/^{238}\text{U}$ values as low as 0.64 (as in section CQ2).

ii. Penetration of oxidising groundwater has resulted in oxidation of the rock adjacent to fissures giving rise to narrow V-shaped oxidised zones extending downwards into the rock. The redox fronts between the oxidised and reduced rock were clearly visible as a change from red to grey marking the $\text{Fe}^{2+}/\text{Fe}^{3+}$ transition. Under these conditions dissolution of uranium as oxidising water reacts with the reduced rock will generate a maximum uranium concentration in the groundwater at the front resulting in diffusion into both the reduced and oxidised rock. The dissolved uranium on the oxidised side of the front is inherently stable in solution but other processes as described above, in particular deposition of oxides of iron and manganese, may lead to removal of uranium from solution. Diffusive movement of uranium away from the redox front into the reduced rock will result in reduction of uranium to the 4+ oxidation state resulting in precipitation in the reduced rock just ahead of the front.

With regard to the HLW repository scenario the model illustrates that the diffusion of nuclides into the rock, the uptake of uranium by fracture-lining minerals and at redox fronts are potentially important components in retarding the far-field movement of radionuclides released from a repository.

4.2.2.2 Rare earth element studies of rock section CQ2

The results for rare earth element analyses of samples from the rock section CQ2 are given in Table 3.6. The plots of REE concentrations against distance from the fracture surface for rock section CQ2 (Figures 4.31a to m) exhibit generally similar trends where, in all cases, maxima are observed in reduced rock close to the redox front (1 - 2 cm) from the fracture and at 4 - 5 cm except for Ho, Yb and Lu where the slight enrichment is displaced to 6 - 7 cm from the fracture surface. Minima are observed in the oxidised rock close to the fracture (0 - 1 cm) and in the reduced rock from about 2 to 4 cm and also in the 7 - 8 cm section.

Comparison of the REE data between sections CQ1 and CQ2 clearly indicates that the concentrations of light REE in CQ1 are about twice those of CQ2. This implies that the light REEs have been lost from the reduced rock in section CQ1 but have been partially scavenged from solution in the oxidised rock, probably by the Fe-Mn oxyhydroxides. Also samples from both sections CQ1 and CQ2 show identical trends for the REE distribution; i.e. a bimodal distribution of elements about the redox front (Figure 4.18 for section CQ1 and Figure 4.31 for section CQ2), similar to patterns in the Pocos de Caldas study (MacKenzie et al., 1992). Yet cerium and europium show no obvious sign of redox induced effects in the concentration profiles shown in Figures 4.31b and f respectively, and also do not exhibit any major deviation from the behaviour of the other REE in this rock section.

Comparison of the uranium and thorium data with those of the REE data indicates: (i) uranium and U/Th concentration ratio maxima over the same area as the REE; and (ii) there is no similarity between thorium and REE

Figure 4.31: Plots of REE concentrations versus distance from the fracture face in the rock section CQ2 from Craignair quarry, Dalbeattie.

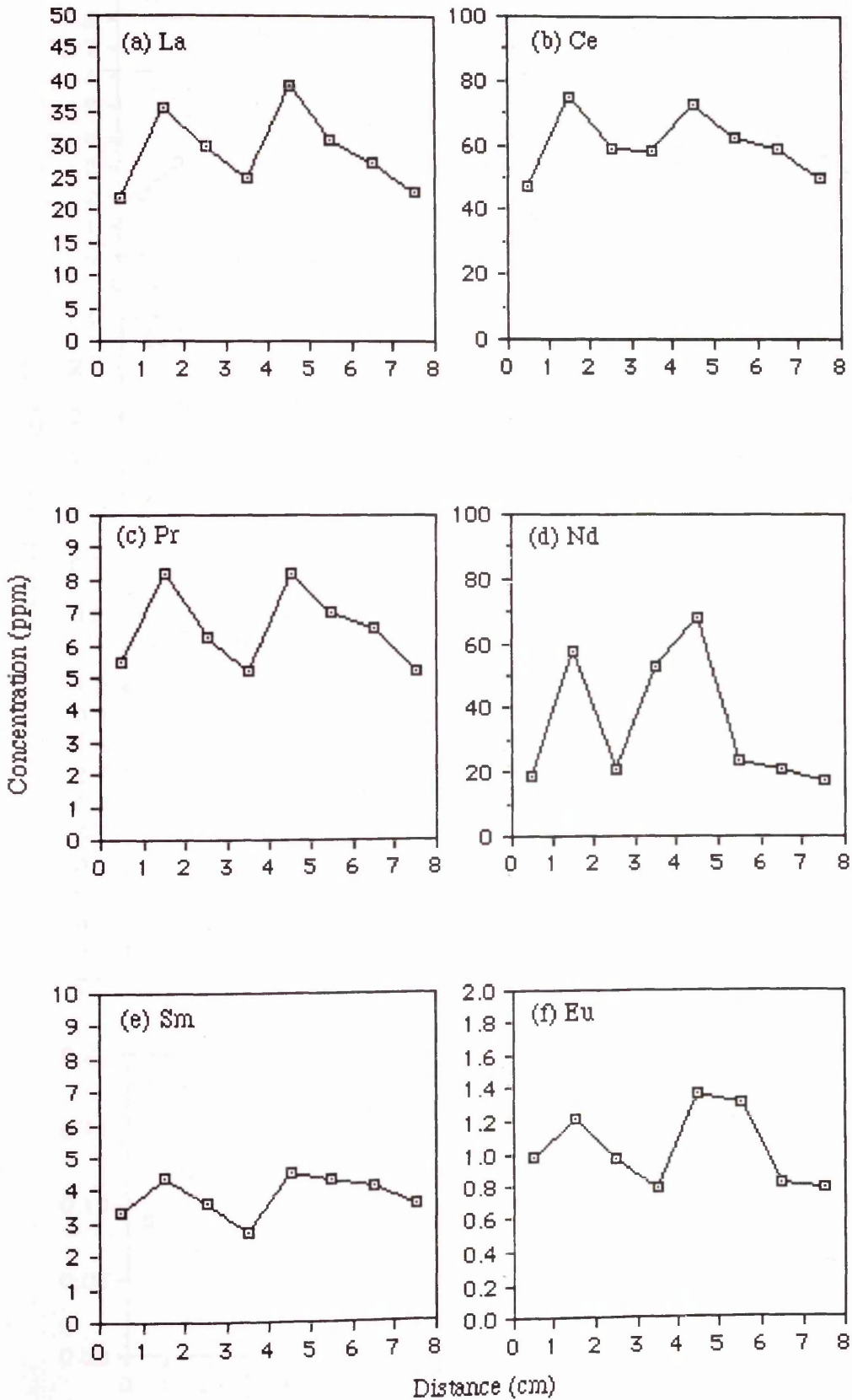
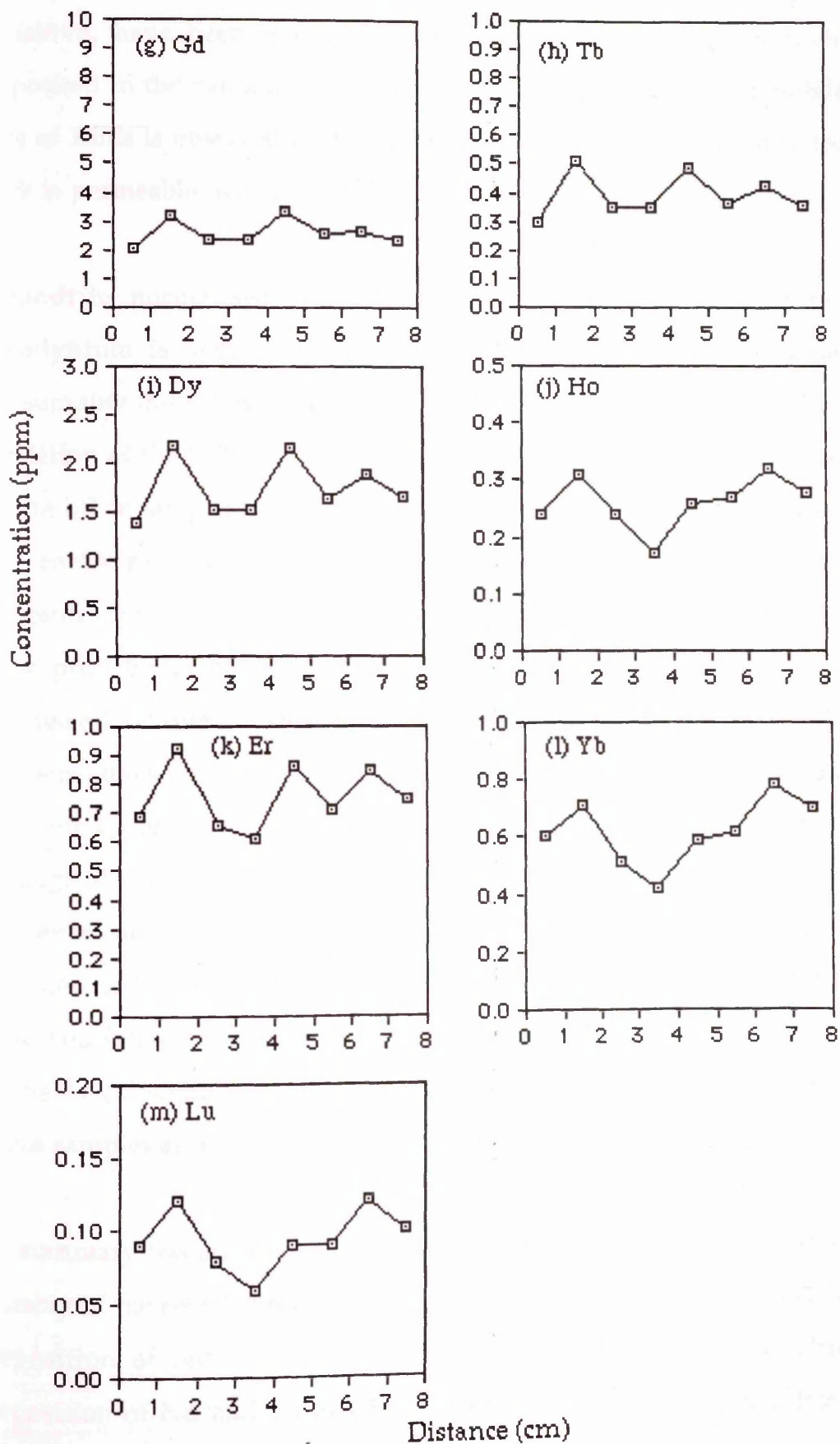


Figure 4.31 (cont.)

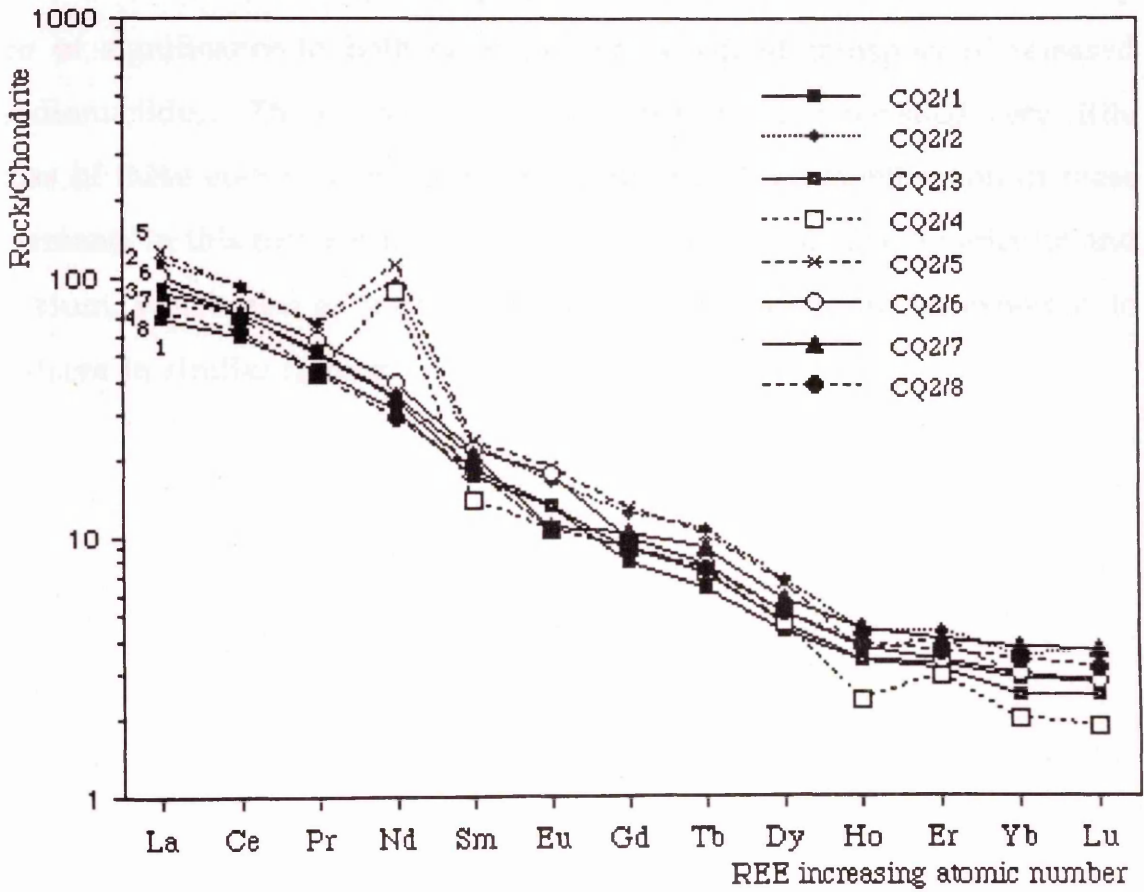


behaviour, indicating that the REE, although not inherently redox-sensitive, have been removed from reduced rock and are partially re-deposited in the oxidised rock, whereas thorium is relatively immobile; (iii) loss of REEs is observed up to 3.5 cm from the fracture, suggesting that the rock is permeable over at least that ^{distant} distance.

Chondrite normalised concentration plots are shown in Figure 4.32. Neodymium is anomalous in samples 2, 4 and 5 in this rock section, presumably indicating re-deposition at these sites. There is generally slight depletion of the REE concentrations apparent in samples 1, 4 and 8, relative to the other samples, indicating that the REE have probably been lost from the rocks represented by these samples. Slight enrichment of REE concentrations were observed in samples 2 and 5, indicating that the REE have probably re-deposited at these sites as with the deposition of Nd, as discussed above. The trends for the chondrite-normalised REE concentrations for all of the samples are very similar, except for Nd and Eu, and this observation forces the conclusion that passage of the redox front through the rock section results in little fractionation of the REE. There is, however, an obvious evident effect on the redox-sensitive REE Eu in samples 1, 7 and 8 where significant depletion of Eu concentration is observed (Figure 4.32). This observation suggests that Eu, which is mobile in the 2+ oxidation state has been lost from the rock close to the fractures by these samples as a result of rock-water interaction.

In summary fractionation of Nd and Eu from the other REE is observed, notably in the reduced rock at about 4.5 cm from the fracture, suggesting re-deposition of Nd and Eu has taken place at the site. The observed deposition of Nd and Eu at 4-5 cm reveals that the weathering front has probably moved to about 4.5 cm in the rock from the fracture surface,

Figure 4.32: Chondrite-normalised REE patterns for sliced samples in rock section CQ2 from Craignair quarry, Dalbeattie.



consistent with the conclusion based on uranium studies as described above. The observed deposition of REE in the reduced rock represents a potentially important radionuclide retardation process and, in the context of radioactive waste disposal, operation of such a process would obviously be of significance in both far-field and near-field transport of released radionuclides. The overall REE data, however, have revealed very little loss of these elements, except for Eu, indicating little mobilisation of these elements in this rock section. By analogy, this suggests that americium and curium, which also exist in 3+ oxidation state would also be expected to behave in similar fashion.

4.3 Natural decay series radionuclide and REE distributions in granite and granodiorite cores from outcrops subject to post-glacial weathering.

In section 4.1 it was demonstrated clearly that the rocks of the Criffel pluton in general have lost uranium. The isotopic data are consistent with this uranium loss having taken place dominantly, but not entirely, during the last 12000 y. From an analogue viewpoint weathering of this type could be regarded as an extreme case of penetration of highly oxidising groundwater into reduced ^{rock}. The behaviour of uranium, thorium, radium and rare earth elements is of interest in this context. Moreover, it is important from a geological viewpoint to evaluate the extent of weathering into the rock if genuinely 'fresh' samples are to be obtained. In order to investigate this phenomenon, natural decay series radionuclide and rare earth element distributions were determined for core samples from a representative granite (GR) from Kinharvie and a granodiorite (GD) from Clifton.

4.3.1 Weathering profile study of a granite core sample from Kinharvie

4.3.1.1 Natural decay series radionuclide distributions

The results for natural decay series analyses for samples from the weathering granite core from Kinharvie (section 2.1.3) are given in Table 3.7. Plots of U and Th concentrations, U/Th concentration ratios, $^{234}\text{U}/^{238}\text{U}$, $^{230}\text{Th}/^{234}\text{U}$ and $^{226}\text{Ra}/^{230}\text{Th}$ activity ratios versus distance from the weathering surface as well as $^{234}\text{U}/^{238}\text{U}$ activity ratio versus $^{230}\text{Th}/^{238}\text{U}$ activity ratio, and $^{226}\text{Ra}/^{230}\text{Th}$ activity ratio versus $^{230}\text{Th}/^{234}\text{U}$ activity ratio, are shown in Figures 4.33 to 4.41. The rock section was observed to be fractured and the fractures were filled with

quartz, carbonate and clay minerals and iron-manganese oxyhydroxides. But the samples themselves were collected from apparently fracture-free core (Plate 2.6).

The plot of uranium concentration against depth for the sample shows a progressive increase from the weathering surface to the end of the core, ranging from 3.0 to 5.1 ppm (Figure 4.33). The concentration of uranium in samples GR-1, 2 and 3 is below the average value of 3.6 ppm for this section of the granite (section 4.1), whereas the remaining samples are above the average. The depletion of uranium in the top three centimetres suggests that it has been leached from the rock by surficial weathering since the last period of glaciation (12000 y BP). The results show relatively constant uranium concentrations (about 4.0 ppm) from 6 cm to a depth of about 14 cm, then an increase to a value of about 5.0 ppm from about 18 cm.

The thorium concentrations in this rock section range from 13.4 to 18.8 ppm and all of the samples are above the average thorium concentration (13.1 ppm) for the MB-zone (Figure 4.34). However thorium concentration was apparently depleted in samples GR-2 and 3 (probably implying slight thorium removal), but this is probably extremely low. Nonetheless this is not reflected in the U/Th concentration ratios in samples from the top of the core to a depth of 14 cm, with a value which is within error constant, ranging between 0.22 and 0.24 and then rising to 0.27 for samples below 14 cm depth (Figure 4.35). The results suggest that, if thorium has remained immobile, and the thorium variation in the core does indicate a variation in mineralogy, then there has been a relatively constant loss of uranium relative to thorium from the rock to a depth of about 15 cm. Thus the uranium and U/Th data suggest that the weathering front may have penetrated to about 15 cm in the rock. There was, however, no visible

Figure 4.33: Uranium concentrations as a function of depth (centimetres from surface rocks) for granite core samples from Kinharvie.

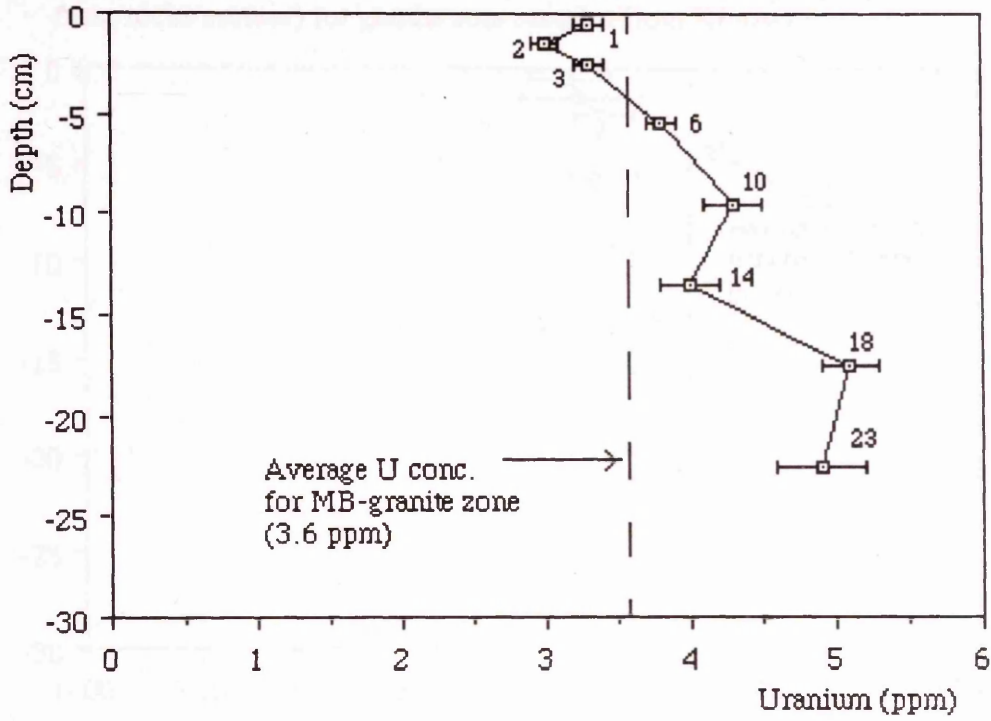


Figure 4.34: Thorium concentrations as a function of depth (centimetres from surface rocks) for granite core samples from Kinharvie.

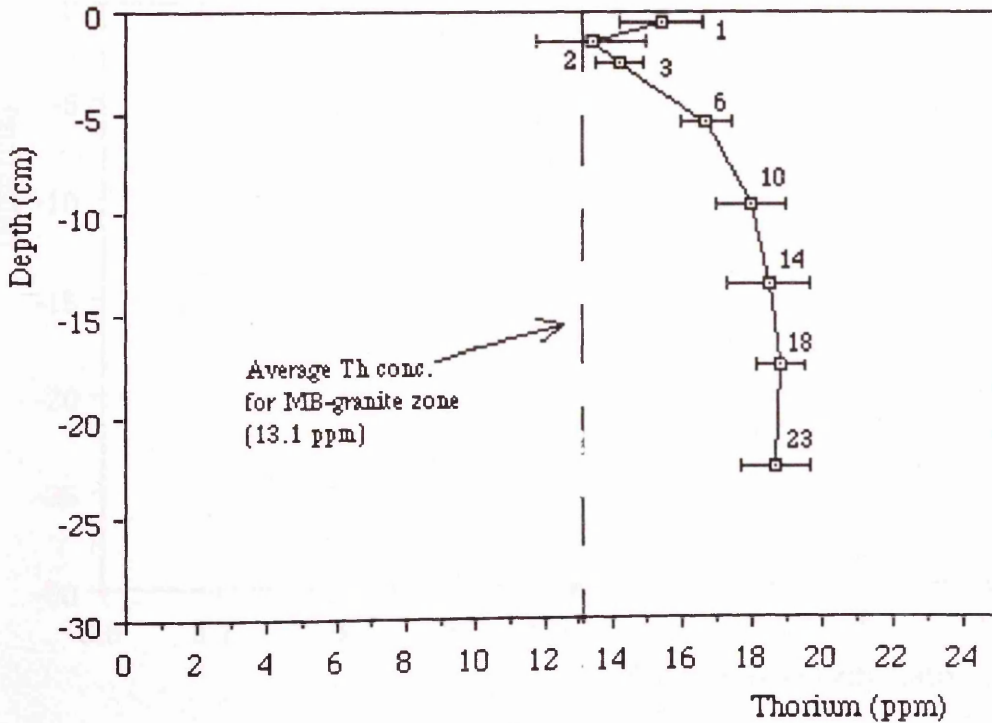


Figure 4.35: U/Th concentration ratio as a function of depth (centimetres from rocks surface) for granite core samples from Kinharvie.

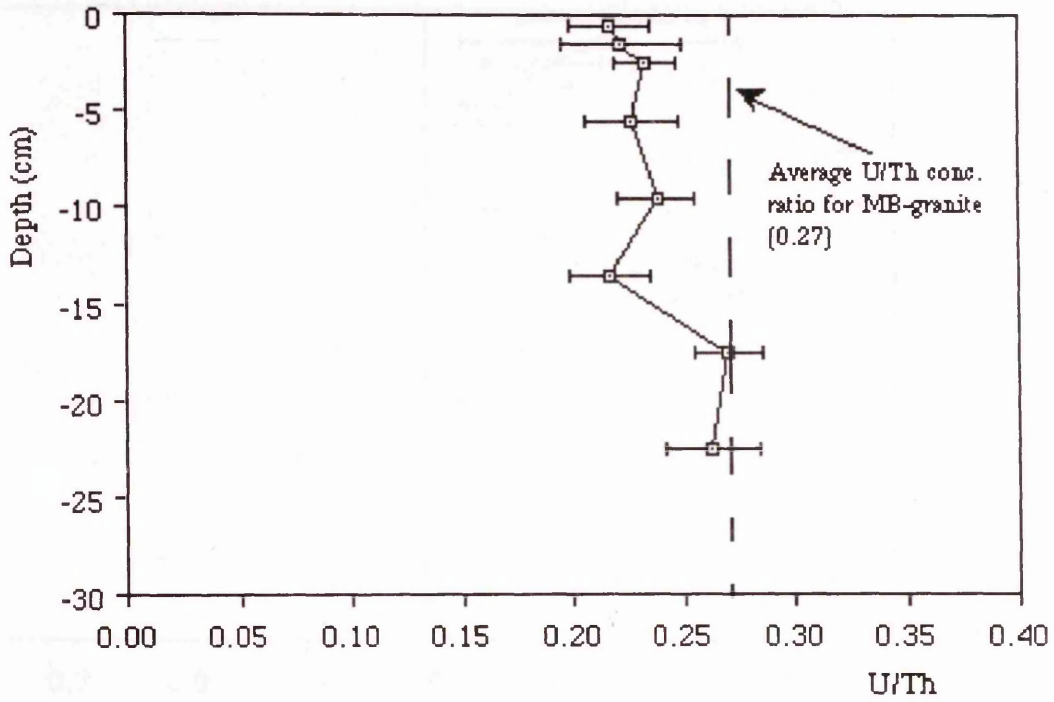


Figure 4.36: $^{234}\text{U}/^{238}\text{U}$ activity ratios as a function of depth (centimetres from rocks surface) for granite core samples from Kinharvie.

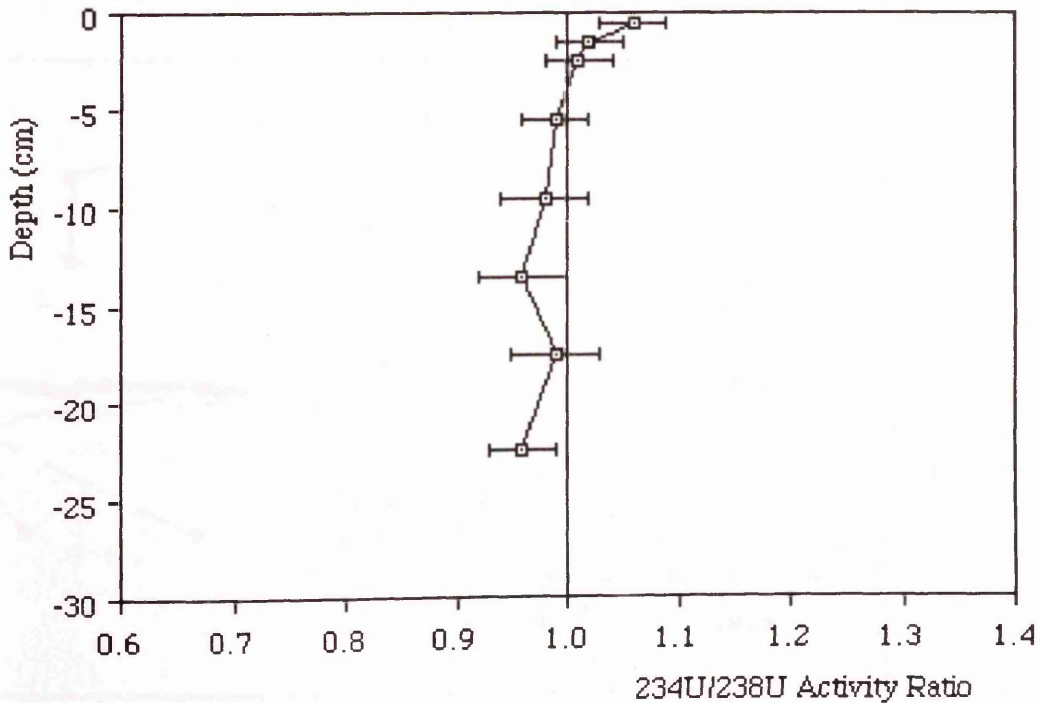


Figure 4.37: $^{230}\text{Th}/^{234}\text{U}$ activity ratios as a function of depth (centimetres from rocks surface) for granite cores samples from Kinharvie.

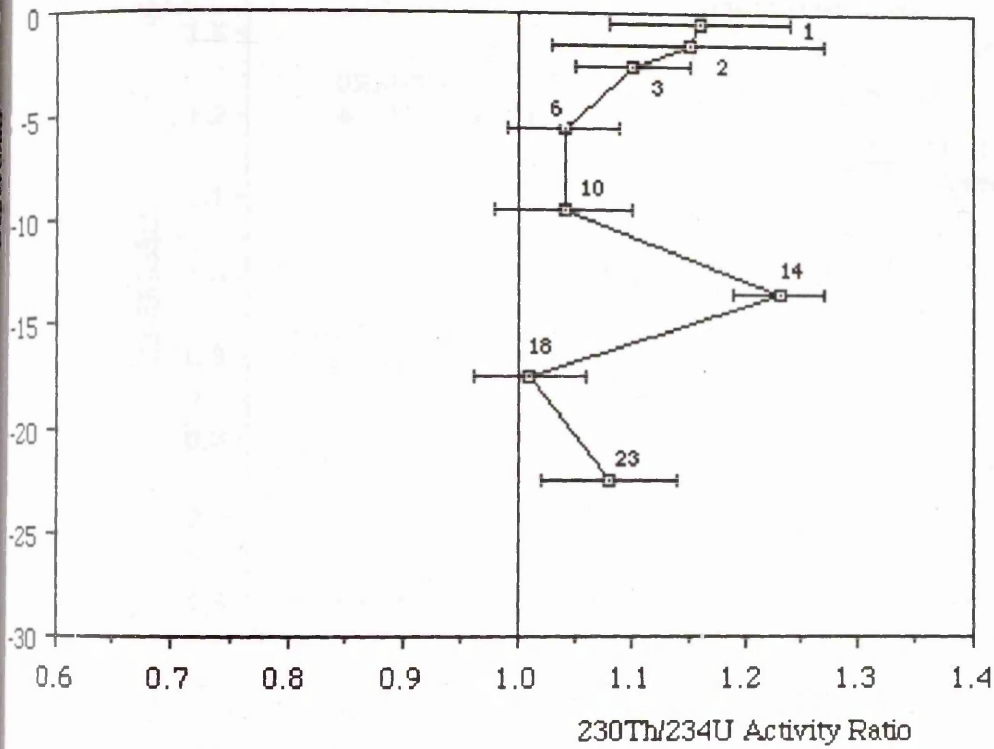


Figure 4.38: Plot of apparent % uranium loss (based on U/Th concentration ratio and $^{230}\text{Th}/^{234}\text{U}$ data) versus depth for granite core GR from Kinharvie.

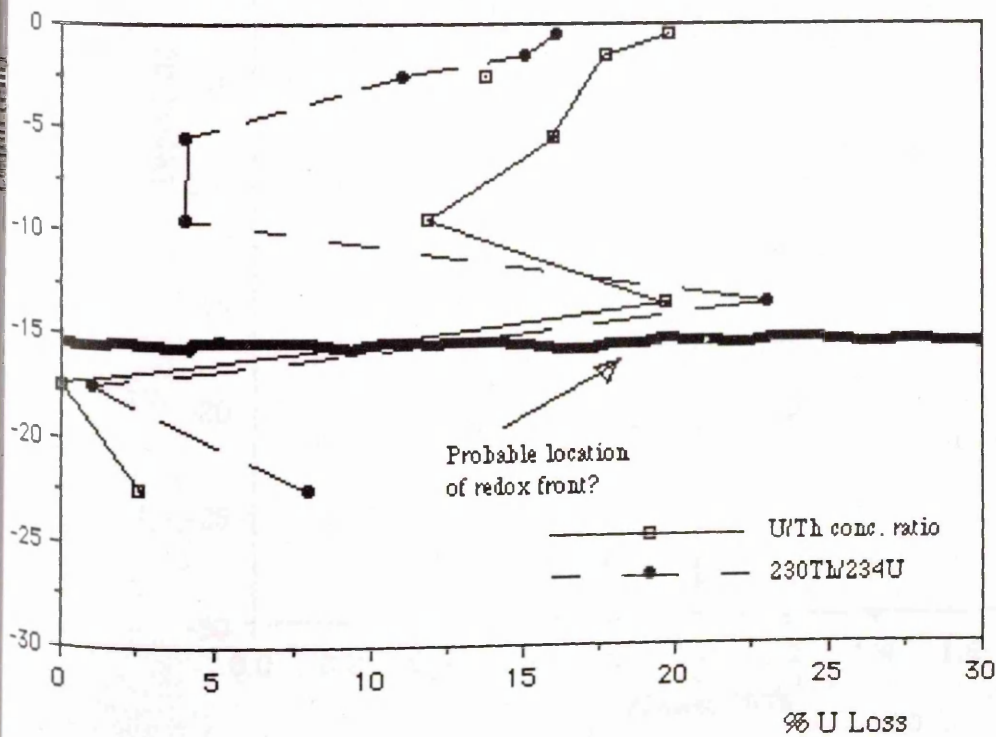


Figure 4.39: $^{234}\text{U}/^{238}\text{U}$ activity ratio versus $^{230}\text{Th}/^{238}\text{U}$ activity ratio diagram for granite core samples from Kinharvie.

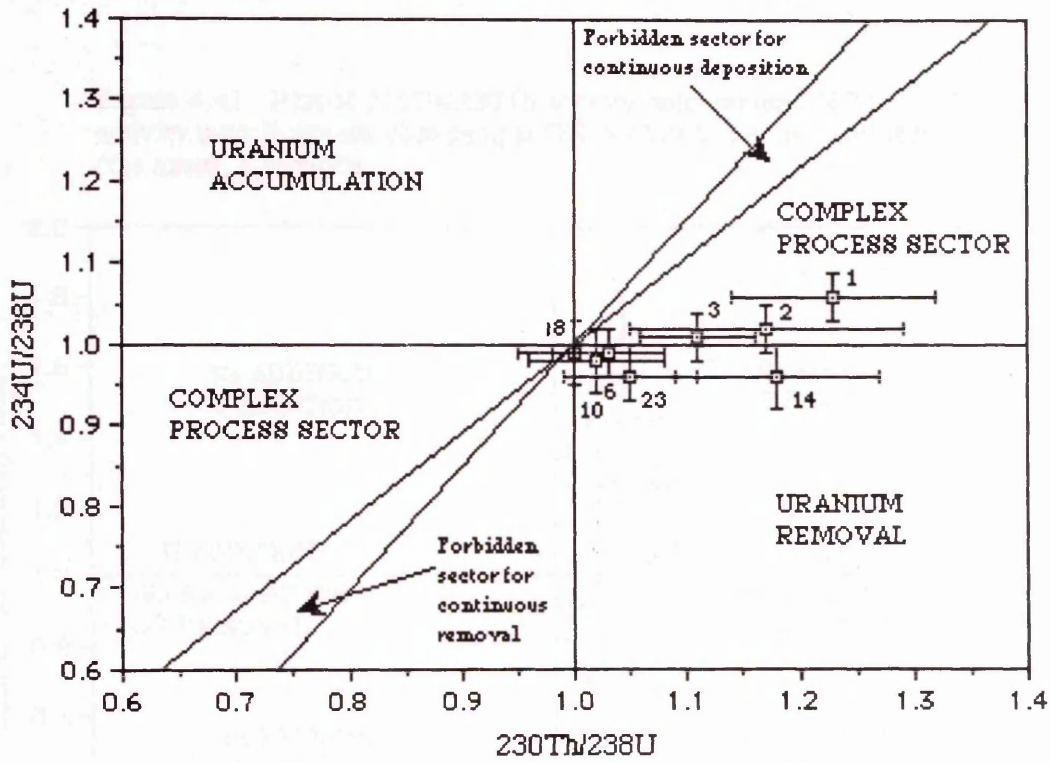


Figure 4.40: $^{226}\text{Ra}/^{230}\text{Th}$ activity ratios as a function of depth (centimetres from rocks surface) for granite core samples from Kinharvie.

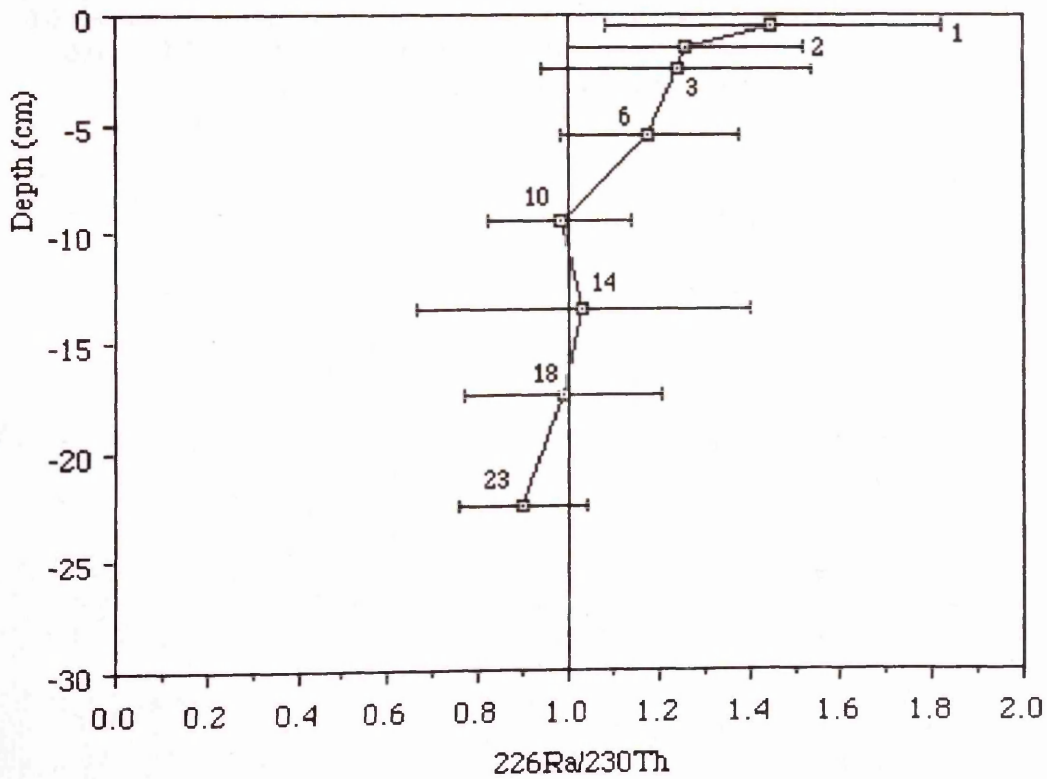
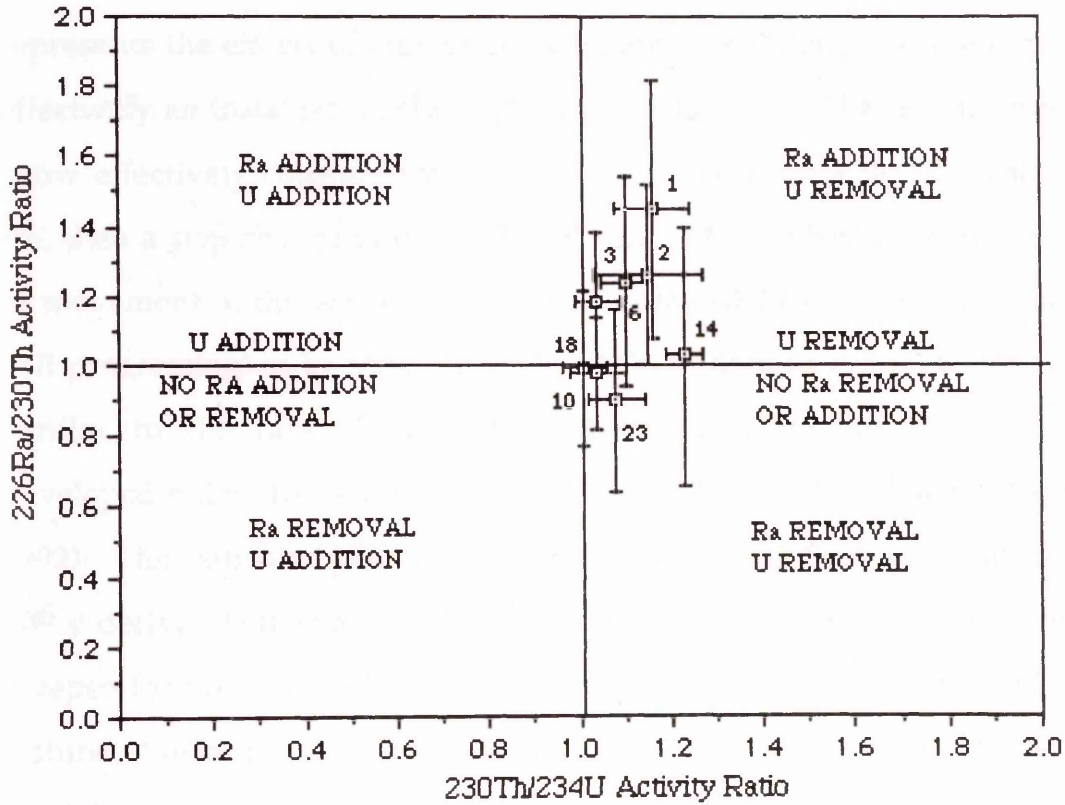


Figure 4.41: Plot of $^{226}\text{Ra}/^{230}\text{Th}$ activity ratio versus $^{230}\text{Th}/^{234}\text{U}$ activity ratio in granite core sample GR relative to secular equilibrium (the axes), Kinharvie.



evidence of an $\text{Fe}^{2+}/\text{Fe}^{3+}$ redox front in the core section. If samples GR-18 and 23 are taken to represent the original U/Th concentration ratio of the rock then the results indicate that a loss of some 30% of the uranium has occurred in this section of rock over 12000 y, consistent with the conclusion derived from $^{230}\text{Th}/^{234}\text{U}$ ratios in section 4.1. This observation thus represents the effects of ingress of weathering conditions into the rock from effectively an instantaneously start about 12000 y ago. The results appear to show effectively constant conditions of weathering to a depth of about 14 cm, then a step change to unweathered rock. On this basis, the average rate of movement of the weathering front is estimated (if it is assumed that it is still progressing) to be about 14 cm in 12000 y (12 m in 10^6 y), which is very similar to the rate of movement observed at the more mature and developed redox fronts at Pocos de Caldas of 12 m in 10^6 y (MacKenzie et al., 1992). The estimated rate of movement of the redox front of up to 12 m in 10^6 y derived here suggests that the proposed rate of far-field movement of a repository-related redox front of up to 50 m in 10^6 y (Neretneiks and Aslund, 1983a, b) is a reasonable value for inclusion in far-field transport models.

Plots of $^{234}\text{U}/^{238}\text{U}$ and $^{230}\text{Th}/^{234}\text{U}$ activity ratios over the length of the core are shown in Figures 4.36 and 4.37 respectively. All of the samples from the core display $^{234}\text{U}/^{238}\text{U}$ activity ratios of about unity but there is an indication of a systematic increase in the ratio towards the surface, with sample GR-1 showing a value of 1.06, suggesting some comparatively recent deposition of uranium (Figure 4.36). The $^{234}\text{U}/^{238}\text{U}$ activity ratio of uranium that has been deposited here is observed to be greater than unity, thus suggesting that it is not exclusively uranium that has been mobilised by recent, rapid dissolution in equilibrium. There is a very smooth trend in

the $^{234}\text{U}/^{238}\text{U}$ data except for sample GR-18 at 17 - 18 cm which has a higher value than the other samples in this section of the rock. This observation again suggests that the weathering front has penetrated to between 14 and 18 centimetres depth since it implies either less removal of uranium at 18 cm or else some re-deposition.

The $^{230}\text{Th}/^{234}\text{U}$ activity ratios (Figure 4.37) are greater than unity throughout the core, indicating uranium loss as a result of recent (relative to the ^{230}Th half life) rock-water interaction. Only three samples, GR6, GR10 and GR18 have $^{230}\text{Th}/^{234}\text{U}$ activity ratios within error of equilibrium, whereas the disequilibrium between ^{230}Th and ^{234}U is quite pronounced for other samples, notably for samples in the top three centimetres of the core, i.e. samples GR-1, 2 and 3 which display $^{230}\text{Th}/^{234}\text{U}$ activity ratios of 1.16, 1.15 and 1.11, respectively, revealing that 10 - 20% of the uranium has been lost from the surface rocks assuming that thorium has remained immobile. So uranium has been lost from the outermost 3 cm of the rock, but the most pronounced loss is observed in sample GR-14 (with a value of 1.23) at 13 - 14 cm. In contrast sample GR-18 at 17 - 18 cm has a $^{230}\text{Th}/^{234}\text{U}$ ratio close to unity. These results, therefore provide strong evidence to support the suggestion of the existence of a weathering front between 14 and 18 cm depth. Assuming thorium has remained immobile in the rock, values for apparent percentage uranium loss from the samples were calculated from (a) the U/Th concentration ratio and (b) the $^{230}\text{Th}/^{234}\text{U}$ activity ratio. The plot of apparent percentage uranium loss versus distance is shown in Figure 4.38. The plot again suggests the existence of the weathering front between 14 and 18 centimetres depth. Thus, these results clearly show that the bulk rock does not act as a retardation barrier except at the very top of the core.

The uranium and thorium isotopic data for the rock section are summarised in a plot of the $^{234}\text{U}/^{238}\text{U}$ activity ratio against the $^{230}\text{Th}/^{238}\text{U}$ activity ratio in Figure 4.39, from which it can be seen that samples GR-6, 10, 14, 18 and 23 lie in the uranium removal sector of the diagram while the rest of the samples (samples GR-1, 2 and 3) all plot in positions in the complex process sector. The results, plotted in this way, reinforce the above suggestion that the weathering front lies in a position between samples GR-14 and 18. Thus, sample GR-14 plots in a position indicative of rapid, recent near-equilibrium dissolution, consistent with being recently affected by oxidising conditions. Samples GR-18 and 23, from deeper within the rock, plot in positions relatively close to the equilibrium (1,1) position suggesting that the influence of weathering has been slight at this depth. Above the putative weathering front, sample GR-10 also lies close to the (1,1) position which suggests that there has been re-deposition of uranium in a near equilibrium at this position relative to sample GR-14. This observation is comparable to that at the Pocos de Caldas analogue site where uranium was effectively scavenged from groundwater by iron oxyhydroxides forming on the oxidised sides of redox fronts. Nearer to the surface there is a systematic trend for samples GR-10, 6, 3, 2 and 1 which lie on a curve projecting into the upper complex process zone, with sample GR-1, which would have been first to be influenced by the weathering front, lying furthest from equilibrium. The trend in the positions of samples GR-10 to 1 suggests that following migration of the weathering front through the rock there is continuing re-distribution of uranium, with a trend towards $^{234}\text{U}/^{238}\text{U}$ disequilibrium as the surface is approached. Since such disequilibrium evolves slowly relative to rapid redox induced re-distribution this also speaks for sample GR-1 having been influenced by the re-distribution processes for the longest time.

Figure 4.40 shows that the $^{226}\text{Ra}/^{230}\text{Th}$ activity ratios of samples GR-1, 2, 3 and 6 from 0 - 10 cm section of the core show ^{226}Ra to be out of equilibrium with ^{230}Th . In these samples a considerable excess of ^{226}Ra (greater than 20%) relative to ^{230}Th has been deposited within the last 8000 y, possibly as a result of radium being removed from the underlying reduced rock (although there is no evidence of radium loss from deeper section of this core) and re-deposited in the oxidised rock in the top section of the core by a co-precipitation process involving iron-manganese oxides. The trend is therefore comparable with that exhibited by the $^{234}\text{U}/^{238}\text{U}$ activity ratio. Thus, taken together there is evidence of uptake of radium and uranium near the surface of the rock, probably in secondary weathering product minerals such as iron-manganese oxyhydroxides. However, the $^{226}\text{Ra}/^{230}\text{Th}$ activity ratios from 10 cm downwards lie within error of secular equilibrium, suggesting that any loss of ^{226}Ra was too little to be detected by the analysis.

The $^{226}\text{Ra}/^{230}\text{Th}$ activity ratio versus $^{230}\text{Th}/^{234}\text{U}$ activity ratio diagram for the core, shown in Figure 4.41, reveals that samples GR-1, 2, 3 and 6 lie in the radium addition/uranium removal sector; sample GR-23 lies in the uranium/radium removal sector; sample GR-14 lies in a position corresponding to uranium removal but no radium removal; and samples GR-10 and 18 lie close to unity indicating little loss of uranium and radium. This observation indicates a weak tendency for ^{226}Ra removal from the reduced rock, possibly from about 23 centimetres downwards, in conjunction with re-deposition in the oxidised rock, whereas uranium loss occurs to a depth of about 14 centimetres in the rock section. Thus, there is evidence that ^{226}Ra , which is not an inherently redox-sensitive element, has moved over distances of the order of 17 centimetres from the reduced

rock to the oxidised rock on a timescale of 10^3 y. The observed deposition of uranium and radium in the oxidised rocks of the granite core represents a potentially important radionuclide retardation process in the geosphere which would not be predicted on the basis of purely thermodynamic considerations. Although as discussed previously in section 4.1, the bulk rock of the pluton does not present a retardation barrier, there is evidence here that the very near surface granite could act, to some extent, as sites of deposition.

In summary, analyses of uranium and thorium in the granite core sample (GR) from the Criffel pluton clearly showed evidence of uranium loss to a depth of about 14 centimetres, thus suggesting the average rate of movement of the weathering front for the granite is about 12 m in 10^6 y. In the context of radioactive waste disposal the estimated rate of movement of the redox front of up to 12 m in 10^6 y derived here suggests that the proposed rate of far-field movement of a repository-related redox front of up to 50 m in 10^6 y (Neretneiks and Aslund, 1983a, b) is a realistic value for inclusion in far-field transport models. Uranium loss is quite pronounced from the top 14 centimetres of the pluton, thus suggesting that the surface rocks have undergone intense surficial weathering since the last period of glaciation (~ 12000 y BP). In addition the results of uranium and thorium in the core are consistent with the expected geochemical behaviour of these two elements in igneous rock i.e. uranium is susceptible to oxidation-induced dissolution and is, consequently, relatively mobile, whereas thorium is effectively immobile. The isotopic results clearly reveal the loss of uranium relative to ^{230}Th , consistent with

the conclusion derived from section 4.1 that the Criffel pluton has experienced a recent, rapid post-glacial removal of uranium from the uppermost section of the rock.

4.3.1.2 Rare earth element studies of granite core GR

The results for rare earth element analyses for samples from the granite core from Kinharvie and chondrite normalising values are given in Table 3.8. The plots of REE concentrations against depth (Figures 4.42a to m) exhibit generally similar trends, with maxima in the oxidised rock from 0 to 2 cm and at 13 - 14 cm, with generally lower values in the section from 2 to 10 cm. This suggests the existence of a weathering front at approximately 14 cm (probably 12 cm depth), consistent with the conclusion derived above from the natural decay series data. On this basis the average rate of movement of the weathering front can be estimated to be about 10 m in 10^6 y, as with the uranium (section 4.3.1.1).

Comparison of the REE data between the granite core GR with rock section CQ1 clearly indicates that the concentrations of light REE in GR are generally slightly less than those of CQ1, suggesting that the light REE have been lost from the reduced rock in section CQ1 but are partially scavenged from solution in the oxidised rock, probably by secondary minerals of Fe-Mn oxyhydroxides. This is consistent with visual observation that the sample contained a substantial amount of Fe-Mn oxyhydroxides in the oxidised rock. In addition, sections CQ1 and CQ2 and granite core GR both show identical bimodal distributions of the REE about the redox fronts

Figure 4.42: Plots of REE concentrations versus depth from the weathered surface in granite core GR from Kinharvie, southwest Scotland.

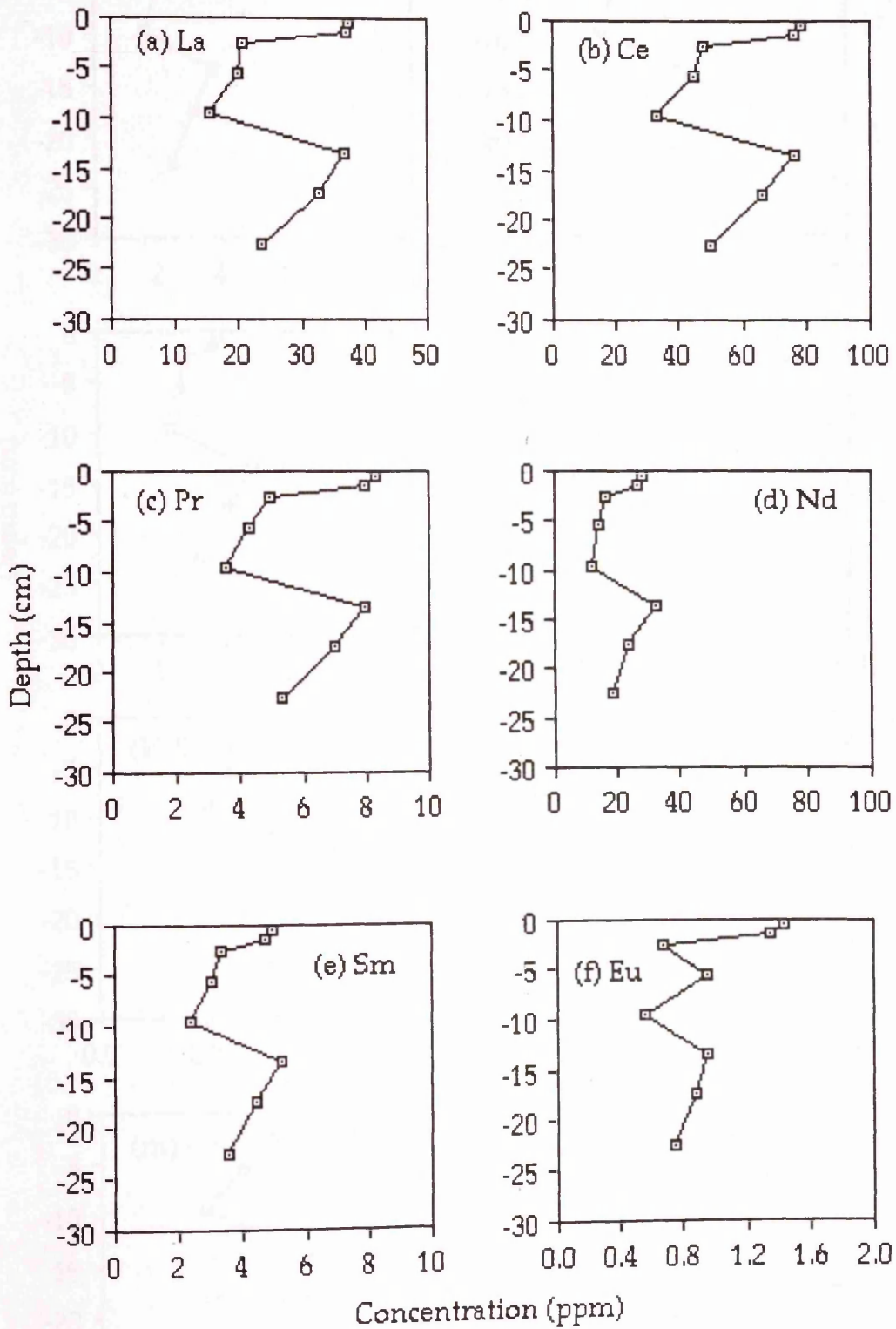
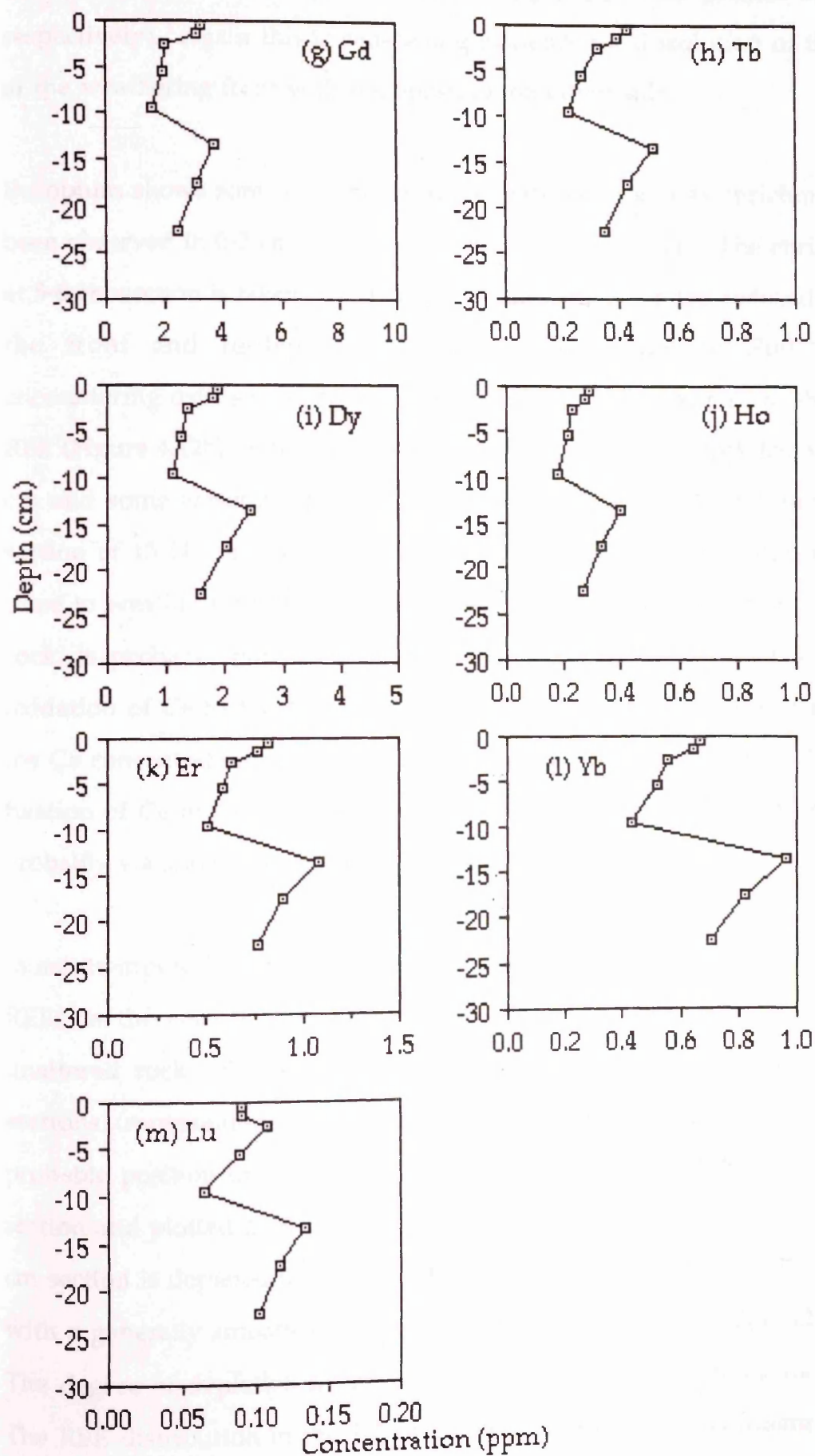


Figure 4.42 (Cont.)

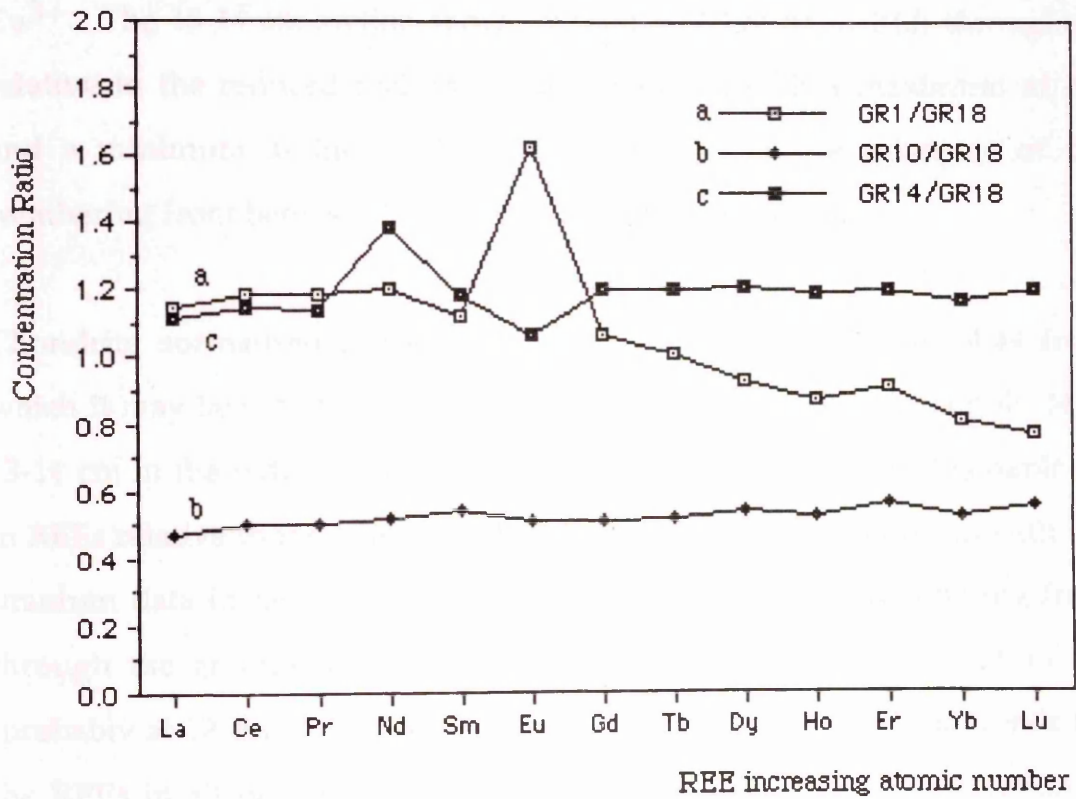


(Figures 4.18, 4.31 and 4.42 for section CQ1, CQ2 and granite core GR respectively). Again this is compelling evidence for dissolution of the REE at the weathering front with re-deposition on either side.

Europium shows some evidence of redox induced effects as enrichment has been observed in 0-2 cm and 5-6 cm sections (Figure 4.42f). The enrichment at 5-6 cm section is taken to indicate Eu^{2+} dissolution on the reduced side of the front and re-deposition, following oxidation to Eu^{3+} upon encountering oxidising conditions. Ce shows a similar pattern to the other REE (Figure 4.42b), with general depletion observed in the rock from 2 to 10 cm and some enrichment in the near surface samples (0-2 cm) and in the section of 13-14 cm. The enrichment pattern observed in the reduced rock close to weathering front suggests that Ce, which is leached from the bulk rock, is probably partially re-deposited at the front, presumably due to oxidation of Ce to the 4+ oxidation state at this site. The enhancement of the Ce concentration in samples 1 and 2 is to be expected given preferential fixation of Ce in 4+ oxidation state in the oxidising conditions, in this case probably via scavenging by iron-manganese oxyhydroxides.

In an attempt to identify possible dissolution and re-deposition effects of the REEs in the core it was assumed that the 17-18 cm section represented unaltered rock. So the REE concentrations in the 1-2 cm and 9-10 cm sections (represented oxidised rock) and 13-14 cm section (represented probable position of weathering front) were divided by those of 17-18 cm section and plotted in Figure 4.43. It is clear from this figure that the 9 - 10 cm section is depleted in the REE relative to the reduced rock at 17 - 18 cm, with a generally smooth trend and no fractionation of individual elements. The degree of depletion in this section decreases slightly along the series. The REE distribution in the 1-2 cm section shows some enrichment for the

Figure 4.43: Plot showing the ratio of REE concentrations in (a) 1-2 cm, (b) 9-10 cm and (c) 13-14 cm sections to concentrations in 17-18 cm section in the reduced rock of the granite core from Kinharvie.

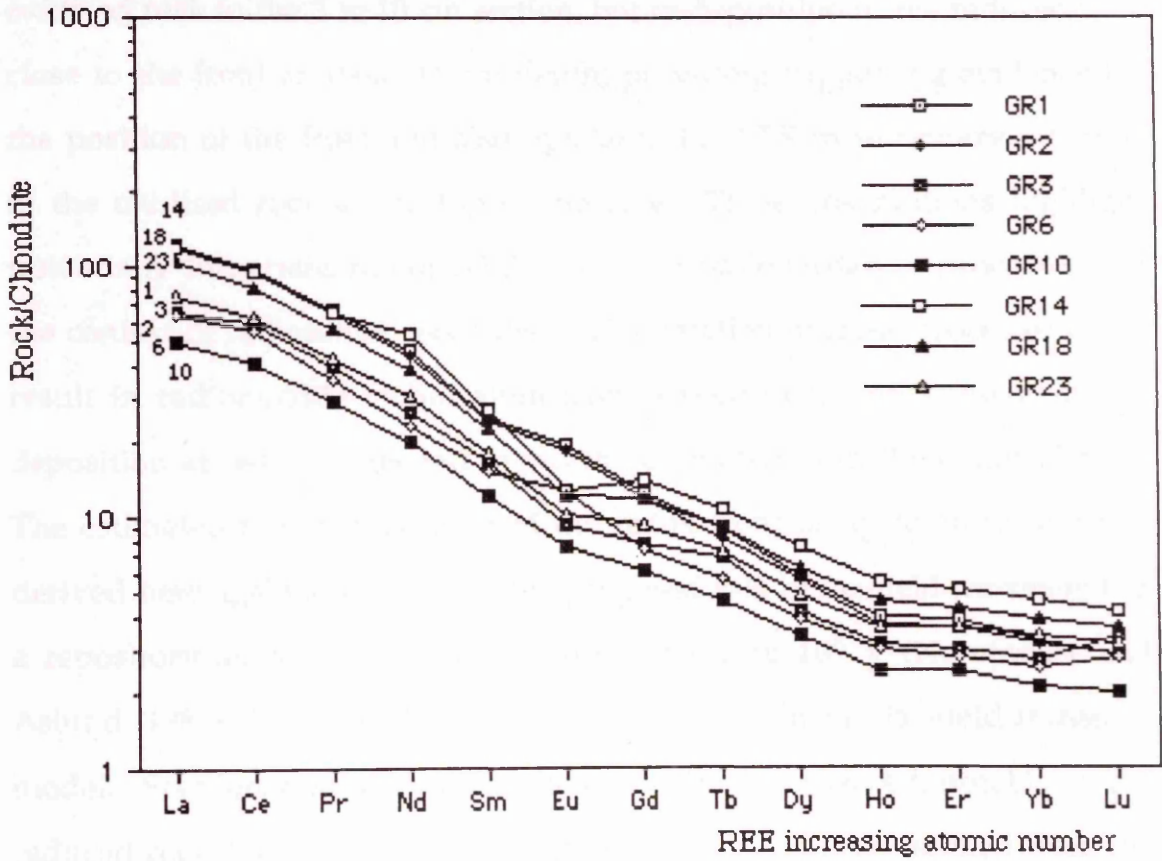


LREE (La - Tb) and depletion in the rest of the REE (the degree of depletion increases along the series with a distinct minimum for Lu) relative to the reduced rock in section 17 - 18 cm. A distinct Eu anomaly is evident in this section, suggesting preferential loss of Eu^{2+} from the reduced rock and re-deposition in the oxidised rock near the surface following oxidation to Eu^{3+} . The 13-14 cm section shows general enrichment in REE throughout relative to the reduced rock in section 17-18 cm, with a maximum at Nd and a minimum at Eu. This observation implies the existence of the weathering front between 13 and 18 cm depth at this location.

Chondrite normalised concentration plots are shown in Figure 4.44 from which it may be seen that there is an enrichment of the REE in sample 14 at 13-14 cm in the reduced rock close to the front, while sample 10 is depleted in REEs relative to the other samples. So again we see evidence (as with the uranium data in section 4.3.1.1 that the penetration of the weathering front through the granite core can attain a distance of between 10 and 14 cm (probably at 12 cm) from the fracture wall. Apart from Eu all the trends for the REEs in all of the samples are similar, implying that the migration of the weathering front through the rock section results in little disturbance in the relative REE concentrations. Obvious evidence of redox induced effects can be seen in sample 14 where significant depletion of Eu concentration is observed (Figure 4.44), suggesting that Eu in the 2+ oxidation state has been lost from this sample.

As discussed in section 1.4, Stephens et al. (1985) used the REE in the classification of the different zones of the pluton. In this context the REE data for sample 18 in the reduced rock at 17 - 18 cm section of the granite core from Kinharvie can be compared to those of Stephens et al. (1985) for sample MB-272 (Table 3.8) located near Kinharvie. The chondrite-

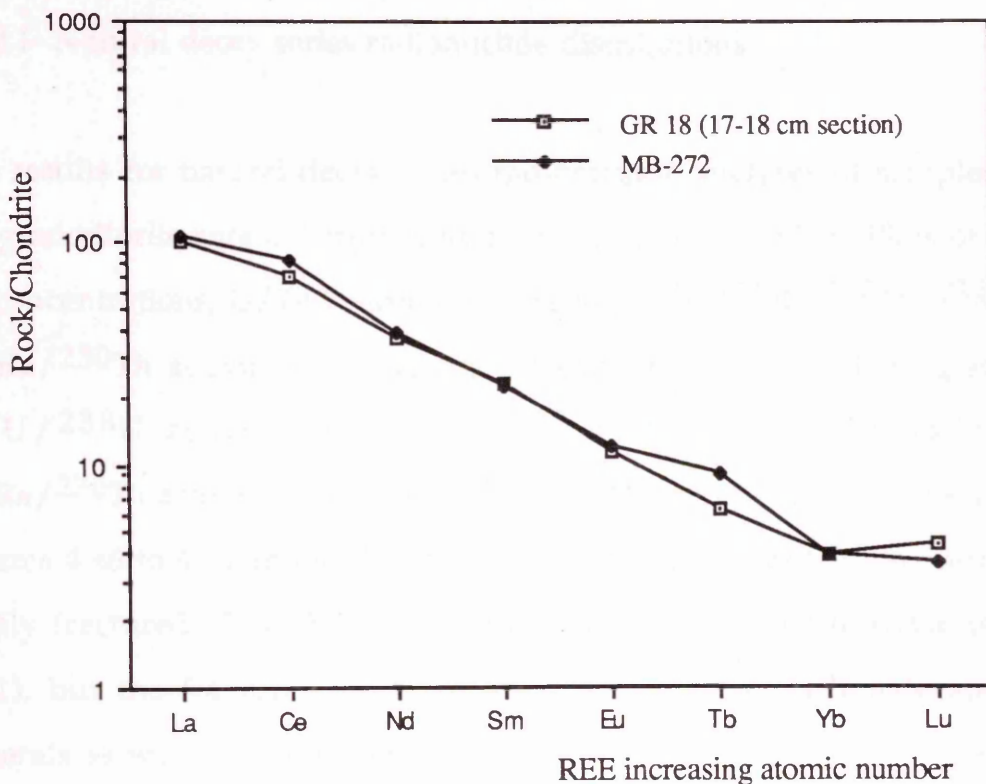
Figure 4.44: Chondrite-normalised REE patterns for sliced samples in granite core GR from Kinharvie, southwest Scotland.



normalised data are found to be comparable and their relationships is shown in Figure 4.45.

In summary the REE data reveal a general loss of these elements from oxidised rock in the 2 to 10 cm section, but re-deposition in the reduced rock close to the front at about 14 cm depth; providing supporting evidence for the position of the front and also uptake of the REE in secondary minerals in the oxidised rock at the top of the core. These observations highlight potentially important radionuclide mobilisation/retardation processes. In the context of radioactive waste disposal, operation of these processes could result in radionuclide mobilisation from a repository and subsequent re-deposition at redox fronts and in weathered materials in the oxidised rock. The estimated rate of migration of the redox front of up to 10 m in 10^6 y derived here again suggests that the proposed rate of far-field movement of a repository-related redox front of up to 50 m in 10^6 y (Neretneiks and Aslund, 1983a, b) is a realistic value for inclusion in the far-field transport model. Fractionation of Eu from the other REE is observed, notably in the reduced rock close to the front, suggesting that it has been leached from the bulk rock in the 2+ oxidation state to be partially re-deposited on the oxidised side upon oxidation to Eu^{3+} .

Figure 4.45: Chondrite-normalised REE patterns for sliced samples at 17-18 cm in the reduced rock of the granite core GR from Kinharvie and sample MB-272 (Stephens et al., 1985) from the Criffel pluton.



4.3.2 Weathering profile study of a granodiorite core sample from Clifton

4.3.2.1 Natural decay series radionuclide distributions

The results for natural decay series radionuclide analyses of samples from the granodiorite core GD from Clifton are given in Table 3.9. Plots of U and Th concentrations, U/Th concentration ratios, $^{234}\text{U}/^{238}\text{U}$, $^{230}\text{Th}/^{234}\text{U}$ and $^{226}\text{Ra}/^{230}\text{Th}$ activity ratios versus distance from the weathering surface, $^{234}\text{U}/^{238}\text{U}$ activity ratios versus $^{230}\text{Th}/^{238}\text{U}$ activity ratios and $^{226}\text{Ra}/^{230}\text{Th}$ activity ratios versus $^{230}\text{Th}/^{234}\text{U}$ activity ratios are shown in Figures 4.46 to 4.53 and 4.55. The rocks in the section at Clifton were more highly fractured (Plate 2.7) than the granite cored from Kinharvie (section 4.3.1), but the fractures too were filled with quartz, carbonate and clay minerals as well as iron-manganese oxyhydroxides.

The plot of uranium concentration against depth (Figure 4.46) reveals small variations in the range 2.6 to 3.7 ppm except for sample 20 which has a value of 6.7 ppm, suggesting that re-deposition of uranium has taken place at this location. Apart from sample 20, all of the remainder have uranium concentrations that are depleted compared with the average value of 3.9 ppm for the CHB-zone. The most pronounced depletions of uranium are observed in samples 1, 2, 10, 15 and 44. This observation suggests that uranium has been leached from the rock as a result of intense surficial weathering since the last period of glaciation (~12000 y BP). This is particularly the case in the top two centimetres judging from those samples, which have experienced intense surface alteration (i.e. they are bleached and friable). The low uranium values at depth probably result from

Figure 4.46: Uranium concentrations as a function of depth (centimetres from rocks surface) for granodiorite samples from Clifton.

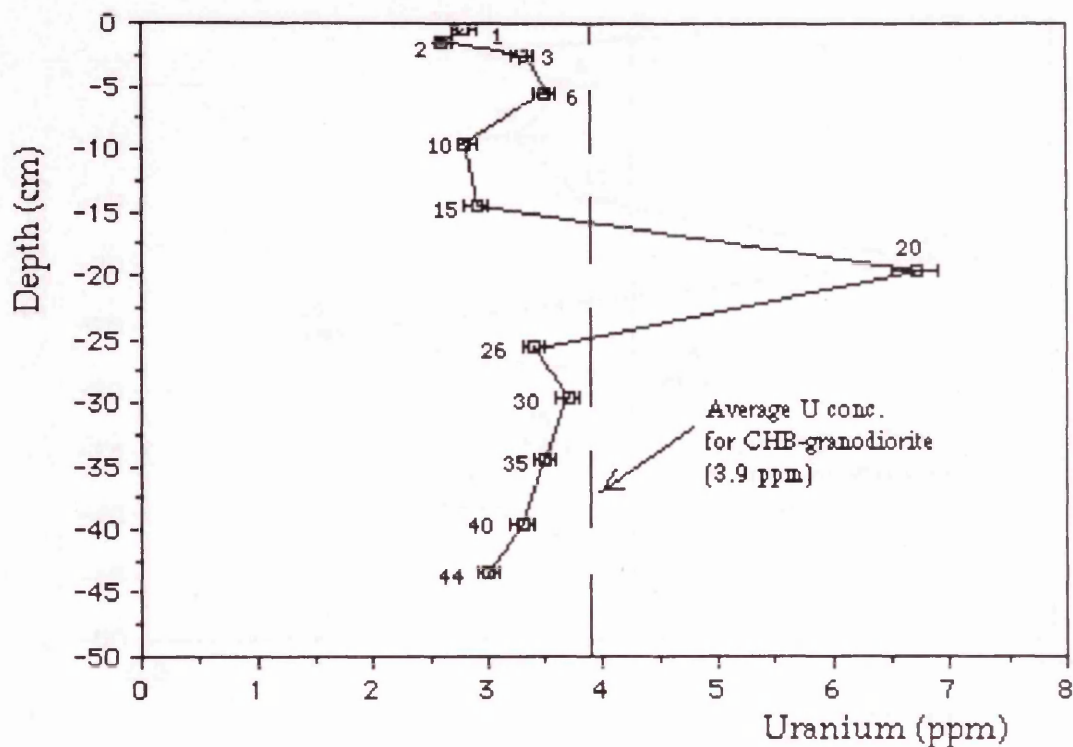


Figure 4.47: Thorium concentrations as a function of depth (centimetres from rocks surface) for granodiorite samples from Clifton.

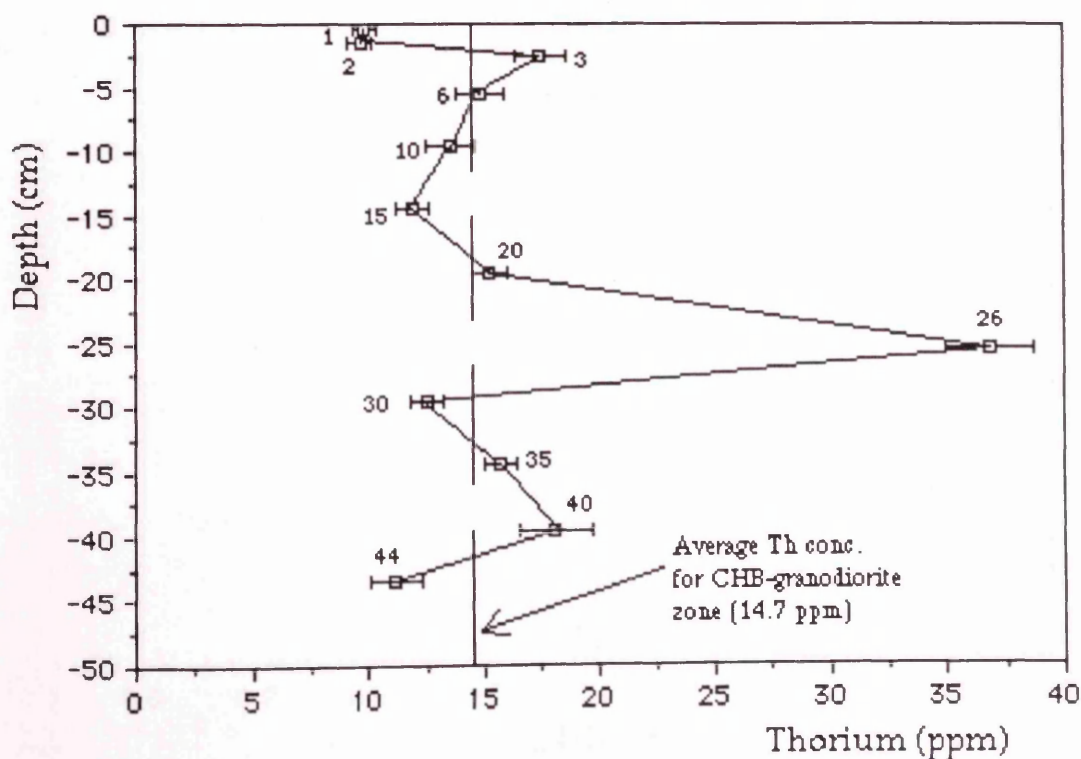


Figure 4.48: Uranium/thorium concentrations ratio as a function of depth (from rocks surface) for granodiorite samples from Clifton.

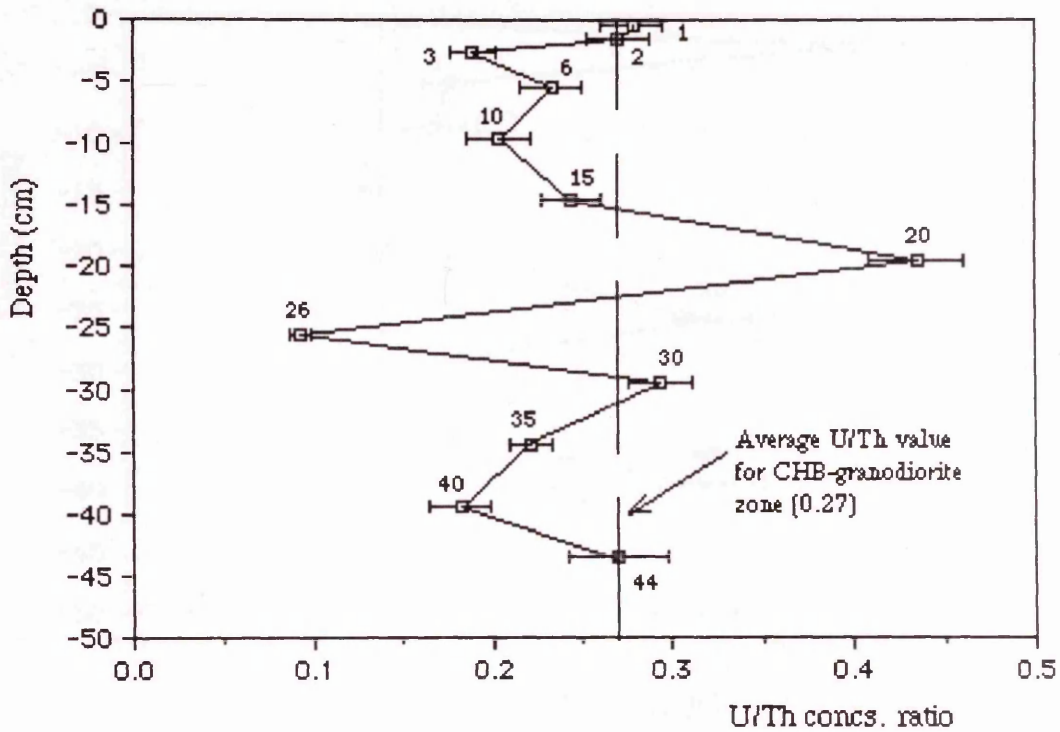


Figure 4.49: $^{234}\text{U}/^{238}\text{U}$ activity ratios as a function of depth (centimetres from rocks surface) for granodiorite samples from Clifton.

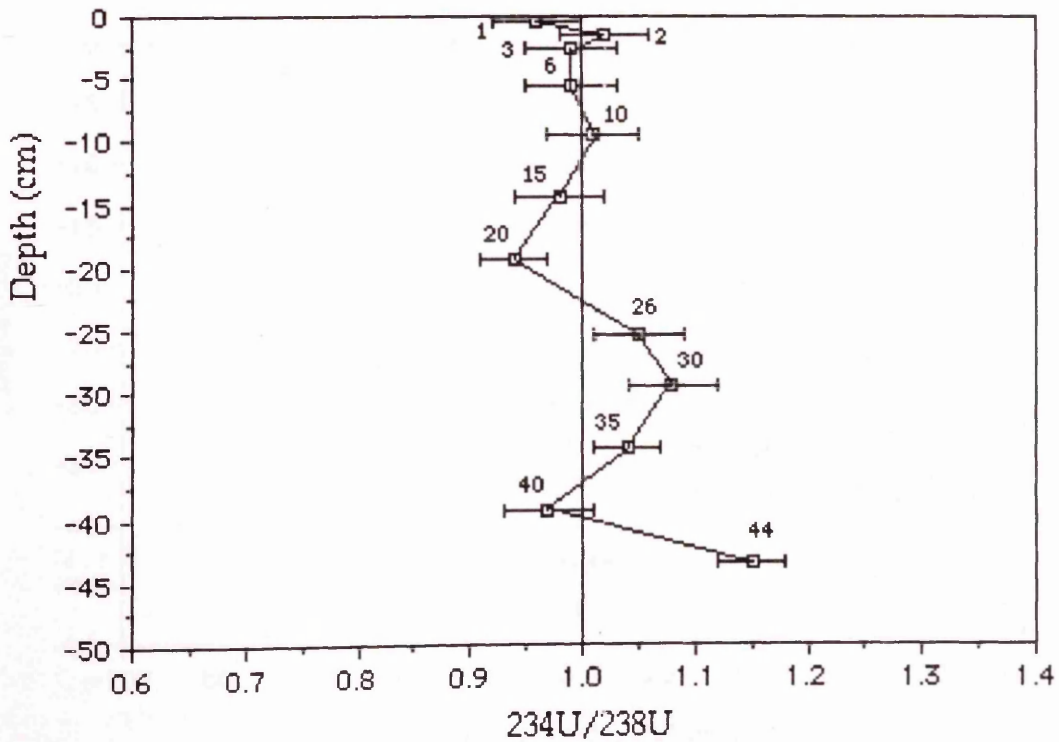


Figure 4.50: $^{230}\text{Th}/^{234}\text{U}$ activity ratios as a function of depth (centimetres from rocks surface) for granodiorite samples from Clifton.

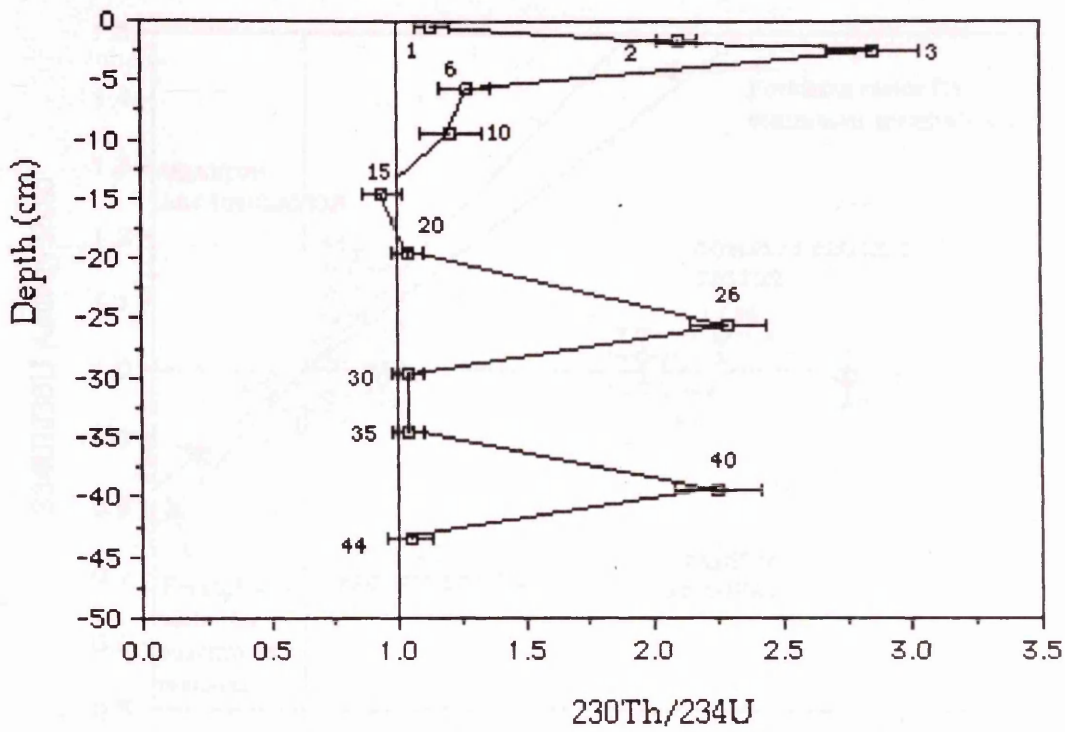


Figure 4.51: Plot of apparent % uranium excess/deficiency based on U/Th concentration ratio and $^{230}\text{Th}/^{234}\text{U}$ activity ratio data versus depth for granodiorite core samples from Clifton.

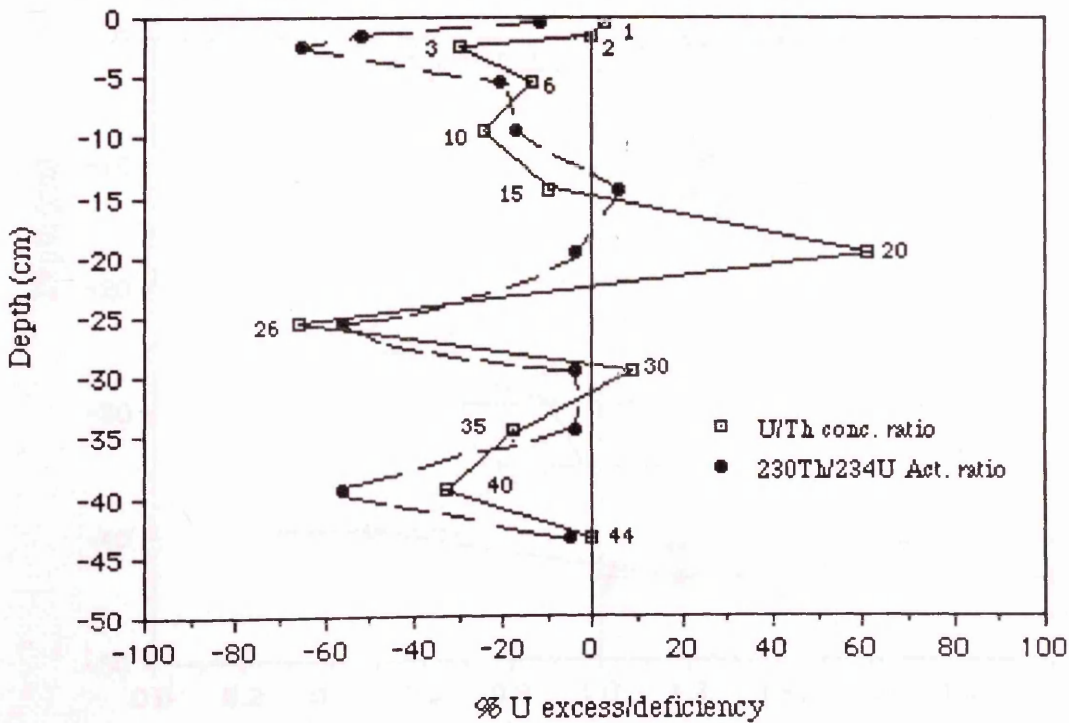


Figure 4.52: $^{234}\text{U}/^{238}\text{U}$ activity ratio versus $^{230}\text{Th}/^{238}\text{U}$ activity ratio diagram for granodiorite samples from Clifton.

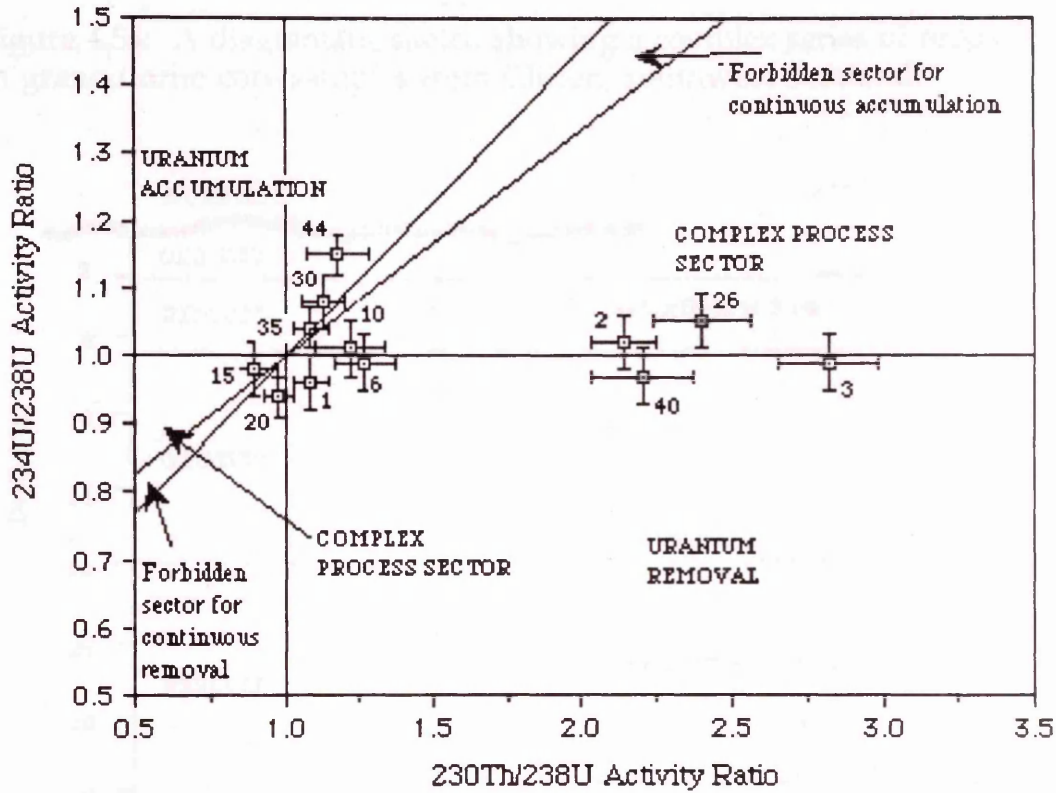


Figure 4.53: $^{226}\text{Ra}/^{230}\text{Th}$ activity ratios as a function of depth (centimetres from rocks surface) for granodiorite samples from Clifton.

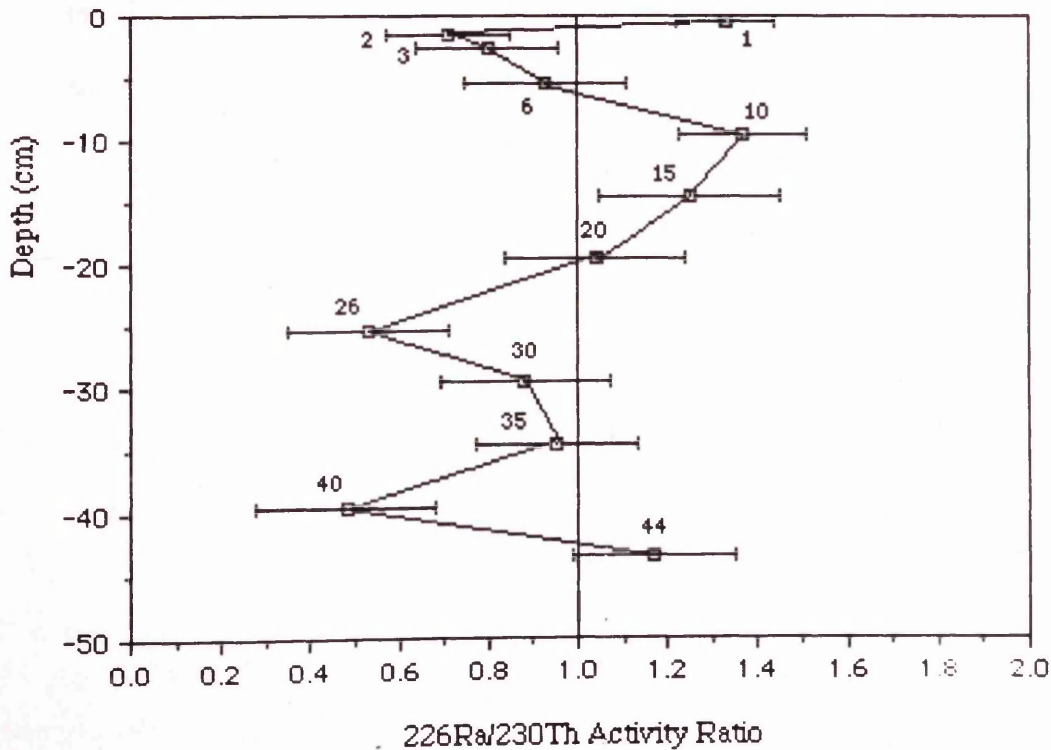


Figure 4.54: A diagrammatic sketch showing a complex series of redox fronts in granodiorite core samples from Clifton, southwest Scotland.

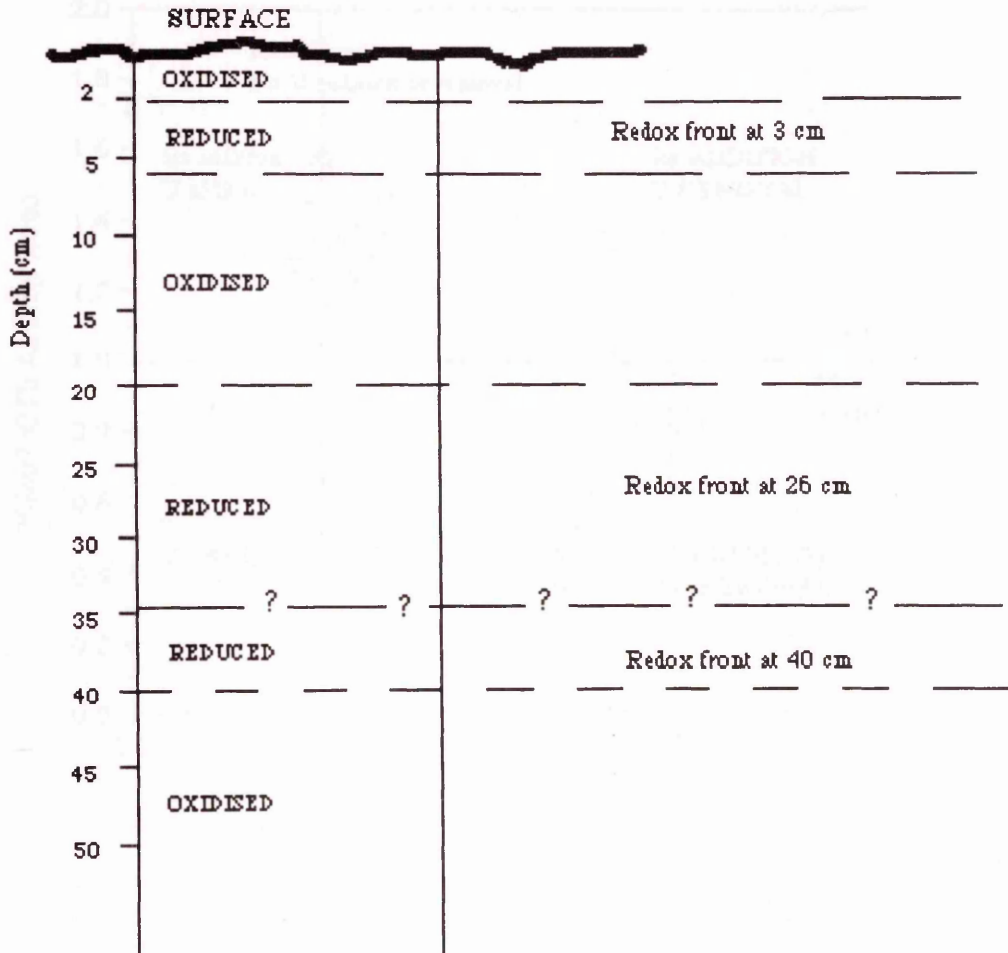
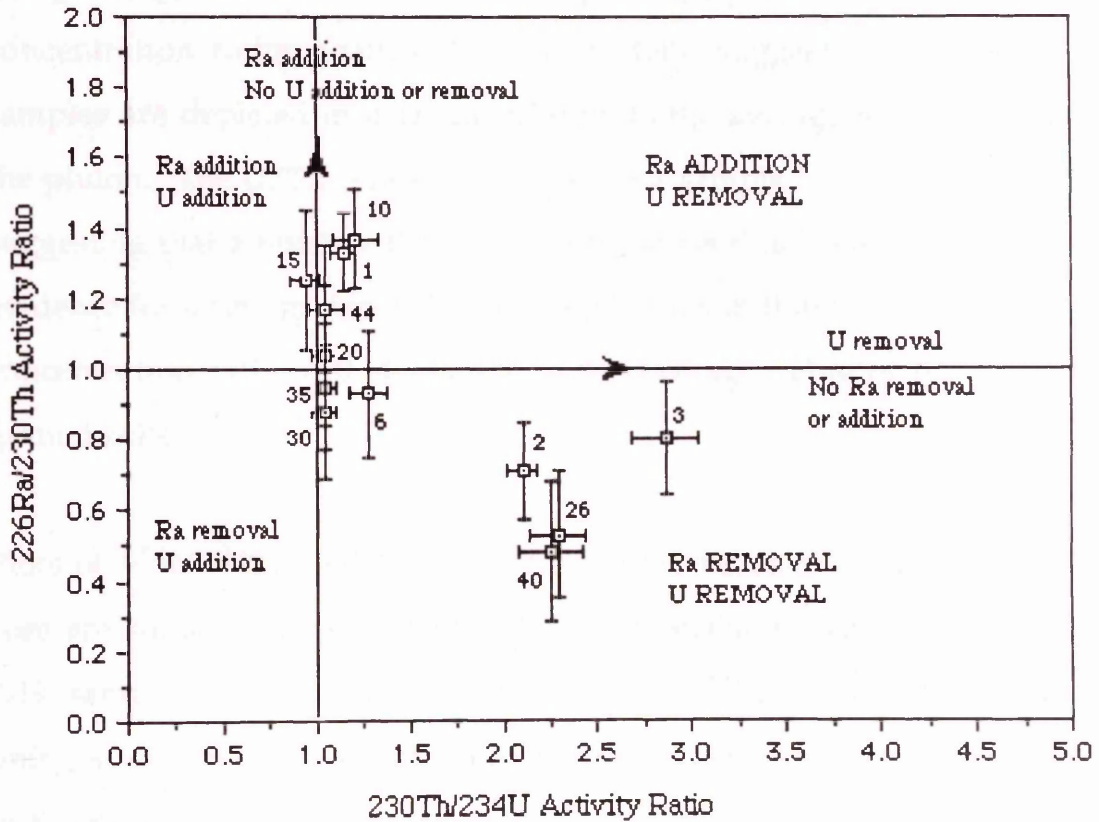


Figure 4.55: Plot of $^{226}\text{Ra}/^{230}\text{Th}$ activity ratio versus $^{230}\text{Th}/^{234}\text{U}$ activity ratio in granodiorite core sample GD relative to secular equilibrium (the axes) from Clifton.



removal of uranium as a result of rock/groundwater interaction along fractures.

The concentration of thorium varies within the range 9.7 to 18.1 ppm, except sample 26 which contains 36.8 ppm (Figure 4.47). The plot of U/Th concentration ratios against depth (Fig. 4.48) suggests that most of the samples are depleted in uranium relative to the average for this section of the pluton. The U/Th concentration ratio for sample 26 is very low (0.093), suggesting that a resistate thorium-bearing mineral is present. There is also evidence for uranium deposition in sample 20 as indicated by its high U/Th concentration ratio of 0.44 relative to the average value of 0.27 for CHB-granodiorite zone.

Plots of $^{234}\text{U}/^{238}\text{U}$ and $^{230}\text{Th}/^{234}\text{U}$ activity ratios over the length of the core are shown in Figures 4.49 and 4.50 respectively. As shown in Figure 4.49, samples 2, 3, 6, 10, 15 and 40 have $^{234}\text{U}/^{238}\text{U}$ ratios, within error, of unity, suggesting either that negligible migration of uranium has occurred in the rocks represented by these samples within the last 10^6 y, or that any process affecting them has been to rapid 'equilibrium'. As in the granite core the data do not exhibit a systematic trend. But there are two samples (1 and 20) which have $^{234}\text{U}/^{238}\text{U}$ activity ratios significantly below unity (Figure 4.49). The low values at 1 and 20 suggest slow, long term loss of ^{234}U , i.e. this signature is retained despite the effects of any recent weathering. Thus there are three explanations for these $^{234}\text{U}/^{238}\text{U}$ ratios; (i) they may have been very low initially (i.e. at 12000 y); (ii) there has been little uranium loss from these samples; and/or (iii) deposition of uranium with $^{234}\text{U}/^{238}\text{U}$ activity ratio less than unity has occurred. As discussed previously, the U/Th concentration ratio for samples 1 and 20 are greater than the average value of the CHB-granodiorite zone, suggesting uranium

deposition at these locations with low $^{234}\text{U}/^{238}\text{U}$ activity ratio. On the other hand, samples 26, 30, 35 and 44 have $^{234}\text{U}/^{238}\text{U}$ activity ratios greater than unity, suggesting accumulation of enriched ^{234}U relative to ^{238}U .

The plot of $^{230}\text{Th}/^{234}\text{U}$ activity ratio against distance from the surface is shown in Figure 4.50. Samples 15, 20, 30, 35 and 44 have $^{230}\text{Th}/^{234}\text{U}$ activity ratios, within error of equilibrium, whereas the remainder have ratios greater than unity, indicating uranium loss as a result of rock-water interaction. The disequilibrium between ^{230}Th and ^{234}U is highly pronounced for some of the samples, notably for 2, 3, 26 and 40 which display $^{230}\text{Th}/^{234}\text{U}$ activity ratios greater than 2.00, indicating of extensive loss of uranium. Intense uranium loss resulting from surface weathering appears to be most pronounced in the 0 - 3 cm range and decreases markedly about 10 cm from the surface. The intense loss of uranium in samples 26 and 40 is probably related to minor fractures. Comparison of the $^{234}\text{U}/^{238}\text{U}$ activity ratio and $^{230}\text{Th}/^{234}\text{U}$ activity ratio data here reveals rapid dissolution and equilibrium loss of uranium because the 1-2 cm, 2-3 cm, 25-26 cm and 39-40 cm sections have $^{234}\text{U}/^{238}\text{U}$ activity ratios near unity and $^{230}\text{Th}/^{234}\text{U}$ activity ratios significantly greater than 2.00.

Assuming thorium has remained immobile in the rock and taking the average U/Th concentration ratio for the CHB-zone to represent 'unweathered' rock, values for apparent percentage excess or deficiency of uranium in the samples (ignoring sample 26 as anomalous) were calculated based upon (a) the U/Th concentration ratio and (b) $^{230}\text{Th}/^{234}\text{U}$ activity ratio. The plot of apparent percentage loss versus distance from the surface shown in Figure 4.51, again suggests that apart from sample 20, almost all of

the samples are depleted in uranium where the U/Th concentration ratio indicates re-deposition. Also the high values of $^{230}\text{Th}/^{234}\text{U}$ activity ratio and thorium content in sample 26 indicate that the sample has been heavily weathered leading to resistate enrichment and Fe-Mn oxyhydroxides along fractures (Plate 4.4).

The uranium and thorium isotopic data for the rock section are summarised in a plot of the $^{234}\text{U}/^{238}\text{U}$ activity ratios against the $^{230}\text{Th}/^{238}\text{U}$ activity ratios in Figure 4.52. Samples 1, 2, 3, 6 and 10 lie in a sequence indicative of recent equilibrium removal/deposition processes; samples 15 and 20 lie close to equilibrium as expected from the operation of long term processes; samples 2, 3, 26 and 40 lie in positions with $^{234}\text{U}/^{238}\text{U}$ activity ratios close to equilibrium and $^{230}\text{Th}/^{238}\text{U}$ activity ratios greater than 2.00, indicating recent equilibrium loss of uranium; and samples 30 and 44 lie in the accumulation sector of the diagram, indicating long term uranium deposition in the order of 10^6 y. As a whole, the isotopic ratios of uranium and thorium for the samples lie in all sectors of the diagram, suggesting that both migration and accumulation processes of uranium have occurred in rocks represented by these samples over the last 10^6 y with recent, rapid perturbation.

The $^{226}\text{Ra}/^{230}\text{Th}$ results for the granodiorite core are plotted in Figure 4.53. Most samples show pronounced deviations from equilibrium. ^{226}Ra depletion is observed in samples 2, 3, 26 and 40, a trend similar to that observed for uranium loss. The comparable loss of Ra and U in samples at 26 and 40 cm from the rock surface indicated by the $^{230}\text{Th}/^{234}\text{U}$ and $^{226}\text{Ra}/^{230}\text{Th}$ data may be explained by dissolution as groundwater flows in fractures. In addition, these samples (2, 3, 26 and 40) have $^{226}\text{Ra}/^{230}\text{Th}$ activity ratios in the range 0.48 to 0.71, implying that at least 30% ^{226}Ra

atoms produced by decay of ^{230}Th are being lost to the aqueous phase. This finding is consistent with the known high permeability of the rock as indicated by a large number of fractures that exist in the sample. The loss of ^{226}Ra at 2-3 cm, 25-26 cm and 39-40 cm is anomalous as this situation is normally observed only on the reduced side of redox fronts. On the other hand a pattern of ^{226}Ra excess is also observed, notably in samples GD1, 10, 15 and 44, suggesting that the dissolved ^{226}Ra is being deposited in the oxidised side of the rock by a co-precipitation process, probably by iron and/or manganese oxides. This observation indicates some deposition and removal of ^{226}Ra along the rock section represented by the core, perhaps because of a complex series of oxidised/reduced zones running through this highly fractured rock (Figure 4.54).

The $^{226}\text{Ra}/^{230}\text{Th}$ activity ratio versus $^{230}\text{Th}/^{234}\text{U}$ activity ratio diagram for the core, shown in Figure 4.55, reveals that samples 1 and 10 lie in the radium addition/uranium removal sector; samples 15, 20 and 44 lie in positions corresponding to radium addition/without uranium addition; samples 30 and 35 correspond to radium removal/without uranium addition, and; samples 2, 3, 6, 26 and 40 lie in the radium/uranium removal sector. As a whole the plot indicates that the samples lie in both radium addition/removal sectors of the diagram, suggesting that both migration and accumulation processes of radium have occurred in these samples over the last 8000 y. Although it has been previously concluded in section 4.1, that the bulk rock of the pluton does not present a retardation barrier, there is evidence here that the very near surface rocks as well as the series of complex redox fronts running through this highly fractured rock could act together as limited sites of deposition.

4.3.2.2 Rare earth element studies of granodiorite core GD

The results for rare earth elements analyses and chondrite normalised values from the granodiorite core GD from Clifton are given in Table 3.10. The plots of REE concentrations against depth (Figures 4.56a to m) exhibit generally similar trends where maxima are observed in samples 1, 2, 3, 6, 26 and 40 and minima are observed in samples 2, 15 and 35. The REE are distributed irregularly in the core, perhaps either because of the original mineralogy of the rocks which is variable with respect to REE content, or because of the results of weathering where REE experience removal as well as deposition throughout the core. The latter possibility again indicates the existence of a series of oxidised/reduced zones in the rock where the maxima represent oxidised zone and the minima represent reduced zone i.e. redox front positions (Figure 4.54), consistent with the conclusion derived above from the natural decay series data. The REE have therefore been removed from the reduced rock close to the front and are re-deposited in the oxidised rock via scavenging by secondary minerals such as iron-manganese oxyhydroxides and clay minerals.

Comparison of the uranium and thorium data with those of the REE data indicates: (i) uranium maxima at REE minima; (ii) thorium maxima coinciding with the REE; (iii) the REE maxima correspond to U/Th minima, and (iv) pronounced enhancement of REE in samples 26 and 40, correlating with $^{230}\text{Th}/^{234}\text{U}$ activity ratios greater than 2.00 relating to the fractures seen in the core (Plate 2.7).

Europium shows little or no evidence of redox induced effects in the concentration profile shown in Figure 4.56f and does not exhibit any major

Figure 4.56: Plots of REE concentrations versus depth from the weathered rock surface in granodiorite core GD from Clifton, southwest Scotland.

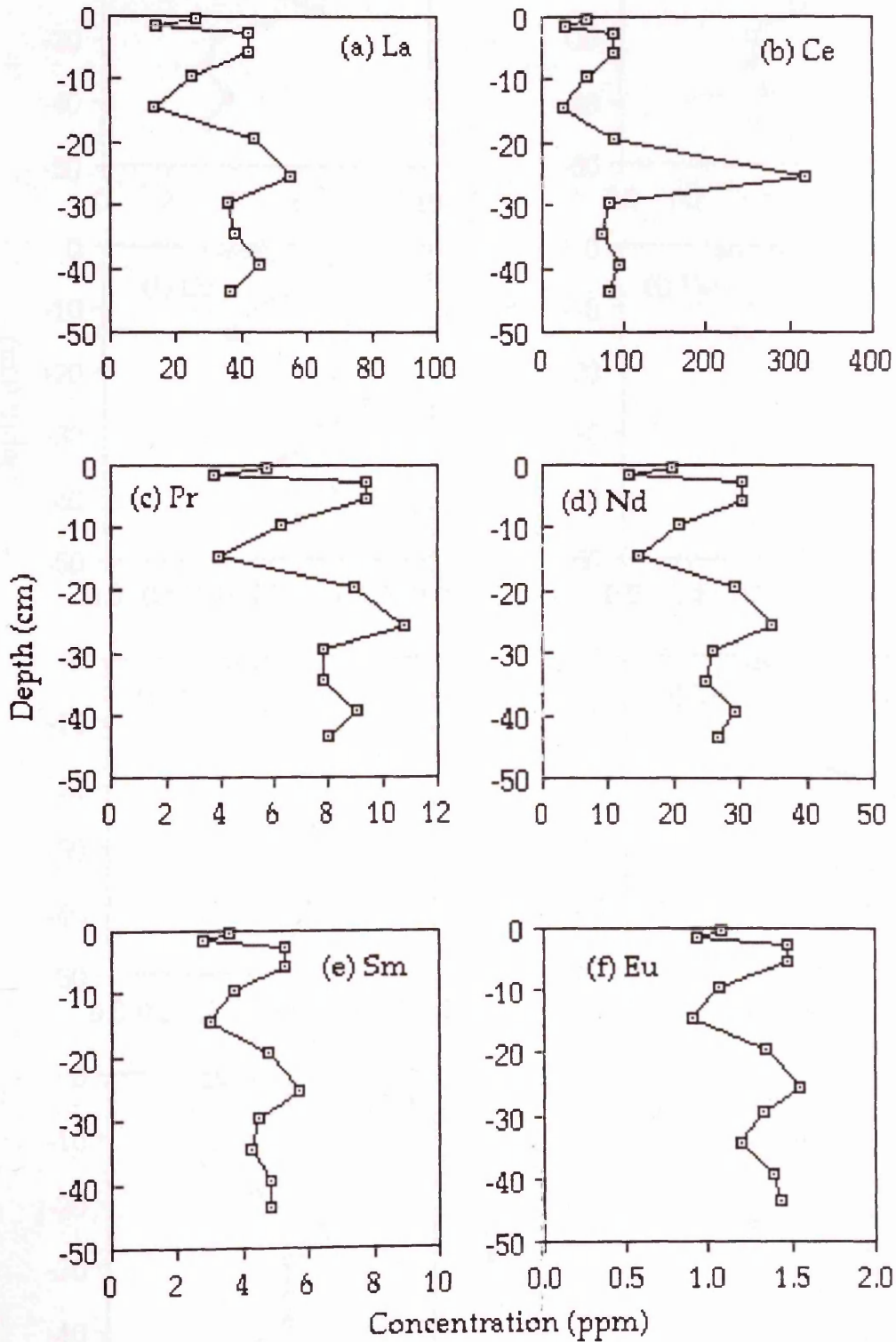
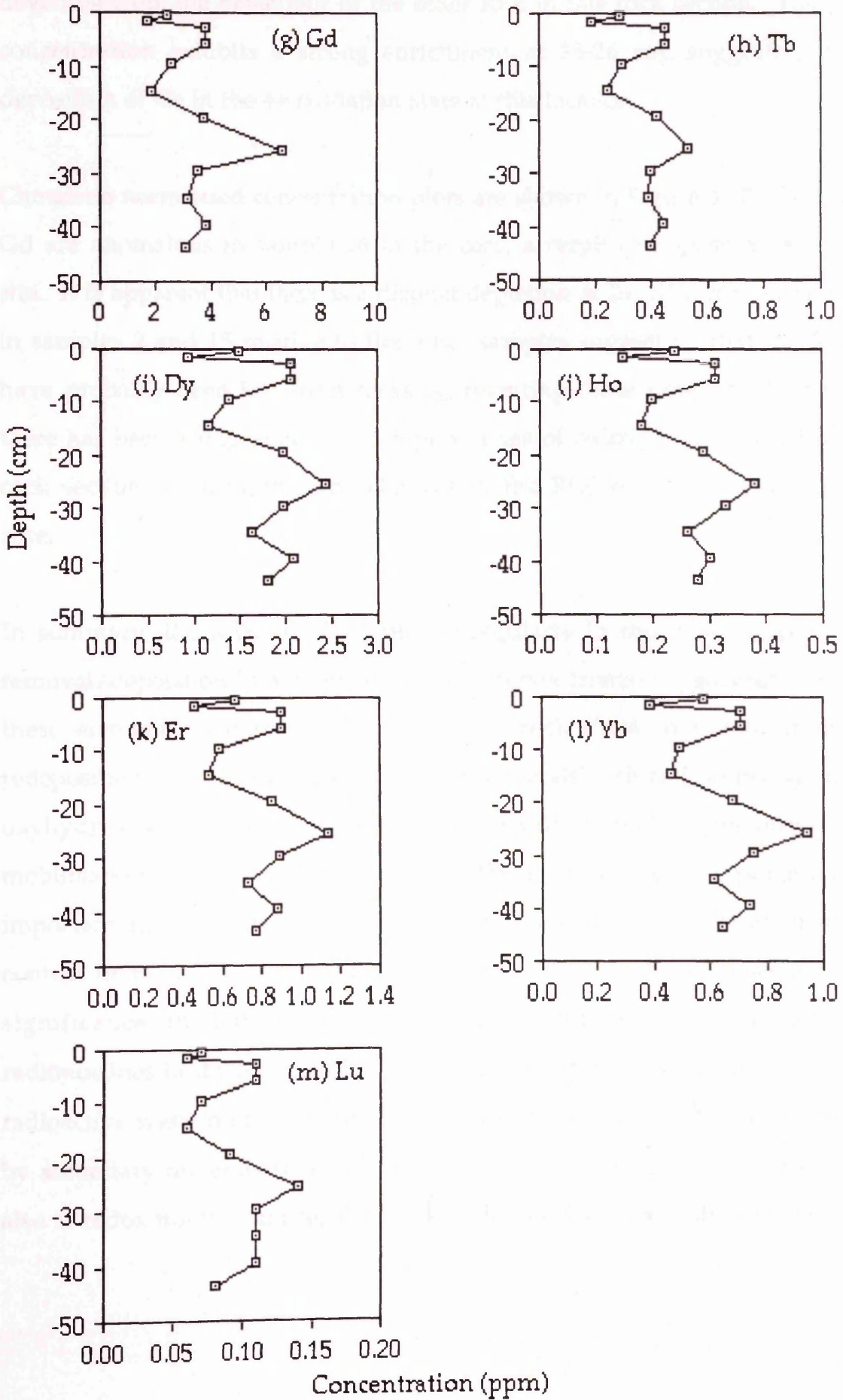


Figure 4.56 (Cont.)

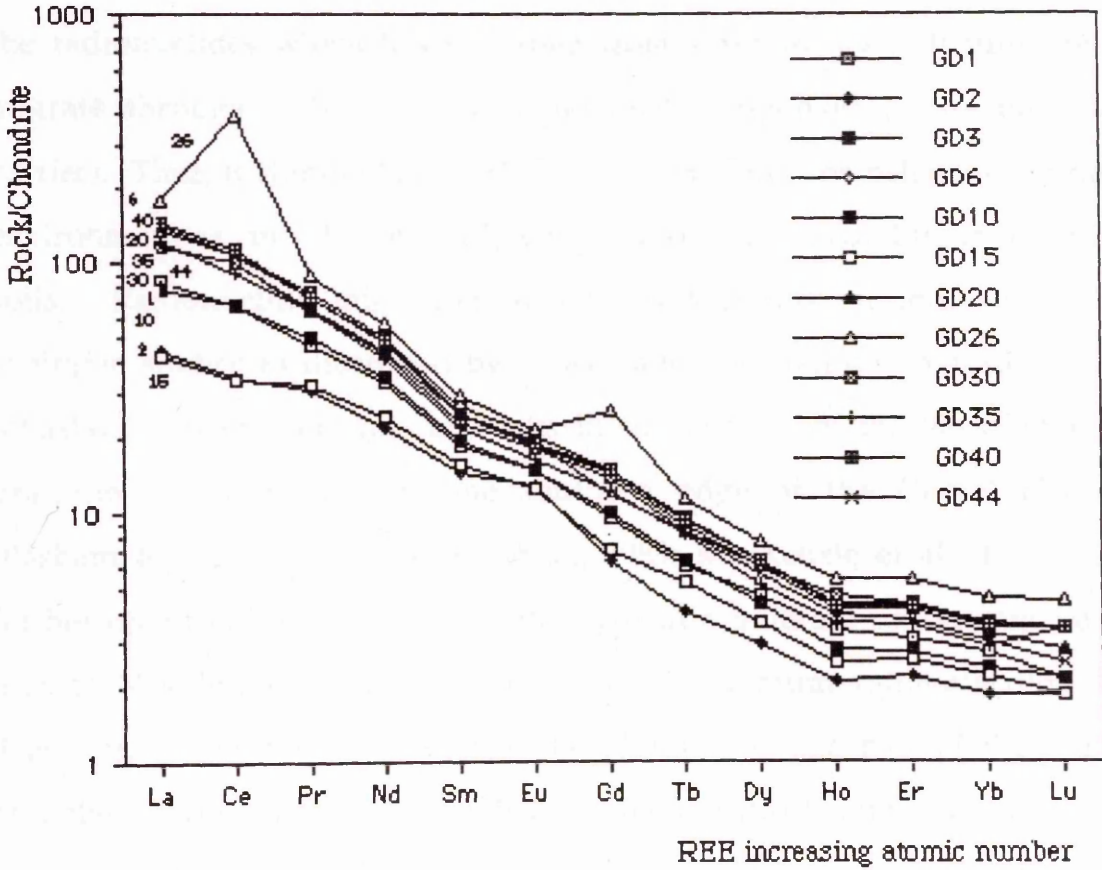


deviation from the behaviour of the other REE in this rock section. The Ce concentration exhibits a strong enrichment at 25-26 cm, suggesting re-deposition of Ce in the 4+ oxidation state at this location.

Chondrite normalised concentration plots are shown in Figure 4.57. Ce and Gd are anomalous in sample 26 in the core, a result of deposition at this site. It is apparent that there is a distinct depletion of the REE concentration in samples 2 and 15 relative to the other samples suggesting that the REE have probably been lost from rocks representing these samples. Perhaps there has been a migration of a complex series of redox fronts through the rock section resulting in some changes in the REE concentrations in the core.

In summary, the REE are distributed irregularly in the core, suggesting removal/deposition in a complex series of redox fronts. A general loss of these elements is observed from reduced rock close to the front, but redeposition has taken place in secondary minerals such as iron-manganese oxyhydroxides and clay minerals in the oxidised rock. The observed mobilisation and deposition of REE in the rock represent a potentially important radionuclide mobilisation/retardation processes. Thus, in the context of radioactive waste disposal, operation of such processes are of significance in both far-field and near-field transport in which radionuclides in the 3+ oxidation state, such as curium and americium, in a radioactive waste repository, could be removed and mobilised while uptake by secondary minerals such as iron oxyhydroxides and clay minerals and also at redox fronts could result in retardation of dissolved radionuclides.

Figure 4.57: Chondrite-normalised REE patterns for sliced samples in granodiorite core GD from Clifton, southwest Scotland.



4.4 Transport and distribution of radionuclides in soil in the vicinity of mineralised uranium veins at Beeswing.

In multi-barrier systems for radioactive waste disposal, it is assumed that the radionuclides which have escaped from a repository will ultimately migrate through soils (i.e. soil is the final component of the far-field barrier). Thus, it is important to characterise radionuclide behaviour in this environment as considerable variations in geochemical conditions occur in soils. Radionuclide migration in soils is therefore of importance in analogue studies as illustrated by investigation of uranium migration and retardation in organic soils and silts in the vicinity of the Needle's Eye uranium mineralisation on the southern edge of the Criffel pluton (Basham et al., 1989; MacKenzie et al., 1989; MacKenzie et al., 1991). A further opportunity for a study of this type in a different soil system from that at Needle's Eye was presented by the uranium mineralisation at Beeswing on the northern edge of the pluton and this part of the work describes an investigation of the distribution and geochemical behaviour of natural decay series radionuclides in the environment in the vicinity of these uranium veins. The gamma spectroscopy techniques employed for ^{210}Pb determination also provided information on the distribution of man-made radiocaesium isotopes and, for completeness, these results are also briefly considered here.

The veins occur in hornfelsed Silurian greywackes on the northern edge of the Criffel pluton (Figure 2.1 and Plate 2.9); the radioactive mineral is mainly uraninite (Gallagher et al., 1971). In the present study the location of the veins was determined using a portable 2" x 2" NaI gamma detector. The results of the measurements are given in Table 3.11, and are shown

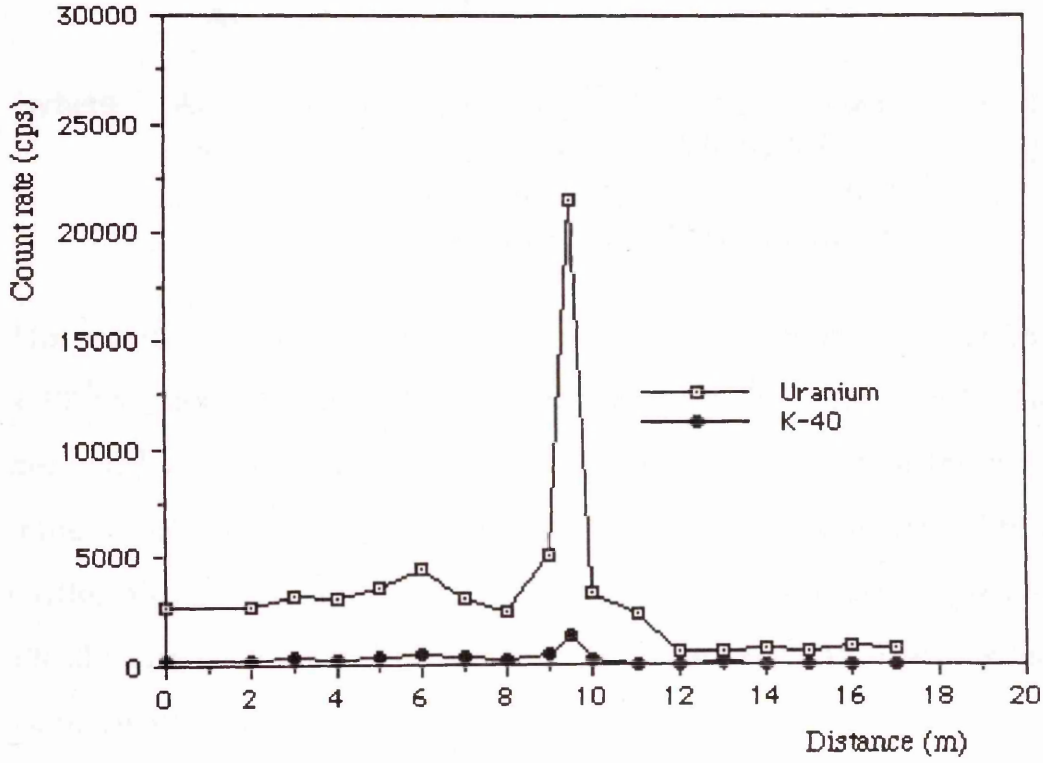
graphically in Figure 4.58. This work has established that the veins represent a possible source of uranium for groundwater flowing through the soil in the area and an attempt was made to characterise the dispersion of uranium into the surrounding soils from the line source of the uraniferous veins (Figure 2.7).

The results for natural decay series radionuclide analysis of bulk material from the exposed section of the vein are given in Table 3.12. The concentrations of uranium and thorium of the vein materials are about 67 and 11 ppm respectively. The sample displays a $^{234}\text{U}/^{238}\text{U}$ activity ratio of 0.94, suggesting that the vein has experienced preferential loss of ^{234}U relative to ^{238}U . This observation suggests that at some time within the last 10^6 y, the vein has been subject to slow dissolution of uranium to allow the development of this weak depletion in ^{234}U relative to ^{238}U .

The $^{230}\text{Th}/^{234}\text{U}$ activity ratio exhibits pronounced disequilibrium, with a value of 1.62, indicating rapid uranium loss as a result of recent rock-water interaction, consistent with the observation that the sample consisted of weathered materials. Taken together the $^{234}\text{U}/^{238}\text{U}$ and $^{230}\text{Th}/^{234}\text{U}$ data suggest two different phases of uranium dissolution i.e. the $^{230}\text{Th}/^{234}\text{U}$ ratio suggests recent, rapid loss of uranium whereas the $^{234}\text{U}/^{238}\text{U}$ activity ratio suggests an older, slow dissolution of uranium. The analysis of the vein material thus confirms that the vein at Beeswing acted as a recent source of uranium to groundwaters in the area.

If it is assumed that an initial state of secular equilibrium applied to the vein material and that it has been disturbed by the onset of the leaching process, a value for the probability of uranium removal by dissolution can

Figure 4.58: Uranium and K-40 count rates over abandoned quarry at Beeswing, southwest Scotland.



be derived following the procedure of Scott et al. (1991) by assuming a value of 12000 y (i.e. corresponding to the end of the last period of glaciation) for the time during which leaching of uranium has occurred. If it is assumed that leaching follows first order kinetics then,

$$A_t = A_0 e^{-kt}$$

where	A_t	= activity ratio of $^{230}\text{Th}/^{234}\text{U}$ at time t	= 1.62
	A_0	= initial activity ratio of $^{230}\text{Th}/^{234}\text{U}$	= 1.00
	k	= removal probability for uranium (y^{-1})	
	t	= time (assumed to be 12000 y in this case)	

This calculation gives a removal probability for uranium dissolution of $4.0 \times 10^{-5} \text{ y}^{-1}$ for the vein materials, comparable to the value of $5.2 \times 10^{-5} \text{ y}^{-1}$ derived by Scott et al. (1991) for uranium dissolution from the bulk vein material of the Needle's Eye mineralisation in the southern edge of the Criffel pluton. The appropriate leaching time may in fact be greater than 12000 years (as indicated by the $^{234}\text{U}/^{238}\text{U}$ activity ratio) so this leaching value should be regarded as an upper limit.

The $^{226}\text{Ra}/^{230}\text{Th}$ activity ratio of the vein material exhibits pronounced disequilibrium, with a value of 1.50, suggesting re-deposition of the ^{226}Ra removed from deeper in the rock. This observation is consistent with the behaviour of ^{226}Ra at redox fronts as described in section 4.2, where removal of ^{226}Ra is observed from reduced rock and re-deposition on the oxidised (weathered) side of the front. The $^{210}\text{Pb}/^{226}\text{Ra}$ activity ratio of the vein material also exhibits pronounced disequilibrium, with a value of 1.38, suggesting either ^{226}Ra loss (or less likely ^{210}Pb deposition). Taken together, the $^{226}\text{Ra}/^{230}\text{Th}$ and $^{210}\text{Pb}/^{226}\text{Ra}$ activity ratios suggest a dynamic regime for radium involving both deposition and removal.

The results of uranium, thorium, organic matter content, ^{210}Pb , ^{226}Ra , ^{134}Cs and ^{137}Cs analyses for the soil cores A, B and C, along with the leaching results for natural decay series radionuclides of 9 soil samples (3 samples from top, middle and bottom positions of each core), are shown in Tables 3.13, 3.14 and 3.15 respectively.

The distribution of uranium and thorium concentrations in the soil cores A, B and C at various levels is shown in {Figure 4.59(i), (ii) and (iii)}. In core A the uranium content is fairly constant (about 3.00 ppm) from the top to about 17 cm depth and then increases systematically with depth to a maximum of 5.8 ppm at 22 - 24 cm. The thorium content of the samples is irregular in the range 4.8 and 8.1 ppm, with a progressive increase from 5 ppm at the top to about 8 ppm at 11 cm and then dropping to about 5 ppm at 17 cm. Below this, the thorium concentration increases again to 8 ppm with a trend paralleling that of uranium {Figure 4.59(i)}. The increase in uranium content at depth could be attributed to leaching of uranium from veins in the outcrop and possibly in the bedrock by groundwater, with subsequent downslope flow and associated uptake of uranium by the soil at depth. Alternatively, the trends in this profile could be interpreted as showing the physical re-distribution of uranium rich mineral or rock particles in the soil since the thorium concentration at depth increases in parallel with the increase in uranium. Assuming that thorium has remained effectively insoluble, the U/Th concentration ratio can be used to identify any differential geochemical movement of uranium and thorium. It was observed that uranium enrichment relative to thorium was significant in the top 6 cm of the core and at depth from about 17 cm downwards {Figure 4.60(i)}. The high uranium content in the shallow samples is consistent with the distribution of organic material in the soil

Figure 4.59: Plots of uranium and thorium concentrations versus depth for soil cores (i) A, (ii) B and (iii) C from Beeswing. Leaching results for samples from top, middle and bottom sections are indicated.

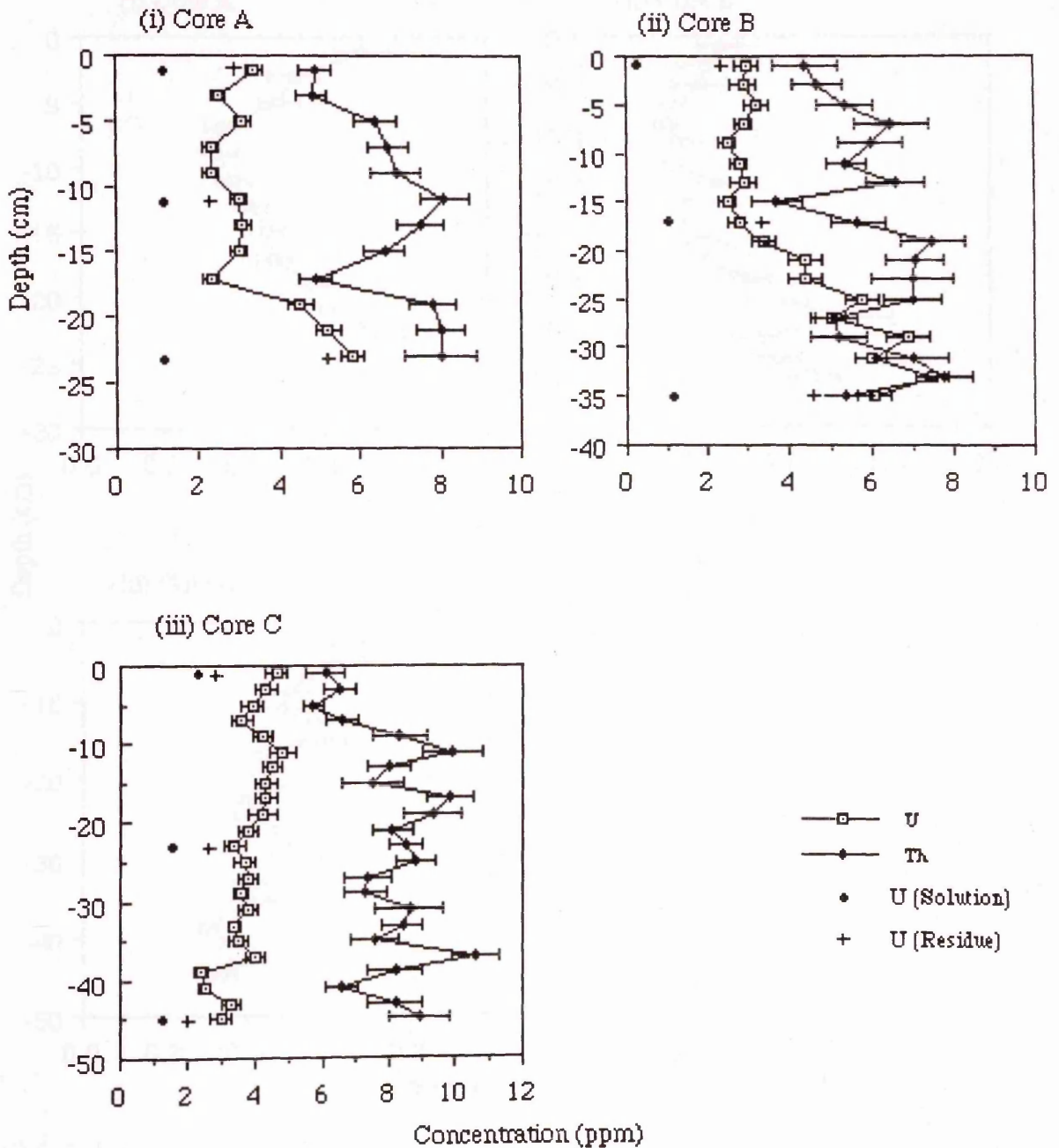
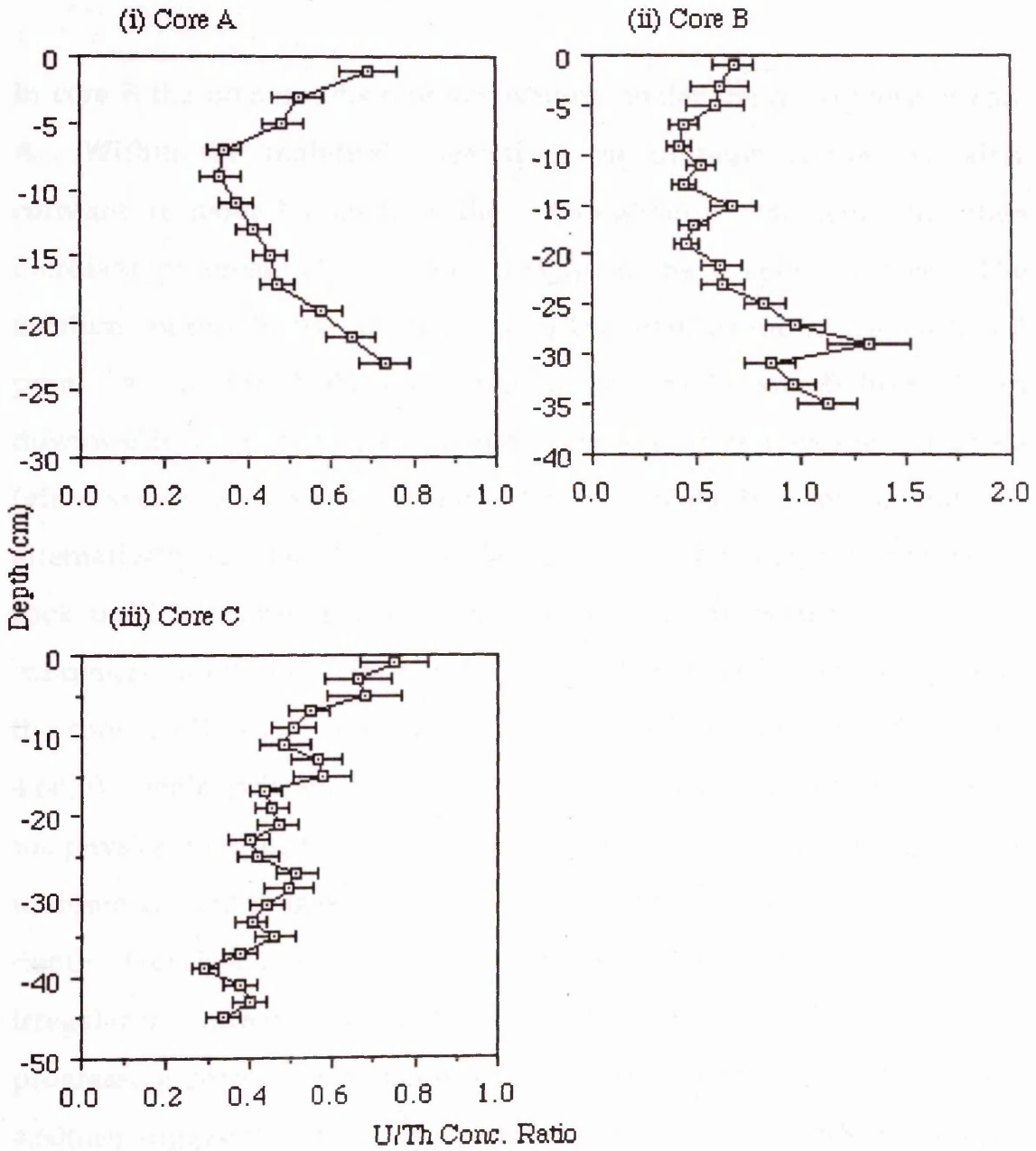


Figure 4.60: Plots of U/Th concentration ratios versus depth for soil cores (i) A, (ii) B and (iii) C from Beeswing.



profile, suggesting uranium association with soil organic materials, whereas the deep samples indicate that the increased uranium at depth does represent re-deposition of uranium from groundwater, probably associated with Fe-Mn sesquioxides.

In core B the uranium distribution exhibits similar trends to those of core A. Within the analytical uncertainty the uranium content is fairly constant at about 3 ppm from the top to about 17 cm depth and then increases progressively to about 7 ppm in the deeper samples. The thorium content in the samples is also irregular, in the range 4.4 to 7.8 ppm. As in core A the high uranium content in core B from 17 cm downwards suggests that uranium may have been re-deposited at depth (via scavenging by Fe-Mn sesquioxides and uptake by clay minerals) or alternatively may be due to the distribution of uranium rich mineral or rock particles since thorium concentration also increases. The U/Th concentration ratio was observed to be slightly enriched in the top 6 cm of the core ($U/Th > 0.5$) and at depth from about 20 cm downwards (Figure 4.60(ii)), again indicating chemical re-deposition of uranium rather than the physical re-distribution of uranium rich detrital minerals. In core C the uranium content ranges from 2.4 to 4.8 ppm and generally decreases with depth (Figure 4.59(iii)). The thorium distribution in the samples is irregular in the range 6.1 to 10.6 ppm. Assuming thorium is immobile, the progressive decrease with depth of the U/Th concentration ratio (Figure 4.60(iii)) suggests retention of uranium in the upper sections of the core. The absence of uranium enrichment at depth suggests that uranium has been largely removed from groundwater before travelling this distance i.e. evidence that uranium dissolved from the vein is relatively quickly taken up by soil materials.

The results therefore indicate uranium deposition at the surface and at depth in core A, at depth in core B and possibly in the surface of core C. This deposition pattern could be produced by a system involving two types of water flow: (a) occasional surface flow during high rainfall, and (b) more regular groundwater flow at depth. An important observation is that the pronounced increase in U/Th ratio in the surface of core A is not seen in core B (about 19 m further from the veins). Thus, the surface flow of uranium and uptake by organic matter is observed only close to the vein i.e. the results suggest highly efficient retardation of uranium by organic matter, resulting in movement over only a few metres, consistent with the conclusion from the Needle's Eye studies (MacKenzie et al., 1989; MacKenzie et al., 1991). Thus, these observations of uranium retention in two different horizons indicate that the soil has a potentially important role as the final component in the geosphere barrier in retarding migration of radionuclides released from a repository.

The leaching experiment revealed that a substantial amount of the uranium was readily leached from the samples (Tables 3.13, 3.14 and 3.15 and {Figure 4.59(i), (ii) and (iii)}) and this was more pronounced for cores A and B than for core C. The results therefore indicate that the majority of the uranium in cores A and B is relatively labile, consistent with it having been recently deposited from groundwater. The lack of lability in core C suggests highly efficient retardation of uranium probably by soil organic matter.

The plots of $^{234}\text{U}/^{238}\text{U}$ activity ratios against depth generally exhibit values about unity for the residual samples and slightly greater than unity for leached samples (Tables 3.13, 3.14 and 3.15). No ^{230}Th was detected in

any of the samples, confirming recent re-distribution of uranium in the soil.

Figure 4.61 shows a schematic cross-section of the study site along A - C (cf. Figure 2.7). The uranium content generally tends to be enriched at depth and near the surface. Uranium-rich soils are apparently located along the bedrock surface, indicating that uranium has been deposited here as a result of leaching of vein materials by groundwater. The U-enriched groundwater flows downwards along the bedrock, thus resulting in slight enrichment of uranium in soil profiles at depth.

The distributions of ^{226}Ra in the soil cores are shown in {Figures 4.62(i), (ii) and (iii)}. In core A the ^{226}Ra specific activity ranges from 69 to 195 Bq kg^{-1} , with an enrichment observed from 17 cm downwards. The high ^{226}Ra content at depth can probably be attributed to leaching of radium from the outcrop and veins in the bedrock surface and retardation by uptake in the soil at depth close to the veins. The ^{226}Ra distributions in cores B and C are irregular ranging from 82.1 to 119.9 Bq kg^{-1} for core B and from 66.9 to 158.8 Bq kg^{-1} for core C. The $^{226}\text{Ra}/^{234}\text{U}$ and $^{226}\text{Ra}/^{238}\text{U}$ activity ratios of the soil cores exhibit pronounced disequilibrium with values range from 1.70 to 3.55. These observations indicate that ^{226}Ra is dissolved from the veins and is subject to relatively efficient retardation by uptake in the soil. No ^{230}Th was detected in these samples, thus indicating recent re-distribution of uranium and radium in the soil. In addition this observation reveals another radium deposition environment, which is its association with soil-materials (the other radium deposition environment is in the rocks on the oxidised side of the front as discussed above and also in section 4.2).

Figure 4.61: Sketch showing distribution of uranium in soil along A-C cross-section, Beeswing.

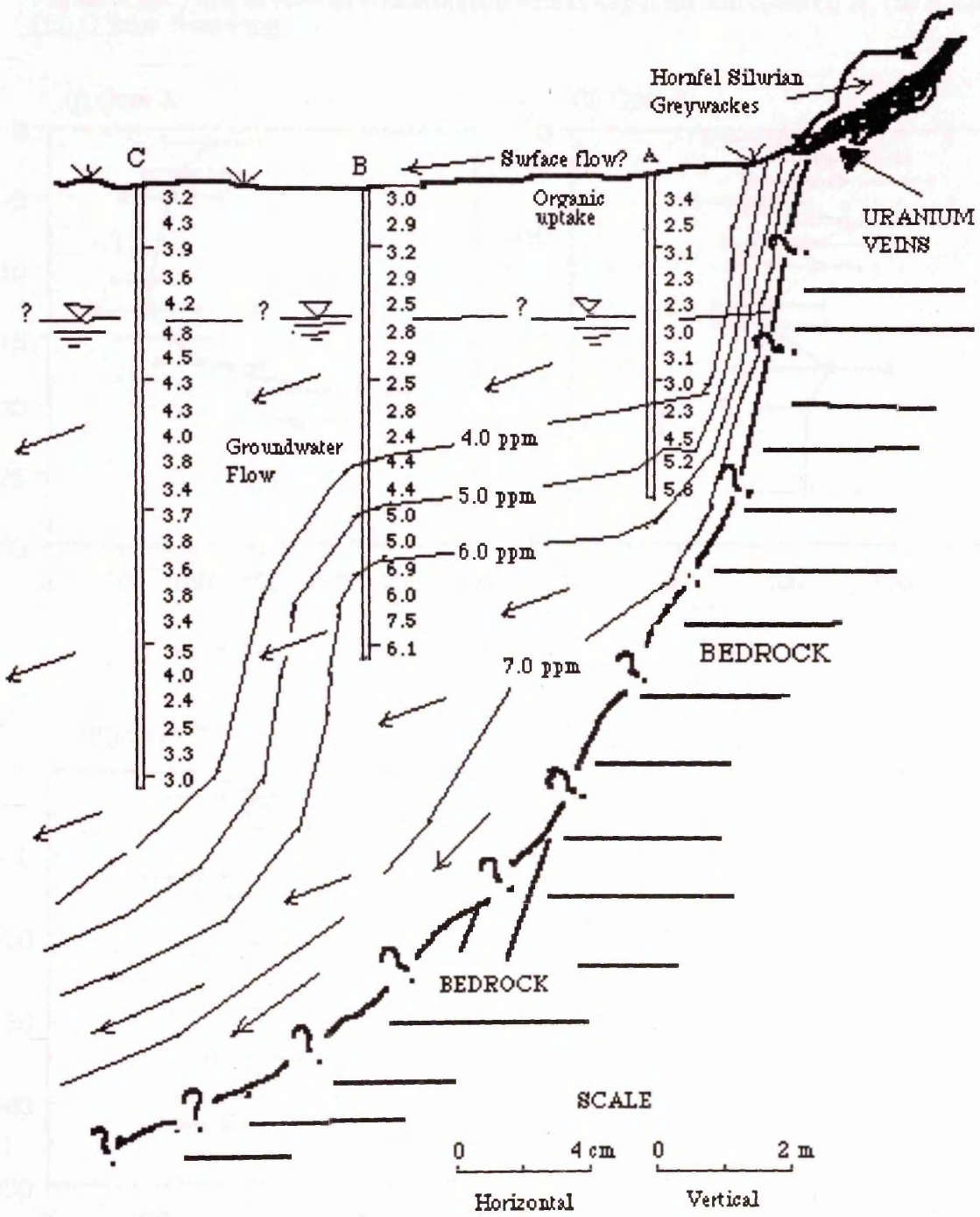
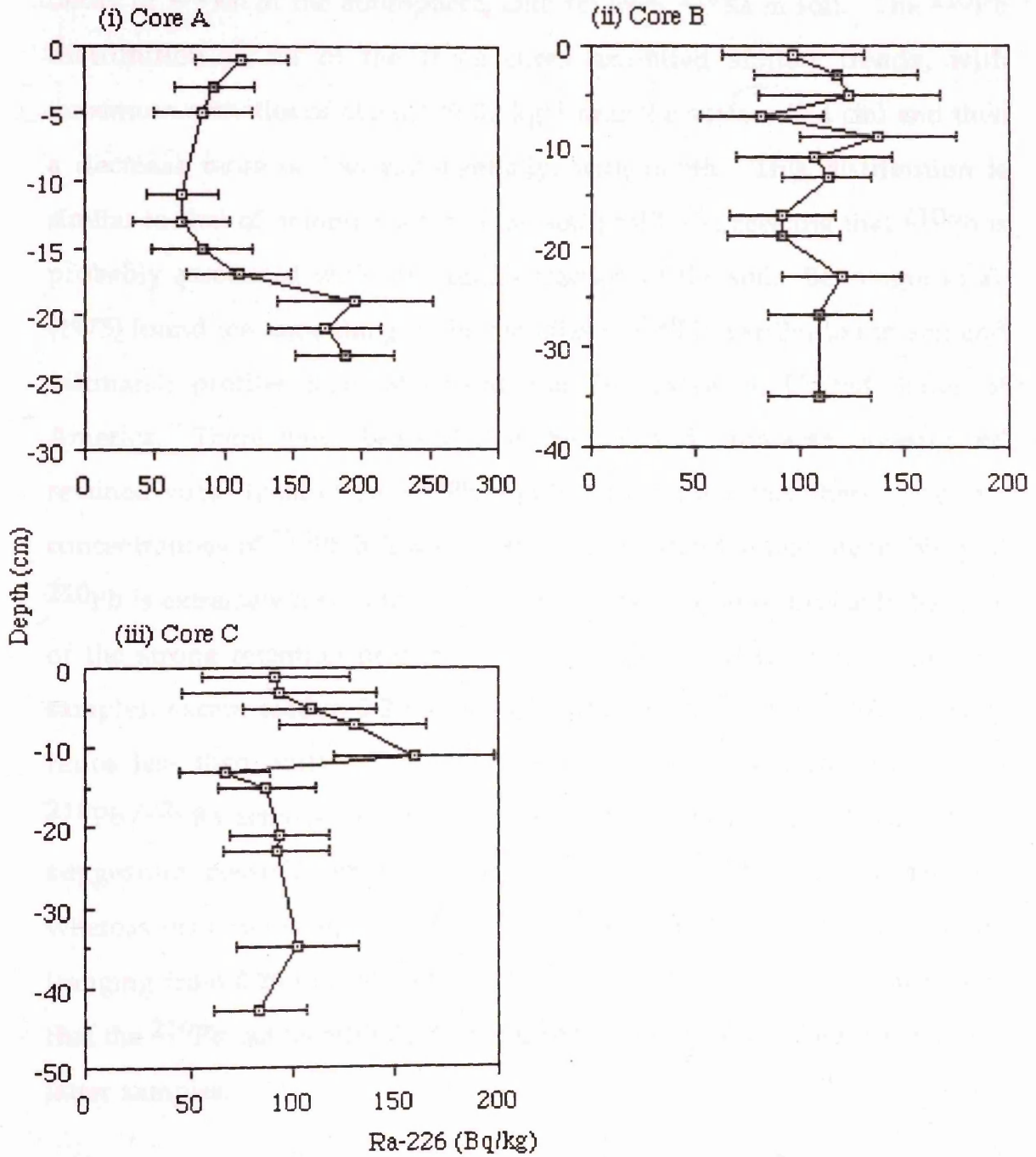


Figure 4.62: Plots of Ra-226 concentration versus depth for soil cores (i) A, (ii) B and (iii) C from Beeswing.



The results of analysis of ^{210}Pb for the three soil cores are given in Tables 3.13, 3.14 and 3.15, and are shown graphically in {Figures 4.63(i), (ii) and (iii)}. ^{210}Pb has three possible sources here: (a) from the vein; (b) from the decay of ^{222}Rn in the atmosphere, and; (c) from ^{226}Ra in soil. The ^{210}Pb distribution in all of the three cores exhibited similar trends, with maximum activities of about 100 Bq kg^{-1} near the surface (0-4 cm) and then a decrease more or less exponentially, with depth. This distribution is similar to that of organic matter in the soil profiles suggesting that ^{210}Pb is probably associated with the organic fraction of the soil. Benninger et al. (1975) found the same thing in their studies of ^{210}Pb distribution in soil and saltmarsh profiles from Maryland and Pennsylvania, United States of America. There they observed that the soil and saltmarsh investigated retained virtually all of the ^{210}Pb supplied from the atmosphere. The low concentrations of ^{210}Pb below 4 cm at Beeswing indicate that the mobility of ^{210}Pb is extremely low in the dissolved phase of the soils, probably because of the strong retention properties of soil organic matter. All of the core samples, except section 0-2 cm of each core, exhibit $^{210}\text{Pb}/^{226}\text{Ra}$ activity ratios less than unity. The surface soil sample of each core displays a $^{210}\text{Pb}/^{226}\text{Ra}$ activity ratio greater than unity (Tables 3.13, 3.14 and 3.15), suggesting possible deposition of excess ^{210}Pb in the surface samples whereas the other samples have $^{210}\text{Pb}/^{226}\text{Ra}$ activity ratios less than unity (ranging from 0.26 to 0.92; but mostly < 0.6). The clear implication here is that the ^{210}Pb can be attributed to in-growth from in-situ ^{226}Ra decay in the latter samples.

The results of analysis of the manmade radiocaesium isotopes for the three cores are presented in Tables 3.13, 3.14 and 3.15 and are shown graphically in {Figures 4.64(i), (ii) and (iii)}. The concentration of ^{137}Cs decreases rapidly

Figure 4.63: Pb-210 concentration profiles for soil cores (i) A, (ii) B and C from Beeswing.

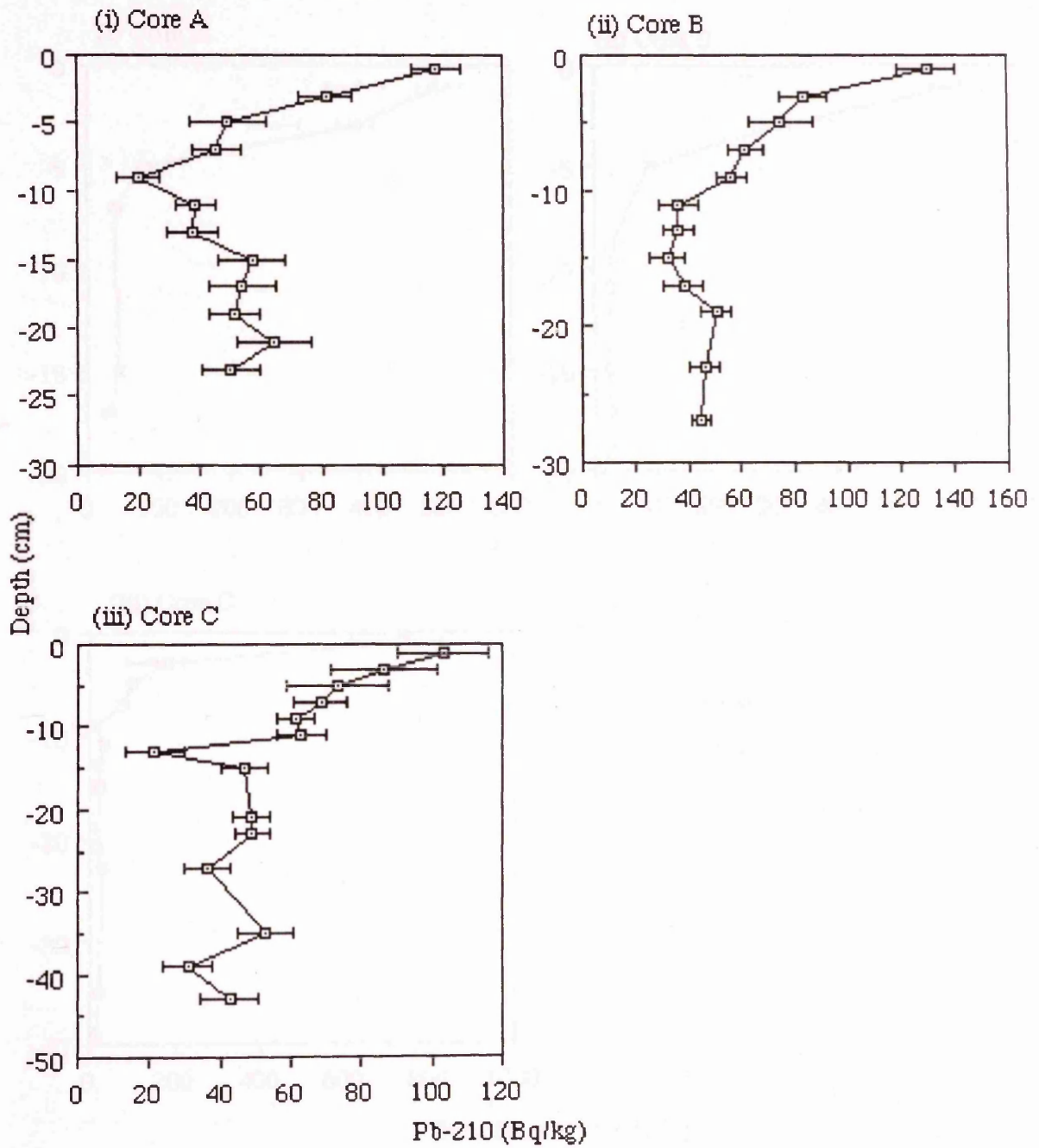
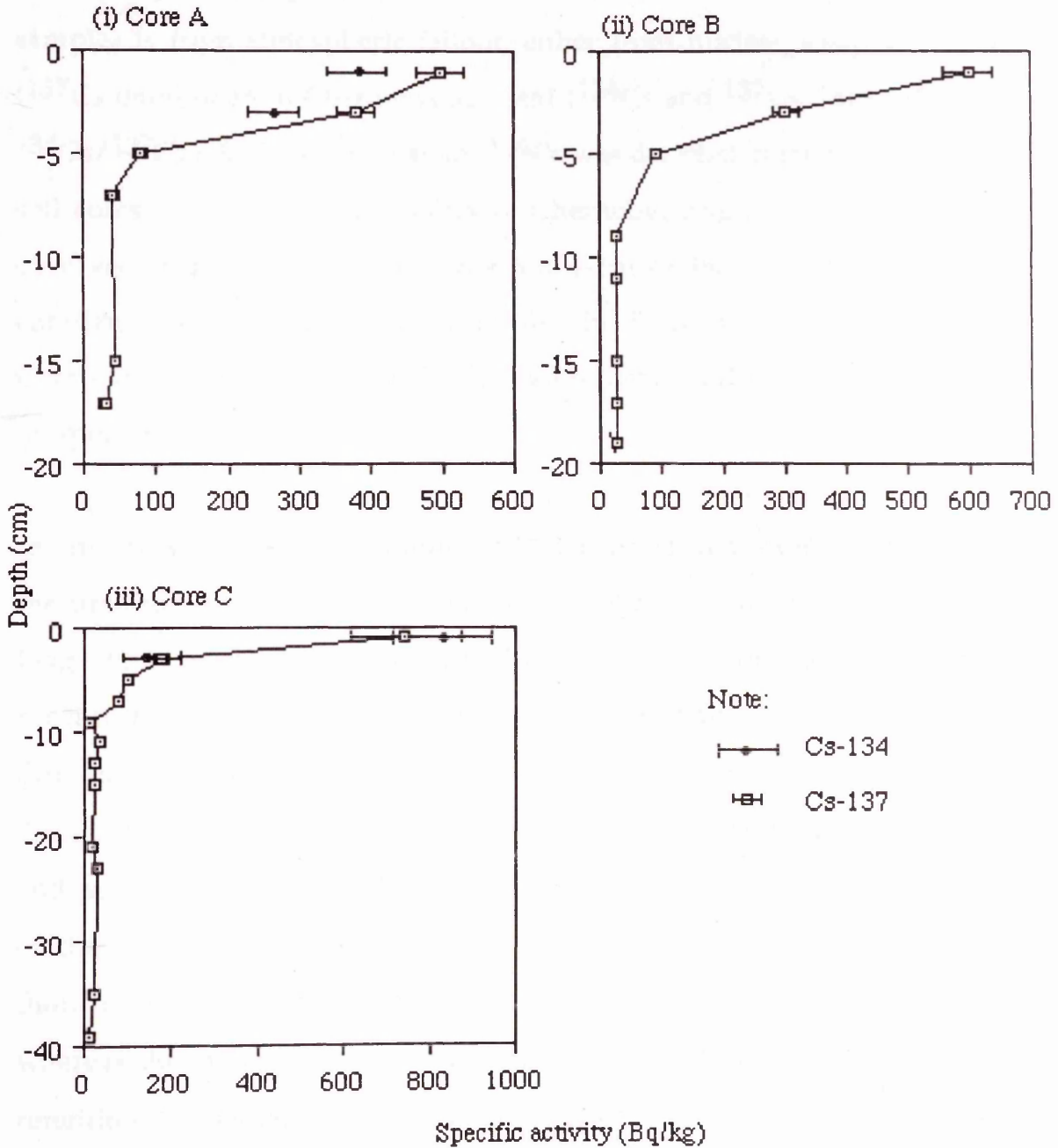


Figure 4.64: Cs-137 and Cs-134 concentration profiles for soil cores (i) A, (ii) B and (iii) C from Beeswing.



with depth, with high concentrations in the top 4 cm of the soil and low and fairly constant concentrations at greater depths. ^{137}Cs is detectable to the bottom of each core, suggesting that downwards migration of ^{137}Cs in the soil is probably quite efficient. The source of the radiocaesium in these samples is from atmospheric fallout, either from nuclear weapons testing (^{137}Cs only) or from Chernobyl accident (^{134}Cs and ^{137}Cs ; May 1986 with $^{134}\text{Cs}/^{137}\text{Cs} = 0.55$) being possible. ^{134}Cs was detected in the top 4 cm of the soil cores A and C which is solely of Chernobyl origin. As ^{137}Cs is also observed to be concentrated in the top 4 cm of the soil, thus providing confirmation that ^{137}Cs contribution in these samples is mostly of Chernobyl origin and probably negligible contribution from the nuclear weapons testing fallout.

In summary analysis of uranium and thorium clearly show evidence that the uranium vein has been subject to two phases of re-distribution i.e. (i) long - term leaching with preferential loss of ^{234}U relative to ^{238}U ; and (ii) recent, rapid loss of uranium with the probability of geochemical dissolution of uranium from the vein being about $5.2 \times 10^{-5} \text{ y}^{-1}$ (upper limit). The observed general behaviour of uranium, thorium, radium, lead and caesium at the study site is consistent with the established geochemistry of these elements. Uranium and radium are relatively mobile whereas thorium is effectively immobile; caesium is relatively mobile in the soil whereas the mobility of lead is extremely low, probably because of strong retention properties of soil organic matter and clay minerals. These findings have implications for radioactive waste disposal in the context of far-field movement of soluble nuclides and highlights the importance of

characterising radionuclide retardation by processes related to groundwater flow in soils (i.e. final component of far-field barrier) eg. uptake of radionuclides by organic matter, clay minerals and iron-manganese sesquioxides.

4.5 Uranium and thorium studies in stream water around the edge of the Criffel pluton

In section 4.1 it was demonstrated that at least the near surface rocks of the Criffel pluton in general have lost uranium, particularly since the end of the last period of glaciation. The dominant mechanism of uranium loss from the pluton is by transport in groundwater which interacts with the rock (described in sections 4.2 and 4.3) and then drains through fissures in the pluton and a portion eventually finds its way to rivers, lakes and the Irish Sea. The rivers thus represent the most readily accessible source of water likely to be fed with uranium and are one of the routes for loss of uranium from the pluton as a result of weathering. But some of the dissolved uranium may simply migrate to depth as part of a continuing major convective or at least advective system.

River water samples collected from 7 localities around the edge of the pluton on two occasions (November 1991 and April, 1992) were analysed for uranium and thorium by ICP-MS and the analytical results are given in Table 3.16, along with the $^{234}\text{U}/^{238}\text{U}$ activity ratio (determined by alpha spectroscopy) of a water sample from Kinharvie Burn. The concentrations of uranium in the river water samples varied from 0.046 to 1.305 ppb with systematically higher values being observed for the samples collected in the April 1992 sampling than those collected in November 1991 (Figure 4.65). The increased uranium concentrations for samples collected in April are possibly indicative of low rainfall resulting in low flow rates of the rivers and increased residence time of groundwater in contact with the rock. In contrast, the low uranium concentrations observed for November 1991 are indicative of higher rainfall, corresponding to higher flow rates and lower

Figure 4.65: Uranium and thorium concentrations of river water samples around the Criffel pluton, southwest Scotland.

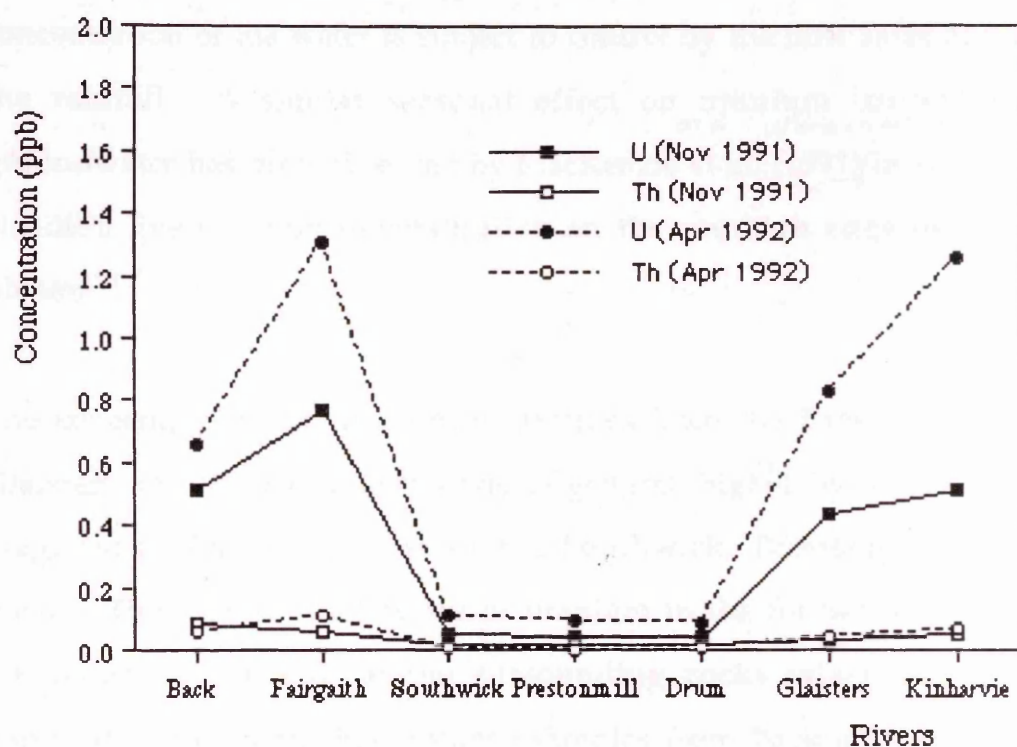
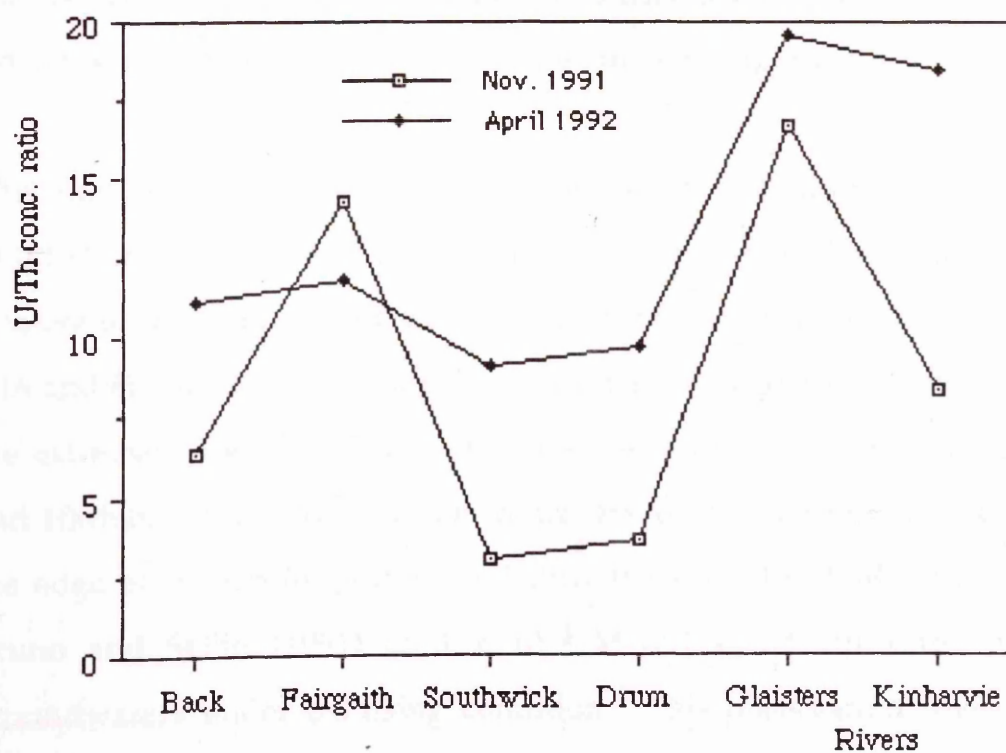


Figure 4.66: U/Th concentration ratio of the river water samples around the Criffel pluton, southwest Scotland.



residence time of groundwater in contact with the rock and dilution of the uranium content in water. The results may indicate that the uranium concentration of the water is subject to control by the flow rates and in turn the rainfall. A similar seasonal effect on uranium concentration in groundwater has been observed by MacKenzie et al. (1991) ^{and Whitton et al. (1992)} in studies at the Needle's Eye uranium mineralisation on the southern edge of the Criffell pluton.

The concentrations of uranium in samples from the Back, Fairgaith lane, Glaisters and Kinharvie burns are, in general, higher by about 1 order of magnitude, than samples from the Southwick, Prestonmill and Drum burns. The high concentrations of uranium in the former samples can be attributed to leaching of the surrounding rocks which are relatively enriched in uranium. For instance samples from Back and Fairgaith lane burns are located in the Sandyhills area which are close to the Needle's Eye and Lot's Wife uranium veins. The high uranium concentrations in river waters from Glaisters and Kinharvie burns may be indicative of the existence of uranium enrichment in the surrounding area.

The concentrations of thorium in the river water samples range from 0.013 to 0.103 ppb with little or no seasonal or geographic variation and are low relative to uranium as indicated by high U/Th concentration ratios (Table 3.16 and Figures 4.65 and 4.66). These values are to be expected considering the extremely low solubility of thorium in most natural waters (Ivanovich and Harmon, 1982). Yet uranium concentration of the river waters around the edge of the Criffell pluton are below the solubility limits reported by Bruno and Sellin (1991) of 3×10^{-4} M (7.1×10^4 ppb) for granitic groundwaters under oxidising condition. This observation reveals that uranium dissolution is subject to both kinetic and thermodynamic control

i.e. solubility data used in models are conservative. In contrast the solubility limit for thorium is about 2×10^{-10} M (0.046 ppb), comparable to thorium concentrations of the river water samples from the pluton.

If the maximum (1.305 ppb), minimum (0.046 ppb) and mean (0.437 ppb) uranium contents of the river water samples are taken in conjunction with the total annual rainfall of 110 cm y^{-1} for the pluton from the Meteorological Service Station at Portling Bay (Whitton et. al., 1992), the resulting regional loss of uranium from the pluton in the last 12000 y are estimated to be 5.6×10^{16} g (6.7×10^{22} Bq), 2.0×10^{15} g (2.4×10^{21} Bq) and 1.9×10^{16} g (2.3×10^{22} Bq) respectively. The results indicate that the regional loss of uranium is about twice the estimated values based on uranium loss from rock to a depth of 20 cm (described in section 4.1). Considering a large scale of uranium budget like this, the results are in reasonably good agreement and indicate that present day leaching over 12000 y could give the observed depletion.

The river water sample from Kinharvie Burn had a uranium concentration of 0.657 ppb (analysed by alpha-spectrometry) and $^{234}\text{U}/^{238}\text{U}$ activity ratio of 1.22, comparable with the observation of a value of 1.5 ± 0.5 by MacKenzie et al. (1991) for a field drain near the Needle's Eye natural analogue study site. The relative enrichment of ^{234}U isotope over ^{238}U in the water sample may be explained by alpha recoil or selective/preferential leaching of ^{234}U or a combination of the two. ^{230}Th was below the detection limit, implying that uranium is dissolved and transported in the virtual absence of thorium.

In summary uranium concentrations in river waters vary in response to the flow rates, the concentration being at a maximum at times of low flow rates and vice versa. The river waters in close proximity to the uranium veins exhibit by about 1 order of magnitude higher uranium content than those from other parts of the pluton indicating that the veins are a significant source of uranium to the river waters. Uranium concentrations in water are less than the predicted solubility values suggesting that the models are conservative.

4.6 Conclusions

On the basis of the preceding discussion, the following major conclusions can be drawn from this study.

The analyses of uranium and thorium in samples from the Criffel pluton are consistent with the expected geochemical behaviour of these two elements in igneous rock, which is that uranium is susceptible to oxidation-induced dissolution and is, consequently, relatively mobile, whereas thorium is effectively immobile. The study shows that the Criffel pluton has experienced a recent, rapid removal of uranium from the uppermost section of the granite, with a removal probability for uranium dissolution of $1.9 \times 10^{-5} \text{ y}^{-1}$. The probability of removal of uranium to solution in groundwater from the Beeswing vein is estimated to be $4.0 \times 10^{-5} \text{ y}^{-1}$, comparable to the value of $5.2 \times 10^{-5} \text{ y}^{-1}$ derived by Scott et al. (1991) for uranium dissolution from the bulk vein material of the Needle's Eye mineralisation on the southern edge of the Criffel pluton. This observation indicates that with no protection whatsoever, pitchblende has been preserved for long time periods with a low probability for uranium dissolution.

Uranium concentrations in river waters draining from the pluton vary in response to flow rate with maximum concentrations at times of low flow rate and vice versa. The river waters in close proximity to the uranium veins exhibited higher uranium concentrations (by about 1 order of magnitude) than those from other parts of the pluton, indicating that the veins are a significant source of uranium to the river waters. This suggests that the control on uranium concentration is kinetic as well as

thermodynamic. Uranium concentrations in water are less than the predicted values from models, thus suggesting that the models are conservative.

The isotopic results for samples from the pluton clearly reveal the loss of uranium relative to ^{230}Th and show that the uranium loss has been a rapid process, with insufficient time to allow the development of detectable disequilibrium between ^{234}U and ^{238}U (i.e. the rate of bulk dissolution has been rapid relative to the rate of preferential loss of ^{234}U). The pronounced disequilibrium between ^{230}Th and ^{234}U is consistent with rapid post-glacial removal of uranium (~ 12000 y).

On a regional basis the *surface part* of the pluton (to a depth of about 20cm) has lost between 20 and 30% of its uranium over the last 12000 y. The absence of significant 'whole-rock' re-deposition within any zone of the pluton suggests that the 'whole-rock' structure of the pluton presents a negligible barrier to uranium migration on a scale of 10 km over a time of about 12000 y. However, there is evidence that the very near surface weathered rocks and those adjacent to fractures and a series of complex redox fronts running through this highly fractured rock act as sites of radionuclide deposition. In the context of far-field movement of soluble nuclides, this observation confirms the assumption adopted in performance assessment modelling that the major features of the far-field barrier which result in radionuclide retardation will be sorption by fracture-lining minerals, matrix diffusion and deposition in the vicinity of redox fronts. In the case of the Dalbeattie quarry samples (rock section CQ1), a distance of 7 cm from the fracture was suggested for the extent of radionuclide migration into saturated rock via matrix diffusion.

Fission track analyses of the samples from the Criffel pluton indicated that uranium is mainly distributed in two ways. Firstly, it is found in association with accessory minerals such as sphene, apatite, monazite and zircon, suggesting that it has been retained in obdurate minerals despite recent weathering. This confirms that these minerals incorporate uranium by crystal lattice substitution and consequently show a high retention capacity of uranium. Thus in the context of a natural analogue study, a mineral such as sphene can retain uranium over a 10^6 y timescale under a variety of geochemical conditions, including recent (12000 y) exposure to oxidising groundwater i.e. if a waste form of comparable durability can be produced then retention for 10^4 to 10^6 y would be obtained. Secondly, uranium is found distributed along crystal boundaries of biotite or at boundaries of crystal inclusions, such as zircons, within biotite. The fission track study suggests that the 'whole-rock' depletion of uranium observed in the samples of the Criffel pluton may be attributed to uranium loss during chemical weathering from interstitial uranium which is present along crystal boundaries of biotite and in altered biotite and feldspars.

The activity ratio data for a representative granite core from the pluton suggest that the average rate of downwards movement of the weathering front in the granite is about 12 m in 10^6 y. In the context of radioactive waste disposal, this rate of movement suggests that the proposed rate of far-field movement of a repository-related redox front of up to 50 m in 10^6 y (Neretneiks and Aslund, 1983a, b) is a realistic value for inclusion in far-field transport models.

As expected, re-deposition of the dissolved uranium occurs in the reduced rock close to the redox fronts in the rock sections at Dalbeattie as a result of the reduction of uranium from the soluble U^{6+} to the insoluble U^{4+} . This

observation thus demonstrates that the redox fronts act as an effective retardation barrier, as indicated by deposition of uranium on the reduced side of the fronts. In an advancing front re-dissolution would, however, occur as the front encroaches into the reduced rock. This is therefore a temporary trapping rather than permanent deposition. Thus, in a HLW repository scenario, development of redox fronts would be expected to lead to retardation of radionuclides with insoluble reduced forms (eg. Pu) released from a repository.

The depth of oxidation in the highly fractured rock at Dalbeattie ranges from 1 to 10m below ground level and, the time-scale for development of the fronts is probably of the order of 12000 y, i.e. since the end of the last glaciation. Uranium is generally removed from the oxidised rock close to the redox front and accumulates just beyond the front in the reduced rock. However, some uranium re-deposition is observed on the oxidised side of the front which would not be expected from a thermodynamic viewpoint and probably involves scavenging by Fe-oxyhydroxides - a process not conventionally incorporated in repository performance assessment models. Also ^{226}Ra and REE diffuse from the reduced rock and accumulate in the oxidised rock, close to the redox front. Taken together, the ^{226}Ra , REE and uranium distributions indicate that both diffusion and advection processes probably control the distribution of radionuclides about the front. The results are consistent with the Pocos de Caldas work by MacKenzie et al. (1992).

^{226}Ra and REE re-distribution about the front is a significant observation for two reasons: firstly, net radium and REE movement is in the opposite direction to that expected for uranium at the front, suggesting that the control of radionuclide and REE movement at the front is both advective

and diffusive; secondly, radium and REE are not inherently redox-sensitive (i.e. Ra is always restricted to the 2+ oxidation state and REE are always in 3+ oxidation state except Ce and Eu). This suggests that radium and REE are released to solution in the reduced rock but are scavenged from solution in the oxidised rock. Either the $\text{Fe}^{2+}/\text{Fe}^{3+}$ and $\text{Mn}^{2+}/\text{Mn}^{4+}$ system or the $\text{S}^{2-}/\text{SO}_4^{2-}$ system could be invoked to explain this observation via scavenging of ^{226}Ra and REE by iron-manganese oxyhydroxides or the formation of secondary sulphates (from sulphides) in the oxidised rock.

The behaviour of elements at the redox front has implications not only for waste disposal, in the context of radionuclide retardation during far-field transportation, but also for genesis of mineral deposits. Thus, the observed enrichment of uranium in the reduced rock close to the fronts indicates the mechanism of formation of low-temperature mineral deposits such as roll-front uranium deposits. Although some of the uranium is caught in the redox fronts as evidenced in the rock sections at Dalbeattie, a proportion is presumably carried down mega-joints where their walls are oxidised. The geometry of the fracture-associated redox fronts is that of an extremely acute arrow pointing downwards, and it is possible to imagine that, at least along significantly permeable structures, the point of that arrow would eventually follow the shape of the flow lines of open convection systems. Thus, it seems feasible to assume that this study provides us with a microcosm of the process that, under appropriate conditions, can lead to precipitation of uranium and other redox-sensitive elements at the discharge points of large-scale hydrothermal convection cells where sulphides, hydrocarbons or even hydrogen act as the electron donors for re-deposition. Although the uranium will eventually leak through in a

small proportion of those natural hydrothermal systems where the source rocks have a relatively high initial oxidation state, it appears from both radiogenic age dating and structural studies that it takes at least 100×10^6 y for the leading edge of such a front to move through the rocks and back to the surface, by this time a benign addition to the uppermost crust (Mohamad et al., 1992).

The study of natural decay series and radiocaesium isotopes from Beeswing revealed significant re-deposition of uranium, radium and lead in soils by uptake in organic materials and secondary minerals and less retardation of caesium. This observation has implication that the soil could play a significant role as the final retardation barrier for radionuclides released from a repository.

In summary, this study has confirmed the expected general behaviour of uranium and thorium during rock water interactions and provided quantitative data for the probability of uranium dissolution from bulk rock and pitchblende. The work verifies that the principal mechanisms of radionuclide retardation during far-field transport are likely to be sorption on rock or fracture lining minerals, matrix diffusion and redox front trapping. The study indicates that these processes may be particularly effective in the near surface rock and further reveals the soil to be the final, additional site of radionuclide retardation. The near surface weathered zone is thus identified as a potentially important final barrier to far-field migration of radionuclide released from a repository - a fact not widely recognised in performance assessment modelling for radioactive waste repositories.

References

- Adams, F. and Dams, R., 1970. Applied gamma-ray spectrometry. Pergamon Press, Oxford, 2nd. Edition, pp 753.
- Alexander, W.R. and Shimmiel, T.M., 1990. Microwave oven dissolution of geological samples: novel application in the determination of natural decay series radionuclides. *J. Radioanal. Nucl. Chem. Letters*, 145/4, , 301-310.
- Alexander, W.R. Scott, R.D., MacKenzie, A.B. and McKinley, I.G., 1988. A natural analogue study of radionuclide migration in a water conducting fracture in crystalline rock. *Radiochimica Acta.*, 44/45, 283-289.
- Alexander, W.R. Scott, R.D., MacKenzie, A.B. and McKinley, I.G., 1989. Natural analogue studies using the natural decay series radionuclides. NAGRA Tech. Rept. (NTB 87 - 08), Baden, Switzerland.
- Andreyev, P.F. and Chumachenko, A.P., 1964. Reduction of uranium by natural organic substances. *Geochem. Intl.* 1, 3-7.
- Arth, J.G. and Barker, F., 1976. Rare earth partitioning between hornblende and dacitic liquid and implications for the genesis of trondhjemitic-tonalitic magmas. *Geology*, 4, 534-536.
- Bacon, M.P. and Rosholt, J.N., 1982. Accumulation rates of Th-230, Pa-231, and some transition metals on the Bermuda Rise. *Geochim. Cosmochim. Acta*, 46, 651-666.
- Barker, F.B. and Scott, R.C., 1958. Uranium and radium in groundwater of the Llamas Estacado, Texas and Mexico. *Am. Geoph. Union*, 39(3), 459-466.
- Basham, I.R., 1981. Some applications of autoradiographs in textural analysis of uranium bearing samples-a discussion. *Econ. Geol.* 76, 974-977.
- Basham, I.R., Milodowski, A.E., Hyslop, E.K. and Pearce, J.M., 1989. The location of uranium in sources and sites of secondary deposition at the Needle's Eye natural analogue site, Dumfries and Galloway. BGS Tech. Rpt., WE/89/56, pp 56.

- Beauchemin, D., Micklethwaite, R.K., vanLoon, G.W. and Hay, G.W., 1992. Determination of metal-organic associations in soil leachates by inductively coupled plasma-mass spectrometry. In: Jarvis, I. and Jarvis, K.E (Eds), *Plasma Spectrometry in the Earth Sciences*. Chem. Geol., 95, 1 - 33.
- BenShaban, Y.A., 1989. Radionuclide movement and geochemistry in intertidal sediments in southwest Scotland. PhD thesis, University of Glasgow, pp 369, (Unpub.).
- Boyle, R.W., 1982. Geochemical prospecting for thorium and uranium deposits. Elsevier Sc. Pub. Co., Amsterdam, Oxford, New York, pp 498.
- Brookins, D.G., 1984. Geochemical aspects of radioactive waste disposal. Springer-Verlag, New York, pp 345.
- Brunfelt, A.O. and Steiness, E., 1969. Neutron activation analysis of silicate rocks with epithermal neutrons. *Analytica Chimica Acta*, 48, 13 - 24.
- CANMET, 1983. Radium-226 in certified uranium reference ores DL-1a, BL-4a, DH-1a and BL-5. CANMET Report 39-9E, Canadian Centre for Mineral and Energy Technology, Ottawa.
- Chalov, P.I., 1959. The $^{234}\text{U}/^{238}\text{U}$ ratio in some secondary minerals. *Geochemistry*, 203-210.
- Chalov, P.I., Tuzova, T.V. and Musin, Y.A., 1964. Isotopic ratio $^{234}\text{U}/^{238}\text{U}$ in natural waters and its use for nuclear geochronology. *Geochem. Intl.*, 1, 402-408.
- Chapman, N.A. and McKinley, I.G., 1987. The geological disposal of nuclear waste. John Wiley and Sons, New York.
- Chapman, N.A., McKinley, I.G. and Smellie, J.A.T., 1984. The potential of natural analogues in assessing systems for deep disposal of high-level radioactive waste. Swiss Federal Institute for Reactor Research, Report No. 545, Wurenlingen, Switzerland, pp 103.
- Chapman, N.A. and Smellie, J.A.T., 1986. The natural analogues systems. *Chem. Geol.*, 55, 167-385.
- Chaudhuri, S. and Faure, G., 1967. Geochemistry of the Keweenawan rocks, White Pine, Michigan. *Econ. Geol.*, 62, 1011-1033.
- Cherdyntsev, V.V., 1971. Uranium-234. Israel program for scientific translation, Monson, Jerusalem, pp 308.
- Cohen, P., 1964. An evaluation of uranium as a tool for studying the hydrogeochemistry of the Truckee Meadows area, Nevada. *J. Geophys. Res.*, 4199-4206.

- Come, B. and Chapman, N.A., 1987. Natural analogues in radioactive waste disposal. Graham and Trotman, Oxford.
- Courrioux, G., 1987. Oblique diapirism: The Criffel granodiorite/granite zoned pluton, SW Scotland. *J. Str. Geol.*, 9, 313-330.
- Craig, G.Y., 1991. *Geology of Scotland*. 3rd. Edition, Alden Press, Oxford.
- Cramer J.J., 1986. Sandstone-hosted uranium deposits in northern Saskatchewan as natural analogues to nuclear fuel waste disposal vaults. *Chem. Geol.*, 55, 269-280.
- Cramer, J., Vilks, P. and Larocque, J.P.A., 1987. Near-field analogue features from the Cigar Lake uranium deposit. In: Come, B. and Chapman, N.A. (Eds.), *Natural analogues of radioactive waste disposal*. Graham and Trotman, Oxford, 59-72.
- Curtis, D., Benjamin, T., Gancarz, A., Loss, R., Rosman, K. DeLaeter, A., Delmore, J. and Maeck, W., 1987. Geochemical controls on the retention of fission products at the Oklo natural fission reactor. In: *Natural analogues in radioactive waste disposal* (Eds. Come, B. and Chapman, N.A.). Graham and Trotman, Oxford, 140-141.
- Darnley, A.G., Chandler, T.R.D., English, T.H., Fiddler, P.A., James, O., Preece, E.R. and Prosser, N.J.D., 1962. Pitchblende from Sandyhills, Kirkcudbrightshire. *Geol. Surv. Great Britain, Age Determination Report*, No. 20, pp 6.
- Date, A.R. and Gray, A.L., 1989. *Applications of Inductively Coupled Plasma Mass Spectrometry*. Blackie, Glasgow, pp 254.
- Davidson C.F. and Bowie S.H.U., 1951. On thucolite and related hydrocarbon-uraninite complexes. *Bull Geol. Surv. Great. Britain*. No. 3, 1-16.
- Dement'yev, V.S. and Syromyatnikov, N.G., 1968. Conditions of formation of a sorption barrier to the migration of uranium in an oxidising environment. *Geochem. Intl.*, 5, 394-399.
- DeSoete, D., Gijbels, R. and Hoste, J., 1972. *Neutron activation analysis*. John Wiley, New York, pp 836.
- Deurden, P., 1990. Alligator Rivers analogue projects. 1st Annual Report 1988-89. *Aust. Nuc. Sc. Tech. Organization*, pp 146.
- Dickson, J.H., Stewart, D.A., Thompson, R., Turner, G., Baxter, M.S., Drndarski, N.D. and Rose, J., 1978. Palynology, paleomagnetism and radiometric dating of Flandrian marine and freshwater sediments of Loch Lomond. *Nature* 274, 548 - 553.

- Doi, K., Hirono, S. and Sakamaki, Y., 1975. Uranium mineralization by ground water in sedimentary rocks, Japan. *Econ. Geol.*, 70, 628-646.
- Dominik, J., Cuccodoro, S., Gourcy, L. and Santiago, S., 1991. A high natural uranium level in the surface and groundwaters of the alpine rhone watershed (Switzerland). *Proc. intl. conf. on heavy metals in the environment* (J.G. Farmer Ed.), I, 342-346.
- Elderfield, H. and Greaves, M.J., 1982. The rare earth elements in seawater. *Nature* 296, 214 - 219.
- Faure, G., 1986. *Principles of Isotope Geology*. John Wiley and Sons (2nd. Edn), New York, 282-304.
- Fleet, A.J., 1984. Aqueous and sedimentary geochemistry of the rare earth elements. In: Henderson, P. (Ed.), *Rare earth geochemistry. Developments in Geochemistry* 2, Elsevier, Amsterdam, 343-369.
- Fleischer R.L., 1966. Uranium micromaps: technique for *in-situ* mapping of distributions of fissionable impurities. *Rev. Sci. Instrum.*, 37, 1738-1739.
- Fleischer, R.L. and Raabe, O.G., 1978. Recoiling alpha emitting nuclei: mechanism for uranium-series disequilibrium. *Geochim. Cosmochim. Acta*, 42, 973-978.
- Fleischer, R.L., 1982a. Alpha-recoil damage and solution effects in minerals: Uranium isotope disequilibrium and radon release. *Geochim. Cosmochim. Acta*, 46, 2191-2201.
- Fleischer, R.L., 1982b. Nature of alpha-recoil damage: evidence from preferential solution effects. *Nucl. Tracks*, 6, 35-42.
- Friedlander, G., Kennedy, J.N., Macias, E.S. and Miller, J.M., 1981. *Nuclear and radiochemistry*. John Wiley and Sons (3rd. Edn.), pp 684.
- Gallagher, M.J., Michie, U.M, Smith, R.T. and Haynes, L., 1971. New evidence of uranium and other mineralization in Scotland. *Trans. Instn. Min. Metall.*, 80, B150-B173.
- Garrels, R.M. and Christ, C.L., 1965. *Solutions, minerals and equilibria*. Harper and Row, New York, pp 450.
- Gascoyne, M. and Schwarcz, H.P., 1986. Radionuclide migration over recent geologic time in a granitic pluton. *Chem. Geol.*, 59, 75-85.
- Gascoyne, M., 1979. *Isotope and geochronologic studies of speleothem*. Ph.D. thesis, McMaster University, Ontario, Canada.

- Gascoyne, M., 1982. Geochemistry of the actinides and their daughters. In: Uranium series disequilibrium applications to environmental problems (Eds. Ivanovich, M. and Harmon, R.S.), Clarendon Press, Oxford.
- Gascoyne, M., 1986. Evidence for the stability of the potential nuclear waste host, sphene, over geological time, from U-Pb ages and U-series measurements. *Applied Geochem.*, 1, 199-210.
- Gordon, G.E., Randle, K., Goles, G.G., Corliss, J.B., Beeson, M.H. and Oxley, S.S., 1968. Instrumental activation analysis of standard rocks with high-resolution γ -ray detectors. *Geochim. Cosmochim. Acta.*, 32, 369-396.
- Govindaraju, K., 1989. 1989 compilation of working values and sample description for 272 geostandards. *Geostand. Newsl.*, 13, 1-113.
- Grauert, B., Seitz, M.G. and Soptrajanova, G., 1974. Uranium and lead gain of detrital zircon studied by isotopic analysis and fission-track mapping. *Earth Planet. Sci. Lett.*, 21, 389-399.
- Greenwood, N.N. and Earnshaw, A., 1984. Chemistry of the elements. Pergamon Press, pp 156.
- Grim, R.E., 1962. Applied clay mineralogy. McGraw-Hill, New York, pp 422.
- Guthrie, V.A. and Kleeman, J.D., 1986. Changing of U distributions during weathering of granite. *Chem. Geol.*, 54, 113-126.
- Guthrie, V.A., 1989. Fission-track analysis of U distribution in granitic rocks. *Chem. Geol.*, 77, 87-103.
- Hadermann, J. and Rosel, F., 1985. Radionuclide chain transport in inhomogeneous crystalline rocks-limited matrix diffusion and effective surface sorption. National Cooperative for the Storage of Radioactive Waste (NAGRA), Rept. No. NTB 85-40, pp 81.
- Hall, G.E.M and Plant, J.A., 1992. Application of geochemical discrimination diagrams for the tectonic interpretation of igneous rocks hosting gold mineralisation in the Canadian Shield. In: Jarvis, I. and Jarvis, K.E. (Eds.), Plasma Spectrometry in the Earth Sciences. *Chem. Geol.*, 95, 157-165.
- Hall, G.E.M., 1989. Inductively coupled plasma-mass spectrometry. In: Thompson, M. and Walsh, J.N. (Eds.), Handbook of Inductively Coupled Plasma-Mass Spectrometry. Blackie, Glasgow, 238-269.
- Hallberg, L., Brise, H., Anderson, S. and Telc, A., 1960. Determination of ^{55}Fe and ^{59}Fe in blood. *Intl J. Appl. Rad. Isotopes*, 9, 100-108.

- Hallberg, R.O., Ostlund, P. and Wadsten, T., 1987. A 17th century bronze cannon as analogue for radioactive waste disposal. In: Natural analogues in radioactive disposal, (Eds. Come, B. and Chapman, N.A.), Graham and Trotman, Oxford, 135-139.
- Halliday, A.N., W.E. Stephens, and Harmon, R.S., 1980. Rb-Sr and O isotopic relationships in 3 zoned Caledonian granitic plutons, Southern Uplands, Scotland: evidence for varied sources and hybridisation of magmas. *J. Geol. Soc. London*, 137, 329-348.
- Hanna, A.G., and Al-Shahristani H., 1977. Resonance activation analysis of biological materials. *J. Radioanal. Chem.*, 37, 581-589.
- Harris, I., 1989. NAA - neutron activation analysis programme. Scottish Universities Research Reactor Centre (Unpub.).
- Hashimoto, T., 1971. Determination of uranium content in seawater by a fission track method with condensed aqueous solution. *Geochim. Cosmochim. Acta.* 56, 347 - 354.
- Heimann, R.B., 1987. A statistical approach to evaluating durability of a simulated nuclear waste glass. In: The geological disposal of high level radioactive wastes (Ed. Brookins, D.G.), Theophrastus Pub., Athens, 181-206.
- Henderson, 1991. Pers. comm.
- Henderson, P., 1982. Inorganic geochemistry. Pergamon Press, Oxford, pp 343.
- Henderson, P., 1984. Rare earth element geochemistry. Elsevier Oxford.
- Holmes D., Pitty A. and Noy D., 1990. Geomorphological and hydrogeological features of the Pocos de Caldas caldera, and the Osamu Utsumi mine and Morro do Ferro analogue study sites, Brazil. The Pocos de Caldas Project, TR 90-14, KBS, Stockholm, Sweden.
- Holmes, J.A., Hales, P.E. and Street-Perrot, F.A., 1992. Trace-element chemistry of non-marine ostracods as a means of paleolimnological reconstruction: An example from the Quarternary of Kashmir, northern India. In: Jarvis, I. and Jarvis, K.E. (Eds.), Plasma Spectrometry in the Earth Sciences. *Chem. Geol.*, 95, 177-186.

- Hooker, P., MacKenzie, A.B., Scott, R.D., Ridgeway, I.M, McKinley, I.G. and West, J.M., 1985. A study of long term (10^3 - 10^4 y) elemental migration in saturated clays and sediments (part 3). Brit. Geol. Surv. Rept., FLPU 85 - 9.
- Hostetler, P.B. and Garrels, R.M., 1962. Transportation and precipitation of uranium and vanadium at low temperatures, with special reference to sandstone type uranium deposits. Econ. Geol. 57, 137-167.
- Hurford, A.J. and Green, P.F., 1982. A user's guide to fission track dating calibration. Earth Planet. Sci. Lett., 59, 343-353.
- IAEA, 1978. Natural fission reactors. Pro. Tech. Com. meeting, Paris, 19-21 Dec., 1977. ST1/PUB/475, Intl Atomic Energy Agency, Vienna.
- IAEA, 1981. Shallow ground disposal of radioactive wastes: a guidebook, Safety Series, 53, Intl Atomic Energy Agency, Vienna.
- IAEA, 1982. Site investigations for repositories for solid radioactive wastes in deep continental geological formations, Tech. Rept. Series, 215, Intl Atomic Energy Agency, Vienna, pp 106.
- IAEA, 1984. Certified Reference IAEA/Soil-7. Intl Atomic Energy Agency Laboratory/243.
- IAEA, 1988. Radioactive waste management advisory programme (WAMAP) in Malaysia. IAEA-TA-2424, pp 54.
- Ivanovich, M. and Harmon R.S., 1982. Uranium series disequilibrium: application to environmental problems. Clarendon Press, Oxford, pp 565.
- Jardine, W.G., 1966. Landscape evolution in Galloway. Trans. Dumfriesshire Natural History and Antiquarian Soc. 2nd Ser. VII. XLIII, pp.13.
- Jardine, W.G., 1993. Pers. comm.
- Jarvis, I. and Jarvis, K.E., 1992. Plasma spectrometry in the earth sciences: Techniques, applications and future trends. Chem. Geol., 95, 1-33.
- Jarvis, K.E., 1988. ICP-MS, a new technique for the rapid or ultra-trace level determination of the REEs in geological materials. Chem. Geol., 68, 31-39.
- Jarvis, K.E., Gray, A.L. and Houk, S., 1991. Handbook of Inductively Coupled Plasma-Mass Spectrometry. Blackie, Glasgow, pp 375.
- Jarvis, K.E., Gray, A.L., Jarvis, I. and Williams, J.(Eds.), 1990. Plasma Source Mass Spectrometry. R. Soc. Chem. London, Spec. Publ., 85, pp 172.

- Kamaneni, D.C., 1986. Distribution of uranium, thorium and rare-earth elements in the Eye-Dashwa Lakes pluton - a study of some analogue elements. *Chem. Geol.*, 55, 361 - 373.
- Katz, J.J., Seaborg, G.T. and Morss, L.R., 1986. The chemistry of the actinide elements. V-2, Chapman and Hall, New York.
- KBS, 1983. Final storage of spent nuclear fuel. KBS-3, Swedish Nuclear Fuel Supply Co. (SKBF/KBS), Stockholm.
- Keller, C., 1988. Radiochemistry. Ellis Horwood Ltd., New York, pp 208.
- Kigoshi, K., 1971. Alpha recoil Th-234: Dissolution into water and the $^{234}\text{U}/^{238}\text{U}$ disequilibrium in nature. *Science*, 173, 47-48.
- Kleeman, J.D. and Lovering, J.F., 1967. Uranium distributions in rocks by fission-track registration in lexan plastic. *Science*, 156, 512-513.
- Kobashi, A., Sato, J. and Saito, N., 1979. Radioactive disequilibrium with uranium, thorium and radium isotopes leached from euxenite. *Radiochim. Acta*, 26, 107-111.
- Krauskopf, K.B., 1986. Thorium and rare-earth elements as analogues for actinide elements. In: The natural analogue systems (Eds. Chapman, N.A. and McKinley, I.G.), *Chem. Geol.*, 55, 323-335.
- Krauskopf, K.B., 1988. Radioactive waste disposal and geology. Chapman and Hill, pp 145.
- Kroom, R.D., Helmke, P.A. and Jackson, M.L., 1980. Associations of trace elements with iron oxides during weathering. *Am. J. Soil Sc.*, 44, 155-159.
- Kuroda, P.K., 1982. The origin of the chemical elements and the Oklo phenomenon. Springer-Verlag, New York, pp 165.
- Lancelot, J.R., Vitrac, A. and Allegre, 1975. The Oklo natural reactor. Age and evolution studies of U-Pb and Rb-Sr systematics. *Earth Plan. Sci. Lett.*, 25, 189 - 196.
- Langmuir, D., 1978. Uranium solution-mineral equilibria at low temperatures with applications to sedimentary ore deposits. *Geochim. Cosmochim. Acta*, 42, 547-569.
- Latham, A.G. and Schwarcz, H.P., 1987a. On the possibility of determining rates of removal of uranium from crystalline igneous rocks using U-series disequilibria, 1: A U-leach model, and its applicability to whole rock data. *Appl. Geochem.*, 2, 55-65.

- Latham, A.G. and Schwarcz, H.P., 1987b. On the possibility of determining rates of removal of uranium from crystalline igneous rocks using U-series disequilibria, 2: A U-leach model, and its applicability to whole rock data. *Appl. Geochem.*, 2, 67-71.
- Latham, A.G. and Schwarcz, H.P., 1987c. The relative mobility of U, Th and Ra isotopes in the weathered zones of the Eye-Dashaw Lakes granite pluton, northwestern Ontario, Canada. *Geochim. Cosmochim. Acta*, 51, 2787-2793.
- Lei, W., Linsalata, P., Franca, E.P. and Eisenbud, M., 1986. Distribution and mobilisation of cerium, lanthanum and neodymium in the Morro do Ferro basin, Brazil. In: *The natural analogue systems* (Eds. Chapman, N.A. and McKinley, I.G.), *Chem. Geol.*, 55, 313-322.
- Levinson, A.A., 1977. Hydrogen - a reducing agent in some uranium deposits. *Can. J. Earth Sci.*, 14, 2679-2681.
- Lopatkina, A.P., 1964. Characteristics of migration of uranium in the natural waters of humid regions and their use in the determination of the geochemical background for uranium. *Geochem. Intl*, 1, 788-794.
- Loveley, D.R., Phillips, E.J.P., Gorby, Y.A. and Landa, E.R., 1991. Microbial reduction of uranium. *Nature*, 350, 413-415.
- Lutze, W., Grambow, B., Ewing, R.C. and Jercinovic, M.J., 1987. The use of natural analogues in the long-term extrapolation of glass corrosion processes. In: *Natural analogues in radioactive waste disposal* (Eds. Come, B. and Chapman, N.A.), *Graham and Trotman, Oxford*, 142-152.
- MacGregor, M., 1937. The western part of the Criffel-Dalbeattie igneous complex. *Quart. J. Geol. Soc. London*, 93, 457-484.
- MacGregor, M., 1938. The evolution of the Criffel-Dalbeattie quartz-diorite; a study of granitisation. *Geol. Mag.* 75, 481-496.
- MacKenzie A.B. Scott R.D. and Smellie J.A.T., 1986. A comparison of neutron activation and alpha spectrometry analyses of uranium in crystalline rocks. *J. Radioanalyt. Nucl. Chem. Lett.*, 103, 321-331.
- MacKenzie A.B., Scott R.D., Linsalata, P. and Miekeley, N., 1992. Natural decay series studies of the redox front system in the Pocos de Caldas uranium mineralization. In: *Chapman, N.A., McKinley, I.G., Shea, M.E. and Smellie, J.A.T. (Eds.), The Pocos de Caldas Project: Natural analogues of processes in a radioactive waste repository. J. Geochem. Expl.* 45, 289-322.

- MacKenzie, A.B. and Scott, R.D., 1982. Radiocaesium and plutonium in intertidal sediments from southern Scotland. *Nature*, 229, 613-616.
- MacKenzie, A.B., Baxter, M.S., McKinley, I.G., Swan, D.S. and Jack, W., 1979. The determination of ^{134}Cs , ^{137}Cs , ^{210}Pb , ^{225}Ra and ^{228}Ra concentrations in nearshore marine sediments and seawater. *J. Radioanalyt. Chem.*, 48, 29-47.
- MacKenzie, A.B., Scott, R.D., Houston, C.M. and Hooker, P.J., 1989. Natural decay series radionuclide studies at the Needle's Eye natural analogue site, 1986-89. BGS Tech. Rept., WE/90/4, pp 59.
- MacKenzie, A.B., Whitton, A.M., Shimmield, T.M., Jemielita, R.A., Scott, R.D. and Hooker, P.J., 1991a. Natural decay series radionuclide studies at the Needle's Eye natural analogue site, II, Tech. Rpt. SURRC, 1989-1991.
- MacKenzie, A.B., Scott, R.D., Linsalata, P., Miekeley, N., Osmond, J.K. and Curtis, D.B., 1991b. Natural radionuclide and stable element studies of rock samples from the Osamu Utsumi mine and Morro do Ferro analogue study site, Pocos de Caldas, Brazil. SKB Tech. Rept. 90-16, Swedish Nuclear Fuel and Waste Management Co., Stockholm, Sweden.
- MacKenzie, A.B., Scott, R.D., McKinley, I.G. and West, J.M., 1983. A study of long term (10^3 - 10^4 y) elemental migration in saturated clays and sediments (Part I). BGS Rept. FLPU 83-6, Bri. Geol. Surv., Keyworth.
- Marsh, G.P., 1982. Materials for HLW containment. *Nucl. Energy*, 21, 253-266.
- Mason, B. and Moore, C.B., 1982. Principles of geochemistry. John Wiley and Sons Inc., (9th Edn.), New York.
- Maynard, J.B., 1983. Geochemistry of sedimentary ore deposits. Springer-Verlag, New York.
- McDonald, P., Cook, G.T., Baxter, M.S. and Thompson, J.C., 1992. The terrestrial distribution of artificial radioactivity in south-west Scotland. *The Science of the Total Environment*, 111, 59-82.
- McKinley, I.G., 1989. Applying natural analogues in predictive performance assessment. In: Risk analysis in nuclear waste management (A.Saltelli et al., Eds.), ECSC, EEC, EAEC, Brussels and Luxembourg, 359-396.
- McKinley, I.G., and Handermann, J., 1984. Radionuclide sorption database for Swiss safety assessments. National Cooperative for the Storage of Radioactive Waste (NAGRA), Report No. 84-40, Baden, Switzerland.

- Means, J.L., Crerar, D.A., Borcsik, M.P. and Duguid, M.L., 1978. Adsorption of selected actinides by Mn and Fe oxides in soils and sediments. *Geochim. Cosmochim. Acta*, 42, 1763-1773.
- Michie, U. McL., Gallagher, M.J. and Simpson, A., 1973. Detection of concealed mineralisation in northern Scotland. In: Jones, M.J. (Ed.), *Geochemical Exploration 1972*, London Insts. Mining Metall., 117-130.
- Miller, J.M. and Taylor, K., 1966. Uranium mineralization near Dalbeattie, Kirkcudbrightshire. *Bull. Geol. Survey*, 25, 1-18.
- Milodowski, A.E., Basham, I.R., Hyslop, E.K. and Pearce, J.M., 1989. The uranium source-term mineralogy and geochemistry at the Broubster natural analogue site. Caithness. *Brit. Geol. Surv. Rept.*, WE/89/50 and DOE Rept. No. DOE/RW/89.073.
- Milodowski, A.E., Pearce, J.M., Hyslop, E.K., Basham, I.R. and Hooker, P.J., 1990. Uranium-mineralised micro-organisms associated with uraniferous hydrocarbons in southwest Scotland. *Nature*, 347, 465-467.
- Mohamad, D.B., 1980. A study of uranium in groundwater around Greyhawk mine, Bancroft, Ontario. M.Sc. thesis, McMaster University, Canada (Unpub.).
- Mohamad, D.B., MacKenzie, A.B., Stephens, W.E. and Russell, M.J., 1992. Exploration methods for nuclear waste repositories or mineral-deposits - from source to sink, where's the front? *Trans. Instns. Min. Metall.*, 101, B139 - B146.
- NAGRA., 1985. Project Gewähr. National Cooperative for the Storage of Radioactive Waste (NAGRA), Technical Report No. 85-09, Baden, Switzerland.
- Nash, J.T. Grainger, H.C. and Adams. S.S., 1981. Geology and concepts of genesis of important types of uranium deposits. *Econ. Geol.* 75th Anniversary Volume, 63-116.
- NEA/OECD, 1977. Objectives, concepts and strategies for the management of radioactive waste arising from nuclear power programmes. Report by a group of experts of the OECD, Paris.
- NEA/OECD, 1984a. Seabed disposal of high level radioactive waste status report. Paris, pp 247.
- NEA/OECD, 1984b. Geological disposal of radioactive waste: An overview of the current status of understanding and development. Paris, pp 266.

- Neretnieks, I. and Aslund, R., 1983a. The movement of radionuclides past a redox front. SKB Report TR 83-66, KBS, Stockholm, Sweden.
- Neretnieks, I. and Aslund, R., 1983b. Two-dimensional movement of redox-front downstream from a repository for nuclear waste. SKB Report TR 83-68, KBS, Stockholm, Sweden.
- Neretnieks, I., 1980. Diffusion in the rock matrix: an important factor in radionuclide retardation? *J. Geophys. Res.*, 85, 4379-4397.
- Neretnieks, I., 1986. Some uses for natural analogues in assessing the function of a HLW repository. *Chem. Geol.*, 55, 175-188.
- Nesbitt, H.W., 1979. Mobility and fractionation of rare earth elements during weathering of a granodiorite. *Nature*, 279, 206-210.
- Norton, D. and Knapp, R., 1977. Transport phenomena in hydrothermal systems: The nature of porosity. *Am. J. Sci.*, 277, 913 - 936.
- Osmond, J.K. and Cowart, J.B., 1976. The theory and uses of natural uranium isotopic variations in hydrology. *Atomic Energy Review*, 14, 621 - 679.
- Patrick, R.A.D and Russell, M.J., 1989. Sulphur isotopic investigation of Lower Carboniferous vein deposits of the British Isles. *Mineral Deposita*, 24, 148-153.
- Phillips, W.J., 1956. The Criffel-Dalbeattie granodiorite complex. *J. Geol. Soc. London.*, 112, 221-240.
- Phillips, W.J., Fuge, R. and Phillips, N., 1981. Convection and crystallization in the Criffel-Dalbeattie pluton. *J. Geol. Soc. London.* 138, 351-366.
- Pine R.J. and Batchelor A.S., 1984. Downward migration of shearing in jointed rock during hydraulic injections. *Int. J. Rock Mechanics Min. Sci.*, 21, 249-263.
- Poupeau, G., 1981. Precision, accuracy and meaning of fission track ages. *Earth Planet. Sci. Lett.*, 90, 403-436.
- Price and Walker, 1963. A simple method of measuring low uranium concentration in natural crystals. *App. Phys. Lett.*, 2, 23-25.
- Riddle, C., VanderVoet, A. and Doherty, W., 1988. Rock analysis using inductively coupled plasma spectrometry: a review. *Geostand. Newsl.*, 12, 203-235.

- Robertson, D.E., 1968. The adsorption of trace elements in seawater on various surfaces. *Analytica Chimica Acta.*, 42, 535-536.
- Roelandts, I. and Deblonde, A., 1992. Rare-earth element composition of Devonian sediments from southern Belgium: application of an inductively coupled-plasma emission spectrometry method. In: Jarvis, I. and Jarvis, K.E. (Eds.), *Plasma Spectrometry in Earth Sciences*. *Chem. Geol.*, 95, 167-176.
- Rogers, J.J.W. and Adams, J.A.S., 1970. Uranium. In: *Handbook of Geochemistry*. K.H. Wedepohl et al. (Eds.). 11-5, Springer-Verlag, Berlin.
- Russell M.J., 1983. Major sediment-hosted exhalative zinc + lead deposits: Formation from hydrothermal convection cells that deepen during crustal extension. Short course in sediment-hosted stratiform lead-zinc deposits. D.F. Sangster (Ed.) *Mineralogical Association of Canada. Short course handbook* 8, 251-282.
- Russell, M.J., 1985. The evolution of the Scottish mineral sub-province. *Scott. J. Geology*, 21, 385-574.
- Russell, M.J. and Hall, J., 1988. Mechanics of downward permeation of water in crystalline rock with application to problems of geothermal energy extraction. *Trans. Insts. Min. and Metall.*, 97, B51-56.
- Russell, M.J. and Skauli, H., 1991. History of theoretical developments in carbonate-hosted base metal deposits and the new tri-level enthalpy classification. *Econ. Geol. Memoir*, 8, 96-116.
- Schnetzler, C.C and Philpotts, J.A., 1970. Partition coefficients of rare earth elements between igneous matrix material and rock-forming mineral phenocrysts, II. *Geochim. Comochim. Acta*, 34, 331 - 340.
- Schwarcz, H.P., Gascoyne, M. and Ford, D.C., 1982. U-series disequilibrium studies of granitic rocks. *Chem. Geol.*, 36, 87-102.
- Scott, R.D., MacKenzie, A.B. and Alexander, W.R., 1992. The interpretation of ^{238}U - ^{234}U - ^{230}Th - ^{226}Ra disequilibrium produced by rock - water interaction. In: Chapman, N.A., McKinley, I.G., Shea, M.E. and Smellie, J.A.T. (Eds.), *The Pocos de Caldas Project: Natural analogues of processes in a radioactive waste disposal repository*. *J. Geochem. Expl.* 45, 323-343.

- Scott, R.D., MacKenzie, A.B., Ben-Shaban, Y.A., Hooker, P.J. and Houston, C.M., 1991. Uranium transport and retardation at Needle's Eye natural analogue site, southwest Scotland. *Radiochimica Acta*, 52/53, 357-365.
- Skagius, K. and Neretneiks, I., 1982. Diffusion in crystalline rocks. In: Lutze, W. (Ed.), *Scientific Basis for Nuclear Waste Management*, 5, Elsevier, Amsterdam, 509 - 518.
- Smellie, J.A. and Papp, T., 1988. Swedish natural analogue research topics. Paper presented at the CEC natural analogue working group meeting, Snowbird near Salt Lake City, USA.
- Smellie, J.A.T., MacKenzie, A.B. and Scott, R.D., 1986. An analogue validation study of natural radionuclide migration in crystalline rocks using uranium series disequilibrium studies. *Chem. Geol.* 55, 233-254.
- Stephens, W.E., 1972. The geochemistry of the Dalbeattie Complex and associated rocks. Ph.D thesis, 1972, U.C.W. Aberyswyth (Unpub.).
- Stephens, W.E. and Halliday, A.N., 1980. Discontinuities in the composition surface of a zoned pluton, Criffel, Scotland. *Geol. Soc. Am. Bull.*, 91, 165-170.
- Stephens, W.E., Whitley, J.E., Thirwall M.F. and Halliday, A.N., 1985. The Criffel zoned pluton: correlated behaviour of rare earth element abundances with isotopic systems. *Mineral. Petrol.*, 89, 226-238.
- Sulaiman, M.Y., 1991. An overview of the rare earth mineral processing industry in Malaysia. *Industrial Minerals Special Review, Rare Earth. Future Prospects*, U.K., 55 - 58.
- Tate, J., 1992. Pers. comm.
- Thiel, K., Herr, W. and Becker, J., 1972. Uranium distribution in basalt fragments of five lunar samples. *EPSL*, 16, 31-44,
- Thiel, K.R., Saager, R. and Stupp, H.D., 1983. ^{235}U fission tracks and ^{238}U -series disequilibria as a means to study recent mobilization of U in Archaean pyritic conglomerates. *Earth Planet. Sci. Lett.*, 65, 249-262.
- Thurber, D.L., 1962. Anomalous $^{234}\text{U}/^{238}\text{U}$ in nature. *J. Geophys. Res.* 67, 4518-4520.
- Thurber, D.L., 1965. The concentrations of some natural radioelements in the waters of the Great Basin. *Bull. Volcanol.*, 28, 195-201.

- Tieh, T.T., Ledger, L.B. and Rowe, M.W., 1980. Release of uranium from granitic rocks during in situ weathering and initial erosion, Central Texas. *Chem. Geol.*, 29, 227-248.
- Toole, J., Hursthouse, A.S., McDonald, P., Sampson, K., Baxter, M.S., Scott, R.D. and McKay, K., 1990. The determination of actinides by ICP-MS. In: Jarvis, K.E., Gary, A.L., Williams, J.G. and Jarvis, I. (Eds), *Royal Society Chemistry*, London, 155 - 162.
- Topping, P.G. and MacKenzie, A.B., 1988. A test of the use of neutron activation analysis for clay source characterisation. *Archeometry* 30, 92-101.
- Totland, M., Jarvis, I. and Jarvis, K.E., 1992. An assessment of dissolution techniques for the analysis of geological samples by plasma spectrometry. *Chem. Geol.*, 95, 35-62.
- Tripathi, V.S., 1979. Comments on "Uranium solution-mineral equilibria at low temperatures with applications to sedimentary ore deposits". *Geochim. Cosmochim. Acta*, 43, 1989-1990.
- USDE, 1988. Site characterisation plan. Yucca Mountain site, Nevada research and development area, Nevada, DOE/RN-0199.
- Waber, N., Schorscher, H.D., MacKenzie, A.B. and Peters, T., 1990. Mineralogy, petrology and geochemistry of the Pocos de Caldas analogue study sites, Minas Gerais, Brazil. I: Osamu Utsumi uranium mine, TR 90-11, KBS, Stockholm, Sweden.
- Wagner, G.A., 1968. Fission track dating of apatites. *Earth Planet. Sci. Lett.*, 4, 411-415.
- White, A.J.R., Chappell, B.W. and Jakes, P., 1972. Coexisting clinopyroxene, garnet and amphibole from an "eclogite", Kakarumi, New Zealand. *Contrib. Mineral. Petrol.*, 34, 185-191.
- White, W.S., 1968. The native copper deposits of northern Michigan. In: Ridge, J.E. (Ed.), *Ore deposits of the United States*. Amer. Inst. Mining Metal. Petrol. Eng., 1, 308-325.
- Whitton, A.M., MacKenzie, A.B., Shimmield, T.M., Scott, R.D. and Hooker, P.j., 1992. Natural decay series radionuclide studies at the Needle's Eye natural analogue site, III, 1991-1992. SURRC Rept. pp 43.
- WHO, 1982. Management of high level radioactive waste. Regional office for Europe, Copenhagen, No. 13, pp 61.

- Williams, J.G. and Gray, A.L., 1988. High dissolved solids and ICP-MS: are they compatible? *Anal. Proc.*, 25, 385-388.
- Yim, W.S.S., Gleadow, A.J.K. and Van Moort, J.C., 1985. Fission track dating of alluvial zircons and heavy mineral provenance in northeast Tasmania. *J. Geol. Soc. London*, 142, 351-356.
- Zhou, Z.H., Fyfe, W.S. and Takazaki, K., 1987. Glass stability in the marine environment. In: *Natural analogues in radioactive waste disposal*. (Come, B. and Chapman, N.A. Eds.), Graham and Trotman, Oxford, 153-164.